Recent Publications in this Series

44/2015 Yuexi Gu
Implications of BRCA1 Mutations in Basal-Like Breast Cancer Development and Treatment
45/2015 Noora Neittaanmäki-Perttu
Diagnosis and Treatment of Premalignant Changes of Photodamaged Skin: Novel Hyperspectral Imaging and New Therapeutical Aspects
46/2015 Tina Loman
Ruokatottumukset, liikunta ja paino: sosioekonomiset erot ja muutokset
47/2015 Terhi Kurko
Deregulation of Nicotine Replacement Therapy Products in Finland: Reasons for Pharmaceutical Policy Changes and Reflections on Smoking Cessation Practices
48/2015 Lotta Hirvenkari
Natural Stimuli and Experimental Setups in the Study of the Neural Basis of Social Interaction
49/2015 Leena Keurulainen
Synthesis and Evaluation of Antichlamydial, Antileishmanial and Antimalarial Activity of Benzimidazole and Benzoxadiazole Derivatives
50/2015 Leena Soininen
The Health of the Finnish Sami in Light of Mortality and Cancer Pattern
51/2015 Mikhail Kislin
Fine Morphological Alterations during Brain Injury and Recovery Analyzed with Intravital Microscopy
52/2015 Laura K. Mäkinen
Atrix Metalloproteinases and Toll-Like Receptors in Early-Stage Oral Tongue Squamous Cell Carcinoma
53/2015 Samuel Sandboge
Early Growth and Adult Health: Focus on Resting Metabolism, Non-alcoholic Fatty Liver Disease, Hypertension, and Regional Differences in Birth Size
54/2015 Merja Laine
Cardiometabolic Health among Male Former Elite Athletes
55/2015 Efthymia Vlachopoulou
HLA-DRB1: Haplotype Diversity, Imputation and Association with Acute Coronary Syndrome
56/2015 Polina Ilina
The Role of the Carrier and the Endocytic Pathway in Non-Viral Gene Delivery
57/2015 Natalia V. Luchkina
Developmentally Regulated Induction and Expression Mechanisms of Long-Term Potentiation at Hippocampal CA3-CA1 Synapses
58/2015 Karoliina Autio
Efficacy and Safety of Oncolytic Vaccinia and Semliki Forest Virus in the Treatment of Canine and Feline Malignant Solid Tumours
59/2015 Martin Reichhardt
Salivary Scavenger and Agglutinin SALSA in Innate Immunity
60/2015 Chakravarthi Kanduri
Genomics Approaches to Study Music Perception and Performance
61/2015 Jussi Kupari
Studies on Peripheral Nervous System Development and Function in Mice Deficient for the Neurturin Receptor GFRα2
62/2015 Anton Tokariev
Studying Connectivity in the Neonatal EEG

Helsinki 2015 ISSN 2342-3161 ISBN 978-951-51-1425-9

DISSERTATIONES SCHOLAE DOCTORALIS AD SANITATEM INVESTIGANDAM
UNIVERSITATIS HELSINKIENSIS

63/2015

EVA MARÍA DEL AMO PÁEZ

Ocular and Systemic Pharmacokinetic Models for Drug Discovery and Development

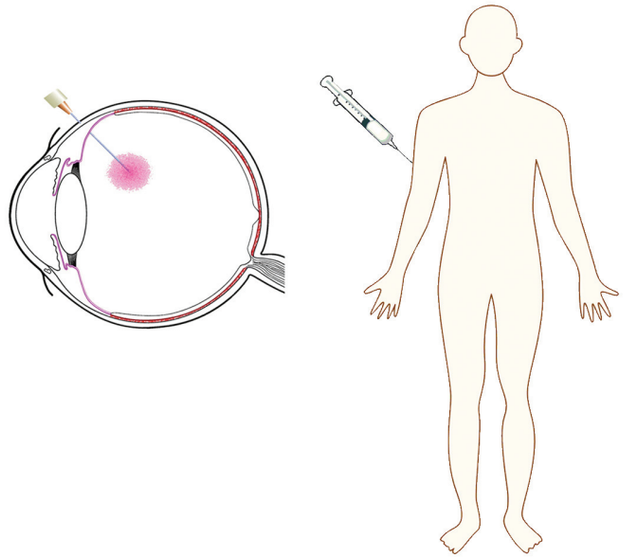

CENTRE FOR DRUG RESEARCH
DIVISION OF PHARMACEUTICAL BIOSCIENCES
FACULTY OF PHARMACY
DOCTORAL PROGRAMME IN DRUG RESEARCH
UNIVERSITY OF HELSINKI

Centre for Drug Research
Division of Pharmaceutical Biosciences
Faculty of Pharmacy
University of Helsinki
Finland

Ocular and systemic pharmacokinetic models for drug discovery and development

Eva María del Amo Páez

ACADEMIC DISSERTATION
To be publicly discussed, with the permission of the Faculty of Pharmacy of the University of Helsinki, in lecture hall MS301, Medistudia building, Yliopistonranta 1A, Kuopio, on Friday, September 11th, 2015, at 12 noon.

Helsinki 2015

Supervisors: Professor Arto Urtti, Ph.D.
Centre for Drug Research
Division of Pharmaceutical Biosciences
Faculty of Pharmacy
University of Helsinki
Finland

Professor Marjo Yliperttula, Ph.D.
Centre for Drug Research
Division of Pharmaceutical Biosciences
Faculty of Pharmacy
University of Helsinki
Finland

Henri Xhaard, Ph.D.
Centre for Drug Research
Division of Pharmaceutical Biosciences
Faculty of Pharmacy
University of Helsinki
Finland

Reviewers: Professor Sara Nicoli, Ph.D.
Department of Pharmacy,
University of Parma
Italy

Rubén Alvarez Sánchez, Ph.D.
Drug Disposition and Safety, Pharmaceutical Sciences
Roche Pharma Research & Early Development
F. Hoffmann-La Roche
Switzerland

Opponent: Emeritus Professor Olavi Pelkonen, Ph.D.
Department of Pharmacology and Toxicology,
University of Oulu
Finland

ISBN 978-951-51-1425-9 (print) 978-951-51-1426-6 (online)
ISSN 2342-3161 (print) 234-317X (online)

Hansaprint Printing House
Helsinki 2015

Abstract

Drug discovery and development is a long process: it takes usually 12 to 15 years before a drug candidate reaches the market. The pharmacokinetics of the drug is an important aspect of drug discovery and development, because the drug must reach its target site and exert the therapeutic response. The pharmacokinetic parameters of new compounds should be investigated early in drug discovery. Pharmacokinetic predictions can be made with Quantitative Structure-Property Relationships (QSPR) which are computational models that correlate chemical features with pharmacokinetic properties. The correlations are based on *in vivo* or *in vitro* pharmacokinetic data and molecular descriptors. QSPR models can be used to predict the pharmacokinetic parameters even before any actual drug synthesis and can be exploited to guide drug discovery. Pharmacokinetic models can also simulate concentration profiles of drugs during the drug discovery and development process.

It was decided to develop QSPR models of pharmacokinetic parameters of drugs to be delivered by the systemic or ocular routes. A combination of Principal Component Analysis and Partial Least Square multivariate statistical methods was used to obtain QSPR equations for volume of drug distribution and fraction of unbound drug in plasma. Parallel modelling of these parameters resulted in acceptable R^2 (0.58 - 0.77) and Q^2 values (0.55 - 0.58). These models are based on a large set of structurally unrelated compounds, they are open and they have a defined applicability domain. Charge and lipophilicity related descriptors were the relevant ones which influenced the volume of distribution and free fraction of drug in plasma.

Pharmacokinetics is an important factor in the development of ocular medications, because the ocular drug targets are difficult to reach, particularly in the posterior tissues such as retina and choroid. Therefore, drugs need to be injected intravitreally in the treatment of retina and choroid diseases (e.g. in exudative age-related macular degeneration) and thus prediction of intravitreal pharmacokinetics would be especially advantageous in ocular drug discovery and development. The first comprehensive collection of intravitreal volume of distribution and clearance values of compounds was collated based on extensive rabbit eye data from the literature. Moreover, predictive QSPR models for intravitreal clearance and half-life were created which had R^2 and Q^2 values of 0.62 – 0.84 for clearance and 0.61 - 0.80 for half-life. $LogD_{7.4}$ and hydrogen bonding capacity defined the intravitreal clearance and half-life of compounds with a molecular weight below 1500 Da. The intravitreal volumes of drug distribution lay within a narrow range (80% within 1.18 - 2.28 ml). The QSPR models for intravitreal clearance and the typical values for intravitreal volumes of distribution were implemented in pharmacokinetic simulation models; the simulated profiles based on the real and predicted pharmacokinetic parameter values were similar. Thus, a combination of QSPR and pharmacokinetic models can be used in drug discovery and development to aid in the design of drugs and drug delivery systems.

A comprehensive comparison of intravitreal pharmacokinetic data between rabbit and human was carried out to clarify the translational value of the rabbit model. The analysis revealed that the rabbit can be considered as a clinically predictive animal model for intravitreal pharmacokinetics of small molecules (18 Da - 1500 Da) and macromolecules (7.1 kDa - 149 kDa). There was a correlation between the intravitreal clearance values in

human patients and healthy rabbits; they showed similar, but not identical, absolute values. The intravitreal pharmacokinetics of small molecules is mainly governed by permeability-limited clearance across blood-ocular barriers and occurs via the posterior route, whereas large molecules are cleared mostly via the anterior route. Although the literature contains some claims about the significance of the viscosity of the vitreous, it seems that this is not a major factor in drug elimination from the eye.

In conclusion, new *in silico* tools were generated for systemic and ocular pharmacokinetics and drug delivery. These models can be exploited in industrial drug discovery and will hopefully speed up the development of new medications.

To Vicente, Rebeca, and Diego.

Acknowledgements

This thesis work was conducted while I was a Ph.D. student in the Centre for Drug Research and at the Division of Biopharmaceutics and Pharmacokinetics (current Division of Pharmaceutical Biosciences), Faculty of Pharmacy, University of Helsinki, from 2010 to 2015. The work was carried out remotely in the Department of Biopharmacy and Pharmaceutical Technology, School of Pharmacy, University of Eastern Finland, Kuopio campus. The FinPharma Doctoral Program and the Finnish Cultural Foundation provided financial support for my research.

I want to express my deepest gratitude to my main supervisor Professor Arto Urtti. He is a good and kind supervisor. He has guided me with patience, humour and has always kept things in perspective. I have enjoyed working with him and his trust in me has meant a lot. I also want to thank my other supervisors: Professor Marjo Yliperttula for her advice and encouragement and Henri Xhaard, Ph.D. for his ideas and suggestions about my thesis.

I send my sincere thanks to the official reviewers Professor Sara Nicoli and Rubén Álvarez Sánchez, Ph.D. for their critical review of this thesis. I am honored to have Professor Olavi Pelkonen as my official opponent. I also want to thank Ewen MacDonald, Ph.D. for revising the language of my thesis.

I want to express my gratitude to the co-authors of the articles of this thesis, Heidi Kidron, Ph.D., Kati-Sisko Vellonen, Ph.D. and Leo Ghemtio, Ph.D. for their important contributions to this work and their support.

In the Kuopio site, I want to thank Professor Jukka Mönkkönen, the current Rector of the University of Eastern Finland. I also wish to thank the current and former Deans of the Faculty of Health Science and Heads of School of Pharmacy. Thank you for giving me the possibility to work here and for providing me with excellent working and learning facilities. It has been a privilege and I have felt comfortably adopted and supported. Thanks especially to all the personnel in the department for their kindness and readiness to help in resolving the many issues that arose during these years, among them Marko, Marja, Riitta, Seija. Thanks to the teachers-consultants, Ossi, Maija, Mika and especially Veli-Pekka. I also want to express my gratitude to Marika, Laura, Eva, Maria and to everyone in the ocular drug delivery group, each of you have added your own flavor to the group: thanks for the sharing of scientific and non-scientific thoughts and for creating such a convivial atmosphere. I also want to remember those who are no longer in the University, Eliisa, Aki, Johanna and those with whom I have shared many lunch time conversations, Tarja, Katja, Kristiina, Päivi, among others.

In the Helsinki site, I want to thank the personnel of the Faculty of Pharmacy, Eija, Tarja, Maija, and the current and former members of the Centre for Drug Research, Polina, Anna-Kaisa, Astrid, Leenas, Melina, Noora, among others: I have always felt warmly welcome on all my visits.

I also want to express my gratitude to Elias Hakalehto, Ph.D. for his trust and the opportunity given to me to take part in his scientific text books, which has helped me to grow as a researcher.

I give thanks to each and all of my friends who have been assisting in this process and especially to Sini who has listened, helped and laughed at the ups and downs of our theses.

I want to thank my parents who have always wanted to give me the best, and my sister Raquel who has encouraged and assuring me so many times.

I want to express my warmest gratefulness to my husband Vicente who has helped me A LOT and who has been so supportive of me, THANK YOU. And thanks with my whole heart to my loving children, Rebeca and Diego, who in their own sweet way have also been supportive to mother and her research in the University.

This thesis has been a very gratifying work and it is the result of many people's participations.

Kuopio, 2015

Eva del Amo Páez

Contents

List of original publications

This thesis is based on the following publications:

I Eva M. del Amo, Leo Ghemtio, Henri Xhaard, Marjo Yliperttula, Arto Urtti, Heidi Kidron. Applying linear and non-linear methods for parallel prediction of volume of distribution and fraction of unbound drug. PLOS ONE 2013, 8 (10), art. no. e74758
http://dx.doi.org/10.1371%2Fjournal.pone.0074758

II Heidi Kidron, Eva M. del Amo, Kati-Sisko Vellonen, Arto Urtti. Prediction of the Vitreal Half-Life of Small Molecular Drug-Like Compounds. Pharmaceutical Research, 2012, 29, 3302-3311.
http://dx.doi.org/10.1007/s11095-012-0822-5

III Eva M. del Amo, Kati-Sisko Vellonen, Heidi Kidron, Arto Urtti. Intravitreal Clearance and Volume of Distribution of Compounds in Rabbits: In Silico Prediction and Pharmacokinetic Simulations for Drug Development. European Journal of Pharmaceutics and Biopharmaceutics, 2015.
http://dx.doi.org/10.1016/j.ejpb.2015.01.003

IV Eva M. del Amo, Arto Urtti. Rabbit as an animal model for intravitreal pharmacokinetics: Clinical predictability and quality of the published data. Experimental Eye Research, 2015, 137, 111-124.
http://dx.doi.org/10.1016/j.exer.2015.05.003

The publications are referred to in the text by their Roman numerals.

Author's contribution

Publication I: Applying linear and non-linear methods for parallel prediction of volume of distribution and fraction of unbound drug. The author designed the study together with her supervisors and co-authors. The author carried out the literature review, obtained the 2-D molecular structures and calculated descriptors of the compounds, as well as undertaking the regression QSPR models with Principal Component Analysis and Partial Least Squares and performing their validation. The author wrote the first draft of the manuscript and actively participated in revising the paper into its final form.

Publication II: Prediction of the Vitreal Half-Life of Small Molecular Drug-Like Compounds. The author obtained the 2-D structures of the compounds of the data set and generated the physicochemical descriptors of the molecules, assisted with resolving pharmacokinetic issues and participated in compiling the final form.

Publication III: Clearance and Volume of Distribution of Compounds in Rabbits: *In Silico* Prediction and Pharmacokinetic Simulations for Drug Development. The author designed the study together with her supervisors and co-authors. The author collected and curated the literature data, participated in the analysis of the primary pharmacokinetic parameters, designed and built the QSPR model and performed the pharmacokinetic simulation models. The author wrote the first draft of the manuscript and actively participated in revising the paper into its final form.

Publication IV: Rabbit as an animal model for intravitreal pharmacokinetics: Clinical predictability and quality of the published data. The author designed the study with her supervisor. The author carried out the literature review and literature data analysis. She analysed the rabbit and human pharmacokinetic data, wrote the first draft of the manuscript and actively participated in revising the paper into its final form.

Abbreviations

A	amount of drug in the body;
ADME	absorption, distribution, metabolism and excretion;
AMD	age-related macular degeneration;
ANN	Artificial Neural Networks;
AUC	area under the curve;
BAB	blood-aqueous barrier;
BNN	Bayesian Neural Networks;
BRB	blood-retinal barrier;
BW	body weight;
C	drug concentration in plasma;
C_0	initial concentration of drug at time zero;
CART	Classification and Regression Trees;
C_{bound}	concentration of protein-bound drug in plasma;
C_{boundT}	concentration of bound drug in the tissue;
CG	Conjugate Gradient;
C_T	drug concentration in tissue;
C_u	concentration of unbound drug in plasma;
C_{uT}	concentration of unbound drug in the tissue;
CL	clearance;
CL_{ivt}	intravitreal clearance;
$CL_{ivt, app}$	apparent intravitreal clearance;
D4	hydrophobic volume descriptor from *Volsurf+® software*;
D_{iv}	intravenous dose;
D_{ivt}	intravitreal dose;
FALS	Fuzzy Adaptive Least Square;
f_b	fraction of drug bound to plasma protein;
f_u	unbound fraction of drug in plasma;
f_{uT}	unbound fraction of drug in tissues;
%FU10	% of fraction unionized at pH 10 descriptor from *Volsurf+® software*;
GA	Genetic Algorithm;
HD	hydrogen bond donor;
HA	hydrogen bond acceptor;
HQSAR	Hologram Quantitative Structure-Activity Relationships;
intravenous	i.v.;
k-NN	k-Nearest-Neighbor;
$K_{p, T}$	distribution coefficient between the tissues and plasma or between the tissues and vitreous;
$LogD_{5.5}$	distribution coefficient at pH 5.5;
$LogD_{7.5}$	distribution coefficient at pH 7.5;
$LogD_{10}$	distribution coefficient at pH 10;
$LogH_{tot}$	logarithm of the sum of hydrogen bond donors and acceptors;

LogHD	logarithm of the hydrogen bond donors;
LogP	partition coefficient;
L3LgS	solubility profiling coefficient descriptor from *Volsurf*+® *software*;
LgS3	logarithm of solubility at pH 3 descriptor from *Volsurf*+® *software*;
LgS10	logarithm of solubility at pH 10 descriptor from *Volsurf*+® *software*;
LogS	logarithm of solubility;
MDA	Mixture Discriminant Analysis;
MLR	Multiple Linear Regression;
MV	molar volume;
NLR	Nonlinear Regression;
PBP	protein binding percentage;
PCA	Principal Component Analysis;
PLS	Partial Least Squares or Projection to Latent Structures;
ρ	Spearman's rank correlation coefficient;
R^2	coefficient of determination;
RF	Random Forest;
SM	Sammon Maps;
SOM	Self Organizing Maps;
SR	Stepwise Regression;
SVM	Super Vector Machine;
SVR	Support Vector Regression;
Q^2	cross-validation;
Q_i^2	correlation coefficient of the internal test set prediction;
Q_e^2	correlation coefficient of the external test set prediction;
QSAR	Quantitative Structure-Activity Relationships;
QSPR	Quantitative Structure-Property Relationships;
QSPkR	Quantitative Structure-Pharmacokinetic Relationships;
RPE	retinal pigment epithelium;
$t_{1/2}$	half-life;
$t_{1/2,\ ivt}$	intravitreal half-life;
V_1	initial volume of distribution;
V_c	volume of the central compartment;
V_{area}	terminal volume of distribution;
V_β	terminal volume of distribution;
V_d	volume of distribution;
V_{plasma}	anatomical volume of plasma;
V_{ss}	volume of distribution at steady state;
$V_{ss,\ ivt}$	intravitreal volume of distribution;
V_T	anatomical volume of the tissue;
V_z	terminal volume of distribution;
W1	hydrophilic volume descriptor from *Volsurf*+® *software*.

1 Introduction

The absorption, distribution, metabolism and excretion (ADME) of drugs are important pharmacokinetic processes that exert an influence on drug efficacy, safety, dosing and patient compliance. These factors need to be investigated at various stages during drug discovery and development since any new drug must possess pharmacokinetic properties that are compatible with successful drug treatment. Pharmacokinetic problems have been identified as an important reason for drug attrition during the clinical stages of drug development (van de Waterbeemd and Gifford, 2003). Currently the vast majority, as many as 90%, of the compounds in the clinical phase, will fail due to many reasons not only lack of efficacy or unacceptable toxicity but also because of pharmacokinetics issues (Kola, 2008). Furthermore, delivery of sufficient amounts of active drug to certain target sites (e.g. brain, retina) is sometimes difficult. Thus, new methods and innovative approaches are needed in pharmacokinetic evaluation and drug delivery to facilitate the development of effective and safe drugs as well as improved delivery systems.

Although the prediction of pharmacokinetics during drug discovery and development has improved in the current century such that today pharmacokinetic properties of new analogs are addressed early in drug discovery, improvements are still needed (Kola and Landis, 2004). There are several computational methods which can be applied in ADME research e.g. Quantitative Structure-Property Relationships (QSPR), pharmacokinetic models, rule-of-5 classification, and the Biopharmaceutics Classification System (Lipinski, 2000, Lipinski et al. 2001, van de Waterbeemd and Gifford, 2003, van de Waterbeemd, 2009). Typically, the *in silico* models utilize prior information from experiments and this is then used to predict the pharmacokinetic features of the new compound. *In vitro* methods are also being widely used to characterize absorption, binding and metabolism of new compounds. These methods include permeability studies with cultured epithelial cells, investigations with transporter expressing cells, drug metabolism studies with microsomes or hepatocytes, and binding studies with plasma proteins (Zhang et al., 2012a, Vellonen et al., 2014, Caldwell et al., 2009). Again, pharmacokinetic models are needed to interpret *in vitro* results, and to translate them to the *in vivo* situation (Jones et al., 2015, Shardlow et al., 2013). *In vitro* methods are suitable for screening studies where one has a large number of compounds and only small quantities of each compound (Caldwell et al., 2009). Finally, only the most promising drug candidates will undergo *in vivo* animal studies, usually with rodents (mice, rats) and dogs or monkeys. Scaling methods are then applied to translate these data to the human patient context (Knibbe et al., 2005, Mahmood, 2007). In clinical studies, pharmacokinetic analyses will be carried out during phase I in healthy volunteers and in phases II and III in patients (Lüllmann et al., 2011, Pandit and Soltis, 2012). Overall, data integration and reliable translation to the clinical situation are highly important goals for the pharmacokinetic investigations undertaken during drug discovery and development. Successful tools can help not only in the compound selection, but also assist in the pharmacokinetic study design, such as devising optimal dosing regimens and administration routes.

The prevalence of ocular diseases affecting the posterior eye segment, such as age-related macular degeneration and diabetic retinopathy, are increasing as the world's

population ages (Zhang et al., 2012b). However, the treatment of these diseases is complicated, because it is difficult to deliver active drug to the retina or choroid. At the moment, local intravitreal injection is the best option to achieve effective drug concentrations in these tissues (del Amo and Urtti, 2008, Urtti, 2006). It is especially important to understand ocular pharmacokinetics after intravitreal injection, since intravitreal injection is such an invasive and unpleasant procedure that a long dosing interval (at least one month) is preferred (Bashshur et al., 2008, Cheung and Eaton, 2013). The dose and primary pharmacokinetic parameters of intravitreal drugs, volume of distribution and clearance determine the vitreal concentration profile of the drug. These parameters have not been investigated in a systematical manner and no QSPR models have been developed to predict intravitreal clearance or volume of drug distribution. One QSPR model has been developed for intravitreal half-life, but it has not been adequately validated (Durairaj et al., 2009). Nonetheless, these kinds of models would be very useful both in their own right and as a component part of pharmacokinetic simulation models. This approach could be expected to advance design of drugs and delivery systems for ocular use.

The rabbit is the most commonly used animal model in ocular pharmacokinetics; there is very little human ocular pharmacokinetic data due to the difficulties in ocular sampling. Recently, the criticism has been raised that the rabbit is a poor model of human intravitreal pharmacokinetics due to differences in eye size, vitreous humour viscosity, and retinal vasculature (Laude et al., 2010, Rowe-Rendleman et al., 2014, Vaishya et al., 2011). However, the rabbit and human pharmacokinetics after intravitreal injection have never been compared in a quantitative and systematic manner. Such information is needed if one wishes to assess the true clinical value of data obtained with the rabbit model i.e. translation of intravitreal pharmacokinetic data.

One goal of thesis project was to build computational models which would describe pharmacokinetics after systemic and intravitreal drug administration. In particular, a QSPR model was developed that combines volume of drug distribution and free fraction in plasma. Furthermore, QSPR and pharmacokinetic models were devised for intravitreally administered drugs in rabbits. Finally, the intravitreal injection data from rabbit and human studies were systematically analysed to assess the translational value of the intravitreal rabbit data.

2 Review of the literature

2.1 Pharmacokinetic processes

2.1.1. ADME

Pharmacokinetics can be defined as the study of the time course of the drug in the body after its administration. It consists of the processes of absorption, distribution, metabolism and excretion, abbreviated as ADME and represented in Figure 1. Drug absorption (A) is the process of drug permeation through body barriers such as skin, intestinal wall and so forth into the bloodstream. Drug distribution (D) is the reversible transfer of the drug from one location in the body (such as the vascular space) to another (such as the extravascular space). Metabolism (M) involves chemical or enzymatic reactions that transform the parent compound into active or inactive metabolites. Excretion (E) is the irreversible removal of the unchanged drug mainly via the kidneys into urine. Metabolism and excretion constitute the elimination process. ADME processes are interrelated and they determine the fate and time course of the drug in the body. The present thesis investigated ocular and systemic drug distribution and ocular elimination.

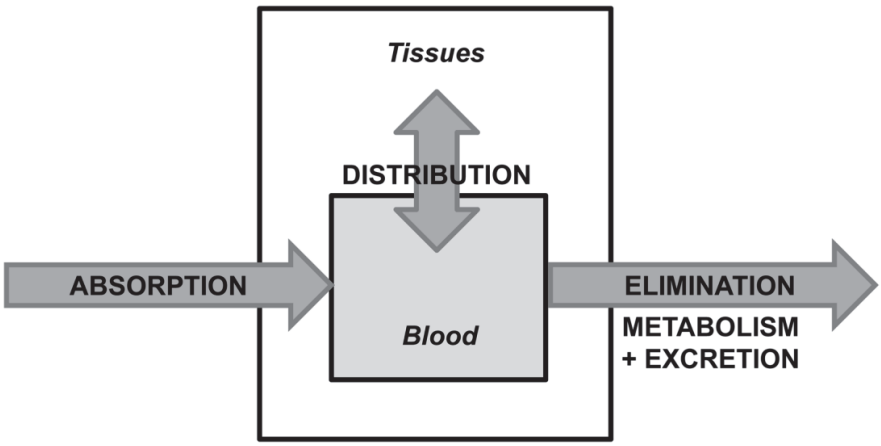

Figure 1 *The ADME processes shown schematically.*

2.1.2 Distribution

After absorption or intravascular injection, the drug is distributed from the blood circulation to the organs and tissues. Distribution is a reversible process that strives to achieve

equilibrium at steady state. Drug distribution from blood to the tissues is influenced by tissue perfusion, drug permeability through the cell membranes (including active transport into or out of the cell) as well as drug binding to the blood and tissue components.

Blood flow. The rate of blood flow in the tissue determines how quickly the drug reaches the tissues; this rate varies widely in different organs (Rowland and Tozer, 2011). For example, liver and kidney have high blood flow rates, whereas bone and adipose tissues are poorly perfused by blood. A drug will distribute faster to the well-perfused organs than to the poorly perfused ones. If the drug easily permeates across the vascular walls in the tissue, the rate of drug distribution is *perfusion rate limited*. On the other hand, if the vascular walls display resistance to the drug distribution, the rate is *permeability limited***.** The rate of drug distribution determines how quickly the target site is reached.

Drug permeation. In order to reach the target cells, the drug must permeate across the vascular walls (endothelial cells), reach the interstitial fluid, and pass across the cell membranes (in the common case where the drug's target is intracellular). The drug may permeate through membrane barriers by several mechanisms.

Paracellular diffusion refers to passage through the intercellular space between the cells. Depending on the leakiness of the intercellular space, this path can play a major or less important role in drug transport (Linnankoski et al., 2010).

Transcellular transport relies on the passage of drug through the cell membranes (Sugano et al., 2010). This can take place as either *transcellular passive diffusion* or *carrier mediated transport*. In the first case, the molecules pass through the membrane from a higher to a lower concentration without any energy requirement. This mechanism is operative in all cell types. In this case, lipophilicity and molecular size are the important physicochemical properties of the drug that influence the transcellular diffusion of the molecule. Typically, increased lipophilicity (characterized with high $LogD_{7.4}$ or LogP values or low hydrogen bonding capacity) and a small molecular weight favor transcellular passive diffusion (van de Waterbeemd and Gifford, 2003, van de Waterbeemd, 2009). The unionized fraction of the weak acids and weak bases is able to diffuse through the lipidic cellular membranes faster than the ionized species.

The *carrier mediated transport* can be classified as either *facilitated transport* (without any need to consume energy) or *active transport* **(**with energy consumption). Active transport can transfer the molecules against their concentration gradient. There are two major superfamilies of transporters: solute carrier transporters (SLC) and ATP-binding cassette (ABC) transporters (e.g. efflux transporters that move the drug in the extruding direction) (International Transporter Consortium et al., 2010). Active transport depends on the expression of the transporter in the particular cell type, it is saturable, and selective i.e. it only transports compounds that are able to bind to the transporter (International Transporter Consortium et al., 2010, Sugano et al., 2010). The net direction of the transport depends on the type of transporter (influx or efflux transport) and the location of the transporter (apical or basolateral side of the cell membrane).

All transport mechanisms coexist and may partly contribute to the overall net transport rate. The contribution of each mechanism depends on the cellular or tissue properties, the chemical features and the concentration of the drug. For example, drug distribution through the paracellular space in the vascular walls is high in those tissues with leaky fenestrated

vascular walls (e.g. liver, muscles), but negligible in the tissues with tight vascular endothelia (e.g. blood-brain barrier, blood-retinal barrier). Transcellular diffusion through the capillary endothelia is the primary mechanism of transport for lipophilic compounds, whereas structure specific distribution is usually associated with the expression of drug transporters.

Drug binding. Drugs may bind to plasma proteins or blood cell components, while in the extravascular space, they may bind to many tissue components. Only the free form of drug in plasma is able to permeate across the vascular walls. This is a prerequisite for drug distribution and localization to the target sites.

In plasma, drugs exist in a reversible equilibrium between the free and protein bound forms. The ratio of unbound to total drug concentration in plasma is the fraction unbound (f_u), in most cases, this is a constant value although the f_u value may change in special situations, such as renal and hepatic diseases (Rowland and Tozer, 2011). Albumin is the most abundant protein in plasma that binds acidic drugs (Hall and Guyton, 2011, Kwon, 2001, Øie and Tozer, 1979). Basic drugs often bind to alpha$_1$-acid glycoprotein and neutral lipophilic drugs to lipoproteins (Kwon, 2001). Furthermore, drugs may bind to extracellular and intracellular sites in the tissues. The free drug in the tissues is available for transcellular diffusion and carrier-mediated transport (Rowland and Tozer, 2011, Pandit and Soltis, 2012) (Figure 2).

Drugs with a high affinity for tissue components will distribute extensively, which means that they have high values of volume of distribution (Tett et al., 1988). Basic drugs tend to display higher extents of distribution than acidic drugs (Rodgers and Rowland, 2007). This may be due to the tissue composition, i.e. cell membranes consist primarily of acidic phospholipids (e.g. in liver, lungs, kidney) that can act as binding sites for positively charged basic drugs. Moreover, basic drugs can become entrapped inside the acidic lysosomes (pH about 5), and once there, an ionized basic drug cannot escape from these organelles and will accumulate extensively (e.g. chloroquine) (Ishizaki et al., 1998). Unionized and lipophilic compounds may favor distribution into the adipose tissue that has a high capacity for binding these types of drugs.

In short, the rate and the extent of drug distribution are influenced by several factors linked 1) to the body, such as blood flow, vascular leakiness, pH, cellular and tissue barriers, and tissue composition and size; 2) to the drug, for example, its physicochemical properties (defining permeability, tissue partitioning) and binding to specific sites (e.g. transporters, other proteins). Birkkett has defined the extent of drug distribution as the ratio of the drug binding to plasma protein and tissue components (Birkett, 2010).

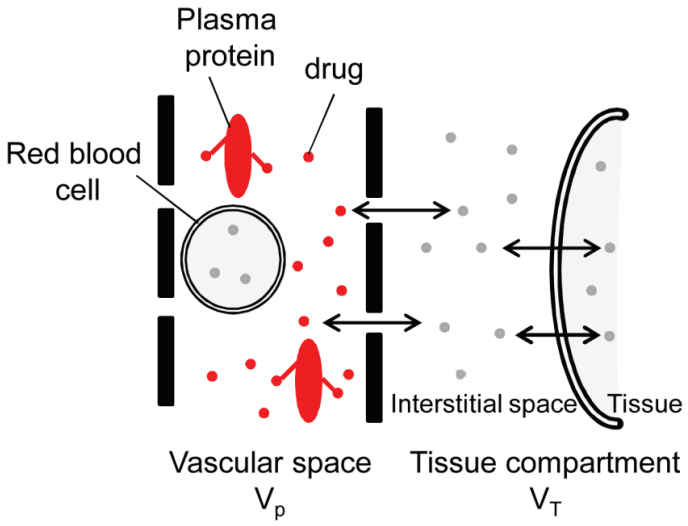

Figure 2 *Schematic description of drug distribution from the vascular space to extravascular space (interstitial space and tissue). Only the free, not the bound, drug can permeate to tissues or blood cells.*

2.2 Pharmacokinetic parameters describing distribution

Pharmacokinetic parameters make it possible to describe the ADME processes in a quantitative manner. There are two independent pharmacokinetic parameters for distribution and elimination i.e. volume of distribution (V_d) and clearance (CL), respectively.

The V_d (units of volume, e.g., L) is defined as

(1) $$V_d = A/C$$

where A is the amount of drug in the body and C is the drug concentration in plasma at any given time. Therefore, V_d is a hypothetical volume that increases with drug binding to the tissues (i.e. A/C increases); it is not an anatomically defined volume. As tissue binding of drugs varies substantially, their volumes of distribution display a wide range of values. For example, erythropoietin is confined to the vascular space and has V_d of 4 L (equal to the volume of the vascular space) (Lim, 1991), whereas hydroxychloroquine (V_d = 49 000 L) extensively accumulates within the cells of many tissues (Tett et al., 1988). The V_d of hydroxychloroquine (700 L/kg) means that only 0.006 % of the drug in the body is present in plasma.

There are different types of V_d values depending on the timing and situation for A/C ratio determination (Toutain and Bousquet-Melou, 2004).

Initial volume of distribution or volume of the central compartment (V_1 or V_c) is the volume of distribution that is determined at the time of intravenous (i.v.) administration (time 0) (Eq. 2):

(2) $$V_1 = D_{iv}/C_0$$

where D_{iv} is the i.v. dose and C_0 is the extrapolated initial concentration of drug (at t=0).

Steady state volume of distribution (V_{ss}) is measured after i.v. infusion at a steady state situation. In that case, the drug has reached an equilibrium distribution between the central compartment (including plasma and tissues where the drug easily distributes) and peripheral compartment(s) (where the drug distributes from plasma with some delay). Therefore, the concentration in plasma is constant, because drug infusion and elimination take place at equal rates.

Terminal volume of distribution (V_z, V_β or V_{area}) is the volume of distribution measured after i.v. injection during the elimination phase. In this case, pseudo-equilibrium prevails between the central and peripheral compartments. The drug concentration in plasma is decreasing due to its elimination and now the drug is diffusing back from the tissues into plasma. Unlike V_{ss}, however, the value of V_z may vary if the elimination rate changes (Toutain and Bousquet-Melou, 2004, Fan and de Lannoy, 2014).

V_z and V_{ss} have often different values for the same drug. The V_z value is always larger than V_{ss}, because the A/C ratio is higher during the terminal elimination phase than at steady state. During the terminal elimination phase, the drug is being eliminated from the central compartment, and drug will be diffusing from the tissues to the central compartment with some delay, leading to elevated A/C values. V_{ss} represents the true equilibrium between the tissues and plasma and therefore, V_{ss} is the best choice if one wishes to correlate the chemical structure with the volume of distribution.

V_{ss} can be compared with the anatomical tissue volumes (Eq. 3).

(3) $$V_{ss} = V_{plasma} + V_{T_1} \times K_{p,T_1} + V_{T_2} \times K_{p,T_2} + V_{T_3} \times K_{p,T_3} \ldots$$

where V_{plasma} is the volume of plasma, V_T describes the anatomical volumes of the tissues and $K_{p,T}$ are the distribution coefficients between the tissues and plasma:

(4) $$K_p = C_T/C$$

where C_T is the concentration in tissue and C is the concentration in plasma including unbound (C_u) and protein-bound drug (C_{bound}). Likewise, C_T includes the unbound (C_{uT}) and bound drug (C_{boundT}) in the tissue. The free fraction of drug in plasma (f_u) is described as:

(5) $$f_u = C_u/C$$

and the unbound fraction of drug (f_{uT}) in tissues as

(6) $$f_{uT} = C_{uT}/C_T$$

Since C_u and C_{uT} are in equilibrium, K_p can be expressed as:

(7) $$K_p = f_u/f_{uT}$$

Thus, V_{ss} can also be expressed as:

(8) $$V_{ss} = V_{plasma} + V_{T_1} \times \left(\frac{f_u}{f_{uT_1}}\right) + V_{T_2} \times \left(\frac{f_u}{f_{uT_2}}\right) + V_{T_3} \times \left(\frac{f_u}{f_{uT_3}}\right) \ldots$$

Thus, V_{ss} depends on the anatomical tissue volumes and the relative extent of drug binding in the plasma and tissues. The equilibrium between tissue and plasma is expressed as f_u/f_{uT}. Therefore, extensive binding in the tissues, as compared to plasma, leads to smaller values of f_{uT} than f_u and high values of V_{ss}. The equilibrium is schematically presented in Figure 3.

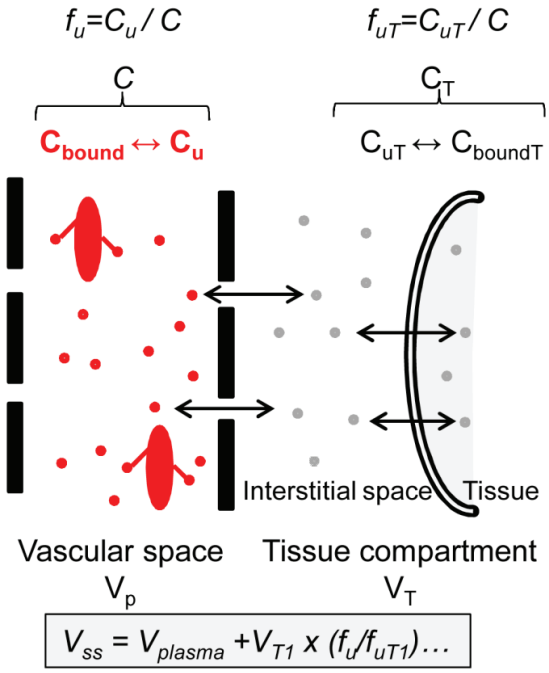

Figure 3 *Drug distribution between the vascular space and extravascular space. At equilibrium, C_u and C_{uT} are equal, and binding in tissue and plasma define the f_u/f_{uT} and V_{ss}.*

2.3 Pharmacokinetics in drug discovery and development

The drug discovery and development process usually last between 12 to 15 years and significant (about 90%) attrition takes place even in the costly clinical phases of drug development (Kola, 2008). It has been recommended that ADME parameters and pharmacokinetic profiles of lead compounds, drug candidates and investigational new drugs should be investigated at various stages of the development process (Zhang et al., 2012a). These investigations can involve *in silico, in vitro* and *in vivo* studies in animals and humans. Both computational and experimental studies are used to predict the pharmacokinetics in humans and to help in the selection of the best compound, optimal routes of administration and potential ways of delivery (Figure 4). In the clinical phase, the pharmacokinetics of the drug candidate will be investigated in healthy volunteers and patients (Figure 4). One important aim of the preclinical investigations is that they involve methods that enable reliable translation to the clinical phases to minimize the costly late stage attrition.

ADME features can be investigated in drug discovery using predictive computational and *in vitro* models (for drug metabolism, lipophilicity, permeation) to help to choose and reject compounds during the early preclinical phases before proof of concept (Caldwell et al., 2009, Zhang et al., 2012a, Maltarollo et al., 2015). The number of compounds being screened at these stages may be enormous but the quantities of compounds available for experiments can be tiny. Therefore, rapid screening methods need to be able to operate either without the drug at all or with only miniscule amounts. *In silico* models can be advantageous in helping to predict volume of distribution and f_u (Balakin et al., 2005, Ekins et al., 2007).

Later, *in vivo* pharmacokinetic studies are conducted in animals (mice, rats, and dogs or monkeys) and the experimental data are used to predict pharmacokinetics in human by applying allometric scaling and physiologically based pharmacokinetic modelling (PBPK) (Zou et al., 2012, Fagerholm, 2007, Sui et al., 2008).

Allometric scaling assumes that pharmacokinetic differences across the species are determined by body size alone. A power function of body weight (Eq. 9) is used for the predictions:

$$Y = a \times BW^{b} \tag{9}$$

where Y is the predicted parameter (for example V_{ss}), BW is the body weight, and a and b are empirically derived constants (Mahmood, 2007, Fan and de Lannoy, 2014). The constant a is a drug-dependent variable whereas b depends on its pharmacokinetic parameters. Allometric scaling predicts only values of the parameters, not concentration profiles. The method is more applicable for V_{ss} prediction than clearance, because there are extensive species differences in drug elimination (e.g. differences in the metabolism).

PBPK represents pharmacokinetics in a physiological context. This method is based on mechanistic equations taking into account the anatomy and physiology of the body. The tissues and organs are represented by different compartments and physiological data such as blood flow, organ size, tissue/blood partition coefficients and clearance in each tissue (Jones et al., 2015, Sy et al., 2014). The concept of physiologically based pharmacokinetic

modelling was introduced by Teorell already in 1937 (Teorell, 1937a, Teorell, 1937b), but this approach has gained significant popularity only after the methods for the prediction and measurement of individual parameters became feasible. *In silico* and *in vitro* parameters are used in building the PBPK model, where they are placed in the physiological and pharmacokinetic context. The model can be tested in animals and then scaled up to humans. The model requires considerable amounts of both *in vitro* and *in vivo* background data, but the ready-made model can be used to predict concentration profiles in plasma and tissues (Jones et al., 2015, Sy et al., 2014, Shardlow et al., 2013). In the V_{ss} prediction, PBPK models based on tissue composition have been applied with *in vitro* data as the input values (Poulin and Theil, 2002, Rodgers and Rowland, 2007). Usually the prediction is carried out during drug development when *in vivo* pharmacokinetic data are available in order to confirm the lack/presence of transporter involvement in drug distribution.

During clinical development, pharmacokinetic studies in humans are conducted first in healthy volunteer subjects (Phase I) in safety tests, then in selected volunteer patients (Phase II) in efficacy tests and finally in patient groups (Phase III) for new drug application approval. The Phase III is the most expensive stage in drug development. In the late stage, in Phase IV, population pharmacokinetics are carried out to determine the possible need for special dosing advice based on age, body weight, co-administered drugs, ethnic background or disease state of patients (Shardlow et al., 2013, Schmidt and Derendorf, 2014).

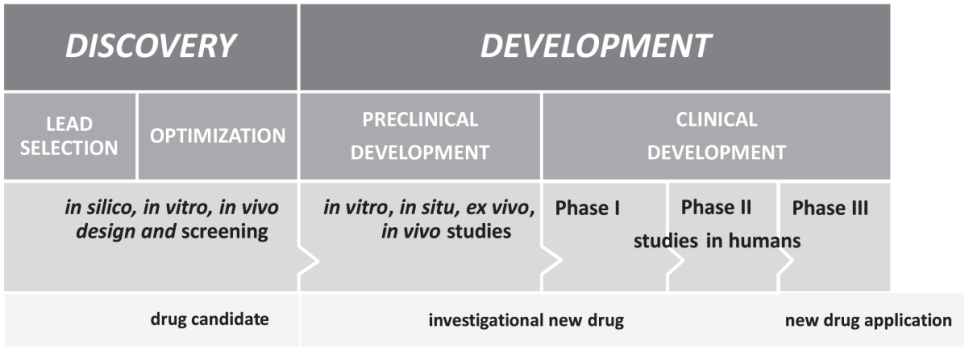

Figure 4 *Scheme of the drug discovery and development process.*

2.4 Quantitative Structure-Property Relationships

Quantitative Structure-Property Relationship methods can be used to correlate pharmacokinetic properties with the chemical structure of the compounds, in this case the abbreviation QSPkR is also used (Quantitative Structure-Pharmacokinetic Relationships) (Mayer and Van de Waterbeemd, 1985). The method uses information from prior experimental ADME data and investigates the relationship between the computational molecular descriptors of the compounds and their measured ADME parameters (Mager, 2006, Maltarollo et al., 2015). With QSPR, it is possible to relate, identify and quantify the structural descriptors that exert an effect on the pharmacokinetic parameter (Eq. 10):

(10) Pharmacokinetic property = f(structural descriptors)

As shown in Eq. 10, the molecular descriptors constitute the X matrix to be correlated to the Y response i.e. the pharmacokinetic property. The molecular descriptors are calculated *in silico* and they range in complexity from one-dimensional, to two- and three-dimensional descriptors (Mager, 2006, Ekins et al., 2007, Leach and Gillet, 2007). The values of the pharmacokinetic property e.g. pharmacokinetic parameters of drugs, are acquired from previous pharmacokinetic studies. After the QSPR model has been built, it can be used for prediction without any additional experiments. Therefore, the approach maximizes the information which can be gained from the experimental data and it can be utilized very early in drug discovery. Valid QSPR models may reduce the use of animals in the preclinical experimental studies. Moreover, QSPR models can be combined with other computational models, such as PBPK (Xu and Mager, 2011).

The relationship between descriptors and a particular pharmacokinetic parameter can be investigated by applying multivariate statistical tools, such as Principal Component Analysis (PCA) and Partial Least Squares (or Projection to Latent Structures, PLS) regression (Eriksson et al., 2006a, Wold et al., 2001a). They are linear statistical methods based on the projection of the descriptor values (and response) into new vectors (principal components or latent variables), which summarize most of the variation of the variables (Eriksson et al., 2006a, Eriksson et al., 2006b). The PCA method can be illustrated by the following analogy: a searchlight is shone on the compounds floating in the descriptor space and the optimal direction is searched in order to obtain the maximum variation of the data in the projected shadow (Figure 5). The projection is graphically represented by the score plot where the axes represent the two latent variables capturing the most relevant information (Eriksson et al., 2006a). PLS adopts a similar approach but the latent variables strive to describe the projection of the variable space X that correlates best with Y (Eriksson et al., 2006a, Wold et al., 2001a, Wold et al., 2001b). The PLS method has the advantage that it allows many responses to be incorporated into one regression model. One should keep in mind that the compounds included in the QSPR should be sufficiently disparate to cause some difference in the response and yet not too heterogeneous that the modelling would be non-viable. The response should also display enough variance in order to be modelled.

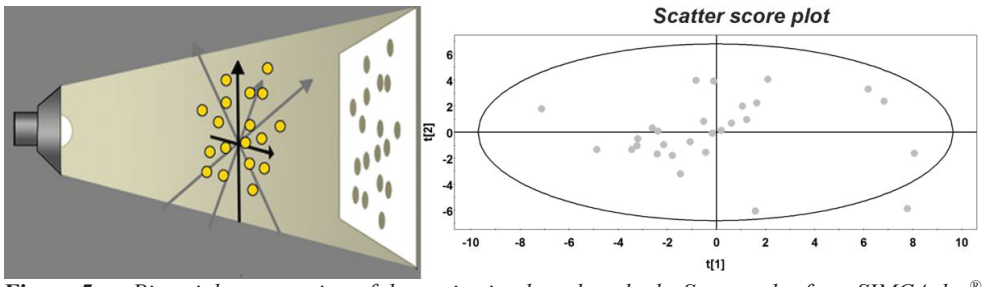

Figure 5 *Pictorial presentation of the projection based methods. Scatter plot from SIMCAplus® summarizes graphically most of the variation in the original data. (http://www.umetrics.com/how-it-works/mva)*

Validation of the model should be conducted by determining the cross-validation value (Q^2), internal, external validations values (Q_i^2, Q_e^2) and performing the Y-randomization test (Eriksson et al., 2003). Q^2 is the parameter that describes the goodness of prediction of the model. Part of the training data are left out and subsequently these are predicted based on a model trained by the remaining data. The goodness of fit (measured by the coefficient of determination, R^2) is calculated for all the parallel models and re-expressed as the cross-validation value Q^2 (the "cross-validated R^{2}"). Q^2 can be calculated leaving out only one compound, which is not such reliable tool (Doweyko, 2008). In the present thesis, one seventh of the data was left out and seven parallel models were generated, Q^2 (leave-1/7-out) (Eriksson et al., 2006a). Q_i^2 and Q_e^2 correspond to R^2 of the regression line of real versus predicted values in the test sets (internal and external respectively). The Y-randomization test involves permuting the response data, e.g. V_{ss} values, to appear in a different order. The models fitted to the shuffled values are expected to display a significantly lower accuracy than the original model, proving the robustness of the original model i.e. that it is not based on chance correlations (Topliss and Edwards, 1979, Eriksson et al., 2003). Moreover, the applicability domain of the model should be investigated to determine the size of the chemical space in which the predictions are applicable (Eriksson et al., 2003, He and Jurs, 2005, Tropsha et al., 2003).

QSPR models can be also classification models that relate the set of descriptor variables to a categorical value of the pharmacokinetic variable and can be developed using non-linear methods such as k-nearest neighbors, artificial neural network, support vector machines or recursive partitioning classification. The Recursive Partitioning classification is a decision tree tool that has been claimed to perform well when modelling complex property. The metrics used for assessing the success of classification model is sensitivity, specificity and the area under curve in receiver operator curve analysis.

2.4.1 Impact of chemical structure on drug distribution and fraction of unbound drug in plasma

The first QSPR model for V_d with purely *in silico* descriptors was built by Hirono and co-workers in 1994 (Hirono et al., 1994) using the Fuzzy Adaptive Least-Squares technique. They modelled V_d using LogP and molecular weight descriptors, but this model failed. V_d is a very complex parameter that depends on drug passage through many cellular and tissue barriers, plasma protein binding, and affinity to the components in the tissues (Rowland and Tozer, 2011, Rodgers and Rowland, 2007, Toutain and Bousquet-Melou, 2004). These factors cannot be described with only a few molecular descriptors. For this reason, the use of too few descriptors can hamper V_d QSPR modelling. Another reason why the modelling may not succeed can be attributed to the inadequate pharmacokinetic *in vivo* data which have been used in building the model. Pharmacokinetic studies should be based on intravenous (not per oral) drug administration to healthy subjects. In this case, the drug dose in the blood circulation at the time of administration is known. Moreover, V_d must be V_{ss}, not V_{area} or $V_{z,}$ because V_{ss} describes the distribution at true equilibrium. The aforementioned reasons are relevant for determining the quality of the input values in model

building. Additionally, it is preferable that the model is not based on a narrow range of molecular structures because that may lead to its limited applicability. This has been the case for some models of V_d and f_u that have been based on small data sets (less than 70 compounds) (Hirono et al., 1994, Karalis et al., 2003, Ghafourian et al., 2004, Ng et al., 2004, Turner et al., 2004, Paul et al., 2010, Li et al., 2011). Such data sets are only suitable for modelling a specific chemical space. Another important point is that the model should be validated in a systematic way (including internal and external validation, and Y-response permutation). The model should be open, transparent and interpretable so that it can be used and understood by other investigators working in this field. In 2008, Obach and co-workers published a curated data set of V_{ss} from intravenous pharmacokinetic studies in healthy subjects (Obach et al., 2008). Subsequently, a few QSPR models of V_{ss} have been published (Berellini et al., 2009, Gombar and Hall, 2013). Tables 1 and 2, present in chronological order the *in silico* QSPR models for V_d and f_u, respectively.

In some of the V_{ss} prediction models, f_u was used as a descriptor (Karalis et al., 2003) or as a hybrid parameter (V_d/ f_u) (Ghafourian et al., 2004). However, no one has used V_{ss} and f_u as responses in the same model for simultaneous prediction. This might well prove to be a valid approach, bearing in mind that the type of binding to tissues (relevant to V_{ss} value) and to protein (affecting the f_u value) may not always be identical (e.g. unspecific tissue binding and relatively specific protein binding). This difference may affect the model. The incorporation of both f_u and V_{ss} as endpoints within the same model is feasible if one utilizes the PLS technique.

Table 1. *Published QSPR models for V_d. Reliable models are those based on V_{ss} from i.v. studies and accurately validated (described in section 2. 4). It is recommended that the applicability domain of the model should be assessed. The initial descriptors correspond only to 2-D unless otherwise specified, f_b: fraction of drug bound to plasma proteins. **ANN**: Artificial Neural Networks; **BNN**: Bayesian Neural Networks; **CART**: Classification and Regression Trees; **FALS**: Fuzzy Adaptive Least Square; **GA**: Genetic Algorithm; **k-NN**: k-Nearest-Neighbor; **MDA**: Mixture Discriminant Analysis; **MLR**: Multiple Linear Regression; **RF**: Random Forest; **SM**: Sammon Maps; **SOM**: Self Organizing Maps; **SR**: Stepwise Regression; **SVM**: Super Vector Machine; **SVR**: Support Vector Regression. The use of a combination of multivariate analysis techniques is indicated by a hyphen.*

References	Data set[a]	Y		X	Multivariate analysis technique	Validation	Relevant descriptors & applicability domain
		V_d type[b]	Route	Initial descriptors			
Hirono et al. 1994	64 non-aromatic (A); 174 aromatic (B); 135 heteroaromatic (C) drugs	V_{ss} & V_{area}	i.v. & oral	MW, LogP, number of specific atoms & functional groups	FALS	Q^2 (leave-one-out)	10 descriptors (A); 22 (B); 21 (C)
Karalis et al. 2002	272 non-congeneric drugs	V_d	-	Variety of physicochemical & molecular descriptors	PCA-PLS	Q^2 (leave-1/7-out)	no predicted model
Karalis et al. 2003[c]	23 cephalosporines	V_d	-	Variety of physicochemical, molecular descriptors & f_b	PCA-PLS	Q^2 (leave-1/7-out) Internal test set (5 drugs)	f_b, LogP & Van der Waals molecular volume
Ng et al. 2004	38 antimicrobial agents	V_{ss}	i.v.	181 including 3-D descriptors	k-NN & PLS	Q^2 (leave-one-out) External test set (6 drugs)	8 descriptors related to molecular surface area, connectivity index, partial charge, LogP (k-NN); 121 descriptors but low predictability (PLS).
Turner et al. 2004	56 non-congeneric compounds	V_{ss}	i.v.	85 hydrophobic, steric & electronic descriptors	ANN	Internal test set External test set (6 drugs each)	4 descriptors related to lipophilicity, connectivity index quotients & atom/functional group
Ghafourian et al. 2004	70 non-congeneric compounds (A+B); 27 acidic (A); 43 basics (B) compounds	$LogV_d$	-	75 descriptors including 3-D descriptors	SR	Internal test set (50% of the drugs)	LogP, $LogD_1$, dipole moment (A+B); lowest atomic charge, MW/volume, $LogD_{7.4}$ (A); $LogD_{7.4}$, Log(fraction $unionized_{7.4}$/pKa), dipole moment (B)
Balakin et al. 2005	253 compounds	V_d	-	>1000 electronic, topological, spatial, structural, thermodynamic descriptors	PCA-SM-SVM-SOM	Q^2 (leave-1/10-out) External test set (12 & 22 drugs)	-
Ghafourian et al. 2006	119 non-congeneric compounds (A+B); 69 acidic (A); 55 basics (B) drugs	$LogV_d$	-	250 including 3-D descriptors	GA-SR	Q^2 (leave-1/4-out)	7 descriptors related to fraction ionized, lipophilicity, electrotopological state, electrostatic potential (A+B); no predicted model (A) nor (B)

Lombardo et al. 2006	384 compounds	V_{ss} & V_{area}	i.v.	1149 including 3-D descriptors	MLR-MDA-RF	Q^2 (leave-1/10-out & leave-class-out) External test set (23 drugs)	31 descriptors describing lipophilicity, ionization, molecular volume, & various molecular fragments.
Gleeson et al. 2006	199 drugs	$LogV_{ss}$	-	123 including 3-D descriptors	PLS; BNN & CART	Q^2 (leave-1/7-out) Internal test set (50 drugs)	23 descriptors (PLS); 30 (BNN); 14 (CART) & its combination, related to lipophilicity, MW, charge state or charge distribution.
Berellini et al. 2009	669 compounds	$LogV_{ss}$	i.v.	312 including 3-D descriptors	RF & PLS	Q^2 (leave-class-out) External test set (29 drugs) Y-response permutation	280 descriptors (RF); 95 or 11 or 95+11 (PLS), related to lipophilicity profile & charge state
Paul et al. 2009	24 quinolone drugs	$LogV_d$	oral	>1500 including 3-D descriptors	MLR	Q^2 (leave-one-out)	Topological & geometrical features related to diffusional interactions
Fatemi et al. 2011	116 non-congeneric compounds	$LogV_d$	-	including 3-D descriptors	SR-ANN or -MLR	Q^2 (leave-five-out) Internal test set External test set (13 drugs each) Y-response permutation	7 descriptors that encode different electronic, steric & lipophilic features (for both MLR & ANN)
Demir-Kavuk et al. 2011 *DemSquare® software*	584 compounds	V_{ss}	i.v.	2 sets including 3-D descriptors: 3642 commercial & 3843 free descriptors	-	Q^2 (leave-1/10-out) Internal test set (246 drugs) External test set (29 drugs) Y-response permutation	Different descriptors depending on the type of validation
Zhivkova et al. 2012	132 acidic non-congeneric drugs	$LogV_{ss}$	i.v.	178 including 3-D descriptors	GA-SR	Q^2 (leave-one-out & leave-1/5-out) External test set (10 drugs)	8 descriptors related to connectivity, electrotopological state indices & atom type numbers.
Gombar et al. 2013	569 compounds	$LogV_{ss}$	i.v.	77 fingerprints (SVR); 365 electrotopological states of two-atom fragments (MLR)	SVR & MLR	Q^2 (leave-1/2.5-out) External test sets (22 & 9 compounds)	-CATS, -ECC3, -CLOGP fingerprint (SVR); 86 electrotopological states descriptors (MLR) & applicability domain defined
Volsurf+® software	> 600 compounds	$LogV_d$	-	*Volsurf+®* descriptors, including 3-D	PCA-PLS	-	-

a: training set & internal test set if selected.

b: V_d term is used when the volume of distribution is apparent or not specified.

c: the only QSPR model included in the table that is not based on solely *in silico* descriptors.

Table 2. *Published QSPR models for f_u. Reliable models are based on V_{ss} from i.v. studies and accurately validated (described in section 2. 4). It is recommended that the applicability domain of the model should be assessed. The initial descriptors correspond only to 2-D unless otherwise specified;* ***PBP****: Protein binding percentage;* ***f_b****: fraction bound to plasma protein;* ***CG****: Conjugate Gradient;* ***HQSAR****: Hologram Quantitative Structure-Activity Relationships;* ***NLR****: Nonlinear Regression. The use of a combination of multivariate techniques is indicated by a hyphen.*

References	Data set[a]	Y	X	Multivariate analysis technique	Validation	Relevant descriptors & applicability domain
		f_u	Initial descriptors			
Saiakhov et al. 2000 *Multiple computer-automated structure evaluation program*	154 compounds	PBP	Graph indices, molecular orbital energies, LogP, solubility & pharmacophores	-	Q^2 (leave-1/10-out)	8 pharmacophores
Yamazaki et al. 2004	159 acidic & zwitterionic drugs (A); 143 basic, neutral & zwitterionic drugs (B)	PBP	LogP, LogD at pH 1,2,…14	NLR	External test set: 15 (A) & 8 (B) drugs	LogP (A); $LogD_{7.4}$ (B)
Turner et al. 2004	56 non-congeneric compounds	f_b	85 hydrophobic, steric & electronic descriptors	ANN	Internal test set (6 drugs) External test set (6 drugs)	5 descriptors related to lipophilicity, atom/functional group & ramification: low predictability for low protein binding
Balakin et al. 2005	549 compounds	PBP	>1000 electronic, topological, spatial, structural, thermodynamic descriptors	PCA-SM-SVM-SOM	Q^2 (leave-1/10-out) External test set (22 & 23 drugs)	-
Votano et al. 2006	808 compounds	PBP	628 topological structure descriptors & LogP	MLR; ANN; kNN & SVM	Q^2 (leave-one-out or leave-1/10-out) External test set (200 compounds)	The top 20 descriptors were atom-type E-state & bond-type indices type & LogP (better predictions with ANN & kNN)
Wang et al. 2006	404 drugs	PBP	941 structural fragments & molecular descriptors including LogP	GA	Q^2 (leave-1/10-out)	47 structural fragments
Gleeson et al. 2007	686 in-house compounds (A) & 245 drugs (B)	$Log((1-f_u)/f_u)$	~ 40 physicochemical descriptors	PLS	Q^2 (leave-1/7-out) External test set: 211 drugs (A) & 82 drugs (B) Y-response permutation	17 descriptors related to lipophilicity, size & charge type/extent of ionization (A), low predictability (B)
Moda et al. 2007	250 compounds	PBP	structural fragments	HQSAR-PLS	Q^2 (leave-one-out) External test set (62 compounds)	fragment distinction related to atoms, bonds, connections & chirality
Ma et al. 2008	692	PBP	951 including 3-D descriptors	GA-CG-SVM	Q^2 (leave-1/5-out) External test set (161 drugs)	29 among them atom-centred fragments, constitutional, topological descriptors
Li et al. 2011	49 antibiotics	$(1-f_b)/f_b$	135 including 3-D descriptors	MLR	Q^2 (leave-1/5-out) External test set (61 drugs)	17 among them aromacity, polarity, hydrogen bond related groups, shape & interaction parameters. Applicability domain defined

2.6 Pharmacokinetics of intravitreal injections

2.6.1 Routes of ocular drug administration

The most common way to administer a drug to the eye is topical treatment (eye drops or ointments) onto the corneal and conjunctival surface. However, topical administration does not achieve therapeutic drug concentrations into the back of the eye (vitreous, retina, choroid) (Urtti, 2006, del Amo and Urtti, 2008). Therefore, topical drug administration is not useful in the treatment of those disorders affecting the posterior eye segment (e.g. macular degeneration, diabetic retinopathy, inherited retinal degenerations) (Zhang et al., 2012b). Other routes of drug administration include systemic delivery and periocular (sub-conjunctival, sub-Tenon or parabulbar) and intravitreal administration (Figure 6). Systemic drug administration (oral, i.v., subcutaneous) is rarely a viable option, because the blood-ocular barriers limit drug entrance to the eye. To overcome these barriers, high systemic doses would be needed and these would most likely be associated with unacceptable side-effects (Urtti, 2006). After periocular administration, drug delivery to the retina is limited by choroidal blood flow and the retinal pigment epithelium (RPE) barrier (Ranta et al., 2010, Ranta and Urtti, 2006).

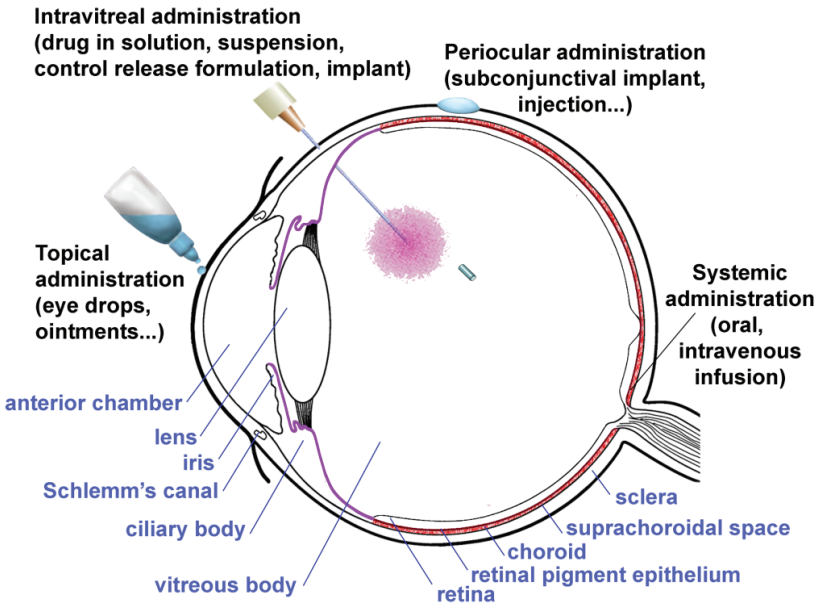

Figure 6 *Scheme of the various routes of ocular drug administration and the anatomy of the eye.*

Intravitreal administration is the most reliable way of delivering adequate drug concentrations to the posterior segment tissues (Urtti, 2006, del Amo and Urtti, 2008). Intravitreal drug delivery can be accomplished either as intravitreal injections (solutions, suspensions) or via controlled release implants (del Amo and Urtti, 2008, Sanford, 2013, Totan et al., 2015). Clinical intravitreal drugs include corticosteroids, non-steroidal anti-inflammatory agents, antibiotics, antivirals, antineoplastics, monoclonal antibodies and soluble receptor (Zhang et al., 2012b, Peyman et al., 2009, Sarao et al., 2014).

In addition to the aforementioned routes of ocular drug delivery in the clinics, there are experimental but rarely used routes of drug administration to the posterior segment. These include suprachoroidal delivery (between the sclera and choroid), intra-scleral delivery, and sub-retinal injections (between the neural retina and RPE). These routes of administration have not gained wider acceptance due to the associated risks and their unexplored pharmacokinetic features, but their clinical applicability may expand in the future with the development of novel drug delivery systems.

2.6.2 Intravitreal pharmacokinetics

The number of intravitreal injections has increased exponentially during the last decade. Earlier, intravitreal injections were used only for rare illnesses e.g. endophthalmitis, viral retinitis, but the situation changed after the introduction of new anti-angiogenic drugs for the treatment of age-related macular degeneration (AMD). Additionally, new generations of ophthalmic drugs for the treatment of AMD, diabetic retinopathy, glaucomatous retinal changes and inherited retinal degenerations are being investigated (Zhang et al., 2012b). These developments may increase further the number of intravitreal injections, since these illnesses are chronic and prevalent. For example, the majority of AMD patients are subjected to an intensive follow-up and injection regime at six weekly intervals (DaCosta et al., 2014, Severn and Hamilton, 2015). This constitutes a burden to the health care system and the patients since these injections are invasive and potentially risky (DaCosta et al., 2014, Dossarps et al., 2015). Therefore, it would be best if the dosing intervals could be as long as possible. In the case of viral and bacterial intraocular infections, shorter treatment periods may be adequate, but the drugs may need to be dosed more frequently (Peyman et al., 2009). It has been speculated that improved drug delivery systems would benefit intravitreal treatment by prolonging the drug residence in the eye for up to several months, thus decreasing the number of injections significantly (del Amo and Urtti, 2008, Sanford, 2013, Totan et al., 2015). For example, the biodegradable Ozurdex implant delivers dexamethasone for six months after its intravitreal administration (Totan et al., 2015).

After intravitreal injection, drugs diffuse throughout the vitreous, distribute into the ocular tissues (lens, iris, ciliary body, retina) and are eliminated into the systemic circulation (Maurice and Mishima, 1984, Maurice, 1976). The ocular distribution of an intravitreally administered drug depends on its permeation and binding to the tissues, while drug clearance from the vitreous is influenced by the ability of the drug to cross the blood-ocular barriers: anterior blood-aqueous barrier (BAB) and posterior blood-retinal barrier (BRB) (Maurice and Mishima, 1984, Maurice, 1976) (Figure 7B). The BAB is formed by the

posterior iris and the inner non-pigmented ciliary epithelia and the tight endothelia around the iris capillaries (Bill, 1975, Freddo, 2013). The BRB consists of the endothelia of the retinal capillaries (inner BRB) and RPE (outer BRB) (Bill, 1975, Cunha-Vaz, 1979, Cunha-Vaz et al., 2011). Intravitreally administered drugs are also eliminated via aqueous humour turnover anteriorly; aqueous humour flows through the pupil into the anterior chamber, and passes through trabecular meshwork into Schlemm's canal and then via a system of collector channels, it is deposited into the venous system (Figure 7A). The anterior clearance corresponds to drug elimination only via aqueous humour outflow (Figure 7A), and posterior clearance refers to elimination through the BAB and BRB and via aqueous humour turnover (Figure 7B). The relative importance of the anterior and posterior routes depends on several properties of the drug (Maurice and Mishima, 1984, Maurice, 1976, Meredith, 1993). Lipophilic drugs which are able to pass through blood-ocular barriers, are eliminated via posterior clearance (Maurice and Mishima, 1984, Maurice, 1976, Meredith, 1993). These kinds of drugs are mainly eliminated through the BRB into the highly vascularized choroid and systemic blood circulation that acts as a sink for the drug (Roh et al., 2006). Permeation across the BRB is the predominant route due to the large membrane surface area and extensive choroidal blood flow (4, in Figure 7B). This leads to relatively fast drug clearance from the eye (Gupta et al., 2000, Maurice, 1976, Shen et al., 2007) (Figure 7B). Large molecules (over 5 kDa) are believed to be eliminated mainly via the anterior route by aqueous humour outflow (Figure 7A), because they have low capabilities of crossing the blood-ocular barriers (Maurice and Mishima, 1984, Maurice, 1976, Meredith, 1993).

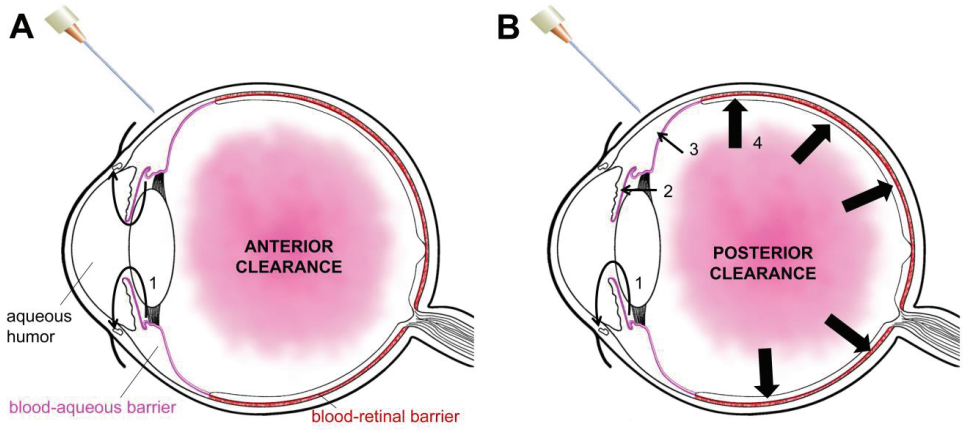

Figure 7 *Routes of drug elimination after intravitreal injection. (A) Anterior clearance of the drug via aqueous humour flow, drug permeates through the trabecular meshwork and reaches the venous system (1). (B) Drug clearance through blood-ocular barriers. The drug permeates through the posterior iris epithelium into the iris vein and is drained by the vortex veins (2), through the non-pigmented ciliary epithelium to ciliary muscles and from the ciliary plexus to the episcleral veins (3), to the retinal capillaries and through the RPE into the choroid and systemic circulation (4).*

The blood-ocular barriers can be disrupted in the diseased eye, for example RPE is compromised in AMD and posterior uveitis while the leakiness of the retinal endothelium of capillaries is increased in diabetic retinopathy and retinal vein-occlusive diseases (Zhang et al., 2012b). These types of changes in the BRB would be anticipated to impact on the intravitreal pharmacokinetics of drugs. On the other hand, there are age-related changes in the vitreous in which the gel volume decreases and the liquid volume increases and these have long been hypothesized to affect the movement of drugs in the vitreous and therefore on drug intravitreal pharmacokinetics (Laude et al., 2010). The diffusion of molecules could increase in the formed *lacunae* pockets of aged-vitreous. However, molecules encounter only a very modest diffusivity difference between vitreous-gel and vitreous-liquid; for example, only a 2.5-fold difference was observed between the diffusivity in pure water versus that in vitreous consisting of nanoparticles of 500 nm diameter (Xu et al., 2013). One would predict that for soluble small compounds and macromolecules, the difference in diffusivity would be even smaller (e.g. bevacizumab has a molecular diameter of 12 nm, other ocular drugs are smaller). This open question could be resolved by undertaking a systematical investigation of the effect of vitreous viscosity on intravitreal pharmacokinetics of small molecular weight drugs and macromolecules.

The intravitreal pharmacokinetics is defined by the primary parameters: volume of distribution ($V_{ss,\,ivt}$) and clearance (CL_{ivt}). In analogy with the systemic pharmacokinetics, $V_{ss,\,ivt}$ can be compared to the anatomical volumes of the ocular tissues:

$$(11) \qquad V_{ss,ivt} = V_{vitreous} + V_{lens} \times K_{p,lens} + V_{ciliary\ body} \times K_{p,ciliary\ body} + V_{retina} \times K_{p,retina} \cdots$$

where V values indicate the anatomical tissue volumes and $K_{p,\,T}$ are the distribution coefficients of the drug between each tissue and vitreous. High $K_{p,\,T}$ values indicate effective drug partitioning to the tissues that should lead to higher $V_{ss,\,ivt}$ values than the anatomical volumes. The minimum of $V_{ss,\,ivt}$ would be $V_{vitreous}$.

CL_{ivt} (units of volume/time, e.g., ml/h) describes the elimination of a compound irreversibly from the eye. CL_{ivt} is expressed as:

$$(12) \qquad CL_{ivt} = \frac{D_{ivt}}{AUC_{ivt}}$$

where D_{ivt} is the intravitreal dose and AUC_{ivt} is the area under the drug concentration in the vitreous curve.

Half-life ($t_{1/2}$) is useful parameter with which to determine the regimen of administration of a drug and it is easy to understand. Although it is the most frequently reported of pharmacokinetic parameters, it is often misunderstood (Toutain and Bousquet-Mélou, 2004). Moreover, $t_{1/2}$ does not make it possible to conduct any mechanistic analyses, because it is not a primary pharmacokinetic parameter, but rather is dependent on V_d and CL.

(13) $$t_{1/2} = \frac{ln2 \times V_d}{CL}$$

Intravitreal pharmacokinetic parameters have not been related to the physiological factors (e.g. tissue volumes, blood flow, and aqueous humour flow) or to the molecular descriptors of the drug in a systematic manner.

2.6.3 Intravitreal pharmacokinetic models: QSPR and pharmacokinetic simulations

The availability of good predictive QSPR models for intravitreal pharmacokinetic parameters ($V_{ss,\ ivt}$, CL_{ivt}, $t_{1/2,\ ivt}$) would benefit ocular drug discovery and development. Previously, a QSPR model for intravitreal half-life ($t_{1/2,\ ivt}$) has been generated using a multiple regression technique, but only a limited set of descriptors was investigated (molecular weight, lipophilicity, and solubility) (Durairaj et al., 2009). Moreover, the model was neither properly validated with either external test set nor evaluated for robustness (Y-permutation test).

Even though $t_{1/2,\ ivt}$ is a useful practical parameter if one wishes to estimate the required dosing frequency, the QSPR prediction of the primary parameters, $V_{ss,\ ivt}$ and CL_{ivt}, can give deeper insights on the influence of the physiological factors on intravitreal pharmacokinetics. However, no QSPR models for $V_{ss,\ ivt}$ and CL_{ivt} have been generated and these values have not been comprehensively determined. Moreover, $V_{ss,\ ivt}$ and CL_{ivt} values can be utilized in pharmacokinetic simulations to predict vitreal drug concentration profiles.

There are various software packages with graphical interfaces which can be used for pharmacokinetic simulations (e.g. *STELLA® Modelling & Simulation software, Berkeley Madonna® Modelling & Analysis of Dynamic Systems*). They are versatile tools that allow compartmental and physiologically based pharmacokinetic modelling, assuming a homogeneous distribution of the drug in each compartment. In addition, a specialized domain package such as *Comsol Multiphysics ® Modelling software* can be used for simulations based on finite element modelling where a 3D replica of the eye can be built and subdivided into thousands of voxels (Kotha and Murtomäki, 2014). Subsequently, the transfer between the voxels is described with equations for diffusion, partitioning and convective flow (Kotha and Murtomäki, 2014).

Hybrid *in silico* tools for ocular pharmacokinetics can be built by combining QSPR models with pharmacokinetic simulations and one could predict that these kinds of simulation models could be very useful in the design of drug delivery systems and drug dosing regimens.

2.6.4 Rabbit as an animal model for intravitreal pharmacokinetics

Ocular pharmacokinetics has only rarely been studied in the human eye, because there are prohibitive ethical issues associated with the invasive sampling from the human eye.

Therefore, ocular pharmacokinetics relies on animal models, and in most cases, the animals have been rabbits.

However, the rabbit has been criticized for being a poor model for intravitreal pharmacokinetics in humans. The criticism is based on the anatomical and physiological differences (Laude et al., 2010, Rowe-Rendleman et al., 2014, Bakri et al., 2007a, Bakri et al., 2007b). In comparison to the human eye, the rabbit eye has a smaller vitreal volume, a larger crystalline lens, a less vascularized retina, a smaller uveoscleral outflow, and less viscous vitreous (Bakri et al., 2007a, Bakri et al., 2007b, Vaishya et al., 2011, Rittenhouse and Pollack, 2000). Nevertheless, no systematic and quantitative analysis of the rabbit and human eye differences in intravitreal pharmacokinetics has ever been performed. Anatomical differences do not necessarily make the animal model invalid. For example, mice and rats are frequently used as animal models in preclinical pharmacokinetics, even though there are evident anatomical and physiological differences between these rodents and humans.

Therefore, there is a need to assess the translational value of the rabbit as an animal model in intravitreal pharmacokinetics.

3. Aims of the study

The overall aim of this thesis was to build predictive chemoinformatic and simulation models for the pharmacokinetics of lead compounds, drug candidates and drug delivery systems. The specific aims were:

1. To develop a QSPR model which could estimate the volume of drug distribution and fraction of unbound drug in plasma based on intravenous drug data in humans.

2. To collect and calculate pharmacokinetic parameters (volume of intravitreal distribution, intravitreal clearance and half-life) from intravitreal injection data in rabbits and humans.

3. To build QSPR models for intravitreal clearance and half-life.

4. To integrate intravitreal clearance and volume of distribution values (from the corresponding QSPR model and reference range) into pharmacokinetic simulation models to allow an estimation of vitreous concentrations of intravitreal drugs.

5. To evaluate the translational value of the rabbit model in intravitreal pharmacokinetics.

4. Overview of the methods

In the present thesis, the following steps and methods were used in assessing either the values or the *in silico* models for human V_{ss} and f_u (**I**), $V_{ss,\ ivt}$, CL_{ivt} and $t_{1/2,\ ivt}$, vitreal and aqueous concentration profiles in rabbits (**II**, **III**) and humans (**IV**):

1. Literature search and data collection of the pharmacokinetic parameters or the concentration-time profiles of drugs (**I - IV**).

2. Extraction of the intravitreal pharmacokinetic parameters from the concentration-time profile data in rabbits using curve fitting with *WinNonlin® software (version 5.3, Pharsight Inc., St. Louis, USA)*. *GetData Graph Digitizer® (version 2.24., Digital River, Inc., Cologne, Germany)* was used to obtain concentration-time numerical values when only the graphs were available (**III**). For human data, *Phoenix WinNonlin® software (version 6.3)* and *GetData Graph Digitizer®* were applied when a balanced concentration profile was available, otherwise calculations of the apparent intravitreal clearance were carried out with *Microsoft Excel® program (2003, Microsoft, Washington, USA)* (**IV**).

3. Generation of the 2-D structure of the compounds with *ACD/Dictionary incorporated in ACDlabs® software (versions 11 and 12, Advanced Chemistry Development, Inc., Toronto, Canada)* (**I - III**) or the PubMed compound database (http://www.ncbi.nlm.nih.gov/pccompound) and the 3-D structure with *Concord within SYBYL® (version 8.0, Tripos International, St. Louis, USA)* (**I**).

4. Generation of molecular descriptors from the 2-D structures using *ACDlabs® software* (**I - III**) and from 3-D structures using *Volsurf+® software* (Cruciani et al., 2000) and *MOE™, Molecular Operating Environment (Chemical Computing Group, Montreal, Canada, 2008)* (**I**).

5. QSPR modelling:

5.1. By PLS Regression and PCA using *SIMCAplus® software (version 10.5, Umetrics AB, Umeå, Sweden)* (**I, II, III**).

5.2. By Recursive Partition (RP) Classification using *Discovery Studio® software (version 3.5, Accelrys Inc., San Diego, USA)* (**I**).

6. QSPR model validation:

The QSPR regression models (in 5.1.) were validated by cross-validation, internal and external test set validation and by performing the Y-randomization test (**I - III**).

The QSPR classification (in 5.2.) was validated by calculating values for sensitivity, specificity and the area under curve in receiver operating characteristics plot metrics as well as undertaking external test set validation and utilizing the Y-randomization test (**I**).

7. Applicability domain of the model to define the chemical space in which the model is able to predict accurately (**I, II**).

8. Implementation of QSPR models into intravitreal pharmacokinetic simulation models using *STELLA® Modelling & Simulation software (version 8.1.1, isee systems, Inc., Lebanon, USA*) in order to simulate the intravitreal concentration profiles of compounds injected either as a solution or in control release systems (**III**). Rabbit and human kinetic data were further explored with the kinetic simulation model *STELLA® Modelling & Simulation software* (*version 10.3)* (**IV**).

5. First article: Applying linear and non-linear methods for parallel prediction of volume of distribution and fraction of unbound drug.

I

Eva M. del Amo, Leo Ghemtio, Henri Xhaard, Marjo Yliperttula, Arto Urtti, Heidi Kidron. Applying linear and non-linear methods for parallel prediction of volume of distribution and fraction of unbound drug. PLOS ONE 2013, 8 (10), art. no. e74758
http://dx.doi.org/10.1371%2Fjournal.pone.0074758

OPEN ACCESS Freely available online

PLOS ONE

Applying Linear and Non-Linear Methods for Parallel Prediction of Volume of Distribution and Fraction of Unbound Drug

Eva M. del Amo[1,2], Leo Ghemtio[1], Henri Xhaard[1], Marjo Yliperttula[2], Arto Urtti[1], Heidi Kidron[1]*

1 Centre for Drug Research, Faculty of Pharmacy, University of Helsinki, Helsinki, Finland, **2** Division of Biopharmaceutics and Pharmacokinetics, Faculty of Pharmacy, University of Helsinki, Helsinki, Finland

Abstract

Volume of distribution and fraction unbound are two key parameters in pharmacokinetics. The fraction unbound describes the portion of free drug in plasma that may extravasate, while volume of distribution describes the tissue access and binding of a drug. Reliable *in silico* predictions of these pharmacokinetic parameters would benefit the early stages of drug discovery, as experimental measuring is not feasible for screening purposes. We have applied linear and nonlinear multivariate approaches to predict these parameters: linear partial least square regression and non-linear recursive partitioning classification. The volume of distribution and fraction of unbound drug in plasma are predicted in parallel within the model, since the two are expected to be affected by similar physicochemical drug properties. Predictive models for both parameters were built and the performance of the linear models compared to models included in the commercial software *Volsurf*+. Our models performed better in predicting the unbound fraction (Q^2 0.54 for test set compared to 0.38 with *Volsurf*+ model), but prediction accuracy of the volume of distribution was comparable to the *Volsurf*+ model (Q^2 of 0.70 for test set compared to 0.71 with *Volsurf*+ model). The nonlinear classification models were able to identify compounds with a high or low volume of distribution (sensitivity 0.81 and 0.71, respectively, for test set), while classification of fraction unbound was less successful. The interrelationship between the volume of distribution and fraction unbound is investigated and described in terms of physicochemical descriptors. Lipophilicity and solubility descriptors were found to have a high influence on both volume of distribution and fraction unbound, but with an inverse relationship.

Citation: del Amo EM, Ghemtio L, Xhaard H, Yliperttula M, Urtti A, et al. (2013) Applying Linear and Non-Linear Methods for Parallel Prediction of Volume of Distribution and Fraction of Unbound Drug. PLoS ONE 8(10): e74758. doi:10.1371/journal.pone.0074758

Editor: Paul Taylor, University of Edinburgh, United Kingdom

Received May 20, 2013; **Accepted** August 7, 2013; **Published** October 7, 2013

Funding: This work has been supported by the Graduate School in Pharmaceutical Research, the Academy of Finland, Biocenter Finland, the Finnish Cultural Foundation, and OrionPharma Ltd. The funders had no role in study design, data collection and analysis, decision to publish, or preparation of the manuscript.

Competing Interests: This work has been supported by Orion Pharma Ltd. The funding occurred through a TEKES (Finnish funding agency for Technology and Innovation) project "IVIVRe". There is no financial or other competing interest by the authors or funders in this work, and this does not alter the authors' adherence to all the PLOS ONE policies on sharing data and materials.

* E-mail: heidi.kidron@helsinki.fi

Introduction

The extent of drug distribution determines the access of a drug to its sites of action and to other tissues, which might give rise to adverse effects. A primary parameter for drug distribution is the volume of distribution (V_d) that is defined as.

$$V_d = \frac{A}{C}$$

where A is the amount of drug in the body, and C is the drug concentration in plasma (both free drug and protein-bound drug). Volume of distribution is an apparent volume that increases with elevated drug binding in the extravascular space of the body and not an anatomically defined volume. Consequently, extensive drug binding outside the blood vessels leads to increasing values of A/C ratio. As tissue binding of drugs varies considerably, volume of distribution displays a wide range of values. For example, erythropoietin is confined to the vascular space presenting a V_d of 4 L (approximately the anatomical volume of vascular space) [1], while hydroxychloroquine with a V_d of 49 000 L strongly accumulates into the cells and tissues [2]. Volume of distribution at steady state (V_{ss}) is measured at equilibrium, therefore, it describes the molecular tissue binding more reliably than other volume of distribution parameters that are dependent on the time after measurement. V_{ss} depends on the access of the drug to the cells and tissues, its affinity to plasma proteins and tissue components, and number of binding sites in plasma and tissues.

Drug concentration in plasma (C) includes both unbound (C_u) and protein-bound drug in plasma. However, only the fraction of free drug in plasma permeates across the cellular membranes and vascular walls in most tissues. The free fraction of drug in plasma (f_u) is described by the ratio C_u/C. Likewise the drug in the tissues also includes both free (C_{uT}) or tissue bound parts. The unbound fraction of drug in tissues is: $f_{uT} = C_{uT}/C_T$, where C_T is the total drug concentration in the tissue. Drug binding to plasma proteins and tissue components influences drug partitioning between the tissues and plasma. Thus, V_{ss} can be presented using the following equation:

$$V_{ss} = V_p + V_{T_1}\left(\frac{f_u}{f_{uT_1}}\right) + V_{T_2}\left(\frac{f_u}{f_{uT_2}}\right)....$$

where V_p is the anatomical volume of plasma and V_T is the true anatomical volume of each tissue. V_{ss} depends on the anatomical volumes of the tissues, and the relative extent of drug binding in the plasma and tissues described as f_u/f_{uT} ratios.

As volume of distribution describes the extent of drug distribution, it is important to predict its value early in drug development before experimental measuring in humans. V_{ss} in humans may be extrapolated from the *in vivo* animal data that is obtained during the drug discovery process, but computational approaches are useful at early stages before animal data has been collected. The volume of distribution used for computational modeling should be collected from intravenous and not from oral pharmacokinetics studies as in some cases [3], [4]. The benefit of intravenous administration is the defined quantity of the drug that is subject to distribution, which avoids the uncertainty associated with incomplete bioavailability after extravascular administration.

Even though quantitative structure-property relationship (QSPR) has been widely used for prediction of V_{ss} [3–16], it remains a challenging problem that has not been adequately solved. The early attempts for predicting volume of distribution were based on small data sets and did not specify the type of volume of distribution that was used as the endpoint or in some cases used several types of volume of distribution for the model building [3-8], [11], [13], [14], [17]. In 2008, a major advance was the publication of a clean, manually curated dataset of V_{ss} [18] that subsequently has been used successfully to build predictive models for V_{ss} [12], [16].

The main difference in the work presented here compared to the previously published models of V_{ss} is that we have included another pharmacokinetic parameter, f_u, to the modeled responses. The f_u in plasma depends on the binding affinity and capacity of plasma proteins, which also affect the volume of distribution. The fraction of unbound drug in plasma can be estimated relatively easily *in vitro*, but computational models for predicting f_u are also available [19-21]. The *VolSurf+* software includes prediction tools for both volume of distribution and plasma protein binding, however, there is limited information of the methodology behind the models and their prediction capacity have not been evaluated in an unbiased manner in the literature. The two parameters, V_{ss} and f_u, are expected to be affected by similar physicochemical drug properties and our hypothesis was that modeling them in parallel would benefit their prediction. We have applied both linear and nonlinear multivariate approaches: linear partial least square (PLS) regression combined with principal component analysis (PCA) and non-linear recursive partitioning (RP) classification. RP has been shown to perform well when dealing with complex endpoints associated with multiple mechanisms, while PLS allows many responses (in our case V_{ss} and f_u) to be incorporated in one regression model, but to our knowledge, this approach has not been used previously in pharmacokinetic QSPR modeling.

Materials and Methods

1. Data Set

The initial dataset collated by Obach and co-workers [18] contains 670 compounds with V_{ss} and f_u values determined after intravenous administration to healthy people. The collection steps, the quality and the diversity of the data have been meticulously detailed in the publication.

The 2D structures of the compounds were obtained from the ACD/Dictionary version 11 [22] or the PubMed compound database (http://www.ncbi.nlm.nih.gov/pccompound Accessed 2010 October). If the compounds were represented as salts in the 2D structure, the counter ion was discarded. The 3D structures were generated using Concord within *SYBYL 8.0* [23]. A set of 648 drugs with both 2D and 3D structures were obtained. For the remaining 22 compounds in Obach's data set either a 2D structure or minimized 3D structure was not obtained or it was not possible to calculate descriptors from the structures. The V_{ss} of artesunate was corrected to 1.5 L/kg based on the work of White [24]. Furthermore, we excluded ibadronic, pamodronic, risedronic and zoledronic bisphosphonates from the set, since these compounds are sequestered to the bones, preventing their detection in the plasma, and leading to underestimated values of V_{ss} [25]. The antimalarial drugs hydroxychloroquine and chloroquine have V_{ss} values of 700 L/kg and 140 L/kg, respectively. These values are far beyond the range of other V_{ss} values (0.035–60 L/kg) and they were excluded to avoid biasing the model.

The final data set of 642 drugs (Figure 1) displays V_{ss} values of 0.035–60 L/kg and f_u values (541 drugs) of 0.0002–1.

2. Calculation of Molecular Descriptors

In this study, molecular descriptors were calculated using *ACDlabs* [26], *Volsurf+* [17] and *MOE* [27]. Input molecular structures were two-dimensional for *ACDlabs* and three-dimensional for *Volsurf+* and *MOE*, for the later Gasteiger-Huckel charges were added. Identical descriptors (i.e. molecular weight, molecular volume) were excluded before combining descriptor sets for modeling. The descriptors that were used for model building are listed in Table 1 and the calculated descriptor values for the data set are available in File S1.

3. PCA and PLS Regression Models

QSPR models were built using linear multivariate analysis tools PCA and PLS (Simca *plus Version 10.5*) [28]. All descriptors were transformed with unit variance scaling and mean centering before PCA and PLS analysis. Moreover, the descriptors with a broad range or unequal distribution across the range were logarithmically transformed to obtain better distributions. Three sets of molecular descriptors were assembled for the regression modeling: (1) *ACDlabs* descriptors and *MOE* logS descriptor; (2) *VolSurf+* descriptors; (3) the combination of *ACDlabs*, *MOE* and *VolSurf+* descriptors.

A workflow of the modeling process is presented in Figure 2. Before modeling, a foreign set of 101 drugs was randomly excluded from the final 642 compound set. The descriptor matrix of the remaining 541 drugs was analysed with PCA to identify the drugs that fall outside the general chemical space of the compound set and descriptors that should be excluded from the model (model calibration). Drugs that were outliers based on their distribution in the PCA plot and whose descriptor values fell outside the boundaries outlined in Table 2 were excluded. Based on the scatter plot of the final PCA plot, an external test set (Figure 3) of 101 compounds representative of the chemical space was selected. The external set comprises molecules within the chemical space of the model, while the foreign set, which was selected before the PCA and model calibration, also includes compounds outside the chemical space used for model building. The remaining compounds constitute the training set for the PLS model building (365 drugs for model 1; 357 drugs for model 2; 361 drugs for model 3). The training sets were used to build PLS models that relate the descriptors to the two simultaneously modelled responses, log V_{ss} and f_u. During initial stages of the analytical process, the number of highly correlated variables observed in the PLS weight plot was gradually reduced in order to equilibrate the influence of the overall set of descriptors on the responses. Subsequent models with improved statistic parameters were

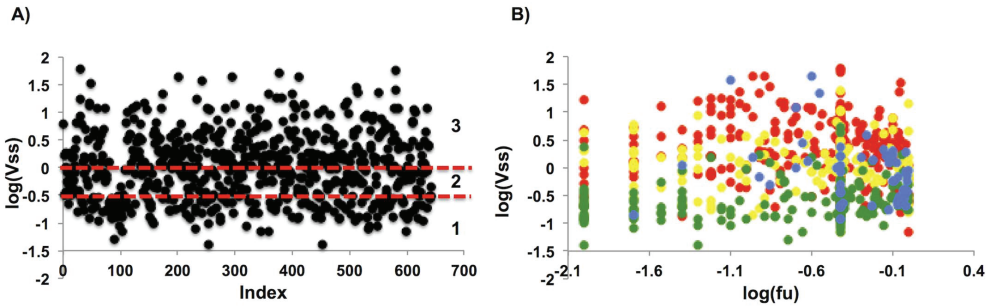

Figure 1. Distribution of compounds in the data set. (A) The distribution of logV_{ss} values in the final dataset. Lines have been draw at 0.3 L/kg and 1 L/kg to indicate the boundaries between the three classes used in the RP models. B) Distribution of compounds based on both log V_{ss} and log f_u values and coloring by compound charge (basic-red, neutral-yellow, acidic-green, zwitterionic-blue).
doi:10.1371/journal.pone.0074758.g001

obtained and variables deemed least influential to the modelled pharmacokinetic parameters were excluded. The decisions were based on the PLS weight plot and confirmed by the variable importance plot results. Moreover, the distribution of the drugs was followed up by the PLS score and Dmod plots, in order to detect outliers.

4. Recursive Partitioning Classification Models

A RP analysis was carried out using *Discovery Studio version 3.5* (Accelrys Inc.) to develop decision trees that categorize the compounds into classes that are based on the V_{ss} values or both V_{ss} and f_u values (Table 3 and 4). Volume of distribution is defined by drug interactions with the main volumes in the body: extracellular space and cellular tissue space. We used these anatomical volumes as rough guidance to classify the volumes into three classes. Class 1 represents the volume of the extracellular fluid (0–0.3 L/Kg), class 2 represents V_{ss} values that take into consideration distribution to the tissues (0.3–1 L/Kg), and class 3 values of V_{ss} represent significant binding to the cellular components (>1 L/Kg). However, it should be noted that V_{ss} is an apparent volume that does not strictly obey anatomical volumes, therefore the anatomical distribution of the compounds cannot be concluded from the V_{ss}. Distribution of compounds into the three classes is shown in Figure 1A. When both V_{ss} and f_u values were predicted, each class

Table 1. The descriptors included in modeling.

ACDlabs descriptors	*Volsurf+* descriptors						*MOE* descriptors
ALogD5	V	WO1	CW5	POL	%FU4	LgS6	logS
ALogD5.5	S	WO2	CW6	MW	%FU5	LgS6	
ALogD7	R	WO3	CW7	FLEX	%FU6	LgS7	
ALogD7.4	G	WO4	CW8	FLEX_RB	%FU7	LgS7.5	
APSA	W1	WO5	ID1	NCC	%FU8	LgS8	
HDonors	W2	WO6	ID2	DIFF	%FU9	LgS9	
HAcceptors	W3	WN1	ID3	LOGP n-Oct	%FU10	LgS10	
FRB	W4	WN2	ID4	LOGP c-Hex	DRDRDR	LgS11	
Rule Of 5	W5	WN3	CD1	PSA	DRDRAC	L0LgS	
Molar Volume	W6	WN4	CD2	HAS	DRDRDO	L1LgS	
MW	W7	WN5	CD3	PSAR	DRACAC	L2LgS	
Surface Tension	W8	WN6	CD4	PHSAR	DRACDO	L3LgS	
Polarizability	D1	IW1	CD5	LgD5	DRDODO	L4LgS	
C ratio	D2	IW2	CD6	LgD6	ACACAC	DD1	
N ratio	D3	IW3	CD7	LgD7	ACACDO	DD2	
NO ratio	D4	IW4	CD8	LgD7.5	ACDODO	DD3	
Num Rings	D5	CW1	HL1	LgD8	DODODO	DD4	
Num Ar Rings	D6	CW2	HL2	LgD9	SOLY	DD5	
	D7	CW3	A	LgD10	LgS3	DD6	
	D8	CW4	CP	AUS7.4	LgS4	DD7	
					LgS5	DD8	

doi:10.1371/journal.pone.0074758.t001

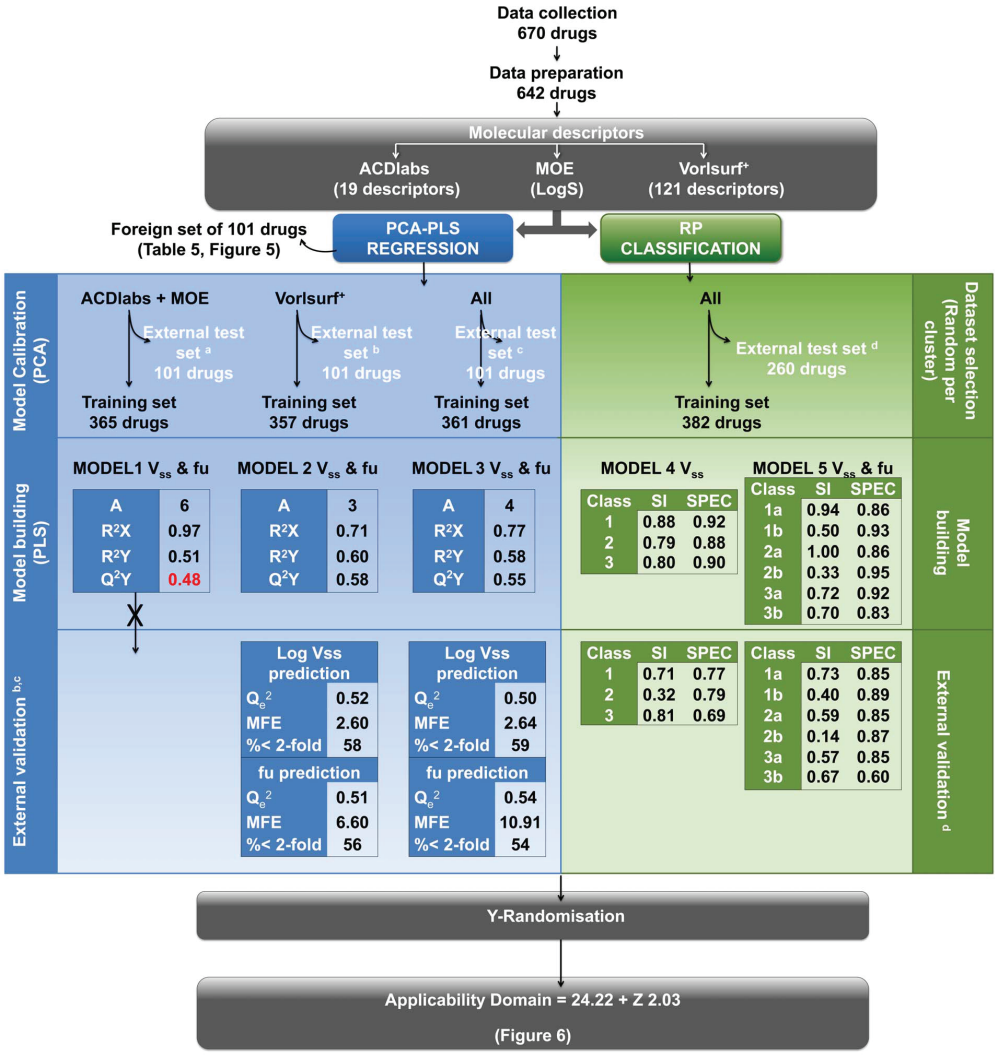

Figure 2. Flowchart of the work process to obtain regression and classification models for V_{ss} and f_u. MFE = mean fold error, SI = Sensitivity, SPEC = specificity.
doi:10.1371/journal.pone.0074758.g002

Table 2. Statistical parameters of the PCA models and the chemical boundaries chosen during the PCA modelling.

	A	R^2X	Q^2X	Criteria of model calibration
Model 1	7	0.90	0.58	MW[a]<940 PSA[b]<205 POL[c]<71 HBD[d]<10 HBA[e]<15 and -7.71<LogS[f]<0.38
Model 2	7	0.79	0.73	MW<940 WO4[g]<100 WO6<2 PSA<205 SOLY[h]<0.93 V[i]<1353 POL<71 LogS9[j]<5.3 W4[k]<483
Model 3	7	0.79	0.72	MW<940 WO4<100 PSA<205 SOLY<0.93 MV[l]<466 Rule of 5<3

[a]**MW:** molecular weight; [b]**PSA:** polar surface area; [c]**POL:** polarizability; [d]**HBD:** hydrogen bond donors; [e]**HBA**: hydrogen bond acceptors; [f]**LogS:** log of solubility; [g]**WO4 and WO6:** hydrogen bond donor volume at different energy levels; [h]**SOLY:** intrinsic solubility; [i]**V:** molecular volume; [j]**LogS9:** log of solubility at pH 9; [k]**W4:** hydrophilic volume; [l]**MV:** molar volume.
doi:10.1371/journal.pone.0074758.t002

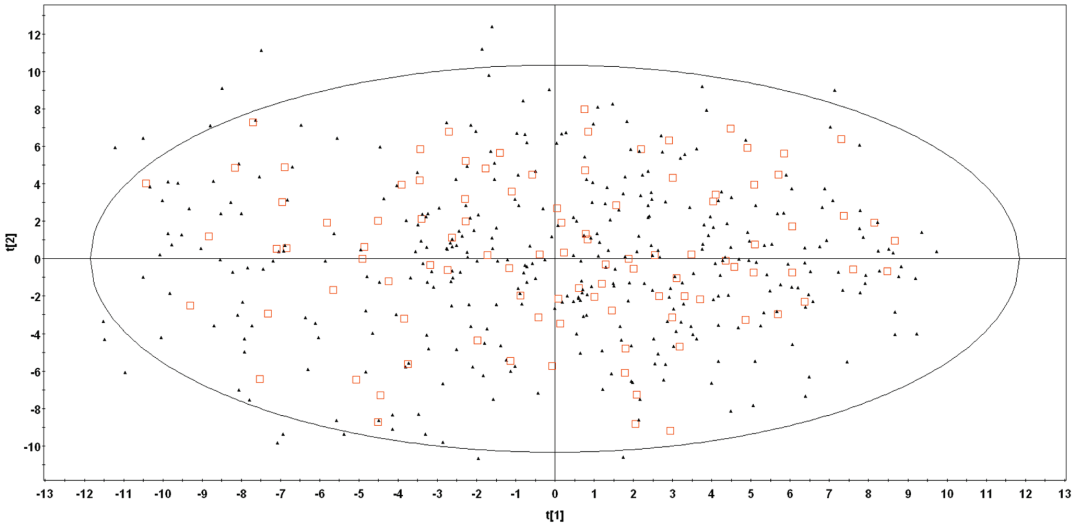

Figure 3. PCA score plot. The final PCA score plot obtained after model 3 calibration where the two principal components explain 27% and 20%, respectively, of the variance in the data set. The open squares represent the drugs in the external test set and the filled triangles the drugs in the training set. The ellipse depicts the 95% confidence region of the model (Hotelling T^2).
doi:10.1371/journal.pone.0074758.g003

was further divided into compounds with low to intermediate (<0.7) or high (>0.7) f_u. Compounds with missing f_u values were addressed by assigning them the mean value of all f_u values and distributing them equally in the training and external test set, which is a standard approach to handle missing values in RP analysis. In our study, balanced forest of RP was used, since it is the appropriate method for imbalanced data [29]. This type of RP contains a relatively small number of trees (in average 10) using a separate bootstrap sample of the original data for each tree. For each tree, the number of members in all classes is equal to the number of members in the smallest class. The number of descriptors that was used as split criterion within each tree was set to the square root of total descriptors. The weighing method was set to "uniform" and the equalize class sizes to true. All others parameters were set to default.

A training set was used to build the decision trees and an external test set was utilized to evaluate the predictive power of the models. To generate the training and external test set for RP analyses, all compounds were first clustered by similarity based on root mean square deviation and each cluster was divided into training and test sets to ensure that both sets included compounds from each cluster. The data set used to train the model consisted of 382 compounds, while 260 compounds were used as an external test set (Figure 2).

Table 3. Division of training and test set compounds into three classes according to observed V_{ss}.

	Class 1	Class 2	Class 3	Total
	V_{ss} = 0–0.3 L/kg	V_{ss} = 0.3–1 L/kg	V_{ss} >1 L/kg	
Training	105	96	181	382
Test	62	71	127	260
Total	167	167	308	642

doi:10.1371/journal.pone.0074758.t003

5. Model validation

The prediction accuracy of the PLS models was determined by internal and external validation. The internal validation is based on the cross-validation value Q^2Y (Q^2) that is calculated by leaving out 1/7 of the data, and predicting these compounds based on a model trained by the remaining data. The external validation is conducted with the external test set. The model was used to predict the log V_{ss} and f_u of the external test set. The predicted responses were plotted against the observed responses (i.e. experimental V_{ss} and f_u). The R^2 value of the regression line for the plot was considered as the Q_e^2 (goodness of prediction of the external test set).

We estimated the predictive ability of the RP classification models using out-of-bag statistics. The external test set was used to estimate the fitting ability of the model on a new dataset that was not used in the model construction. The performance of the RP models is based on three metrics: true positive rate (recall or sensitivity), specificity, and the area under the curve (AUC) of the receiver operating characteristics (ROC) plot [30]. AUC represents the probability that a classifier will be estimated correctly, with values >0.5 indicating better than random prediction and 1 signifying perfect prediction. In the case of more than two classes (multiclassification), a confusion matrix is a square of NxN, where N is the number of classes. AUC is computed as defined by Hand and Till (2001) as an average over components generated from several ROC plots for a Y property and cannot be plotted [30]. For instance, when N (A, B, C) is 3, the classifier's performance is computed per class as follows for class A:

Table 4. Division of training and test set compounds into six classes according to observed V_{ss} and f_u.

	Class 1a	Class 1b	Class 2a	Class 2b	Class 3a	Class 3b	Tota
	V_{ss} =0–0.3 L/kg & f_u >0.7	V_{ss} =0–0.3 L/kg & f_u <0.7	V_{ss} =0.3–1 L/kg & f_u >0.7	V_{ss} =0.3–1 L/kg & f_u <0.7	V_{ss} >=1 L/kg & f_u >0.7	V_{ss} >=1 L/kg & f_u <0.7	l
Training	18	87	22	68	38	149	382
Test	11	51	17	51	21	109	260
Total	29	138	39	119	59	258	642

doi:10.1371/journal.pone.0074758.t004

Actual/predicted	*ClassA*	*ClassB*	*ClassC*
ClassA	T_A	F_{B1}	F_{C1}
ClassB	F_{A2}	T_B	F_{C2}
ClassC	F_{A3}	F_{B3}	T_C

$$Sensitvity = \frac{T_A}{T_A + F_{B1} + F_{C1}}$$

$$Specificity = \frac{T_B + T_C}{T_B + F_{A2} + T_C + F_{A3}}$$

6. Y-randomization test

In addition to the internal and external validation, the Y-randomization test (response permutation test) was performed, which estimates the robustness of models [31]. The X data are left intact, whereas the Y data are permuted to appear in a different order (random shuffling). A model is then fitted to the permuted Y-data and the model statistics are computed for the derived model. It is expected that the models from randomized activities would have significantly lower accuracy values.

7. The applicability domain of models

An applicability domain (AD) of the model is needed to avoid making predictions for compounds, which differ substantially from the training set molecules. The AD is used to estimate which compounds are suitable for model predictions and avoid unjustified extrapolation of predictions. We used a method introduced by Zhang et al. (2006) for defining the AD based on the distribution of similarities between each compound and its nearest neighbours in the training sets [32]. The AD was calculated as follows:

$$AD = <d> + Z\sigma$$

The average of Euclidean distances between all points of the training set were calculated from Similarity and Clustering Canvas of Schrödinger modeling package [33], with 32 bit linear Daylight fingerprint. Data for estimation of the Euclidean distance and application of the AD on new compounds are available in Files S2-S5. Then, using the distances lower than the average, a new average distance <d> and standard deviation σ between these distances were calculated. Z is an arbitrary parameter to control the significance level and considerably affects the number of compounds within the applicability domain. Increasing Z will include compounds that are more dissimilar in the AD. We set the value of Z to 0.7 to calculate the compounds within the AD of the models in the foreign test set.

Results

1. PLS Regression Models

The linear regression model of log V_{ss} and f_u was attempted with three descriptor sets: (1) 19 descriptors from *ACDlabs* and *MOE*, (2) 121 descriptors from *VolSurf+* and (3) 140 descriptors from the combination of the two previous sets. The three sets were first analyzed with PCA. In Table 2, the final PCA model statistics for the three strategies are presented as well as the criteria of selection chosen in each case. In Figure 3, the score plot of the final PCA model of data set 3 is shown as an example. Similar plots were obtained for the other data sets.

The statistical values of the final models are present in Figure 2. Model 1 resulted in a non-predictive model, yielding a Q^2Y smaller than 0.50, and therefore the analysis of this set was not taken any further. The final models were based on 332 compounds and 9 descriptors from *Volsurf+* (model 2) and 353 compounds and 11 descriptors combined from *Volsurf+*, *ACDlabs* and *MOE* (model 3). The PLS weight plot of model 3 is presented in Figure 4, showing the relationships between the X-descriptors and Y-responses, V_{ss} and fu, at the same time. A detailed description of PLS weight interpretation is presented in the legend. The final equations for model 2 and model 3 are:

Model 2.

$$\log V_{ss} = 0.1521 - 0.1173L1LgS + 0.2858L3LgS - 0.0123SOLY + 0.0122LOGPn - Oct + 0.0463LgD9 - 0.0083WN5 - 0.0002W1 + 0.2811ID3 + 0.0026A$$

$$f_u = 0.8134 - 0.0348L1LgS + 0.1096L3LgS + 0.0733SOLY - 0.0523LOGPn - Oct - 0.0227LgD9 + 0.0005WN5 - 0.0001W1 + 0.5579ID3 - 0.0272A$$

Model 3.

$$\log V_{ss} = 0.2464 + 0.0909LgS3 - 0.0269LgS10 - 0.0099\log S + 0.3894L3LgS + 0.0465LgD10 + 0.0514ALogD5.5 + 0.0010\%FU10 + 0.0004MV - 0.0005W1 + 0.0023D4 + 0.0174HD$$

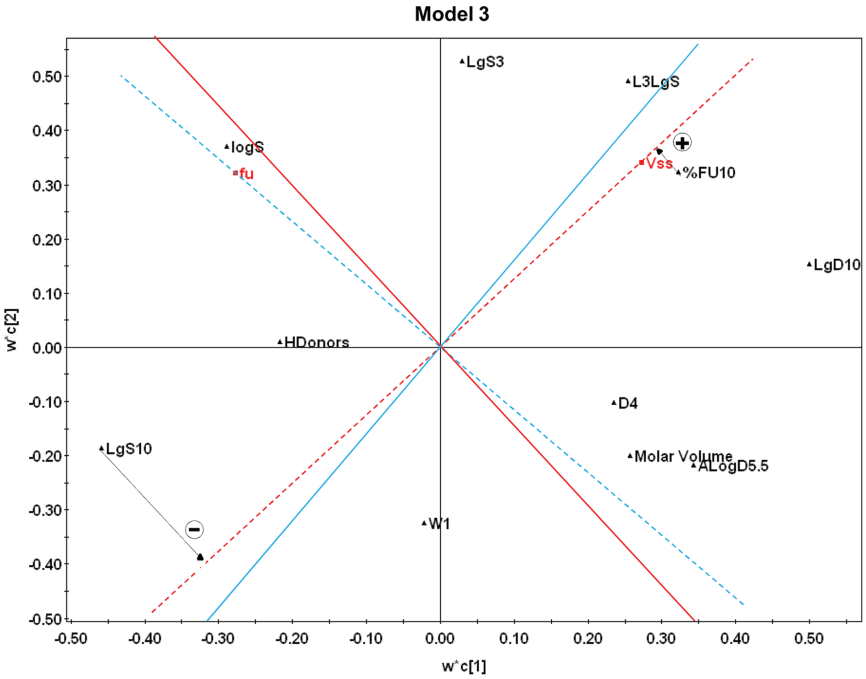

Figure 4. PLS weight plot of model 3. The plot illustrates the relationships between the eleven descriptors (in black) and V_{ss} and f_u (in red). The dashed red line crosses the origo and the V_{ss} response, and the continuous red line (perpendicular to the dashed line) represents the borderline between negative and positive influences of the descriptors. The respective lines for f_u are blue. Impact of descriptors is interpreted in the following manner: the V_{ss} descriptors that show orthogonal projection on the same side as V_{ss} (on the right from red borderline) have positive impact on V_{ss}, and the descriptors on the left side of the borderline show negative impact on V_{ss}. The farther away from the origo the projection of the descriptors lies, the stronger is the impact on the corresponding response. As an example of the variables influence on V_{ss}, two arrows have been drawn that represent the orthogonal projections of variable LgS10 (negatively correlated to V_{ss}) and %FU10 (positively correlated to V_{ss}). Likewise, the descriptors on the left side of blue borderline show positive impact on f_u, and the descriptors on the right side of the borderline have negative influence on f_u.
doi:10.1371/journal.pone.0074758.g004

$$f_u = 0.7052 + 0.0091LgS3 - 0.0024LgS10 + 0.0600\log S + 0.0277L3LgS - 0.0153LgD10 - 0.0583ALogD5.5 + 0.0009\%FU10 - 0.0007MV + 0.0001W1 - 0.0025D4 + 0.0026HD$$

Where L1LgS and L3LgS are solubility profiling coefficients, logS is the logarithm of solubility, LgS3 and LgS10 are the logarithms of solubility at pH 3 and pH 10, respectively, SOLY is intrinsic solubility, LOGP n-Oct is the partitioning coefficient in octanol/water, LgD9, LgD10 and ALogD5.5 are distribution coefficients at pH 9, pH 10 and pH 5.5, respectively, WN5 is hydrogen bond acceptor volume, W1 is hydrophilic volume, ID3 is hydrophobic integy moment, A is amphiphilic moment, %FU10 is % of fraction unionized at pH 10 (not to be confused with f_u), MV is molar volume, D4 is hydrophobic volume and HD is hydrogen bond donor.

Model 2 and model 3 were internally validated by cross-validation, gaining Q^2 values of 0.58 and 0.55, respectively. In external validation of the models we determined their accuracy in predicting log V_{ss} and f_u with the external test sets. In log V_{ss} prediction by model 2, two outliers were excluded (ribavirin and bilobalide), while in f_u prediction by model 2, four outliers (acetylcysteine, amiodarone, aripiprazole, repaglinide) were excluded and in f_u prediction by model 3, five outliers were excluded (ethambutol, atovaquone, beclomethasone dipropionate, drotaverine, irbesartan). The statistical results of the predictions are presented in Figure 2. The Y-randomization test after 50 permutations provided R^2Y- and Q^2Y-intercepts smaller than the recommended limits of 0.3 and 0.05 for both log V_{ss} and f_u, respectively (data not shown).

The AD was estimated from the compounds belonging to the training set as:

$$A = 24.22 + Z2.03$$

With Z = 0.7, AD is 25.641 that represent the maximum distance between compounds in the training set and new compound to be predicted. The compounds in the foreign test set that fell inside this AD were selected, yielding a set of 35 drugs for model 2, and 30 drugs for model 3. The statistical parameters of log V_{ss} and f_u predictions for the foreign set are presented in Table 5 and plots of the observed and predicted responses of

Table 5. Statistical parameters for log Vss and f_u predictions of the foreign set compounds inside the applicability domain of the models, calculated with Z = 0.7.

	Log V_{ss} prediction of foreign set			f_u prediction of foreign set		
	Q_f^2	MFE	% <2-fold	Q_f^2	MFE	%<2-fold
Model 2	0.62	2.85	60	0.59	5.58	54
Model 3	0.70	2.41	67	0.54	7.04	52

doi:10.1371/journal.pone.0074758.t005

model 3 and *VolSurf+* ADME models are presented in Figure 5. A comparison of the predicted and the observed values is found Table S1. Increasing Z increases the number of compounds in the foreign test set that are considered to be within the applicability domain but decreases the accuracy of prediction due to inclusion of dissimilar nearest neighbors (Figure 6).

2. RP Classification Models

The AUC for the in-bag training data for all trees in the forest model is 0.96 and 0.92, and the out-of-bag AUC is 0.81 and 0.79 for the V_{ss} and V_{ss} & f_u models, respectively. The in-bag results use predictions for the records used to train the tree, while the out-of-bag results use predictions for the left-out records. The statistics for the training set data presented in Figure 2 are derived from the in-bag results. The external test set including 260 compounds (described in Methods section) was used to evaluate the predictive ability of the two models. All compounds were classified according to their V_{ss} or V_{ss} & f_u values without applying AD. The overall prediction accuracy, calculated as ROC curve, was 0.78 and 0.82, respectively, and the sensitivity and specificity values are presented

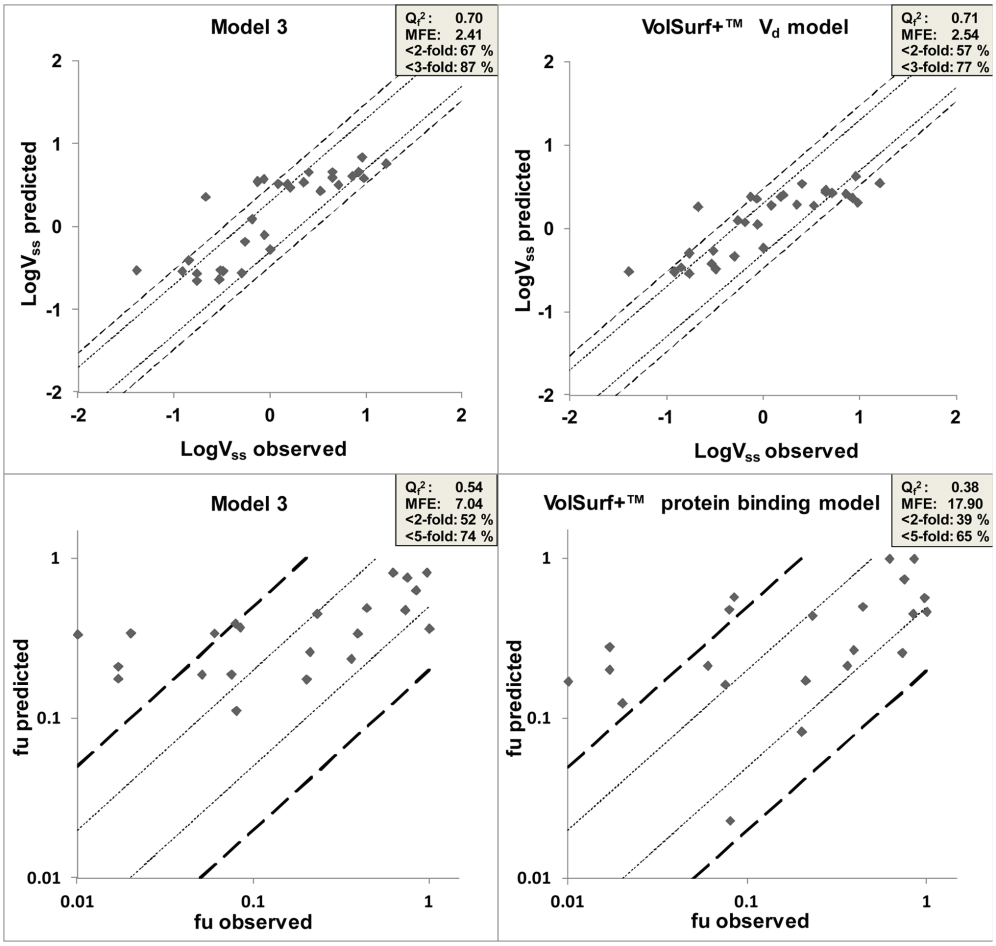

Figure 5. Log V_{ss} and f_u prediction plots of model 3 versus *VolSurf+ ADME* models (V_d and protein binding). Dot lines represent 2-fold error, dashed lines represent 3 –fold error and long dash lines represent 5-fold error. MFE: mean fold error.
doi:10.1371/journal.pone.0074758.g005

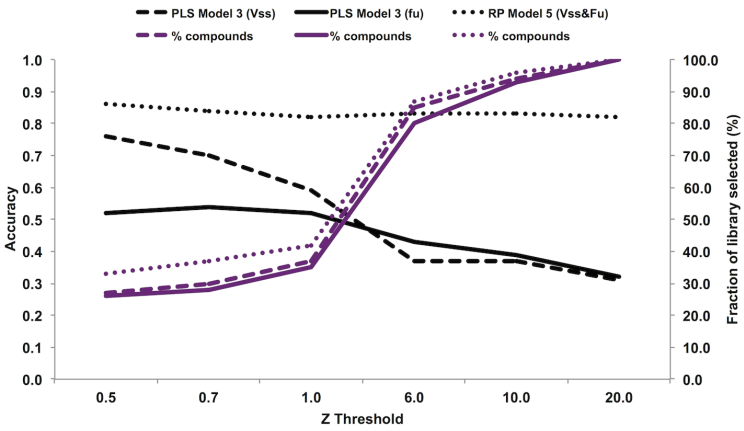

Figure 6. The effect of the AD on the prediction accuracy and chemical space coverage. Dashed black line: Q^2 of the V_{ss} foreign set predicted with PLS model 3. Dashed purple line: percentage of compounds from the V_{ss} foreign set predicted with PLS model 3. Black line: Q^2 of the f_u foreign set predicted with PLS model 3. Purple line: percentage of compounds from the f_u foreign set predicted with PLS model 3. Dotted black line: AUC of the test set predicted with RP classification. Dotted purple line: percentage of compounds from the test set predicted with RP classification.
doi:10.1371/journal.pone.0074758.g006

in Figure 2. The confusion matrices are presented in Tables S2-S7.

In general, the sensitivity of the models is high for compounds with a very low or high volume of distribution, while compounds belonging to class 2, with V_{ss} values between 0.3 and 1 L/kg are more difficult to classify correctly. The V_{ss} model performed well on the training set, with sensitivity 0.79 in class 2, but less than half of the class 2 compounds in the training set (42 of 93 compounds, leading to a sensitivity of 0.45) were predicted to the correct class in the out-of bag results (Table S3). Similarly, the model was able to identify class 1 and class 3 compounds form the external test set (sensitivity 0.71 and 0.81, respectively), while recognition of class 2 test set compounds was not as successful (sensitivity 0.32, Figure 2, Table S6). Interestingly, in the V_{ss} & f_u model, compounds with high f_u were predicted more accurately, with 10 of 17 compounds of the test set compounds correctly classified (sensitivity 0.59), but only 7 of 51 compounds with low f_u (sensitivity 0.14) (Figure 2, Table S7). The Y-randomization test was performed four times, and the AUC values for the model using the data set with experimental V_{ss} and V_{ss} & f_u values were significantly higher than those obtained from the dataset with randomized values (data not shown), indicating that our models are statistically robust. The AD was applied to the test set and its effect analyzed on the V_{ss} & f_u model (Figure 6). The prediction accuracy was highest with low Z cutoff, as expected, and slowly decreasing as the cutoff was increased to 1. However, increasing the cutoff from 1 to 20 did not markedly affect the prediction accuracy, while increasing the coverage of the test set from 39% to 100%. The small decrease in prediction accuracy is probably due to the cluster-based approach used to select the training and test set (described in Methods) that make the chemical space covered by two set similar.

One aid for interpretation of forest models is a set of descriptor importance measures, which indicate the relative importance of the descriptors in distinguishing among the different classes in the data. The percent selection frequency empirically appears to best distinguish truly important descriptors from others. It represents the percent of the time that the descriptor was selected for a split when a split was possible. A summary of descriptors ranked as top 10 based on their frequency of occurrences in the models are given in Table 6. It should be noted that size, polarity and lipophilicity are predominant in all models. The simple importance measures reported here are known to have bias in some cases [34]. However, if all descriptors have the same character as in our cases (e.g. they are all continuous numerical properties), then bias is generally not an issue.

Discussion

We have predicted V_{ss} and f_u with linear PLS models and nonlinear RP classification models, aiming for models that rely on *in silico* descriptors only and therefore are suitable for screening. V_{ss} is affected by the f_u in plasma, and we wanted to explore if predicting both parameters in parallel would help to find relevant physicochemical descriptors affecting these parameters. PLS can easily be used to correlate descriptors with several related responses, but to our knowledge, this approach has not been used in pharmacokinetic QSPR modeling.

The RP classification model was reasonably successful in classifying compounds with high ($\geq$1 L/kg) or low (0–0.3 L/kg) V_{ss}, while it had difficulties to identify the compounds with moderate (0.3–1 L/kg) V_{ss}. Interestingly, the level of binding to plasma proteins had an influence on the prediction accuracy, which was seen most clearly in the moderate V_{ss} class, where compounds with high f_u were correctly predicted in 59% of the test set, but only 14% of those with low f_u (Figure 2, Table S7). The attempt to create a PLS model for V_{ss} and f_u (model 1) starting with only 19 descriptors from *ACDlabs* and *MOE* was not successful, but using a wider range of descriptors from *Volsurf+* resulted in a predictive model (model 2) (Table 1 and Figure 2). The combination of all descriptors to model 3 did not significantly improve the prediction of the external set (V_{ss} $Q_F^2 = 0.50$, f_u $Q_F^2 = 0.54$) compared to model 2 (V_{ss} $Q_F^2 = 0.52$, f_u $Q_F^2 = 0.51$) (Figure 2). However, model 3 had better success in predicting the V_{ss} of the compounds in the foreign set (model 3 $Q_F^2 = 0.70$, model 2 $Q_F^2 = 0.62$) (Table 5). Notably, the prediction of the compounds in the foreign set within the AD was better than for the

Table 6. Most influential descriptors in the classification models.

V_{ss}				V_{ss} and f_u			
Descriptor	**Type**	**Number of Chances**	**Percent Selection Frequency**	**Descriptor**	**Type**	**Number of Chances**	**Percent Selection Frequency**
Rule Of 5	Drug like	12	8.3	PSAR	Polar area	4	25
CD3	Hydrophobic area	31	6.4	Num Rings	Topology	5	20
FLEX_RB	Size/Shape	69	5.8	W8	Hydrophilic area	5	20
L1LgS	Solubility	53	5.7	R	Size/Shape	10	10
CD6	Hydrophobic area	37	5.4	DRDRDO	Pharmacoforic	12	8.3
CW8	Hydrophilic area	20	5	D8	Hydrophobic area	26	7.7
LgS11	Solubility	66	4.5	LgD9	LogD	32	6.3
C ratio	Topology	45	4.4	ALogD5	LogD	34	5.9
NO ratio	Topology	48	4.2	CP	Shape	17	5.9
LgS5	Solubility	72	4.2	AUS7.4	Charge	35	5.7

doi:10.1371/journal.pone.0074758.t006

external set for both model 2 and 3. The AD was not used to filter compounds for prediction in the external set, which might be one reason for the improved performance on the foreign set. The use of an AD prevents extrapolation beyond the limits of chemical space that was used to build the model and can be used to identify the compounds for which predictions are reliable.

The impact of the descriptors on the responses can be observed graphically in the PLS weight plot (model 3 in Figure 4, model 2 in Figure S1). In model 3, the descriptors L3LgS, %FU10 and LgD10 have the highest positively correlated impact to V_{ss} (L3LgS, LogP n-oct and LgD9 in model 2, Figure S1), while LgS3, D4, Molar Volume and ALogD5.5 have a more moderate positive influence on V_{ss} (A in model 2). LgS10 has the largest negative correlation to V_{ss} (L1LgS in model 2), while W1, HDonors and LogS have smaller negative correlation in model 3 (Wn5, SOLY, W1 and ID3 in model2). On the other hand, LogS, LgS3 and LgS10 have the highest positive correlation with f_u (SOLY in model 2), while LogD10 and AlogD5.5 have the highest negative correlation (LogD9 and LOGP n-Oct in model 2). All in all, this suggests that charge and lipophilicity of the drug affect drug distribution, albeit with an inverse relationship. Thus, the lipophilicity descriptors have high correlation with the two responses, positive with V_{ss} and negative with f_u, while reversely, the charge and solubility descriptors have negative correlation with V_{ss} and positive with f_u. There is a complex relationship between f_u and V_{ss} and increasing the f_u of a compound does not inevitably lead to a higher volume of drug distribution, as is stated in many pharmacokinetic textbooks [35], [36]. This is easy to understand, since structural changes influencing the drugs ability to bind to plasma proteins may also affect the tissue binding of the drug.

Similar descriptors were found to be important in both the RP classification models (Table 6) and the PLS models. These include solubility descriptors, LogD at pH 9 or 5, as well as hydrophilic and hydrophobic area and volume descriptors. Due to the complexity of V_{ss} and f_u, many descriptors were always required to yield good prediction capability. Previously, trends have been observed between V_{ss} and LogP, polar surface area and hydrogen bond descriptors for the data set we have used [18]. Using the same data set, Berellini et al. (2009) found hydrogen bonding, LogD at pH 5–10, flexibility of the molecule and the *Volsurf+* descriptors DRDRDO, DRDRAC to be important in their V_{ss} model [12]. DRDRDO and DRDRAC are pharmacophoric descriptors of the maximum area of the triangles derived from Dry (DR), H-bond acceptor (AC) and H-bond donor (DO) points in a molecule. DRDRDO and flexibility were among the ten most influential descriptors in the RP models, but in the PLS models they did not have equally high importance. However, when comparing our descriptor selection to previous models of V_{ss} it must be kept in mind that we have modeled both V_{ss} and f_u parameters. Therefore a comparison is not directly applicable as descriptors having high influence on one parameter, but no correlation with the other parameter, are likely to be removed in our models.

Outliers are usually interesting, and the analysis of outliers can sometimes give a deeper understanding of the mechanisms under investigation. However, it is difficult to analyse the outliers in this study, because we do not know the reason for their exceptional behavior. Deviations in V_{ss} may be due to the active transport (influx or efflux) or compound specific binding to the tissues. As an example, let's consider the outliers in the prediction of V_{ss} by the PLS models (ribavirin, bilobalide, tamsulosin, decitabine). Ribavirin and decitabine are substrates of widely expressed nucleoside transporters, and extensive active transport might lead to outlier profiles of ribavirin and decitabine [37]. Tamsulosin is a substrate of alpha1 adrenergic receptors and bilobalide binds to GABA, glycine, and 5-HT3 receptors [38]. We cannot be sure, however, if these transport and binding phenomena take place substantially enough to cause exceptional V_{ss} values. Clearly, V_{ss} and f_u are complex phenomena that are affected by numerous factors. Therefore, explanations for the outlier behavior are not on firm ground and the reasons can be identified only by extensive experimental work.

We compared the performance of our model 3 with the volume of distribution and plasma protein binding models available in the *Volsurf+* package (Figure 5). As no AD is reported for the *Volsurf+* models, we have applied our AD with the Z cutoff value of 0.7 to select the compounds from the foreign test set for both models. For the practical use of AD in V_{ss} and f_u prediction, see File S2. It should be noted that we are not aware of which compounds have been used to train the *Volsurf+* model, and it is possible that some, or all, of the compounds used in our test set have been used to for that purpose. The same considerations apply for the *Volsurf+* plasma protein binding model. Our model achieved higher accuracy than the *Volsurf+* model in predicting f_u ($Q_f^2 = 0.54$ and

$Q_f^2 = 0.38$, respectively) (Figure 5), while the prediction of V_{ss} was comparable to the *Volsurf+* model (V_{ss} $Q_f^2 = 0.70$ and $Q_f^2 = 0.71$ for model 3 and *Volsurf+* models, respectively). The best predictions with our model were obtained at f_u values above 0.05. Predictions of the compounds with f_u values above 0.05 in the foreign set had a MFE of only 2.2 for model 3, compared to 7.04 for the whole foreign set (Figure 5, table 5). The predictions at f_u values below 0.05 give high FE values (>5-fold), whereas % error in this region is low. However, FE is pharmacologically a more relevant parameter, because the free drug concentration in plasma, C_u, is defined as f_u x C. Therefore, 3-fold change in f_u is expected to result in 3 fold change in C_u Unfortunately, we do not have an explanation for the poor results for the compounds that have very low f_u values, however, the compounds that were badly predicted by our models were also badly predicted by the *Volsurf+* model (Table S1), suggesting that the exceptional behavior is drug dependent and not due to the model.

The physical complexity of the V_{ss} and f_u parameters makes their prediction very challenging, and we were not able to reach models with optimal predictability. One way to improve prediction accuracy is to build the model using a narrower range of more similar compounds. We divided the data set of 642 compounds based on structural features or chemical properties and used these data sets to build several sub-models. However, the models were not able to achieve much higher accuracy than the more global models presented here (data not shown), but presented a much narrower AD and therefore more limited use.

Conclusions

The PLS models of V_{ss} showed similar performance to the commercial *Volsurf+* model, while the f_u prediction accuracy was slightly better. The RP classification models were able to distinguish between compounds with high or low V_{ss} values, but accurate classification of moderate V_{ss} or of low f_u values were not as successful. Due to the complex nature of V_{ss} and f_u parameters, a fairly large number of descriptors were needed for meaningful models. The advantages of the models compared to previous models is that they are based on a large set of structurally unrelated compounds, they are open, and they have a defined AD, which aids in identifying compounds for which reliable predictions can be made.

Supporting Information

Figure S1 PLS model 2 weight plot.
(TIF)

Table S1 Table of predicted vs. observed values for foreign set with PLS models.
(XLSX)

Table S2 Confusion matrix in-bag training results for the V_{ss} classification model.
(DOCX)

Table S3 Confusion matrix out-of-bag training results for the V_{ss} classification model.
(DOCX)

Table S4 Confusion matrix in-bag training results results for the V_{ss} & f_u classification model.
(DOCX)

Table S5 Confusion matrix out-of-bag training results results for the V_{ss} & f_u classification model.
(DOCX)

Table S6 Confusion matrix external test results for the V_{ss} classification model.
(DOCX)

Table S7 Confusion matrix external test results for the V_{ss} and f_u classification model.
(DOCX)

File S1 Final data set used for models.
(SDF)

File S2 Instructions for use of applicability domain.
(DOCX)

File S3 Training set for RP models.
(SDF)

File S4 Training set for PLS model 2.
(SDF)

File S5 Training set for PLS model 3.
(SDF)

Acknowledgments

The authors would like to thank Dr. Ossi Korhonen and Dr. Jari Pajander (School of Pharmacy, University of Eastern Finland) for their valuable help in the initial stages of the project, Dr. Veli-Pekka Ranta for his readiness to discuss pharmacokinetic questions (School of Pharmacy, University of Eastern Finland) and Dr. Mikko Kolehmainen (Dpt of Enviromental Science, University of Eastern Finland) for his experience in the use of multivariate analyses tools.

Author Contributions

Conceived and designed the experiments: EMA LG HX MY AU HK. Performed the experiments: EMA LG. Analyzed the data: EMA LG HX MY AU HK. Contributed reagents/materials/analysis tools: HX MY AU. Wrote the paper: EMA LG HX MY AU HK.

References

1. Lim VS (1991) Recombinant human erythropoietin in predialysis patients. Am J Kidney Dis 18: 34–37.
2. Tett SE, Cutler DJ, Day RO, Brown KF (1988) A dose-ranging study of the pharmacokinetics of hydroxy-chloroquine following intravenous administration to healthy volunteers. Br J Clin Pharmacol 26: 303–313.
3. Paul Y, Dhake AS, Parle M, Singh B (2010) In Silico Quantitative Structure Pharmacokinetic Relationship Modeling for Quinolone Drugs: Biological Half-Life. 22: 4880–4890.
4. Gleeson MP, Waters NJ, Paine SW, Davis AM (2006) In silico human and rat Vss quantitative structure-activity relationship models. J Med Chem 49: 1953–1963.
5. Hirono S, Nakagome I, Hirano H, Yoshii F, Moriguchi I (1994) Non-congeneric structure-pharmacokinetic property correlation studies using fuzzy adaptive least-squares: volume of distribution. Biol Pharm Bull 17: 686–690.
6. Karalis V, Tsantili-Kakoulidou A, Macheras P (2002) Multivariate statistics of disposition pharmacokinetic parameters for structurally unrelated drugs used in therapeutics. Pharm Res 19: 1827–1834.
7. Karalis V, Tsantili-Kakoulidou A, Macheras P (2003) Quantitative structure-pharmacokinetic relationships for disposition parameters of cephalosporins. 20: 115–123.
8. Lombardo F, Obach RS, Dicapua FM, Bakken GA, Lu J, et al. (2006) A hybrid mixture discriminant analysis-random forest computational model for the prediction of volume of distribution of drugs in human. J Med Chem 49: 2262–2267.
9. Ng C, Xiao Y, Putnam W, Lum B, Tropsha A (2004) Quantitative structure-pharmacokinetic parameters relationships (QSPKR) analysis of antimicrobial agents in humans using simulated annealing k-nearest-neighbor and partial least-square analysis methods. J Pharm Sci 93: 2535–2544.

10. Turner JV, Maddalena DJ, Cutler DJ (2004) Pharmacokinetic parameter prediction from drug structure using artificial neural networks. Int J Pharm 270: 209–219.
11. Balakin KV, Ivanenkov YA, Savchuk NP, Ivashchenko AA, Ekins S (2005) Comprehensive computational assessment of ADME properties using mapping techniques. Curr Drug Discov Technol 2: 99–113.
12. Berellini G, Springer C, Waters NJ, Lombardo F (2009) In silico prediction of volume of distribution in human using linear and nonlinear models on a 669 compound data set. J Med Chem 52: 4488–4495.
13. Fatemi MH, Ghorbannezhad Z (2011) Estimation of the volume of distribution of some pharmacologically important compounds from their structural descriptors. 76: 1003–1014.
14. Demir-Kavuk O, Bentzien J, Muegge I, Knapp E (2011) DemQSAR: predicting human volume of distribution and clearance of drugs. J Comput Aided Mol Des 25: 1121–1133.
15. Zhivkova Z, Doytchinova I (2012) Prediction of steady-state volume of distribution of acidic drugs by quantitative structure-pharmacokinetics relationships. J Pharm Sci 101: 1253–1266.
16. Gombar VK, Hall SD (2013) Quantitative Structure-Activity Relationship Models of Clinical Pharmacokinetics: Clearance and Volume of Distribution. J Chem Inf Model.
17. Cruciani G, Crivori P, Carrupt P, Testa B (2000) Molecular fields in quantitative structure–permeation relationships: the VolSurf approach. 503: 17–30.
18. Obach RS, Lombardo F, Waters NJ (2008) Trend Analysis of a Database of Intravenous Pharmacokinetic Parameters in Humans for 670 Drug Compounds. Drug Metab Dispos 36: 1385–1405.
19. Gleeson MP (2007) Plasma protein binding affinity and its relationship to molecular structure: an in-silico analysis. J Med Chem 50: 101–112.
20. Moda TL, Montanari CA, Andricopulo AD (2007) Hologram QSAR model for the prediction of human oral bioavailability. Bioorg Med Chem 15: 7738–7745.
21. Ma CY, Yang SY, Zhang H, Xiang ML, Huang Q, et al. (2008) Prediction models of human plasma protein binding rate and oral bioavailability derived by using GA-CG-SVM method. J Pharm Biomed Anal 47: 677–682.
22. *ACD/Dictionary*, Advanced Chemistry Development, Inc., Toronto, On, Canada. Available: www.acdlabs.com.
23. *SYBYL 8.0*, Tripos International, St. Louis, Missouri, USA.
24. White NJ (1994) Clinical pharmacokinetics and pharmacodynamics of artemisinin and derivatives. Trans R Soc Trop Med Hyg 88 Suppl 1: S41–3.
25. Watts NB, Diab DL (2010) Long-term use of bisphosphonates in osteoporosis. J Clin Endocrinol Metab 95: 1555–1565.
26. *ACDlabs software*, Advanced Chemistry Development, Inc., Toronto, On, Canada. Available: www.acdlabs.com.
27. *MOE*, Molecular Operating Environment, Chemical Computing Group: Montreal, Canada, 2008.
28. *SIMCAplus software*, Umetrics AB, Box 7960, SE-90719 Umeå, Sweden.
29. Chen C, Liaw A, Breiman L (2004) Using Random Forest to Learn Imbalanced Data. Technical report 666, Department of Statistics, University of Berkeley.
30. Hand DJ, Till RJ (2001) A Simple Generalisation of the Area Under the ROC Curve for Multiple Class Classification Problems. Machine Learning 45: 171–186.
31. Tropsha A, Gramatica P, Gombar VK (2003) The Importance of Being Earnest: Validation is the Absolute Essential for Successful Application and Interpretation of QSPR Models. 22: 69–77.
32. Zhang S, Golbraikh A, Oloff S, Kohn H, Tropsha A (2006) A Novel Automated Lazy Learning QSAR (ALL-QSAR) Approach: Method Development, Applications, and Virtual Screening of Chemical Databases Using Validated ALL-QSAR Models. 46: 1984–1995.
33. *Suite 2012: Maestro* (2012) version 9.3, Schrödinger, LLC, New York, NY.
34. Strobl C, Boulesteix AL, Zeileis A, Hothorn T (2007) Bias in random forest variable importance measures: illustrations, sources and a solution. BMC Bioinformatics 8: 25.
35. Lüllmann H, Mohr K, Hein L, Bieger D (2005) Color Atlas of Pharmacology. p. 402.
36. Rowland M, Tozer TN (2011) Clinical Pharmacokinetics and Pharmacodynamics: Concepts and Applications. p. 864.
37. King AE, Ackley MA, Cass CE, Young JD, Baldwin SA (2006) Nucleoside transporters: from scavengers to novel therapeutic targets. Trends Pharmacol Sci 27: 416–425.
38. Thompson AJ, Duke RK, Lummis SC (2011) Binding sites for bilobalide, diltiazem, ginkgolide, and picrotoxinin at the 5-HT3 receptor. Mol Pharmacol. 80: 183–190.

6. Second article: Prediction of the Vitreal Half-Life of Small Molecular Drug-Like Compounds.

II

Reprinted with permission of Springer: Heidi Kidron, Eva M. del Amo, Kati-Sisko Vellonen, Arto Urtti. Prediction of the Vitreal Half-Life of Small Molecular Drug-Like Compounds. Pharmaceutical Research, 2012, 29, 3302-3311.
http://dx.doi.org/10.1007/s11095-012-0822-5

Pharm Res (2012) 29:3302–3311
DOI 10.1007/s11095-012-0822-5

RESEARCH PAPER

Prediction of the Vitreal Half-Life of Small Molecular Drug-Like Compounds

Heidi Kidron • Eva M. del Amo • Kati-Sisko Vellonen • Arto Urtti

Received: 6 May 2012 / Accepted: 22 June 2012 / Published online: 10 July 2012

ABSTRACT

Purpose To build a fast, user-friendly computational model to predict the intravitreal half-lives of drug-like compounds.

Methods We used multivariate analysis to build intravitreal half-life models using two data sets, one with experimental data derived from both pigmented and albino rabbits and another including only data from experiments with albino rabbits.

Results The final models had a Q^2 value of 0.65 and 0.75 for the mixed and albino rabbit models, respectively. The models performed well in predicting the intravitreal half-life of an external test set. In addition, the models are physiologically interpretable, containing mainly hydrogen bonding and lipophilicity descriptors.

Conclusion The developed models enable reliable predictions of intravitreal half-lives for use in the early drug development stages, without the need for prior experimental data.

KEY WORDS blood-retinal barrier · intravitreal injection · multivariate analysis · ocular drug delivery · QSPR

ABBREVIATIONS

FRB	freely rotatable bonds
HA	number of hydrogen bond acceptors
HD	number of hydrogen bond donors
H_{tot}	total number of putative hydrogen bonds, i.e. HD +HA
logP	the logarithm of the octanol-water partition coefficient of the neutral form
log $t_{½}$	the logarithm of the intravitreal half-life, $logD_x$, the logarithm of the octanol-water partition coefficient at pH x
MW	molecular weight
PCA	principal component analysis
P-gp	P-glycoprotein
PLS	partial least squares
QSPR	quantitative structure-property relationship
RMSE	root mean squared error
RMSEP	root mean squared error of prediction
VIP	variable importance in the projection

INTRODUCTION

Intravitreal therapy is used to treat ocular diseases in the posterior segments of the eye, for example, age-related macular degeneration and diabetic macular edema. Intravitreal drug administration must be used, because topical eye drop treatment does not lead to adequate drug concentrations in the posterior target sites (retina, choroid, vitreous). The drug is injected directly into the vitreous, which is a hydrophilic gel consisting of a network of well separated hyaluronic acid and collagen type II fibers, allowing diffusion of drug molecules, even macromolecules, to the retina and choroid. One advantage of the intravitreal injections is

H. Kidron (✉) • E. M. del Amo • A. Urtti
Centre for Drug Research, Faculty of Pharmacy, University of Helsinki
P.O. Box 56, FIN-00014 Helsinki, Finland
e-mail: heidi.kidron@helsinki.fi

E. M. del Amo • K.-S. Vellonen
Division of Biopharmacy and Pharmacokinetics, Faculty of Pharmacy
University of Helsinki
Helsinki, Finland

Present Address:
K.-S. Vellonen
School of Pharmacy, University of Eastern Finland
Kuopio, Finland

that it generally leads to minimal systemic exposure of the drug. However, due to the invasive nature of the injections, other ways of delivering drugs to the posterior eye segment have been attempted, but the topical, systemic and subconjunctival delivery routes generally fail in reaching effective concentrations in the vitreous body (1).

After an injection into the vitreous there are two routes by which the molecule can be eliminated: 1) anteriorly via flows of aqueous humor and uveal blood circulation; 2) posteriorly through the blood-retinal barrier to retinal and choroidal blood circulation (2). The blood-retinal barrier is composed of the retinal pigment epithelium and the tight walls of retinal capillary. The cells in the blood-retinal barrier express transporters, which in principle may affect drug elimination from the vitreous, but the effect of transporters on drug elimination *in vivo* is still unclear (3). The posterior route presents a large surface area surrounding the vitreous, but the cells in the blood-retinal barrier form a tight layer, allowing efficient elimination of lipophilic compounds. The anterior route, in contrast, is limited by the small area that is available for diffusion from the vitreous into the posterior and anterior chambers. In general, elimination through the posterior route takes place rapidly, whereas drug elimination via the anterior route is slower (2).

Intravitreal drugs can be administered as injections or implants that release drug over prolonged times. In all cases, drug concentrations in vitreous are dependent on the rate of drug elimination from the vitreous. Slow intravitreal drug elimination is desirable, since it will prolong the duration of drug action after intravitreal injections and minimizes the required drug loading in the controlled release formulations. The intravitreal half-life of a compound must be determined *in vivo* by injecting the compound into the vitreous of an animal, usually rabbit, and measuring the concentration of the compound in the vitreous at certain time-points after the injection. Pharmacokinetic evaluation is typically carried out using many time points (often 5–10) and several replicates of each time point is needed (more than 5). Thus, for plotting a reliable time-concentration curve at least 20 animals are needed, which makes this method unacceptable for drug screening. There is a need for an alternative method that would enable screening of molecules before *in vivo* studies and also reduce and refine animal experiments related to development of ocular drugs and intravitreal drug delivery systems.

A computational method like quantitative structure-property relationships (QSPR) modeling is optimal for rapid virtual evaluation and pre-selection of compounds. Even though QSPR models are widely used to study the relationship between physicochemical properties and the pharmacokinetic properties of molecules, surprisingly few attempts have been made to predict the intravitreal half-life of injected drugs. Some prior studies have established that compounds with a high molecular weight are preferably eliminated by the anterior route (4), and that molecular weight (MW) and lipophilicity do have an influence on the intravitreal half-life (5–7). However, some studies (5,6) have been done using small sets of structurally and chemically similar compounds and, therefore, those models are not broadly applicable to diverse compounds. Durairaj and co-workers used a large set of molecules, including small molecules and macromolecules, with a MW range from 32 to 149 000 Da, but explored only a limited set of variables, including only molecular weight, lipophilicity and solubility variables to derive QSPR models by multiple regression (7).

We aimed to build a computational model for virtual prediction of drug elimination from the vitreous. The models are focused on compounds with molecular weight below 1500 Da, thus excluding macromolecules. The use of a lower, narrower MW range will make the model more applicable for prediction of small molecules. We have made a careful literature search and collected experimental data on the intravitreal half-lives of 47 compounds in albino and pigmented rabbits. The data set contains molecules with diverse structural and chemical features. The relationship between the intravitreal half-life and 33 physicochemical descriptors was determined by multivariate analysis. Simple mathematical equations were derived, enabling reliable prediction of the intravitreal half-life for a compound without any experimental data.

MATERIALS AND METHODS

Compound Data Set

A data set of 47 compounds (Table I) was collected from an an extensive literature search for intravitreal injections (5,8–49). The half-lives of the compounds included in the dataset have been measured in either albino or pigmented rabbits. A subset was constructed from this dataset, containing 39 compounds with experimental data collected from only albino rabbits (Table I). An average value was calculated for compounds with more than one reference. The model is focused on molecules with molecular weight less than 1500 Da. In addition, we only included data from experiments with compounds that were dissolved in water or buffer solution and injected into normal, healthy eyes. When the intravitreal half-life had not been reported for a compound, the half-life was calculated from the reported concentrations. Compounds for which the intravitreal concentrations had been measured during a time-span that was less than two half-lives, were excluded from the data set.

Data that was deemed of insufficient quality due to for instance large standard deviations or an irregular time-concentration curve was also excluded. For two-compartment models, the half-life of the terminal phase was used, except for moxifloxacin and fluorouracil, where the alpha phase was dominant.

Table I Calculated Descriptors Used in the Final Models and Experimentally Determined Intravitreal Half-Life of Compounds in the Data Sets

compound	albino/pigmented	$t_{1/2}$ (h)mix	$t_{1/2}$ (h)alb	H_{tot}	$LogD_{7.4}$	FRB	Reference
1-heptanol	albino	2.6	2.6	2	2.37	6	(8)
1-pentanol[b,d]	albino	1.2	1.2	2	1.35	4	(8)
1-propanol	albino	1.0	1.0	2	033	2	(8)
Å6 peptide	albino	19.4	19.4	38	−8.68	28	(9)
acyclovir[d]	albino	3.0	3.0	12	−0.62	5	(10)
amikacin[a,c]	albino	25.9	25.9	35	−10.59	22	(11)
ampicillin[b]	albino	8.8	8.8	11	−1.84	5	(12)
aztreonam	albino/pigmented	7.9	8.3	18	−4.32	7	(12,13)
candesartan	abino	6.8	6.8	11	1.45	7	(14)
carbenicillin	albino/pigmented	4.3	3.5	11	−3.62	5	(15,16)
cefazolin	albino	3.8	3.8	14	−4.41	7	(17)
cefepime[a]	pigmented	14.6	–	15	−2.29	7	(18,19)
ceftazidime[b]	pigmented	18.0	–	18	−2.95	9	(19)
ceftizoxime	pigmented	5.7	–	14	−4.35	5	(19)
ceftriaxone[c]	albino/pigmented	11.6	14.1	20	−4.58	8	(19,20)
cephalexin[d]	albino	3.1	3.1	11	−2.93	5	(17)
cephalothin	albino	2.4	2.4	10	−3.62	7	(17)
cidofovir[a]	albino	21.0	21.0	14	−5.41	7	(21)
ciprofloxacin	albino	4.4	4.4	8	−0.29	3	(5)
clarithromycin[b,d]	albino	2.0	2.0	18	2.06	12	(22)
clindamycin[c]	albino	3.0	3.0	11	0.70	10	(23)
cyclosporin A	albino	7.6	7.6	28	2.79	16	(24)
dexamethasone[b]	pigmented	3.5	–	8	2.03	5	(25)
fleroxacin[a]	albino	3.4	3.4	7	−3.09	4	(5)
fluconazole[d]	albino	3.2	3.2	8	0.45	6	(26)
fluorescein	albino	2.5	2.5	7	2.68	2	(27,28)
fluorouracil	pigmented	12.8	–	6	−1.64	0	(29)
ganciclovir[b]	albino/pigmented	6.0	5.3	14	−0.74	7	(10,30–32)
gentamicin[c]	albino/pigmented	22.7	22.0	23	−7.81	13	(33,34)
grepafloxacin[a]	albino/pigmented	3.5	3.5	8	0.62	3	(35)
kanamycin[b,d]	albino	10.3	10.3	30	−8.86	17	(36)
lincomycin	albino	12.6	12.6	13	−0.36	11	(37)
methanol	albino	0.9	0.9	2	−0.69	0	(8)
methicillin	albino	6.2	6.2	10	−2.71	5	(38)
methotrexate[c]	albino	7.6	7.6	20	−5.10	9	(39)
moxalactam[a]	albino	16.1	16.1	19	−7.31	10	(40)
moxifloxacin	pigmented	1.7	–	9	0.31	4	(41)
netilmicin[b,d]	albino	26.6	26.6	23	−6.79	14	(12,42)
ofloxacin[b]	albino	3.0	3.0	8	−0.39	2	(5)
penicillin	not known	4.2	–	8	−1.81	4	(43,44)
piperacillin	albino	8.9	8.9	15	−2.73	6	(12)
quinidine[a]	albino	2.0	2.0	5	0.98	5	(28,45)
sparfloxacin[c]	albino	2.8	2.8	11	0.83	4	(5)
tobramycin	albino	31.5	31.5	29	−9.54	16	(46)
trifluorothymidine[b]	albino	3.2	3.2	10	−0.20	4	(47)

Table I (continued)

compound	albino/pigmented	$t_{1/2}$ (h)mix	$t_{1/2}$ (h)alb	H_{tot}	$LogD_{7.4}$	FRB	Reference
vancomycin	pigmented	62.3	–	54	−4.49	23	(48)
voriconazole[d]	albino	2.5	2.5	7	1.21	6	(49)

[a] The compound was excluded from the mixed data set prior to model building and included in the external test set, [b] The compound was selected to the internal test set from the mixed data set based on the PCA, [c] The compound was excluded from the albino data set prior to model building and included in the external test set, [d] The compound was selected to the internal test set from the albino data set based on the PCA.

Molecular Descriptors

The chemical structure of the compounds in the data set were retrieved from ACD/Dictionary (50), or the the PubChem database (http://pubchem.ncbi.nlm.nih.gov/). The ACDLabs software package version 12 was used to calculate the molecular descriptors for these compounds (50). A total of 33 descriptors were chosen for this study; pKa, LogD at pH 2, 5.5, 6.5, 7, 7.4 and 10, LogP, MW, PSA (polar surface area), FRB (freely rotatable bonds), HD (hydrogen bond donors), HA (hydrogen bond acceptors), H_{tot} (HD + HA), molar refractivity, molar volume, parachor, index of refraction, surface tension, density, polarizability, C ratio, N ratio, NO ratio, hetero ratio, halogen ratio, number of rings and number of aromatic, 3-, 4-, 5- and 6-membered rings.

Multivariate Data Analysis

Before data analysis, an external data set of seven compounds was randomly extracted from the collected data set of 47 compounds from pigmented and albino rabbits (mixed set), while six compounds were randomly extracted from the albino data set of 39 compounds (Table I). The compounds in the external data sets were not used for model building or training. A logarithmic transformation was performed for those variables that had a broad range or were not equally distributed over the range. A principal component analysis (PCA) including all molecular descriptors was calculated to analyze the diversity of the data set. The logarithm of intravitreal half-life ($\log_{t1/2}$) was correlated to the molecular descriptors by Partial Least Squares (PLS) analysis using Simca-P (version 10.5) (51). Based on the distribution of the compounds in the PCA plot training sets of 30 and 25 compounds and internal test sets of ten compounds and eight compounds were generated, respectively, for the mixed and albino data set. Only the compounds in the training set were used to calculate the models. Both cross-validation and prediction of the intravitreal half-life of the compounds in the internal tests sets were used to evaluate the predictive capability of the models. For cross-validation, the training set is divided into seven groups and the intravitreal half-life for the compounds in each group is predicted using the data in the other groups. The sum of squared errors between the actual and predicted data is calculated and converted into the Q^2 value (cross validated R^2). The half-life for the compounds in the internal test sets were predicted for further evaluation of the models. Ultimately, the final models were assessed by predicting the half-life of the external data sets that were extracted before data analysis (Table I).

The statistical significance of the models was assessed by Y-scrambling, i.e. the model is fitted to scrambled half-life values and R^2Y (equivalent to the R^2 coefficient) and Q^2 are calculated. After repeating the process 50 times, the results are plotted with the R^2Y values on the Y-axis and the Q^2 values on the X-axis and regression lines are fitted to the points. For statistically valid models, the intercepts should be below 0.3 and 0.05 for R^2Y and Q^2, respectively.

RESULTS

Literature Search

Initially, we found 83 reported intravitreal half-lives for compounds by literature searches. Twenty of these half-lives were excluded from the data set, since they did not fulfill the criteria as described in the Materials and Methods section. Among the compounds that were left out from the data set is triamcinolone acetonide, which is a well-studied and widely used drug in ocular therapy. However, it was excluded from the study as it is poorly soluble and precipitates in the vitreous after injection, thus, its long half-life is due to the slow dissolution of the drug particles in the vitreous. The remaining 63 reported half-lives were used to build the mixed data set of 47 compounds, containing data from both pigmented and albino rabbits, as well as the subset of 39 compounds from albino rabbits (Table I). An average value was calculated for those compounds with more than one study that reported a half-life. The terminal half-life, in the case of two-compartment models, was used as the elimination half-life in all cases except two: moxifloxacin and fluorouracil. For moxifloxacin the half-life of the first phase was used, since it is the dominant phase, while an effective half-life was calculated for fluorouracil, taking into account both the first phase (alpha) and the terminal phase (beta), $(t_{1/2,\ eff}=(AUC_{alpha}/AUC_{tot})x\ t_{1/2alpha}+(AUC_{beta}/AUC_{tot})x\ t_{1/2beta})$(52). For fluorouracil, the first phase accounted for approximately one third of the total

elimination based on the AUC of the alpha phase. Therefore, the effective half-life deviates from terminal half-life and is a more representative indicator for drug concentration decay in the vitreous. The unusual elimination profile of moxifloxacin might be due to its ability to strongly bind to melanin (53).

Molecular Diversity of the Compounds

The compounds in the mixed data set cover a broad range of structurally and chemically diverse molecules, with an intravitreal half-life from 0.9 to 62.3 h. The molecular weights of the compounds varied from 32 to 1449 Da and the $LogD_{7.4}$ from -10.60 to 2.68. All calculated descriptors were used to perform PCA for both mixed and albino dataset (Fig. 1). The mixed data set resulted in a PCA model with five principal components that explained 81% of the variance in the data set, while the PCA model for the albino data set contained four principal components explaining 80% of the variance. The PCA score plots of the two first principal components, explaining 44% and 18%, respectively, of the variance in the mixed data set and 42% and 18%, respectively, of the variance in the albino data set, are shown in Fig. 1. Methanol lies outside the elliptic 95% tolerance volume of both the mixed and albino PCA models, but it was not excluded from model building, since 5% of the data set is allowed outside the tolerance volume. The compounds in the data sets were divided into training sets (30 and 25 compounds in the mixed and albino training sets, respectively) and internal test sets (10 and 8 compounds in the mixed and albino test sets, respectively) based on their distribution in the PCA score plot (Fig. 1, Table I).

PLS Analysis of Training Set Compounds and Evaluation of Derived Models with Internal Test Set Compounds

The PLS model using all the 33 calculated descriptors and the 30 compounds of the mixed training set had a R^2Y= 0.65 and Q^2=0.59, and the PLS model with all descriptors

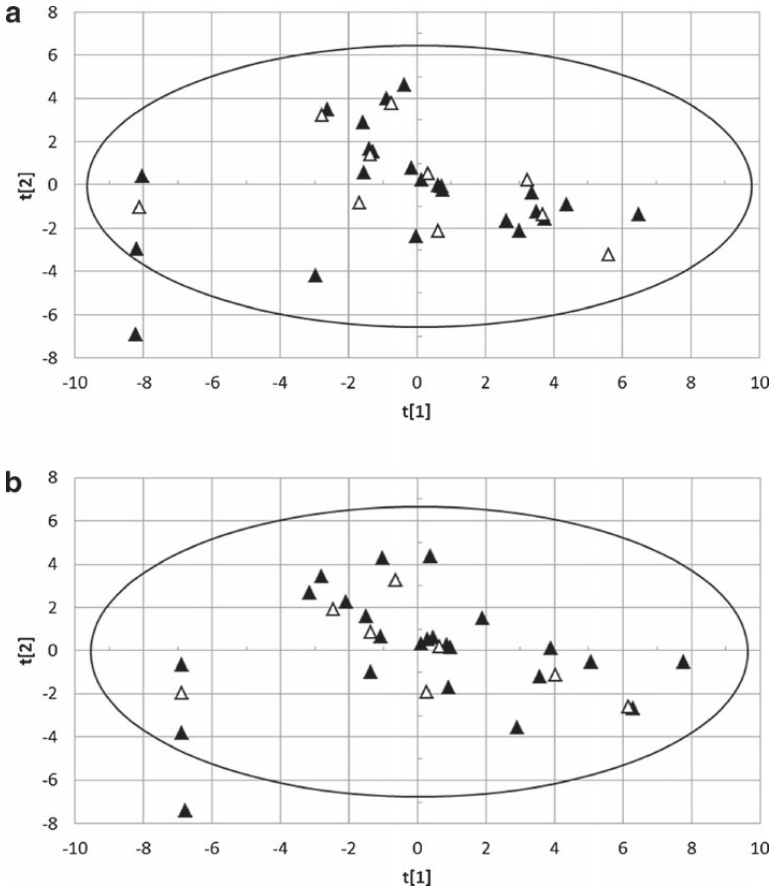

Fig. 1 PCA score plot of (**a**) the 47 compounds in the mixed data set and (**b**) the 39 compounds in the albino data set. The black triangles represent compounds in the training set and the unfilled triangles the compounds in the internal test set. The ellipse depicts the 95% tolerance volume based on hotelling T^2 (0.05).

for the albino set had similar values, R^2Y=0.69 and Q^2= 0.55 (Table II). In order to construct a simpler model, we excluded those descriptors that according to SIMCAs variable influence on projection (VIP) function were deemed the least influential (Fig. 2). A VIP value above 1 specifies the descriptor as more influential than average in explaining the modeled response. A threshold of 1.2 and 1.1 was chosen for the mixed and the albino data set, respectively, leading to models with 14 descriptors for both data sets. The models had improved statistics with higher R^2 and Q^2 values than the initial models (Table II). The descriptors were related to lipophilicity (LogD at pH 5.5, 6.5, 7 and 7.4), hydrogen bonding (H_{tot}, HD, HA and PSA) and mass (MW, MV, polarizability, molar refractivity and parachor), as well as the amount of rotatable bonds, defined with the variable FRB. Subsequently, we excluded the descriptors with high correlation coefficients (> 0.9) with H_{tot}, $LogD_{7.4}$ or MW. The H_{tot} variable was chosen since it combined the information from the HD and HA descriptors, which it is highly correlated to. The MW descriptor was selected since it had the highest VIP value of the correlated coefficients, while the $LogD_{7.4}$ descriptor was chosen for its physiological relevance. This resulted in a four-variable model for both data sets, including the descriptors H_{tot}, MW, $LogD_{7.4}$ and FRB. Both models had good statistics, with R^2Y=0.64, Q^2=0.61 for the mixed model and R^2Y=0.73, Q^2=0.71 in the albino model. The predictability of these models was evaluated on the internal test set, with a Q^2int value of 0.61 and 0.67 for the mixed and albino model, respectively. Exclusion of the FRB descriptor in the mixed model improved the statistics and the prediction of the internal test set (Table II), while creating a three-variable model by removing any of the other descriptors led to markedly decreased predictability of the internal test set (data not shown). Similarly, exclusion of the MW descriptor in the albino data set improved the model statistics and predictability of the internal test set, while creating a three-variable model by exclusion of any of the other variables did not have a beneficial impact. Furthermore, a two-variable model with good statistics and better predictability for the internal data set was obtained for the mixed data sets using only the H_{tot} and $LogD_{7.4}$ descriptors (Table II). A two-variable model for the albino data using the same descriptors resulted in a model with a lower Q^2 value, but good predictability of the internal test set.

The two-variable model was chosen for the mixed data set, while the three-variable model was chosen for the albino data set for further evaluation. The final models are described by the following equations:

$$\log t_{1/2,\text{mixed}} = -0.046 - 0.051(\log D_{7.4}) + 0.640(\text{LogH}_{\text{tot}})$$

$$\log t_{1/2,\text{albino}} = -0.164 - 0.032(\log D_{7.4}) + 0.435(\text{LogH}_{\text{tot}}) + 0.461(\text{Log}(\text{FRB} + 1))$$

The statistical significance of the predictive capability of these final models was evaluated with the *validate* function in Simca-P. The R^2Y and Q^2 Y-intercepts were -0.06 and -0.16 for the mixed model and -0.02 and -0.18 for the albino model, respectively. Both are well below the upper limits of a statistically valid model.

Evaluation of the Final Models on an External Test Set

The final models were used to predict the intravitreal half-life of the compounds in the external data sets that were removed prior to model building (Table I). Both models predicted the compounds in the external data sets with good accuracy, with an external Q^2 value of 0.81 and 0.88, respectively, for the mixed and albino models.

Table II PLS Models Obtained from the Mixed Data Set Compounds and the Albino Dataset Compounds

Variables	A[a]	R^2X	Training set		RMSEE[b]	Internal test set	
			R^2Y	Q^2		Q^2	RMSEP[c]
Mixed data set							
33	1	0.42	0.65	0.59	0.256	0.68	0.229
14	1	0.72	0.66	0.63	0.252	0.60	0.255
Htot, MW, $LogD_{7.4}$, FRB	1	0.74	0.64	0.61	0.260	0.61	0.255
Htot, MW, $LogD_{7.4}$	1	0.75	0.66	0.65	0.232	0.63	0.245
Htot, $LogD_{7.4}$	1	0.80	0.66	0.64	0.250	0.69	0.225
Albino data set							
33	1	0.43	0.69	0.55	0.220	0.70	0.256
14	1	0.68	0.72	0.68	0.206	0.74	0.263
Htot, MW, $LogD_{7.4}$, FRB	1	0.74	0.73	0.71	0.205	0.67	0.287
Htot, $LogD_{7.4}$, FRB	1	0.75	0.75	0.75	0.196	0.74	0.276
Htot, $LogD_{7.4}$	1	0.79	0.70	0.66	0.218	0.76	0.239

[a]Number of principal components in the PLS model. [b]RMSEE, Root Mean Squared Error of Estimation. [c]RMSEP, Root Mean Squared Error of Prediction

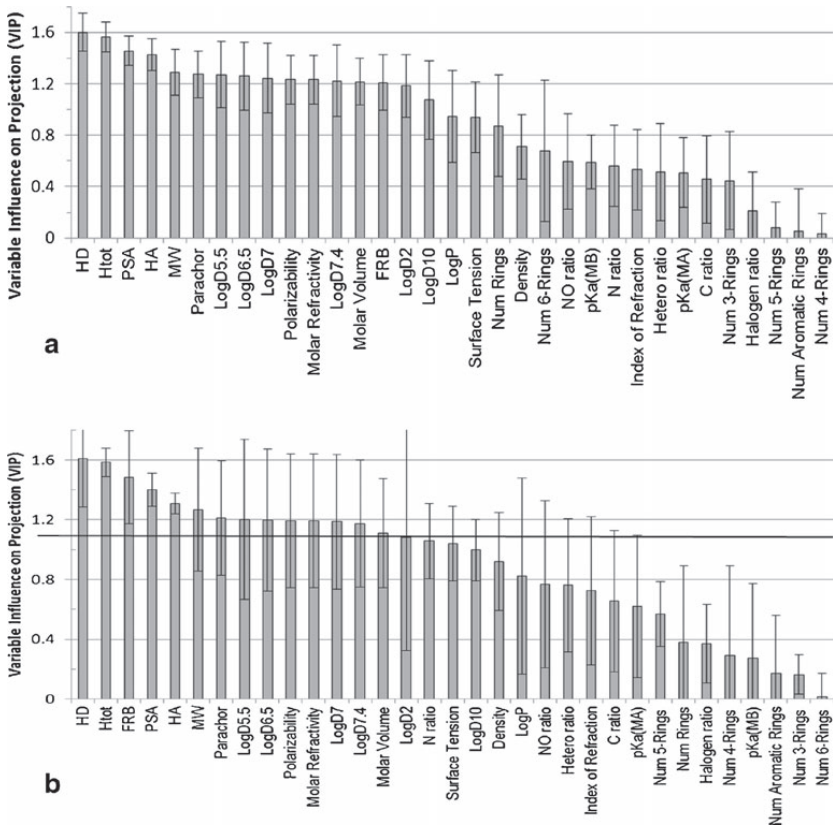

Fig. 2 VIP plots, with confidence intervals, from PLS analysis using all variables and the training set compounds for (**a**) the mixed data set and (**b**) the albino data set. A horizontal line has been drawn in (**b**) to indicate the 1.1 VIP threshold.

DISCUSSION

Two models for the prediction of intravitreal half-life were obtained, one specifically for albino rabbits and one that is suitable both for albino and pigmented rabbits. Due to the limited amount of data available for pigmented rabbits (only 13 compounds), we did not attempt to build a specific model for pigmented rabbits. Both of the final models had good statistical values, with the R^2Y and Q^2 of the albino higher (both values 0.75) compared to those of the mixed set model (0.66 and 0.64, respectively). The ability of the models to predict the intravitreal half-life was verified both on internal test sets as well as on randomly selected external test sets (Fig. 3). The models performed well, as the difference in observed and predicted half-life for the most poorly predicted compound in the mixed test sets was 2.3-fold (cidofovir in the external test set) and all in all, only four other compounds had more than a two-fold difference to the experimental value. In the albino test sets, clarithromycin was predicted to have a 3.4-fold longer half-life than observed experimentally, but on the other hand, there was only one other compound, kanamycin, with a two-fold error in its predicted half-life, while all the other compounds had less than two-fold error-prediction.

The final models contained only two or three variables, H_{tot} and $LogD_{7.4}$ in the model for the mixed data set, and H_{tot}, $LogD_{7.4}$ and FRB for the albino set. Both models had better R^2Y and Q^2 values than the models using all 33 calculated variables and also slightly improved values compared to the four-variable models (Table II). Furthermore, the variables that are included in the final models are easily interpretable. A higher $LogD_{7.4}$ value leads to a shorter half-life, which is likely due to increased permeability of the cell membranes in the blood-retinal barrier, while increasing the amount of hydrogen bond donors and acceptors results in longer half-lives, as polar compounds have more difficulties to permeate membranes. According to the albino model, flexible compounds that have a high amount of rotatable bonds have longer half-lives.

Previous studies have linked intravitreal half-life to MW and lipophilicity (4–7). In our study, MW was also an influential descriptor with a relatively high VIP value, but still its exclusion improved the predictivity of the models. One possible explanation is that our model focuses on low MW

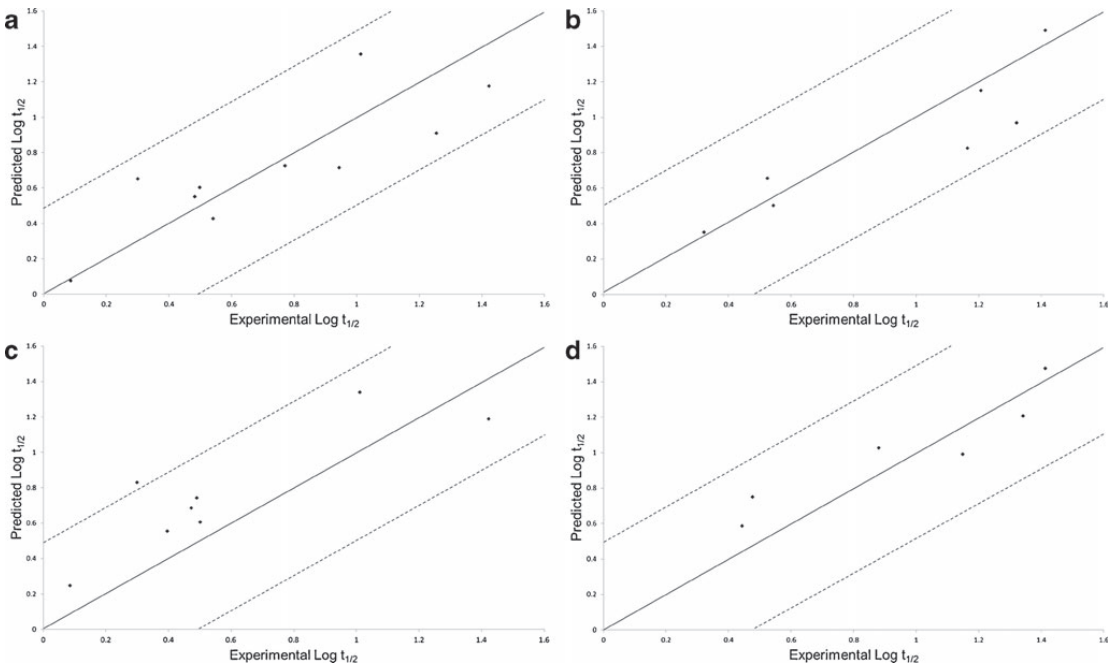

Fig. 3 Predicted *versus* observed log $t_{1/2}$ values based on the final models. Prediction of the mixed data set compounds in the internal test set (**a**) and external test set (**b**) and the albino data set compounds in the internal test set (**c**) and external test set (**d**). A diagonal line has been drawn in $R^2Y = 1$ to facilitate interpretation and the dashed lines represent a 3-fold prediction range.

compounds and, thus, does not highlight the effect MW on the half-life, and a more clear effect might only be observed when significantly larger compounds, like macromolecules with MW of several thousand Da are included. Macromolecules, like proteins, have a slower rate of diffusion in the vitreous and they are predominantly eliminated from the vitreous through the anterior route. These compounds have significantly longer half-lives than molecules that can permeate the blood-retinal barrier. However, we have only included compounds that have MW <1500 Da in our study, and therefore this size effect may not be evident in our data set. Another likely explanation could be that the number of rotatable bonds as well as hydrogen bonds generally tends to increase with the size of molecules and, therefore, the successful use of MW in describing membrane permeability is due to its correlation with increased polarity and flexibility (54), which in our model is described by the H_{tot} and FRB variables. However, Veber and co-workers found that the number of FRB influences membrane permeability of compounds independently of MW (54).

Some compounds in the data set are known substrates for transporters in the retinal pigment epithelium cells. For example, carbenicillin and quinidine have been identified as substrates for P-glycoprotein (P-gp) (15,28,45). Interestingly, these compounds are not outliers in our model, which might be due to the relatively small increase (1.5–2.5-fold) in intravitreal half-life of these compounds when a P-gp inhibitor is coadministered. For the same reason the model is quite accurate in predicting the half-lives of these transporter substrates, as the effect of active transport apparently falls within the 3-fold prediction error of the model for the compounds in this study. The lack of influence of active transport on the estimation of half-lives suggests that active transport is not highly significant for intravitreal elimination for the compounds included in this study.

The two models that were generated in this study are quite similar, which either can point to similar pharmacokinetics in

Table III Comparison of Half-Lives Obtained in Both Albino and Pigmented Rabbits

compound	$t_{1/2}$,albino (h)	$t_{1/2,}$ pigmented (h)	references
aztreonam	8.3	7.5	(12,13)
carbenicillin	3.5	5	(15,16)
ceftriaxone	14.1	9.1	(19,20)
ganciclovir	5.24*	7.9	(10,30–32)
gentamicin	22*	24	(33,34)
grepafloxacin	3.5	3.5	(35)

*average value

the eye of albino and pigmented rabbits, or to a bias of albino rabbits due to the majority of data acquired from albino rabbits. However, based on a comparison of the half-lives of six compounds for which the half-life had been reported both in albino and pigmented rabbits (Table III), there is no clear trend for longer elimination times in either albino or pigmented, suggesting similar rate of vitreal elimination. It is well known that many drugs are able to bind to the pigmentation (e.g. ganciclovir (10,30–32), gentamicin (33,34) and grepafloxacin (35) in our data set) and this may affect drug distribution in the tissues, such as retinal pigment epithelium. This is not reflected in the elimination rate constants, because even though some fraction of the intravitreally injected drug would bind to the melanin granules in the retinal pigment epithelium, it will mostly enter plasma that acts as a sink rather than distributing back to the vitreous.

The QSPR model presented is expected to be a useful tool in ocular drug research. The model will provide an early virtual estimate of the drug elimination rate. Thus, it will be easy to estimate drug concentration profiles after intravitreal injections at different dosing levels. With straightforward modeling approaches concentration predictions can be extended to administration of suspensions and drug delivery systems. In that case, drug dissolution or release rate can be used as input rate and the QSPR based elimination as output rate. There are some limitations in the use of the QSPR model. Firstly, we recommend that the models are used to predict the intravitreal half-life for compounds in the same chemical space as the test compounds, i.e. the descriptor values should be in the same range as the descriptor values in the model. Secondly, the half-lives in the human eye may not be the same as in the rabbit eye. The dimensions of the human eye are slightly bigger than in the rabbit eye, but the physiological factors of drug elimination (blood retina barrier, aqueous humor flow, blood aqueous humor barrier) are similar. Geometrical scaling methods can be used to obtain estimates for elimination in human eyes.

CONCLUSIONS

We have built a QSPR model for the prediction of intravitreal half-life of drug-like compounds. The model encompasses a broad chemical space and 33 *in silico* descriptors were used to build an optimal model. Overall, the QSPR model will be a useful tool in ocular drug discovery and development as it will help to reduce and refine animal experiments.

ACKNOWLEDGMENTS AND DISCLOSURES

The Academy of Finland, Magnus Ehrnooth Foundation, Medicinska Understödsföreningen för Liv och Hälsa, Orion-Farmos Research Foundation, and the Graduate School in Pharmaceutical Research are acknowledged for their support.

REFERENCES

1. Del Amo EM, Urtti A. Current and future ophthalmic drug delivery systems. A shift to the posterior segment. Drug Discov Today. 2008;13(3–4):135–43.
2. Maurice DM, Mishima S. Ocular pharmacokinetics. In: Sears ML, editor. Handbook of experimental pharmacology. Berlin-Heidelberg: Springer Verlag; 1984. p. 16–119.
3. Mannermaa E, Vellonen KS, Urtti A. Drug transport in corneal epithelium and blood-retina barrier: emerging role of transporters in ocular pharmacokinetics. Adv Drug Deliv Rev. 2006;58 (11):1136–63.
4. Maurice DM. Injection of drugs into the vitrous body. In: Leopold IH, Burns RP, editors. Symposium on ocular therapy. New York: Wiley; 1976. p. 59–72.
5. Liu W, Liu QF, Perkins R, Drusano G, Louie A, Madu A, *et al.* Pharmacokinetics of sparfloxacin in the serum and vitreous humor of rabbits: physicochemical properties that regulate penetration of quinolone antimicrobials. Antimicrob Agents Chemother. 1998;42 (6):1417–23.
6. Dias CS, Mitra AK. Vitreal elimination kinetics of large molecular weight FITC-labeled dextrans in albino rabbits using a novel microsampling technique. J Pharm Sci. 2000;89(5):572–8.
7. Durairaj C, Shah JC, Senapati S, Kompella UB. Prediction of vitreal half-life based on drug physicochemical properties: quantitative structure-pharmacokinetic relationships (QSPKR). Pharm Res. 2009;26(5):1236–60.
8. Atluri H, Mitra AK. Disposition of short-chain aliphatic alcohols in rabbit vitreous by ocular microdialysis. Exp Eye Res. 2003;76 (3):315–20.
9. Koh HJ, Cheng L, Bessho K, Jones TR, Davidson MC, Freeman WR. Intraocular properties of urokinase-derived antiangiogenic A6 peptide in rabbits. J Ocul Pharmacol Ther. 2004;20(5):439–49.
10. Hughes P, Krishnamoorthy R, Mitra A. Vitreous disposition of two acylguanosine antivirals in the albino and pigmented rabbit models: a novel ocular microdialysis technique. J Ocular Pharmacol Ther. 1996;12:209–24.
11. Zheng S, Hu C, Wei H, Lu Y, Zhang Y, Yang J, *et al.* Intravitreal pharmacokinetics of liposome-encapsulated amikacin in a rabbit model. Ophtalmology. 1993;100(11):1640–4.
12. Miglioli PA, Dorigo MT. Antibiotic levels in aqueous and vitreous humor after intraocular administration. Chemotherapy. 1989;35 (6):406–9.
13. Barza M, McCue M. Pharmacokinetics of aztreonam in rabbit eyes. Antimicrob Agents Chemother. 1983;24(4):468–73.
14. Lee JE, Lim DW, Park HJ, Shin JH, Lee SM, Oum BS. Intraocular toxicity and pharmacokinetics of candesartan in a rabbit model. Invest Ophthalmol Vis Sci. 2011;52(6):2924–9.
15. Schenk AG, Peyman GA, Paque JT. The intravitreal use of carbenicillin (Geopen) for treatment of pseudomonas endophalmitis. Acta Ophthalmol (Copenh). 1974;52:707–17.
16. Barza M, Kane A, Baum J. The effects of infection and probenecid on the transport of carbenicillin from the rabbit vitreous humor. Invest Ophthalmol Vis Sci. 1982;22(6):720–6.
17. Macha S, Mitra AK. Ocular pharmacokinetics of cephalosporins using microdialysis. J Ocul Pharmacol Ther. 2001;17(5):485–98.
18. Jay WM, Shockley RK. Toxicity and pharmacokinetics of cefepime (BMY-28142) following intravitreal injection in pigmented rabbit eyes. J Ocul Pharmacol 1988 Winter;4(4):345-349.

19. Barza M, Lynch E, Baum JL. Pharmacokinetics of newer cephalosporins after subconjunctival and intravitreal injection in rabbits. Arch Ophthalmol. 1993;111(1):121–5.
20. Shockley RK, Jay WM, Friberg TR, Aziz AM, Rissing JP, Aziz MZ. Intravitreal ceftriaxone in a rabbit model. Dose- and time-dependent toxic effects and pharmacokinetic analysis Arch Ophthalmol. 1984;102(8):1236–8.
21. Dolnak DR, Munguia D, Wiley CA, De Clercq E, Bergeron-Lynn GL, Boscher C, *et al.* Lack of retinal toxicity of the anticytomegalovirus drug (S)-1-(3-hydroxy-2-phosphonylmethoxypropyl) cytosine. Invest Ophthalmol Vis Sci. 1992;33(5):1557–63.
22. Unal M, Peyman GA, Liang C, Hegazy H, Molinari LC, Chen J, *et al.* Ocular toxicity of intravitreal clarithromycin. Retina. 1999;19(5):442–6.
23. Fiscella R, Peyman GA, Fishman PH. Duration of therapeutic levels of intravitreally injected liposome-encapsulated clindamycin in the rabbit. Can J Ophthalmol. 1987;22(6):307–9.
24. Pearson PA, Jaffe GJ, Martin DF, Cordahi GJ, Grossniklaus H, Schmeisser ET, *et al.* Evaluation of a delivery system providing long-term release of cyclosporine. Arch Ophthalmol. 1996;114(3):311–7.
25. Kwak HW, D'Amico DJ. Evaluation of the retinal toxicity and pharmacokinetics of dexamethasone after intravitreal injection. Arch Ophthalmol. 1992;110(2):259–66.
26. Gupta SK, Velpandian T, Dhingra N, Jaiswal J. Intravitreal pharmacokinetics of plain and liposome-entrapped fluconazole in rabbit eyes. J Ocul Pharmacol Ther. 2000;16(6):511–8.
27. Anand BS, Atluri H, Mitra AK. Validation of an ocular microdialysis technique in rabbits with permanently implanted vitreous probes: systemic and intravitreal pharmacokinetics of fluorescein. Int J Pharm. 2004 Aug 20;281(1–2):79–88.
28. Majumdar S, Hippalgaonkar K, Srirangam R. Vitreal kinetics of quinidine in rabbits in the presence of topically coadministered P-glycoprotein substrates/modulators. Drug Metab Dispos. 2009 Aug;37(8):1718–25.
29. Jarus G, Blumenkranz M, Hernandez E, Sossi N. Clearance of intravitreal fluorouracil. Normal and aphakic vitrectomized eyes Ophthalmology. 1985 Jan;92(1):91–6.
30. Macha S, Mitra AK. Ocular disposition of ganciclovir and its monoester prodrugs following intravitreal administration using microdialysis. Drug Metab Dispos. 2002 Jun;30(6):670–5.
31. Lopez-Cortes LF, Pastor-Ramos MT, Ruiz-Valderas R, Cordero E, Uceda-Montanes A, Claro-Cala CM, *et al.* Intravitreal pharmacokinetics and retinal concentrations of ganciclovir and foscarnet after intravitreal administration in rabbits. Invest Ophthalmol Vis Sci. 2001 Apr;42(5):1024–8.
32. Macha S, Duvvuri S, Mitra AK. Ocular disposition of novel lipophilic diester prodrugs of ganciclovir following intravitreal administration using microdialysis. Curr Eye Res. 2004 Feb;28 (2):77–84.
33. Peyman GA, May DR, Ericson ES, Apple D. Intraocular injection of gentamicin. Toxic effects of clearance Arch Ophthalmol. 1974 Jul;92(1):42–7.
34. Kane A, Barza M, Baum J. Intravitreal injection of gentamicin in rabbits. Effect of inflammation and pigmentation on half-life and ocular distribution Invest Ophthalmol Vis Sci. 1981 May;20 (5):593–7.
35. Solans C, Bregante MA, Garcia MA, Perez S. Ocular penetration of grepafloxacin after intravitreal administration in albino and pigmented rabbits. Chemotherapy. 2004 Jun;50(3):133–7.
36. Peyman GA, Nelsen P, Bennett TO. Intravitreal injection of kanamycin in experimentally induced endophthalmitis. Can J Ophthalmol. 1974 Jul;9(3):322–7.
37. Schenk AG, Peyman GA. Lincomycin by direct intravitreal injection in the treatment of experimental bacterial endophthalmitis. Albrecht Von Graefes Arch Klin Exp Ophthalmol. 1974;190 (4):281–91.
38. Daily MJ, Peyman GA, Fishman G. Intravitreal injection of methicillin for treatment of endophthalmitis. Am J Ophthalmol. 1973 Sep;76(3):343–50.
39. Velez G, Yuan P, Sung C, Tansey G, Reed GF, Chan CC, *et al.* Pharmacokinetics and toxicity of intravitreal chemotherapy for primary intraocular lymphoma. Arch Ophthalmol. 2001 Oct;119 (10):1518–24.
40. Leeds NH, Peyman GA, House B. Moxalactam (Moxam) in the treatment of experimental staphylococcal endophthalmitis. Ophthalmic Surg. 1982 Aug;13(8):653–6.
41. Iyer MN, He F, Wensel TG, Mieler WF, Benz MS, Holz ER. Clearance of intravitreal moxifloxacin. Invest Ophthalmol Vis Sci. 2006 Jan;47(1):317–9.
42. Sloane H, Peyman GA, Raichand M, West S. Netilmicin: new aminoglycoside effective against bacterial endophthalmitis. Can J Ophthalmol. 1981 Jan;16(1):22–6.
43. Gardiner PA, Michaelson IC, Rees RJ, Robson JM. The Effects of various Types of Penicillin Injected into the Vitreous. Br J Ophthalmol. 1948 Oct;32(10):768–75.
44. Duguid JP, Ginsberg M, Fraser IC, Macaskill J, Michaelson IC, Robson JM. Experimental Observations on the Intravitreous use of Penicillin and Other Drugs. Br J Ophthalmol. 1947 Apr;31 (4):193–211.
45. Duvvuri S, Gandhi MD, Mitra AK. Effect of P-glycoprotein on the ocular disposition of a model substrate, quinidine. Curr Eye Res. 2003 Dec;27(6):345–53.
46. Kim EK, Kim HB. Pharmacokinetics of intravitreally injected liposome-encapsulated tobramycin in normal rabbits. Yonsei Med J. 1990 Dec;31(4):308–14.
47. Pang MP, Branchflower RV, Chang AT, Peyman GA, Blatt H, Minatoya HK. Half-life and vitreous clearance of trifluorothymidine after intravitreal injection in the rabbit eye. Can J Ophthalmol. 1992 Feb;27(1):6–9.
48. Coco RM, Lopez MI, Pastor JC, Nozal MJ. Pharmacokinetics of intravitreal vancomycin in normal and infected rabbit eyes. J Ocul Pharmacol Ther. 1998 Dec;14(6):555–63.
49. Shen YC, Wang MY, Wang CY, Tsai TC, Tsai HY, Lee YF, *et al.* Clearance of intravitreal voriconazole. Invest Ophthalmol Vis Sci. 2007 May;48(5):2238–41.
50. Advanced Chemistry Developement, Toronto, Canada.
51. Umetrics AB, Box 7960, SE-90719 Umeå, Sweden. Simca-P. ;10.5.
52. Boxenbaum H, Battle M. Effective half-life in clinical pharmacology. J Clin Pharmacol. 1995 Aug;35(8):763–6.
53. Siefert HM, Kohlsdorfer C, Steinke W, Witt A. Pharmacokinetics of the 8-methoxyquinolone, moxifloxacin: tissue distribution in male rats. J Antimicrob Chemoter 1999 May; 43 SupplB: 61-67
54. Veber DF, Johnson SR, Cheng HY, Smith BR, Ward KW, Kopple KD. Molecular properties that influence the oral bioavailability of drug candidates. J Med Chem. 2002 Jun 6;45(12):2615–23.

7. Third article: Intravitreal Clearance and Volume of Distribution of Compounds in Rabbits: *In Silico* Prediction and Pharmacokinetic Simulations for Drug Development.

III

Reprinted with permission of Elsevier B.V.: Eva M. del Amo, Kati-Sisko Vellonen, Heidi Kidron, Arto Urtti. Intravitreal Clearance and Volume of Distribution of Compounds in Rabbits: In Silico Prediction and Pharmacokinetic Simulations for Drug Development. European Journal of Pharmaceutics and Biopharmaceutics, 2015.
http://dx.doi.org/10.1016/j.ejpb.2015.01.003

European Journal of Pharmaceutics and Biopharmaceutics xxx (2015) xxx–xxx

Contents lists available at ScienceDirect

European Journal of Pharmaceutics and Biopharmaceutics

journal homepage: www.elsevier.com/locate/ejpb

Research paper

Intravitreal clearance and volume of distribution of compounds in rabbits: *In silico* prediction and pharmacokinetic simulations for drug development

Eva M. del Amo [a,b,*], Kati-Sisko Vellonen [b], Heidi Kidron [a], Arto Urtti [a,b]

[a] Centre for Drug Research, Division of Pharmaceutical Biosciences, University of Helsinki, Helsinki, Finland
[b] School of Pharmacy, University of Eastern Finland, Kuopio, Finland

ARTICLE INFO

Article history:
Received 19 August 2014
Accepted in revised form 7 January 2015
Available online xxxx

Chemical compounds studied in this article:
1-heptanol
Amikacin
Ceftriaxone
Dexamethasone phosphate
Erythromycin
Fluorouridine
Fomivirsen
Ganciclovir
Oxacillin
Sulphacetamide
Tobramycin
Voriconazole

Keywords:
Intravitreal injection
Volume of distribution
Clearance
QSPR
Ocular drug delivery
Pharmacokinetic simulation

ABSTRACT

The aims of this research were to (1) create a curated universal database of intravitreal volumes of distribution ($V_{ss,\ ivt}$) and clearances (CL_{ivt}) of small molecular weight compounds and macromolecules and (2) to develop quantitative structure property relationship (QSPR) and pharmacokinetic models for the estimation of vitreal drug concentrations based on the compound structure.

$V_{ss,\ ivt}$ and CL_{ivt} values were determined from the available literature on intravitreal drug administration using compartmental models and curve fitting. A simple QSPR model for CL_{ivt} of small molecular weight compounds was obtained with two descriptors: $\mathrm{Log}D_{7.4}$ and hydrogen bond donor capacity. The model predicted the internal and external test sets reliably with a mean fold error of 1.50 and 1.33, respectively ($Q^2Y = 0.62$). For 80% of the compounds the $V_{ss,\ ivt}$ was 1.18–2.28 ml; too narrow range for QSPR model building. Integration of the estimated $V_{ss,\ ivt}$ and predicted CL_{ivt} parameters into pharmacokinetic simulation models allows prediction of vitreous drug concentrations after intravitreal administration.

The present work presents for the first time a database of CL_{ivt} and $V_{ss,\ ivt}$ values and the dependence of the CL_{ivt} values on the molecular structure. The study provides also useful *in silico* tools to investigate *a priori* the intravitreal pharmacokinetic profiles for intravitreally injected candidate compounds and drug delivery systems.

1. Introduction

Diseases affecting the posterior segment of the eye are becoming more and more prevalent in the ageing populations. These disorders include age-related macular degeneration, diabetic retinopathies, glaucoma, and rare retinal degenerations [1]. Currently, intravitreal drug administration is the best option to ensure therapeutic concentrations of drug in the vitreous humour, retina

Abbreviations: BAB, blood-aqueous barrier; BRB, blood-retinal barrier; CL, clearance; CL_{ivt}, intravitreal clearance; $C_{ss,\ ivt}$, steady state drug concentration in the vitreous; CV%, coefficient of variation; E, extraction ratio; $E_{aqueous\ humour}$, extraction ratio from vitreous to the anterior chamber; $E_{ciliary\ body}$, ciliary body extraction ratio; $E_{choroid}$, choroid extraction ratio; E_{iris}, iris extraction ratio; E_{ocular}, ocular extraction ratio; E_{retina}, retina extraction ratio; DDS, drug delivery system; FRB, freely rotatable bonds; HA, hydrogen bond acceptors; HD, hydrogen bond donors; Htot, total number of putative hydrogen bonds i.e. HD + HA; K_p, distribution coefficient between the tissue and vitreous; MW, molecular weight; PCA, principal component analysis; PLS, linear partial least square; PSA, polar surface area; Q, blood flow; $Q_{aqueous\ humour}$, aqueous humour flow; $Q_{ciliary\ body}$, blood flow in the ciliary body; $Q_{choroid}$, blood flow in the choroid; Q_{iris}, blood flow in the iris; Q_{ocular}, ocular blood flow; Q_{retina}, blood flow in the retina; QSPR, quantitative structure property relationship; RPE, retinal pigment epithelium; $t_{1/2}$, half-life; $t_{1/2,\ ivt}$, intravitreal half-life; V_{ss}, volume of distribution; $V_{ss,\ ivt}$, intravitreal volume of distribution.

* Corresponding author. School of Pharmacy, University of Eastern Finland, P.O. Box 1627, 70211 Kuopio, Finland. Tel.: +358 403 553 883; fax: +358 17162424.
E-mail address: eva.delamo@uef.fi (E.M. del Amo).

http://dx.doi.org/10.1016/j.ejpb.2015.01.003
0939-6411/

and choroid [2]. The drug concentrations in the vitreous are governed by $V_{ss,\ ivt}$ and CL_{ivt} of the drug. After intravitreal injection the dissolved drug will diffuse throughout the vitreous, distribute into the ocular tissues and eliminate into the systemic circulation. There are two main ocular barriers in the eye that affect the intravitreal pharmacokinetics: the blood-aqueous barrier (BAB) located in the anterior part of the eye and the blood-retinal barrier (BRB) located in the posterior part. Both barriers have epithelial and endothelial components with intercellular tight junctions. The BAB is formed by the inner non-pigmented ciliary epithelium and posterior iris epithelium and the endothelium of iris capillaries. The BRB consists of the endothelium of retinal capillaries and retinal pigment epithelium (RPE).

The volume of distribution (V_{ss}) is an apparent volume that describes the extent of drug distribution and binding to the tissues. As we have described elsewhere [3], the systemic V_{ss} values after intravenous administration can oscillate between 4 l (V_{ss} of erythropoietin contained in plasma) and 49,000 l (V_{ss} of hydroxychloroquine that accumulates in tissues). After intravitreal administration, the $V_{ss,\ ivt}$ should reflect the extent of drug distribution and binding to the ocular tissues, but these values are still mostly unknown. The CL_{ivt} represents the ocular volume that is being cleared of drug per unit of time. Thus, CL_{ivt} quantitatively describes irreversible drug elimination from the vitreous. In general, clearance (CL) can be defined by the Eq. (1):

$$CL = Q \times E \tag{1}$$

where Q is the blood flow of the organ and E the extraction ratio that varies between zero and one. Thus, CL_{ivt} is dependent on the aqueous humour flow ($Q_{aqueous\ humour}$), the blood flow in the ocular tissues (Q_{ocular}), the ability of the drug to reach the anterior chamber and get across the barriers (BRB, BAB) to the blood circulation (ocular extraction ratio or E_{ocular}). The CL_{ivt} values are rarely determined or related to the chemical structure of the drug or to the fluid flow (blood, aqueous humour) values in the eye. The intravitreal half-life ($t_{1/2,\ ivt}$) is more widely used, but this is a secondary parameter that is dependent on the primary pharmacokinetic parameters ($V_{ss,\ ivt}$ and CL_{ivt}) according the general equation of half-life ($t_{1/2}$):

$$t_{1/2} = \frac{ln2 \times V_{ss}}{CL} \tag{2}$$

QSPR approach is used to establish relationship between the chemical structure and pharmacokinetics. Intravitreal $t_{1/2}$ of compounds can be predicted with QSPR models [4,5], but the values and prediction tools of the primary intravitreal pharmacokinetic parameters, $V_{ss,\ ivt}$ or CL_{ivt}, are not available. Universal $V_{ss,\ ivt}$ and CL_{ivt} values and derived QSPR models would be very useful allowing structure based calculation of these parameters early in drug discovery. Unlike $t_{1/2,\ ivt}$, the estimated $V_{ss,\ ivt}$ and CL_{ivt} values can be used to predict vitreal drug concentrations after their inclusion in the pharmacokinetic simulation models.

In this study, we determined the $V_{ss,\ ivt}$ and CL_{ivt} values using all published literature reports with adequate quality. These values for small molecular weight (MW) compounds were used for QSPR and pharmacokinetic model building to provide tools for vitreal drug concentration predictions in drug discovery and development.

2. Materials and methods

2.1. Intravitreal primary pharmacokinetic parameters

The primary pharmacokinetic parameters for intravitreally injected compounds (CL_{ivt}, $V_{ss,\ ivt}$) were calculated from all published studies that met the quality requirements using the following procedure.

A search in PubMed database was conducted using different combinations of the key words: "intravitreal" "rabbit" and "pharmacokinetic" or "clearance". The intravitreal rabbit studies were used, since the available human data are too limited. The search yielded 367 references (1947–2013), but the number was reduced to 158 studies. For example, the studies in diseased or manipulated rabbit eyes or with suspensions and drug delivery systems (DDS) were removed, because suspensions and DDS retain in the vitreous much longer than free drug and they release drug gradually. Therefore, total and free intravitreal drug concentrations after suspension and DDS administration do not represent purely pharmacokinetics (CL_{ivt}, $V_{ss,\ ivt}$) of the drug. Further selection of data from injected intravitreal solutions was carried out (Fig. 1). When drug quantities instead of concentrations were used in the publications, the amounts were divided by the reported volume of the vitreous or by the reference value of 1.15 ml (for reference volume, see Supplementary data, Table A.1a). Average concentration values were used in the pharmacokinetic analyses.

Curve fitting with *WinNonlin® software (version 5.3, Pharsight Inc., St. Louis, USA)* was used for the analysis of $V_{ss,\ ivt}$ and CL_{ivt}. The numerical values were collected from the tables or they were extracted from the pharmacokinetic graphs using *GetData Graph Digitizer® (version 2.24. Digital River, Inc., Cologne, Germany).* For salts the equivalent dose of the free drug was used. Different compartmental models and weighting schemes were used to achieve the optimal data fitting. The level of correlation between the primary pharmacokinetic parameters had to be below 0.95 and their coefficient of variation (CV%) below 35%. The model with the lowest Akaike's information criterion (AIC) was considered to be the best one.

2.2. Generation of molecular descriptors

From small molecules, the ∗.sdf format of the structure was obtained and used as input in *ACDlabs® software (version 12, Advanced Chemistry Development, Inc., Toronto, Canada)* to generate 30 molecular descriptors: pK_a for the most acidic molecular form, pK_a for the most basic form, Log*D* at pH 5.5 and 7.4, Log*P*, MW, PSA (polar surface area), FRB (freely rotatable bonds), HD (hydrogen bond donors), HA (hydrogen bond acceptors), Htot (HD + HA), rule of 5, molar refractivity, molar volume, parachor, index of refraction, surface tension, density, polarizability, C ratio, N ratio, NO ratio, hetero ratio, halogen ratio, number of rings and number of aromatic, 3-, 4-, 5- and 6-membered rings. No computational descriptors were generated for macromolecules, because their 3D structures were not accessible.

2.3. Multivariate QSPR model generation

Multivariate QSPR models were generated for the 40 small MW molecules with $V_{ss,\ ivt}$ and CL_{ivt} values (Fig. 2). Principal component analysis (PCA) and linear partial least square (PLS) (*Simca plus®, version 10.5, Umetrics AB, Umeå, Sweden*) were used to analyse the chemical space and the relationship between the primary kinetic parameters ($V_{ss,\ ivt}$ and CL_{ivt}) and the molecular descriptors of the compound set. The descriptors were transformed with unit variance scaling and mean centring. The parameters requiring normal distribution were logarithmically transformed. Before data analysis, an external set was randomly chosen. These compounds were not used for model building, but for validating the model.

In the PCA analysis the chemical space of the compounds was defined, and outlier compounds and descriptors with too narrow range were excluded. Based on the scatter plot of the final PCA

Please cite this article in press as: E.M. del Amo et al., Intravitreal clearance and volume of distribution of compounds in rabbits: *In silico* prediction and pharmacokinetic simulations for drug development, Eur. J. Pharm. Biopharm. (2015), http://dx.doi.org/10.1016/j.ejpb.2015.01.003

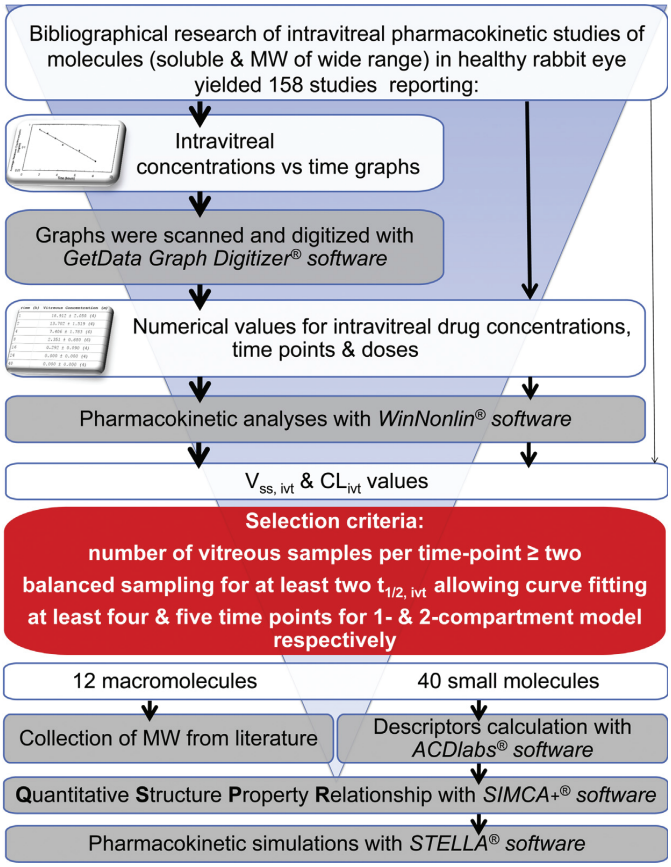

Fig. 1. The chart of the work flow.

model, a representative internal test set was selected. The training set compounds were used to calculate the PLS models of $V_{ss,\ ivt}$ and CL_{ivt}. Highly correlated variables and the variables with small influence were excluded based on the plots of PLS weight and coefficient. Furthermore, the predictions with the internal test set were carried out to confirm the improvement in the prediction accuracy.

2.4. Validation of the models

The PLS models were validated by an internal and external validation. The internal validation involved cross-validation (Q^2Y) and the regression coefficient (Q_i^2) when plotting the prediction of the internal test set against the observed experimental values. The external validation was presented as the regression coefficient (Q_e^2) when plotting the prediction of the external test set against the observed experimental values. For the three parameters (Q^2Y, Q_i^2, Q_e^2), values above 0.5 were regarded as acceptable (for more detailed description of the parameters see Supplementary material, Doc. 1).

The *Y*-randomization test (response permutation) was performed to estimate the robustness of the model [6]. The performance of the original model was compared with models built with the response data (i.e. CL_{ivt} values) randomly shuffled (appearing in a different order). When the accuracy of the permutated models was statistically significantly lower than the original one, the validity of the original model was proved (Supplementary data, Doc. 1).

2.5. Pharmacokinetic simulations

The QSPR equation for the CL_{ivt} was linked as a parameter in pharmacokinetic simulation models using *STELLA® Modelling & Simulation software* (*version 8.1.1, isee systems, Inc., Lebanon, USA*). Intravitreal concentration profiles of the small MW compounds were simulated with the predicted and observed values of CL_{ivt} and $V_{ss,\ ivt}$ using one-compartmental simulation model. Moreover, simulations of intravitreal controlled release systems were conducted. Firstly, first-order release kinetics (rate constant 0.0016 h^{-1}) at different drug loading levels was simulated. We investigated the required loading levels to reach concentrations of 1, 10, 100, 1000, 10,000, and 100,000 nM in the vitreous three months after a single injection. Secondly, we examined the relationship between zero-order release rate and steady state drug concentration ($C_{ss,\ ivt}$) in the vitreous humour at three months after drug dosing. The simulations were conducted using a fourth-order Runge–Kutta algorithm using time intervals (DT) of 0.1 h for the DDS of small compounds.

Please cite this article in press as: E.M. del Amo et al., Intravitreal clearance and volume of distribution of compounds in rabbits: *In silico* prediction and pharmacokinetic simulations for drug development, Eur. J. Pharm. Biopharm. (2015), http://dx.doi.org/10.1016/j.ejpb.2015.01.003

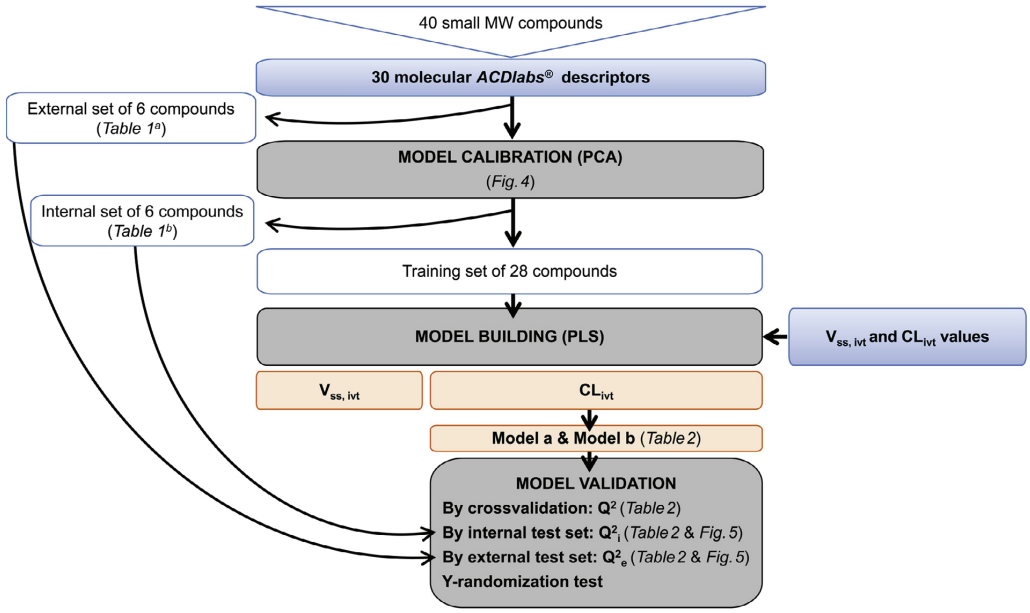

Fig. 2. The scheme of the QSPR model process.

3. Results

3.1. Literature search and pharmacokinetic analysis

The selected 158 studies reported the concentration–time profile and the dose. For most of them, $V_{ss,\ ivt}$ and CL_{ivt} were determined. Most of the compounds followed one-compartment model, but a few obeyed two-compartmental kinetics (for individual cases, see Supplementary material, Table A.2). Many studies (92, data not shown) were excluded from the analysis due to quality reasons (i.e. they did not fulfill the selection criteria in Fig. 1). The final set of 40 small compounds and 12 macromolecules with CL_{ivt} and $V_{ss,\ ivt}$ was collected (Table 1). More detailed information of the analyses based on the 66 accepted studies has been compiled in Table A.2 (Supplementary material). The final set included the intravitreal rabbit studies that used whole vitreous analysis or microdialysis and fulfilled the quality criteria (Fig. 1).

3.2. MW vs $V_{ss,\ ivt}$ and CL_{ivt} of macromolecules and small compounds

The MW of the 52 compounds ranged from 18 Da to 148 kDa. The CL_{ivt} values spanned over a wide range of values from 0.011 to 1.530 ml/h (Table 1, Fig. 3A). The $V_{ss,\ ivt}$ values showed narrow range of 0.72–3.6 ml (Table 1, Fig. 3B). No correlation between MW and $V_{ss,\ ivt}$ was observed, but an inverse proportionality between MW and CL_{ivt} was seen (regression coefficient = 0.67) (Fig. 3). Semi-logarithmic plot of MW vs $V_{ss,\ ivt}$ and logarithmic plot of MW vs $t_{1/2,\ ivt}$ were also included in Supplementary material (Figs. A.1 and A.2, respectively).

3.3. Multivariate QSPR with small MW compounds

The QSPR modelling was done with small MW compounds (range of 18–1449 Da). For these compounds, the range of the $V_{ss,\ ivt}$ and CL_{ivt} values was 0.72–3.14 ml and 0.031–1.530 ml/h, respectively. The values of $\mathrm{Log}D_{7.4}$ and HD varied from −10.59 to 2.79 and from 1 to 21, respectively (Table 1). After exclusion of the external set (Table 1), the QSPR analysis was carried out with the remaining 34 compounds. Their chemical space is represented in the PCA score plot (Fig. 4), where two first principal components ($t[1]$ and $t[2]$) explained the 42% and 21% of the variance in the data set, respectively.

Based on the PCA score plot the data set was divided in training set (28 compounds) and internal test set (6 compounds) that were well distributed all over the chemical space (Fig. 4, Table 1). The training set was used to build the PLS predictive models, and the internal set was used for the internal validation. Due to the narrow range of values, no PLS model could be generated for the $V_{ss,\ ivt}$ response. However, a PLS model for predicting $\mathrm{Log}CL_{ivt}$ was obtained and optimized. During the modelling process water was excluded as an outlier (Fig. 4) and the least influential descriptors were discarded.

As final output, a model based on the descriptors HD, $\mathrm{Log}D_{7.4}$ and PSA with a goodness of fit R^2X of 0.784 and R^2Y of 0.663 and a goodness of prediction Q^2Y of 0.633 was obtained (model **a** in Table 2). The exclusion of the PSA descriptor yielded model **b** with a goodness of fit R^2X of 0.835 and R^2Y of 0.637. The goodness of prediction Q^2Y was lower in model **b** (0.620; shown in Table 2). Both final models were built on 27 compounds and their corresponding equations were bestowed in Table 2.

Model **b** presented better predictability of the internal test set than model **a** (Q_i^2 of 0.853 vs 0.749) (Table 2). The CL_{ivt} predictions of all the compounds in both models were within the 3-fold error range (Fig. 5).

Moreover, the models were externally validated and the predictive plots and prediction accuracy are presented in Fig. 5, with a Q_e^2 of 0.905 for model **a** and improved Q_e^2 of 0.919 for model **b**. For both models, all predictions of external test set were within 3-fold error limits.

The statistical robustness of these final models was evaluated by *Y*-randomization after 50 permutations showing the validity of the models (data shown in Supplementary data, Doc. 1).

Please cite this article in press as: E.M. del Amo et al., Intravitreal clearance and volume of distribution of compounds in rabbits: *In silico* prediction and pharmacokinetic simulations for drug development, Eur. J. Pharm. Biopharm. (2015), http://dx.doi.org/10.1016/j.ejpb.2015.01.003

Table 1
The list of $V_{ss,\ ivt}$, CL_{ivt}, $t_{1/2,\ ivt}$, MW, Log$D_{7.4}$ and HD values of the curated selection of intravitreal compunds. A solid line separates the small MW molecule set and the macromolecule set.

Compound	Albino/pigmented	$V_{ss,\ ivt}$ (ml)	CL_{ivt} (ml/h)	$t_{1/2,\ ivt}$ (h)	MW	Log$D_{7.4}$	HD	References
1-Heptanol	Albino	1.84	0.718	*2.92*	116.2	2.37	1	[7]
1-Pentanol	Albino	2.16	1.530	0.98	88.15	1.35	1	[7]
Amikacin	Albino	1.37	0.035	26.94	585.6	−10.59	17	[8,9]
Aztreonam	Pigmented	1.39	0.125	7.73	435.43	−4.32	5	[10]
Carbenicillin	Albino/pigmented	1.22	0.176	4.90	378.4	−3.62	3	[11,12]
Cefazolin	Albino	1.72	0.165	7.24	454.51	−4.41	2	[13]
Cefepime	Pigmented	1.30	0.060	15.09	481.57	−2.29	4	[14]
Cefotetan	Pigmented	1.36	0.109	8.69	575.62	−3.43	5	[15]
Ceftazidime	Pigmented/albino	1.47	0.070	14.48	547.58	−2.95	5	[16–18]
Ceftriaxone[a]	Albino	1.45	0.109	9.21	554.58	−5.32	5	[19]
Cefuroxime	Pigmented	1.29	0.235	3.80	424.39	−3.48	4	[20]
Ciprofloxacin	Albino/pigmented	1.32	0.336	2.84	331.34	−0.29	2	[21,22]
Clarithromycin	Albino	0.72	0.320	1.55	747.95	2.06	4	[23]
Cyclosporine A	Albino	3.06	0.484	4.38	1202.61	2.79	5	[24]
Dexamethasone phosphate	Albino/pigmented	1.54	0.324	*18.15*	472.44	−4.64	4	[25,26]
Erythromycin[a]	Albino	1.40	0.190	5.11	733.93	1.16	5	[27]
Flomoxef[b]	Albino	1.46	0.179	5.64	496.47	−6.03	3	[28]
Fluconazole	Albino	1.93	0.753	4.69	306.27	0.45	1	[29]
Fluorouracil[b]	Pigmented	1.49	0.173	5.97	130.08	−1.64	2	[30]
Fluorouridine[a]	Pigmented	1.77	0.267	4.59	262.19	−1.97	4	[31]
Fluorouridine-5′phosphate	Albino	3.14	0.315	*21.16*	342.17	−8.09	5	[32]
Foscarnet	Pigmented	1.39	0.057	16.86	126.01	−6.91	3	[33]
Ganciclovir	Pigmented/albino	1.34	0.153	*7.18*	255.23	−1.61	5	[34–36]
Gentamicin[b]	Albino/pigmented	1.18	0.031	26.50	463.57	−8.36	12	[37–39]
Hesperetin	Albino	1.31	0.501	1.82	302.28	1.52	3	[40]
HPMPC (cidofovir)[b]	Albino	2.44	0.095	*24.84*	279.19	−5.41	5	[41]
Kanamycin	Albino	1.63	0.115	9.81	484.5	−8.67	14	[42]
Ketorolac[b]	Albino	1.48	0.283	5.98	255.27	−0.34	1	[43]
Methanol	Albino	1.17	1.300	0.62	32.04	−0.69	1	[7]
Methicillin	Albino	2.19	0.218	7.66	380.42	−2.71	2	[44]
Methotrexate	Albino	1.72	0.197	6.05	454.44	−5.1	7	[45]
Netilmicin	Albino	1.74	0.055	22.06	475.58	−6.79	11	[46]
Oxacillin[b]	Albino	2.29	0.310	5.11	401.44	−1.18	2	[47]
Penicillin	–	1.06	0.126	5.85	334.39	−1.81	2	[48]
Quinidine	Albino	0.93	0.448	1.44	324.42	0.98	1	[49]
Sulphacetamide[a]	–	2.28	0.148	10.71	214.24	−2.52	3	[48]
Tobramycin[a]	Albino	1.22	0.040	23.58	467.51	−9.54	15	[50,51]
Vancomycin	Albino/pigmented	1.46	0.039	25.89	1449.25	−4.49	21	[52,53]
Voriconazole[a]	Albino	1.37	0.421	2.25	349.31	1.21	1	[54]
Water[c]	Pigmented		1.250		18.02	−1.38	2	[55]
Aflibercept	Pigmented	1.57	0.019	56.44	97,000			[56]
Bevacizumab	Pigmented	2.02	0.019	77.17	149,000			[57,58]
Bevasiranib	Pigmented	1.10	0.022	34.83	14,224			[59]
Conbercept	Pigmented	2.10	0.015	93.73	143,000			[60]
Erythropoietin	Albino	1.21	0.014	58.14	34,000			[61]
Fomivirsen (ISIS2922)	Albino	2.22	0.027	56.18	7122			[62]
Pegaptanib	Albino	1.45	0.011	91.64	50,000			[63]
PF-04523655[c]	Pigmented	3.60	0.071	35.00	12,000			[64]
Ranibizumab	Pigmented	1.91	0.025	53.18	48,000			[58,65]
rhuMAbHER2[c]	Albino	1.78	0.015	*134.40*	148,000			[66]
Rituximab	Albino	2.76	0.016	119.34	145,000			[67]
sEphB4	–	2.28	0.011	143.58	57,800			[68]

The $t_{1/2,\ ivt}$ values in italics correspond to the terminal $t_{1/2,\ ivt}$ of two-compartmental drug, for dexamethasone phosphate and ganciclovir many pharmacokinetic studies with different compartmental models were available, then an average of the terminal and one-compartmental $t_{1/2,\ ivt}$ was calculated and marked in italic. In other cases, $t_{1/2,\ ivt}$ is based on one-compartment model.

[a] The compounds of the external test set.

[b] The compounds of the internal test set.

[c] $V_{ss,\ ivt}$ and CL_{ivt} values are from the original reference (for justification, see Supplementary material, Table A.2).

3.4. Pharmacokinetic simulations

Primary intravitreal pharmacokinetic parameters were integrated to pharmacokinetic simulation models for prediction of drug concentrations in the vitreous. Since no QSPR model for $V_{ss,\ ivt}$ was obtained, upper and lower reference values were incorporated in the simulations. This range (1.18–2.28 ml) (Table 3) represented 80% of the $V_{ss,\ ivt}$ values in the dataset. In the case of CL_{ivt}, the QSPR model **b** equation was integrated to the pharmacokinetic simulation model. The selected compounds for the simulations were heptanol and amikacin with typical high and low CL_{ivt} levels, respectively (Fig. 3). In Table 3, we presented the predicted and observed primary pharmacokinetic parameter values for the compounds.

Firstly, pharmacokinetic simulation models with the dose of 100 μg of intravitreal solution of the compounds were performed and presented (Fig. 6). The simulations with CL_{ivt} values from QSPR model yielded concentration profiles that were close to the simulations with the observed CL_{ivt} values.

Please cite this article in press as: E.M. del Amo et al., Intravitreal clearance and volume of distribution of compounds in rabbits: *In silico* prediction and pharmacokinetic simulations for drug development, Eur. J. Pharm. Biopharm. (2015), http://dx.doi.org/10.1016/j.ejpb.2015.01.003

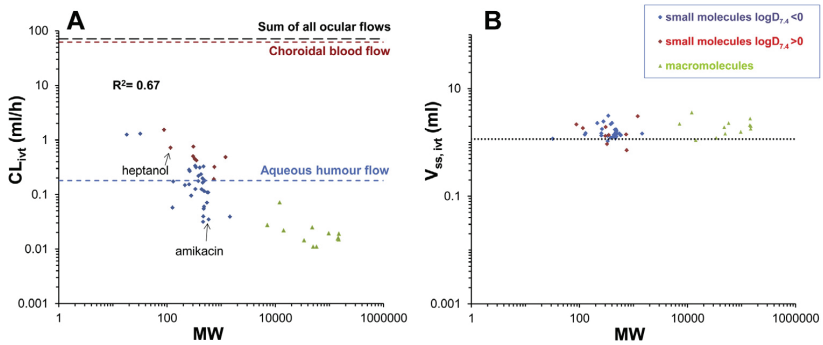

Fig. 3. The relationships between (A) MW and CL_{ivt} and (B) MW and $V_{ss,\ ivt}$ for the whole set of compounds (40 small molecular compounds and 12 macromolecules). The diamonds represent the small MW compounds with $Log D_{7.4}$ below 0 (blue symbols) and $Log D_{7.4}$ above 0 (red symbols). The triangles represent the macromolecules. In (A) the long dashed line represents the sum of the choroidal, retinal, iridial and ciliary body blood flows [69] and the aqueous humour flow [70], the short dashed lines correspond to the choroidal blood flow [69] (red) and aqueous humour flow [70] (blue). The two small compounds with the typical levels within CL_{ivt} range are pointed out. In (B) the dotted line represents the anatomical volume of the vitreous 1.15 ml (Supplementary data, Table A.1a). (For the interpretation of the references to colour in this figure legend, the reader is referred to the web version of this article.)

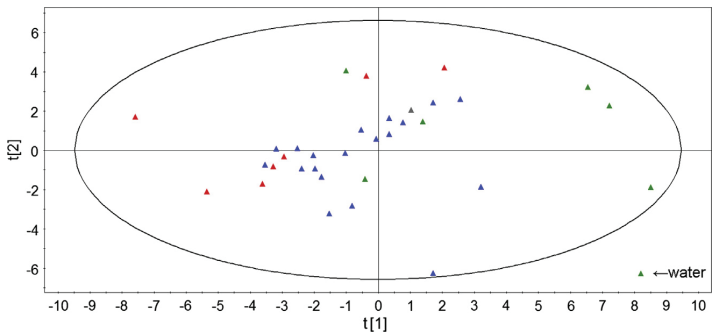

Fig. 4. The PCA score plot of the 34 intravitreal compounds that were acidic (blue), basic (red), neutral (green) and zwitterionic (grey). The ellipse depicts the 95% tolerance volume based on hotelling T^2. (For the interpretation of the references to colour in this figure legend, the reader is referred to the web version of this article.)

Table 2
The PLS models for CL_{ivt} of small MW compounds with the statistical parameter values.

	Variables	A^a	R^2X	Training set		Internal test set	External test set
				R^2Y	Q^2Y	Q_i^2	Q_e^2
Model ***a***							
$Log CL_{ivt} = -0.17411 - 0.38180\ (Log HD) - 0.00117\ PSA + 0.03686\ (Log D_{7.4})$	$+Log D_{7.4} - HD - PSA$	1	0.784	0.663	0.633	0.749	0.905
Model ***b***							
$Log CL_{ivt} = -0.25269 - 0.53747\ (Log HD) + 0.05189\ (Log D_{7.4})$	$+Log D_{7.4} - HD$	1	0.835	0.637	0.620	0.853	0.919

[a] Number of principal component.

Moreover, we simulated the administration of compounds in DDS with first-order and zero-order release kinetics. During the first-order drug release, the doses that were required to keep minimum concentrations at 1–100,000 nM for three months were simulated (Fig. 7B). Also, the intravitreal C_{max} values after different drug loadings in the DDS were modelled using the real and predicted pharmacokinetic parameters (Fig. 7C). For a dose of 10 mg (feasible with DDS injection volume of 100 µl), we estimated the intravitreal concentrations (Fig. 7A). At three months, for the high CL_{ivt} compound concentration of ≈6 µM was reached, while low CL_{ivt} drug had a simulated concentration of ≈26 µM (Fig. 7B). Thus, the minimum concentration for drug activity should be below those levels. Moreover, the expected C_{max} after delivery of 10 mg was about ≈190 µM for the high CL_{ivt} compound and ≈650 µM for the drug with low CL_{ivt} (Fig. 7C).

We used the simulations also the other way: knowing the minimum therapeutic concentration, we simulated the release rate and dose required to maintain the vitreal drug concentrations ($C_{ss,\ ivt}$) above a threshold levels. In the case of DDS with zero-order release, the release rate constants and doses required to reach $C_{ss,\ ivt}$ in the range of 1–10,000 nM were presented in Fig. 8. The simulation results based on the observed and predicted CL_{ivt} parameter overlapped. The $V_{ss,\ ivt}$ had no influence on the level of $C_{ss,\ ivt}$.

Please cite this article in press as: E.M. del Amo et al., Intravitreal clearance and volume of distribution of compounds in rabbits: *In silico* prediction and pharmacokinetic simulations for drug development, Eur. J. Pharm. Biopharm. (2015), http://dx.doi.org/10.1016/j.ejpb.2015.01.003

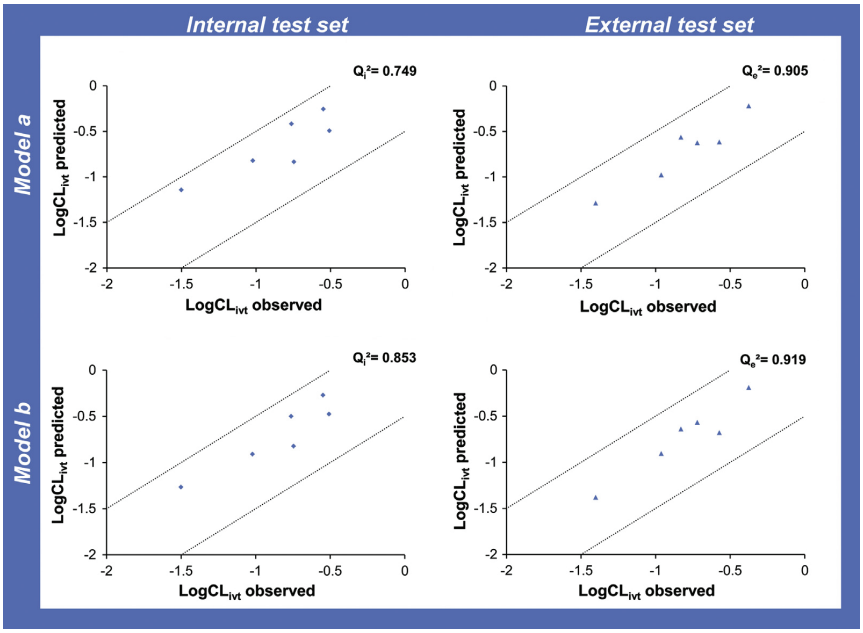

Fig. 5. The LogCL_{ivt} prediction plots of model **a** and model **b**. The diamonds represent the internal test set and the triangles represent the external test set. The dotted lines represent 3-fold error range.

Table 3
The primary PK parameter values in the simulations (1 and 2 based on predicted values and 3 in observed values).

	High CL_{ivt} compound (heptanol)		Low CL_{ivt} compound (amikacin)		Simulation numbers (shown in Figs. 6–8)
	CL_{ivt} (ml/h)	$V_{ss,\ ivt}$ (ml)	CL_{ivt} (ml/h)	$V_{ss,\ ivt}$ (ml)	
Predicted values	0.742	1.18[a]	0.034	1.18[a]	1
		2.28[b]		2.28[b]	2
Observed values	0.718	1.84	0.035	1.37	3

[a,b] Lower and upper reference values of $V_{ss,\ ivt}$ respectively.

4. Discussion

4.1. Intravitreal clearance

Even though the intravitreal pharmacokinetics are dependent on both $V_{ss,\ ivt}$ and CL_{ivt}, the CL_{ivt} seemed to have the main role in defining the ocular drug concentrations. The $V_{ss,\ ivt}$ had very narrow range of values (about 4-fold), whereas the CL_{ivt} spanned more than 100-fold range of values (Fig. 3). Therefore, the $t_{1/2,\ ivt}$ was principally affected by the CL_{ivt}.

QSPR models for CL_{ivt} of small MW compounds were built with good statistical values (R^2X and R^2Y over 0.5), namely model **b** showed a good prediction ability for both internal and external test sets (Fig. 5) with a mean fold error of 1.50 and 1.33, respectively. The model **b** descriptors (Log$D_{7.4}$, and HD) showed positive and negative influence on the CL_{ivt}. Similar dependence is seen for $t_{1/2,\ ivt}$ in the rabbit eyes [5]. The hydrogen bonding capacity and Log$D_{7.4}$ correlate with drug permeability in biomembranes supporting the role of blood-retina barrier as defining factor of CL_{ivt}.

The CL_{ivt} of the whole compound set, including macromolecules, varied between 0.011 and 1.53 ml/h. The macromolecules had smaller CL_{ivt} than the small molecules (Fig. 3), which is in line with the previous study [4]. However, MW did not determine CL_{ivt} of the small molecular compounds indicating that their diffusion in the vitreous was not rate-limiting factor or determinant of CL_{ivt}.

Intravitreal drugs can be eliminated from the eye via aqueous humour flow (1, Fig. 9A) and via permeation into the ocular vascular system, i.e. across the blood-ocular barriers to the systemic circulation (2–4, Fig. 9B). The first mechanism is operative for all drugs. The aqueous humour is formed in the ciliary processes and its convective flow drags drugs from the vitreous into the anterior chamber, where they are eliminated via the trabecular meshwork (Fig. 9A). Elimination to the ocular blood stream is relevant for the molecules that are able to cross BAB and BRB (Fig. 9B) in the anterior part (iris and ciliary body capillaries) or in the posterior part (retinal and choroidal capillaries). The posterior route of elimination is dominating due to the wide surface area of permeation and high choroidal blood flow. Lipophilic compounds have higher CL_{ivt} in line with their permeation across the BRB.

The aqueous humour flow mediated CL_{ivt} (Fig. 9A) can be defined as equation (Fig. 10):

$$CL_{ivt} = Q_{aqueous\ humour} \times E_{aqueous\ humour} \quad (3)$$

where $E_{aqueous\ humour}$ is the extraction ratio from vitreous to the anterior chamber of the eye. The average $Q_{aqueous\ humour}$ in rabbits

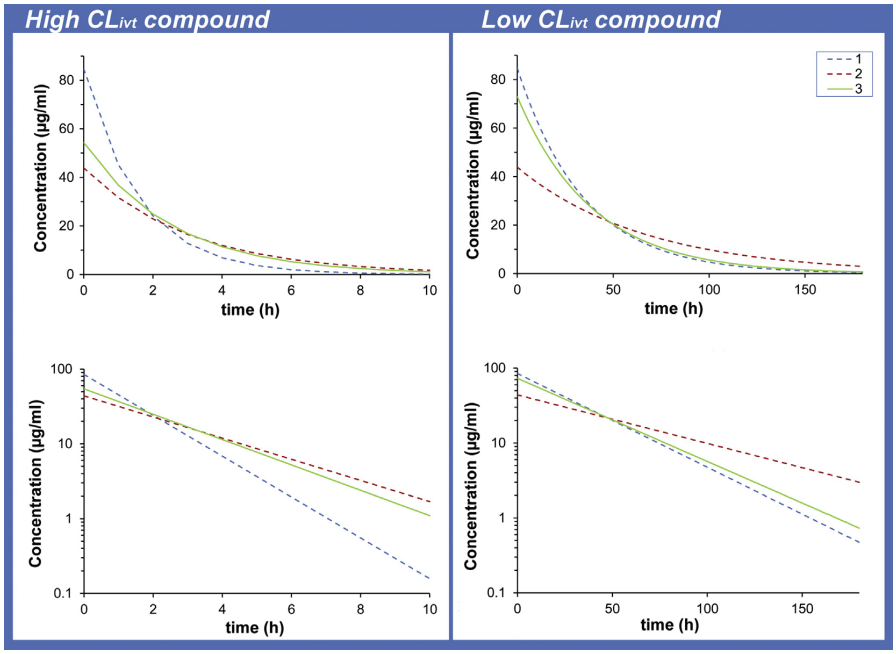

Fig. 6. The simulations of intravitreal injection of 100 µg dose of high and low CL_{ivt} compounds. The drug concentrations in the vitreous were simulated. The dashed lines correspond to simulations using the predicted CL_{ivt} values with the low $V_{ss,\ ivt}$ of 1.18 ml (blue, 1) and the high $V_{ss,\ ivt}$ of 2.28 ml (red, 2) and the solid lines are simulations with the experimental CL_{ivt} and $V_{ss,\ ivt}$ values (green, 3) (see Table 3). The simulation length for high CL_{ivt} compound was of 10 h and DT was 0.0005. For low CL_{ivt} compound the duration was 180 h and DT = 0.01. (For the interpretation of the references to colour in this figure legend, the reader is referred to the web version of this article.)

is 0.18 ml/h [70]. The compounds that are eliminated mainly by the aqueous humour flow are expected to be macromolecules that are incapable to get across BRB and BAB. Their CL_{ivt} values are 0.01–0.07 ml/h, meaning that the $E_{aqueous\ humour}$ is 0.06–0.55. This may be due to the barriers of lens, iris, ciliary body and zonules that are limiting drug transfer between the vitreal cavity and anterior chamber [71]. Interestingly, removal of the lens in rabbits decreases the $t_{1/2,\ ivt}$ of small CL_{ivt} drug, amikacin, from 25.5 to 14.3 h [9] (CL_{ivt} estimates of 0.08 and 0.05 ml/h). Even though the lens removal increased the CL_{ivt} values, it was still less than $Q_{aqueous\ humour}$ (0.18 ml/h) suggesting that the lens is only one of the factors that limit molecular exchange between the vitreous and the anterior chamber.

The CL_{ivt} of small molecular compounds can be defined with the following equation (Fig. 10):

$$CL_{ivt} = Q_{choroid} \times E_{choroid} + Q_{retina} \times E_{retina} + Q_{ciliary\ body} \times E_{ciliary\ body} + Q_{iris} \times E_{iris} + Q_{aqueous\ humour} \times E_{aqueous\ humour} \quad (4)$$

where the blood flows and the extraction ratios in choroid, retina, ciliary body and iris are represented by Q and E, respectively, with the corresponding subscripts. The values of the blood flows in the rabbit eye are: $Q_{choroid}$ = 62 ml/h, Q_{retina} = 0.66 ml/h, $Q_{ciliary\ body}$ = 4.91 ml/h, Q_{iris} = 3.72 ml/h [69] and $Q_{aqueous\ humour}$ = 0.18 ml/h [70]. $Q_{choroid}$ contributes about 87% of the total ocular flow (71.47 ml/h) (Fig. 3). If all E_{ocular} values in the equation would be equal to 1.0, the CL_{ivt} would be 71.4 ml/h. The highest CL_{ivt} was 1.53 ml/h (1-pentanol), indicating that the E_{ocular} values are $\ll$1.0, particularly in the case of drug elimination to the choroid. Therefore, CL_{ivt} is limited by blood-ocular barrier permeability, not blood flow rate. Since choroid is the main contributor in the ocular flows (Fig. 3), the E_{ocular} value must be highly dependent on the permeability in the RPE, the barrier that separates choroidal blood flow from the vitreous humour. Unlike the changes in the ocular blood flow, the changes in the RPE permeability (e.g. disease state, drug structure) should have a significant impact on the CL_{ivt}.

4.2. Intravitreal volume of distribution

No QSPR model for $V_{ss,\ ivt}$ of small compounds was constructed, because the $V_{ss,\ ivt}$ values represented so narrow range. In principle, the $V_{ss,\ ivt}$ is defined by the equation (Fig. 10):

$$V_{ss,ivt} = V_{vitreous} + V_{T_1} \times Kp_1 + V_{T_2} \times Kp_2 \ldots \quad (5)$$

where $V_{vitreous}$ is the volume of the vitreous cavity and V_T terms are the anatomical volumes of the ocular tissues (lens, ciliary body, choroid, retina…) (Table A.1, Supplementary material) and K_p values are the distribution coefficients between the tissue and vitreous. Thus, $V_{ss,\ ivt}$ depends on the tissue volumes, and the distribution coefficients for each tissue. The volume of vitreous is much higher than the tissue volumes (Table A.1), and the impact of K_p values on the $V_{ss,\ ivt}$ is only moderate. Therefore, the $V_{ss,\ ivt}$ values showed only a narrow range (Fig. 3B), and two-compartmental intravitreal pharmacokinetics was not common (Supplementary data, Table A.2). Likewise, we did not see significant effects in the $V_{ss,\ ivt}$ values in albino and pigmented rabbits.

The physiological factors affecting $V_{ss,\ ivt}$ and CL_{ivt} were summarized in Fig. 10. The anatomical volume of the vitreous is the most relevant factor for $V_{ss,\ ivt}$, whereas the permeability and surface area of RPE and choroidal blood flow are the key parameters for CL_{ivt} of small molecules.

Please cite this article in press as: E.M. del Amo et al., Intravitreal clearance and volume of distribution of compounds in rabbits: *In silico* prediction and pharmacokinetic simulations for drug development, Eur. J. Pharm. Biopharm. (2015), http://dx.doi.org/10.1016/j.ejpb.2015.01.003

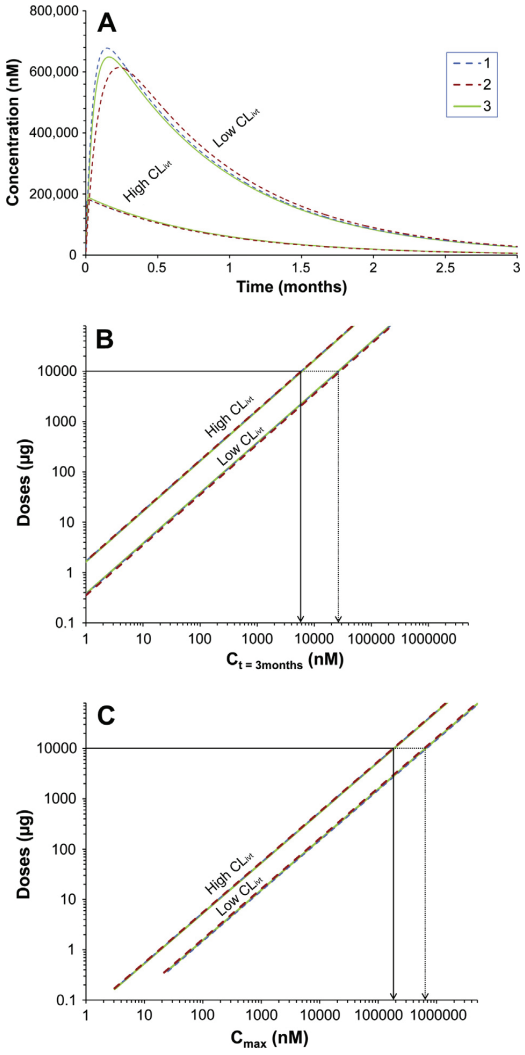

Fig. 7. The simulations of intravitreal drug delivery with first-order release DDS. The high and low CL_{ivt} compounds were released at the rate of 0.0016 h^{-1}. (A) The simulations of the observed and predicted intravitreal pharmacokinetic profiles of the DDS loaded with 10 mg of the compounds. (B) The doses required to achieve the drug concentrations on the *x*-axis after three months. (C) The doses required to achieve different C_{max} values in the vitreous. The dashed lines show the simulations with predicted CL_{ivt} values with low $V_{ss,\ ivt}$ value (blue, 1) and high $V_{ss,\ ivt}$ value (red, 2) and solid lines are the simulations with the observed values (3). The solid and dotted arrows show the concentrations achieved at the dose of 10 mg of the high and low CL_{ivt} molecules respectively. (For the interpretation of the references to colour in this figure legend, the reader is referred to the web version of this article.)

4.3. Pharmacokinetic simulations

Even though $V_{ss,\ ivt}$ could not be predicted from the molecular structure, its lower and upper limiting values were defined reliably, since 80% of the compounds had $V_{ss,\ ivt}$ of 1.18–2.29 ml. Due to the narrow scale of the $V_{ss,\ ivt}$ values and predictability of QSPR model for CL_{ivt}, the estimates of $V_{ss,\ ivt}$ and CL_{ivt} were used in the pharmacokinetic simulations. Such simulations can be done early in drug discovery and development, even before the drug synthesis. For drug solutions, the simulated profiles were close to the observed values (Fig. 6). This was excellent level of prediction taking into account that these simulations were solely based on computational parameters.

The *in silico* tools were also used for dosage form design to estimate the required release rates that are needed to reach the target product profile. For example, the dose required in first-order release DDS for achieving a target concentration was simulated (Fig. 7B). The required doses were ≈4-fold bigger for the high CL_{ivt} compound than for the low CL_{ivt} drug. In addition, we calculated the expected C_{max} values (Fig. 7C); in this case 3.5-fold smaller value was seen for the high CL_{ivt} compound compared to the low CL_{ivt} one. In the case of zero-order release, required dosing for a target $C_{ss,\ ivt}$ was 20 times higher for high CL_{ivt} than low CL_{ivt} compounds (Fig. 8B). These dosing predictions are relevant for drug formulators, because only small doses can be loaded in small intravitreal formulations (maximum volume is about 100 µl) and it is often difficult to formulate drug at high concentrations.

This approach can be used for any controlled release system or release profile, but it is important to note that the simulated input rate is *in vivo* release rate that may differ from the *in vitro* rate. Pharmacokinetics of the free drug is governed by CL_{ivt} and $V_{ss,\ ivt}$. In general, the CL_{ivt} and $V_{ss,\ ivt}$ values are not modified by the clinically used DDS or other controlled release systems (implants, inserts, microspheres, gels). However, CL_{ivt} and $V_{ss,\ ivt}$ might be affected in the case of experimental intracellular targeting systems (e.g. liposomes, nanoparticles).

4.4. Importance of the data and models

This study presented for the first time a universal view on the $V_{ss,\ ivt}$ and CL_{ivt} values that could be related to the physiology and anatomy of the eye to yield mechanistic understanding of drug distribution and elimination. Furthermore, the presented CL_{ivt} and $V_{ss,\ ivt}$ values of individual compounds (Tables 1 and A.2) may be used for the predictions of intravitreal drug concentrations in the context of DDS design (e.g. dosing levels, release rate effects). Likewise, predicted CL_{ivt} and $V_{ss,\ ivt}$ values can be used to guide delivery of the new drug candidates to the vitreous.

These *in silico* tools do not replace *in vivo* studies, but they may reduce and refine rabbit experiments, accelerate preclinical ocular drug development, and augment clinical study design. Even though our model is based on rabbit data, it can be further scaled up to the human eye, since both species are similar, but not identical, in terms of drug binding to tissues, ocular flows and barriers affecting the intravitreal pharmacokinetic (Fig. 10). For example, bevacizumab has a similar CL_{ivt} in human and in rabbit, 0.025 ml/h [72] and 0.019 ml/h (Table 1), respectively. The $V_{ss,\ ivt}$ value in human is 3.17 ml [72] and 2.02 ml in rabbit (Table 1), both of them being close to the anatomical volumes of vitreous (i.e. 4 ml in humans [73] and 1.15 ml in rabbits (Supplementary data, Table A.1a). However, the disease state might render blood-ocular barriers more leaky and, thereby, the CL_{ivt} values might change. The liquefaction of vitreous in the elderly patients is another factor that might affect ocular pharmacokinetics [74]. However, diffusion coefficients of small compounds are very similar in vitreous and water and therefore, this factor may not be important. Bevacizumab is a large molecule with established pharmacokinetics in rabbit (Table 1) and human [72] vitreous. In this case, only moderate difference is seen between the CL_{ivt} values of healthy rabbits and human patients with exudative macular degeneration. Based on these arguments, we propose that our *in silico* models can be further developed for intravitreal pharmacokinetics in humans.

Please cite this article in press as: E.M. del Amo et al., Intravitreal clearance and volume of distribution of compounds in rabbits: *In silico* prediction and pharmacokinetic simulations for drug development, Eur. J. Pharm. Biopharm. (2015), http://dx.doi.org/10.1016/j.ejpb.2015.01.003

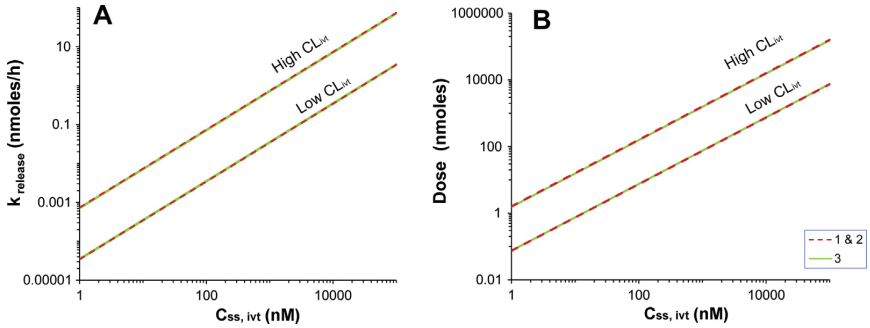

Fig. 8. The simulations of intravitreal zero-order drug delivery. (A) The relationship between the release rate and steady-state concentrations in the vitreous for low and high CL_{ivt} compounds. (B) The relationship between the dose delivered in three months and the steady-state concentrations in the vitreous for low and high CL_{ivt} compounds. The dashed red lines correspond to simulations using the predicted CL_{ivt} value (1 and 2) and the solid green lines correspond to simulations using the experimental CL_{ivt} (3) (see Table 3). (For the interpretation of the references to colour in this figure legend, the reader is referred to the web version of this article.)

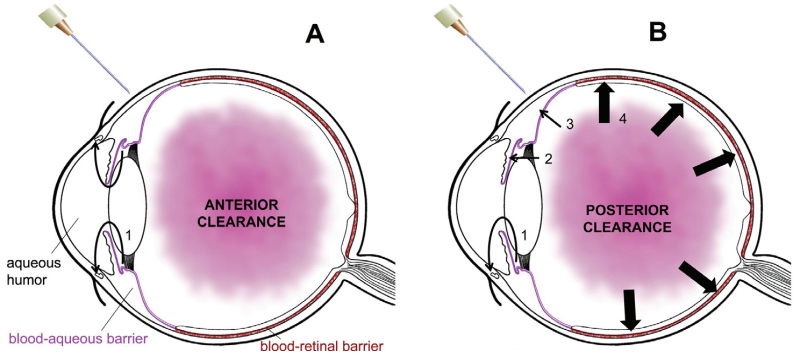

Fig. 9. The routes of drug elimination after intravitreal injection. (A) Anterior elimination of the drug by aqueous humour flow (1). (B) Drug elimination through blood-ocular barriers. The drug permeates through the posterior iris epithelium into iris vein and is drained by vortex veins (2), through the non-pigmented ciliary epithelium to ciliary muscles and from the ciliary plexus to the episcleral veins (3), to the retinal capillaries and through the RPE into the choroid and systemic circulation (4).

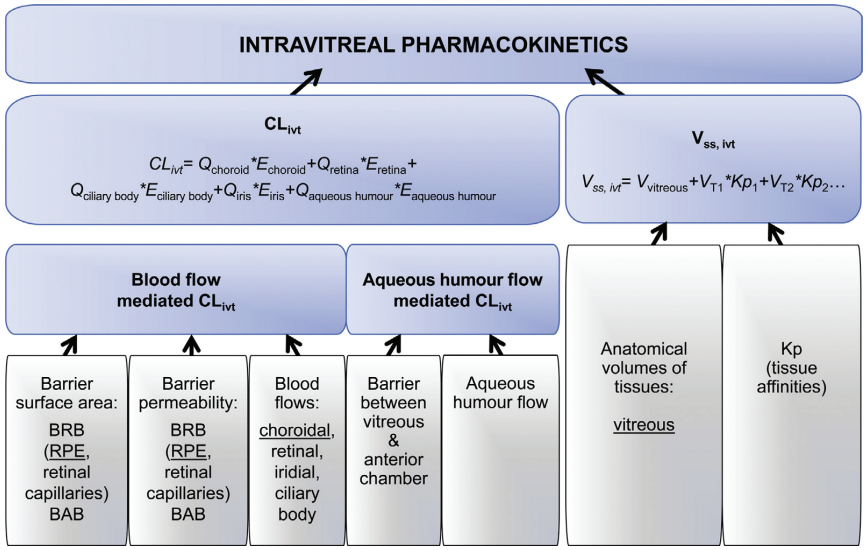

Fig. 10. Physiological factors affecting the intravitreal pharmacokinetics. The most important factors have been underlined.

Please cite this article in press as: E.M. del Amo et al., Intravitreal clearance and volume of distribution of compounds in rabbits: *In silico* prediction and pharmacokinetic simulations for drug development, Eur. J. Pharm. Biopharm. (2015), http://dx.doi.org/10.1016/j.ejpb.2015.01.003

5. Conclusions

The $V_{ss,\ ivt}$ and CL_{ivt} predictions are needed for the ocular pharmaceutical research and development. In our study, CL_{ivt} was highly dependent on molecular structure, but it could be predicted reliably with two to three molecular descriptors. On the contrary, the $V_{ss,\ ivt}$ was almost constant regardless of the molecular structure. These models were linked to pharmacokinetic models to estimate drug delivery system properties in pharmacokinetic context. These data and computational tools will improve the ocular pharmacokinetic understanding and give valuable guidance in the design of compounds and drug delivery systems.

Conflict of interest

There are no conflicts of interest.

Acknowledgements

This study was supported by the Finnish Cultural Foundation (Eva M. del Amo) and Academy of Finland (Kati-Sisko Vellonen, Heidi Kidron, Arto Urtti). The authors would like to thank Dr. Veli-Pekka Ranta (School of Pharmacy, University of Eastern Finland) and Dr. Maija Lahtela-Kakkonen (School of Pharmacy, University of Eastern Finland) for the discussions and practical help during the research process.

Appendix A. Supplementary material

Supplementary data associated with this article can be found, in the online version, at http://dx.doi.org/10.1016/j.ejpb.2015.01.003.

References

[1] K. Zhang, L. Zhang, R.N. Weinreb, Ophthalmic drug discovery: novel targets and mechanisms for retinal diseases and glaucoma, Nat. Rev. Drug Discov. 11 (2012) 541–559.
[2] E.M. del Amo, A. Urtti, Current and future ophthalmic drug delivery systems. A shift to the posterior segment, Drug Discov. Today 13 (2008) 135–143.
[3] E.M. del Amo, L. Ghemtio, H. Xhaard, M. Yliperttula, A. Urtti, H. Kidron, Applying linear and non-linear methods for parallel prediction of volume of distribution and fraction of unbound drug, PLoS One 8 (2013) e74758.
[4] C. Durairaj, J.C. Shah, S. Senapati, U.B. Kompella, Prediction of vitreal half-life based on drug physicochemical properties: quantitative structure-pharmacokinetic relationships (QSPKR), Pharm. Res. 26 (2009) 1236–1260.
[5] H. Kidron, E.M. del Amo, K.S. Vellonen, A. Urtti, Prediction of the vitreal half-life of small molecular drug-like compounds, Pharm. Res. 29 (2012) 3302–3311.
[6] A. Tropsha, P. Gramatica, V.K. Gombar, The importance of being earnest: validation is the absolute essential for successful application and interpretation of QSPR models, QSAR Comb. Sci. 22 (2003) 69–77.
[7] H. Atluri, A.K. Mitra, Disposition of short-chain aliphatic alcohols in rabbit vitreous by ocular microdialysis, Exp. Eye Res. 76 (2003) 315–320.
[8] S. Zeng, C. Hu, H. Wei, Y. Lu, Y. Zhang, J. Yang, G. Yun, W. Zou, B. Song, Intravitreal pharmacokinetics of liposome-encapsulated amikacin in a rabbit model, Ophthalmology 100 (1993) 1640–1644.
[9] B.A. Mandell, T.A. Meredith, E. Aguilar, A. el-Massry, A. Sawant, S. Gardner, Effects of inflammation and surgery on amikacin levels in the vitreous cavity, Am. J. Ophthalmol. 115 (1993) 770–774.
[10] M. Barza, M. McCue, Pharmacokinetics of aztreonam in rabbit eyes, Antimicrob. Agents Chemother. 24 (1983) 468–473.
[11] A.G. Schenk, G.A. Peyman, J.T. Paque, The intravitreal use of carbenicillin (Geopen) for treatment od pseudomonas endophthalmitis, Acta Ophthalmol. (Copenh) 52 (1974) 707–717.
[12] M. Barza, A. Kane, J. Baum, The effects of infection and probenecid on the transport of carbenicillin from the rabbit vitreous humor, Invest. Ophthalmol. Vis. Sci. 22 (1982) 720–726.
[13] L. Ficker, T.A. Meredith, S. Gardner, L.A. Wilson, Cefazolin levels after intravitreal injection. Effects of inflammation and surgery, Invest. Ophthalmol. Vis. Sci. 31 (1990) 502–505.
[14] W.M. Jay, R.K. Shockley, Toxicity and pharmacokinetics of cefepime (BMY-28142) following intravitreal injection in pigmented rabbit eyes, J. Ocul. Pharmacol. 4 (1988) 345–349.
[15] W. Philipp, K. Schmid, H.J. Steiner, B. Pumpel, F. Allerberger, H.P. Aichberger, W. Mayer, Toxicity and clearance of intravitreal cefotetan, Graefes Arch. Clin. Exp. Ophthalmol. 228 (1990) 475–480.
[16] W.M. Jay, P. Fishman, M. Aziz, R.K. Shockley, Intravitreal ceftazidime in a rabbit model: dose- and time-dependent toxicity and pharmacokinetic analysis, J. Ocul. Pharmacol. 3 (1987) 257–262.
[17] K. Mochizuki, Y. Yamashita, M. Torisaki, M. Komatsu, T. Tanahashi, K. Kawasaki, Intraocular kinetics of ceftazidime (Modacin), Ophthalmic Res. 24 (1992) 150–154.
[18] T.A. Meredith, Antimicrobial pharmacokinetics in endophthalmitis treatment: studies of ceftazidime, Trans. Am. Ophthalmol. Soc. 91 (1993) 653–699.
[19] R.K. Shockley, W.M. Jay, T.R. Friberg, A.M. Aziz, J.P. Rissing, M.Z. Aziz, Intravitreal ceftriaxone in a rabbit model. Dose- and time-dependent toxic effects and pharmacokinetic analysis, Arch. Ophthalmol. 102 (1984) 1236–1238.
[20] S. Koul, A. Philipson, B.T. Philipson, E. Kock, P. Nylen, Intraocular levels of cefuroxime in uninflamed rabbit eyes, Acta Ophthalmol. (Copenh) 68 (1990) 455–465.
[21] P.A. Pearson, D.P. Hainsworth, P. Ashton, Clearance and distribution of ciprofloxacin after intravitreal injection, Retina 13 (1993) 326–330.
[22] A.L. Marchese, V.S. Slana, E.W. Holmes, W.M. Jay, Toxicity and pharmacokinetics of ciprofloxacin, J. Ocul. Pharmacol. 9 (1993) 69–76.
[23] M. Unal, G.A. Peyman, C. Liang, H. Hegazy, L.C. Molinari, J. Chen, S. Brun, P.J. Tarcha, Ocular toxicity of intravitreal clarithromycin, Retina 19 (1999) 442–446.
[24] P. Pearson, G.J. Jaffe, D.F. Martin, et al., Evaluation of a delivery system providing long-term release of cyclosporine, Arch. Ophthalmol. 114 (1996) 311–317.
[25] R.O. Graham, G.A. Peyman, Intravitreal injection of dexamethasone. Treatment of experimentally induced endophthalmitis, Arch. Ophthalmol. 92 (1974) 149–154.
[26] H.W. Kwak, D.J. D'Amico, Evaluation of the retinal toxicity and pharmacokinetics of dexamethasone after intravitreal injection, Arch. Ophthalmol. 110 (1992) 259–266.
[27] H.I. Meisels, G.A. Peyman, Intravitreal erythromycin in the treatment of induced staphylococcal endophthalmitis, Ann. Ophthalmol. 8 (1976) 939–943.
[28] K. Mochizuki, M. Torisaki, Y. Yamashita, M. Komatsu, T. Tanahashi, Intravitreal flomoxef sodium in rabbits, Ophthalmic Res. 25 (1993) 128–136.
[29] S.K. Gupta, T. Velpandian, N. Dhingra, J. Jaiswal, Intravitreal pharmacokinetics of plain and liposome-entrapped fluconazole in rabbit eyes, J. Ocul. Pharmacol. Ther. 16 (2000) 511–518.
[30] G. Jarus, M. Blumenkranz, E. Hernandez, N. Sossi, Clearance of intravitreal fluorouracil. Normal and aphakic vitrectomized eyes, Ophthalmology 92 (1985) 91–96.
[31] D.S. Huang, M.S. Blumenkranz, E. Hernandez, M. Hartzer, Uptake and clearance of 5-fluorouridine following subconjunctival and intravitreal injection, Retina 8 (1988) 205–209.
[32] K.K. Assil, M. Hartzer, R.N. Weinreb, M. Nehorayan, T. Ward, M. Blumenkranz, Liposome suppression of proliferative vitreoretinopathy. Rabbit model using antimetabolite encapsulated liposomes, Invest. Ophthalmol. Vis. Sci. 32 (1991) 2891–2897.
[33] C. Claro, R. Ruiz, E. Cordero, M.T. Pastor, L.F. Lopez-Cortes, M. Jimenez-Castellanos, M. Lucero, Determination and pharmacokinetic profile of liposomal foscarnet in rabbit ocular tissues after intravitreal administration, Exp. Eye Res. 88 (2009) 528–534.
[34] L.F. Lopez-Cortes, M.T. Pastor-Ramos, R. Ruiz-Valderas, E. Cordero, A. Uceda-Montanes, C.M. Claro-Cala, M.J. Lucero-Munoz, Intravitreal pharmacokinetics and retinal concentrations of ganciclovir and foscarnet after intravitreal administration in rabbits, Invest. Ophthalmol. Vis. Sci. 42 (2001) 1024–1028.
[35] S. Duvvuri, K.G. Janoria, D. Pal, A.K. Mitra, Controlled delivery of ganciclovir to the retina with drug-loaded Poly(d, L-lactide-co-glycolide) (PLGA) microspheres dispersed in PLGA–PEG–PLGA gel: a novel intravitreal delivery system for the treatment of cytomegalovirus retinitis, J. Ocul. Pharmacol. Ther. 23 (2007) 264–274.
[36] K.G. Janoria, S.H. Boddu, Z. Wang, D.K. Paturi, S. Samanta, D. Pal, A.K. Mitra, Vitreal pharmacokinetics of biotinylated ganciclovir: role of sodium-dependent multivitamin transporter expressed on retina, J. Ocul. Pharmacol. Ther. 25 (2009) 39–49.
[37] G.A. Peyman, D.R. May, E.S. Ericson, D. Apple, Intraocular injection of gentamicin. Toxic effects of clearance, Arch. Ophthalmol. 92 (1974) 42–47.
[38] A. Kane, M. Barza, J. Baum, Intravitreal injection of gentamicin in rabbits. Effect of inflammation and pigmentation on half-life and ocular distribution, Invest. Ophthalmol. Vis. Sci. 20 (1981) 593–597.
[39] P.H. Fishman, G.A. Peyman, T. Lesar, Intravitreal liposome-encapsulated gentamicin in a rabbit model. Prolonged therapeutic levels, Invest. Ophthalmol. Vis. Sci. 27 (1986) 1103–1106.
[40] R. Srirangam, K. Hippalgaonkar, S. Majumdar, Intravitreal kinetics of hesperidin, hesperetin, and hesperidin G: effect of dose and physicochemical properties, J. Pharm. Sci. 101 (2012) 1631–1638.
[41] D.R. Dolnak, D. Munguia, C.A. Wiley, E. De Clercq, G.L. Bergeron-Lynn, C. Boscher, J.D. Connor, C. Sherwood, E. Capparelli, R. Armani, Lack of retinal toxicity of the anticytomegalovirus drug (S)-1-(3-hydroxy-2-phosphonylmethoxypropyl) cytosine, Invest. Ophthalmol. Vis. Sci. 33 (1992) 1557–1563.
[42] G.A. Peyman, P. Nelsen, T.O. Bennett, Intravitreal injection of kanamycin in experimentally induced endophthalmitis, Can. J. Ophthalmol. 9 (1974) 322–327.
[43] M. Wang, W. Liu, Q. Lu, H. Zeng, S. Liu, Y. Yue, H. Cheng, Y. Liu, M. Xue, Pharmacokinetic comparison of ketorolac after intracameral, intravitreal, and suprachoroidal administration in rabbits, Neurosurgery (2012).

Please cite this article in press as: E.M. del Amo et al., Intravitreal clearance and volume of distribution of compounds in rabbits: *In silico* prediction and pharmacokinetic simulations for drug development, Eur. J. Pharm. Biopharm. (2015), http://dx.doi.org/10.1016/j.ejpb.2015.01.003

[44] M.J. Daily, G.A. Peyman, G. Fishman, Intravitreal injection of methicillin for treatment of endophthalmitis, Am. J. Ophthalmol. 76 (1973) 343–350.
[45] G. Velez, P. Yuan, C. Sung, et al., Pharmacokinetics and toxicity of intravitreal chemotherapy for primary intraocular lymphoma, Arch. Ophthalmol. 119 (2001) 1518–1524.
[46] H. Sloane, G.A. Peyman, M. Raichand, S. West, Netilmicin: new aminoglycoside effective against bacterial endophthalmitis, Can. J. Ophthalmol. 16 (1981) 22–26.
[47] R.T. Kasbeer, G.A. Peyman, Intravitreal oxacillin in experimental staphylococcal endophthalmitis, Albrecht Von Graefes Arch. Klin. Exp. Ophthalmol. 196 (1975) 279–286.
[48] J.P. Duguid, M. Ginsberg, I.C. Fraser, J. Macaskill, I.C. Michaelson, J.M. Robson, Experimental observations on the intravitreous use of penicillin and other drugs, Br. J. Ophthalmol. 31 (1947) 193–211.
[49] S. Duvvuri, M.D. Gandhi, A.K. Mitra, Effect of P-glycoprotein on the ocular disposition of a model substrate, quinidine, Curr. Eye Res. 27 (2003) 345–353.
[50] T.O. Bennett, G.A. Peyman, Use of tobramycin in eradicating experimental bacterial endophthalmitis, Albrecht Von Graefes Arch. Klin. Exp. Ophthalmol. 191 (1974) 93–107.
[51] E.K. Kim, H.B. Kim, Pharmacokinetics of intravitreally injected liposome-encapsulated tobramycin in normal rabbits, Yonsei Med. J. 31 (1990) 308–314.
[52] H.E. Aguilar, T.A. Meredith, A. el-Massry, A. Shaarawy, M. Kincaid, J. Dick, D.J. Ritchie, R.M. Reichley, M.K. Neisman, Vancomycin levels after intravitreal injection. Effects of inflammation and surgery, Retina 15 (1995) 428–432.
[53] R.M. Coco, M.I. Lopez, J.C. Pastor, M.J. Nozal, Pharmacokinetics of intravitreal vancomycin in normal and infected rabbit eyes, J. Ocul. Pharmacol. Ther. 14 (1998) 555–563.
[54] Y.C. Shen, M.Y. Wang, C.Y. Wang, T.C. Tsai, H.Y. Tsai, Y.F. Lee, L.C. Wei, Clearance of intravitreal voriconazole, Invest. Ophthalmol. Vis. Sci. 48 (2007) 2238–2241.
[55] S. Sirossian, J.I. Usansky, D.D. Tang-Liu, Ocular distribution and elimination of 3H-inulin and 3H2O following intravitreal administration to Dutch-belted rabbits, Pharm. Res. 12 (Suppl.) (1995) (Abstract 8052).
[56] J.B. Christoforidis, M.M. Williams, S. Kothandaraman, K. Kumar, F.J. Epitropoulos, M.V. Knopp, Pharmacokinetic properties of intravitreal I-124-aflibercept in a rabbit model using PET/CT, Curr. Eye Res. 37 (2012) 1171–1174.
[57] S.J. Bakri, M.R. Snyder, J.M. Reid, J.S. Pulido, R.J. Singh, Pharmacokinetics of intravitreal bevacizumab (Avastin), Ophthalmology 114 (2007) 855–859.
[58] J.B. Christoforidis, M.M. Carlton, M.V. Knopp, G.H. Hinkle, PET/CT imaging of I-124-radiolabeled bevacizumab and ranibizumab after intravitreal injection in a rabbit model, Invest. Ophthalmol. Vis. Sci. 52 (2011) 5899–5903.
[59] N.S. Dejneka, S. Wan, O.S. Bond, D.J. Kornbrust, S.J. Reich, Ocular biodistribution of bevasiranib following a single intravitreal injection to rabbit eyes, Mol. Vis. 14 (2008) 997–1005.
[60] H. Li, N. Lei, M. Zhang, Y. Li, H. Xiao, X. Hao, Pharmacokinetics of a long-lasting anti-VEGF fusion protein in rabbit, Exp. Eye Res. 97 (2012) 154–159.
[61] J.F. Zhang, Y.L. Wu, J.Y. Xu, W. Ye, Y. Zhang, H. Weng, W.D. Shi, G.X. Xu, L. Lu, W. Dai, S.H. Sinclair, W.Y. Li, G.T. Xu, Pharmacokinetic and toxicity study of intravitreal erythropoietin in rabbits, Acta Pharmacol. Sin. 29 (2008) 1383–1390.
[62] J.M. Leeds, S.P. Henry, L. Truong, A. Zutshi, A.A. Levin, D. Kornbrust, Pharmacokinetics of a potential human cytomegalovirus therapeutic, a phosphorothioate oligonucleotide, after intravitreal injection in the rabbit, Drug Metab. Dispos. 25 (1997) 921–926.
[63] Eyetech Study Group, Preclinical and phase 1A clinical evaluation of an anti-VEGF pegylated aptamer (EYE001) for the treatment of exudative age-related macular degeneration, Retina 22 (2002) 143–152.
[64] T.R. Johnson, , Pharmacokinetic and ocular distribution of PF-04523655 and RTP801-inhibiting siRNA, following intravitreal administration in rabbits, Invest. Ophthalmol. Vis. Sci. 51 (2010) (E-Abstract 2442).
[65] S.J. Bakri, M.R. Snyder, J.M. Reid, J.S. Pulido, M.K. Ezzat, R.J. Singh, Pharmacokinetics of Intravitreal Ranibizumab (Lucentis), Ophthalmology 114 (2007) 2179–2182.
[66] J. Mordenti, K. Thomsen, V. Licko, L. Berleau, J.W. Kahn, R.A. Cuthbertson, E.T. Duenas, A.M. Ryan, C. Schofield, T.W. Berger, Y.G. Meng, J. Cleland, Intraocular pharmacokinetics and safety of a humanized monoclonal antibody in rabbits after intravitreal administration of a solution or a PLGA microsphere formulation, Toxicol. Sci. 52 (1999) 101–106.
[67] H. Kim, K.G. Csaky, C.C. Chan, P.M. Bungay, R.J. Lutz, R.L. Dedrick, P. Yuan, J. Rosenberg, A.J. Grillo-Lopez, W.H. Wilson, M.R. Robinson, The pharmacokinetics of rituximab following an intravitreal injection, Exp. Eye Res. 82 (2006) 760–766.
[68] M. Brar, L. Cheng, R. Yuson, F. Mojana, W.R. Freeman, P.S. Gill, Ocular safety profile and intraocular pharmacokinetics of an antagonist of EphB4/EphrinB2 signalling, Br. J. Ophthalmol. 94 (2010) 1668–1673.
[69] S.F.E. Nilsson, A. Alm, Determination of ocular blood flows with the microsphere method, in: Determination of Ocular Blood Flows with the Microsphere Method. Ocular Blood Flow, Springer, 2012.
[70] Y.E. Barany, V.E. Kinsey, The rate of flow of aqueous humor; the rate of disappearance of para-aminohippuric acid, radioactive rayopake, and radioactive diodrast from the aqueous humor of rabbits, Am. J. Ophthalmol. 32 (Pt. 2) (1949) 177–188.
[71] D.M. Maurice, S. Mishima, Ocular pharmacokinetics, in: Ocular Pharmacokinetics Pharmacology of the Eye, Springer-Verlag, 1984.
[72] Q. Zhu, F. Ziemssen, S. Henke-Fahle, O. Tatar, P. Szurman, S. Aisenbrey, N. Schneiderhan-Marra, X. Xu, Tubingen Bevacizumab Study Group, S. Grisanti, Vitreous levels of bevacizumab and vascular endothelial growth factor-A in patients with choroidal neovascularization, Ophthalmology 115 (2008) 1750–1755 (1755.e1).
[73] A.J. Ruby, G.A. Williams, M.S. Blumenkranz, Vitreous humor, in: Vitreous humor, Lippincott Williams & Wilkins, 2006.
[74] A. Laude, L.E. Tan, C.G. Wilson, G. Lascaratos, M. Elashry, T. Aslam, N. Patton, B. Dhillon, Intravitreal therapy for neovascular age-related macular degeneration and inter-individual variations in vitreous pharmacokinetics, Prog. Retin. Eye Res. 29 (2010) 466–475.

Please cite this article in press as: E.M. del Amo et al., Intravitreal clearance and volume of distribution of compounds in rabbits: *In silico* prediction and pharmacokinetic simulations for drug development, Eur. J. Pharm. Biopharm. (2015), http://dx.doi.org/10.1016/j.ejpb.2015.01.003

8. Fourth article: Rabbit as an animal model for intravitreal pharmacokinetics: Clinical predictability and quality of the published data.

IV

Eva M. del Amo, Arto Urtti. Rabbit as an animal model for intravitreal pharmacokinetics: Clinical predictability and quality of the published data. Experimental Eye Research, 2015, 137, 111-124.
http://dx.doi.org/10.1016/j.exer.2015.05.003

Experimental Eye Research 137 (2015) 111–124

Contents lists available at ScienceDirect

Experimental Eye Research

journal homepage: www.elsevier.com/locate/yexer

Review

Rabbit as an animal model for intravitreal pharmacokinetics: Clinical predictability and quality of the published data

Eva M. del Amo [a, b], Arto Urtti [a, b, *]

[a] School of Pharmacy, University of Eastern Finland, Kuopio, Finland
[b] Centre for Drug Research, Division of Pharmaceutical Biosciences, Faculty of Pharmacy, University of Helsinki, Finland

ARTICLE INFO

Article history:
Received 5 March 2015
Received in revised form
7 May 2015
Accepted in revised form 10 May 2015
Available online 12 May 2015

Keywords:
Ocular pharmacokinetics
Drug delivery
Intravitreal
Animal model
Rabbit

ABSTRACT

Intravitreal administration is the method of choice in drug delivery to the retina and/or choroid. Rabbit is the most commonly used animal species in intravitreal pharmacokinetics, but it has been criticized as being a poor model of human eye. The critique is based on some anatomical differences, properties of the vitreous humor, and observed differences in drug concentrations in the anterior chamber after intravitreal injections. We have systematically analyzed all published information on intravitreal pharmacokinetics in the rabbit and human eye. The analysis revealed major problems in the design of the pharmacokinetic studies. In this review we provide advice for study design. Overall, the pharmacokinetic parameters (clearance, volume of distribution, half-life) in the human and rabbit eye have good correlation and comparable absolute values. Therefore, reliable rabbit-to-man translation of intravitreal pharmacokinetics should be feasible. The relevant anatomical and physiological parameters in rabbit and man show only small differences. Furthermore, the claimed discrepancy between drug concentrations in the human and rabbit aqueous humor is not supported by the data analysis. Based on the available and properly conducted pharmacokinetic studies, the differences in the vitreous structure in rabbits and human patients do not lead to significant pharmacokinetic differences. This review is the first step towards inter-species translation of intravitreal pharmacokinetics. More information is still needed to dissect the roles of drug delivery systems, disease states, age and ocular manipulation on the intravitreal pharmacokinetics in rabbit and man. Anyway, the published data and the derived pharmacokinetic parameters indicate that the rabbit is a useful animal model in intravitreal pharmacokinetics.

1. Introduction

Age-related macular degeneration, glaucoma, diabetes, and various rare ocular diseases may impair the functionality of the retina leading to visual impairment and blindness. Even though this is a growing problem in the aging populations, effective treatments are not available to most patients with retinal diseases.

New mechanisms of action and drug candidates are being discovered for the retinal diseases (Zhang et al., 2012), but drug delivery to the retina is very difficult (and often impossible) from topical eye drops or systemic medications (such as tablets). Therefore, the intravitreal injections have emerged as the primary method of drug administration to the retina and choroid (del Amo and Urtti, 2008; Urtti, 2006). The number of annual intravitreal injections has increased rapidly being nearly 400,000 in the United Kingdom (Severn and Hamilton, 2015) and probably an order of magnitude higher numbers in Europe and U.S.A. For example, bevacizumab (Avastin®), ranibizumab (Lucentis®), pegaptanib sodium (Macugen®), aflibercept (Eylea®) and triamcinolone acetonide (Kenalog®) are widely used as intravitreal injections to treat neo-vascular macular degeneration and other retinal diseases.

ABBREVIATIONS: AIC, Akaike's information criterion; AUC, area under the curve; C_0, drug concentration at time zero; C_{calc}, calculated concentration; CL_{ivt}, intravitreal clearance; CL_{RPE}, intravitreal clearance across the RPE; C_{obs}, observed concentration; CV%, coefficient of variation; D_{ivt}, intravitreal dose; E, extraction ratio; $k_{elimination}$, first-order elimination rate constant; $f_{u,\ vitreous}$, fraction of unbound drug in vitreous; $f_{u,\ tissue}$, fraction of unbound drug in the tissue; K_p, distribution coefficient between the tissue and vitreous; MW, molecular weight; P, permeability in the membrane; ρ, Spearman's rank correlation coefficient; R^2, coefficient of determination; Q, flow; RPE, retinal pigment epithelium; S, membrane surface area; $t_{1/2,\ ivt}$, intravitreal half-life; TEER, trans-epithelial electrical resistance; V, anatomical tissue volume; $V_{ss,\ ivt}$, intravitreal volume of distribution; Y, actual concentration; Y hat, predicted concentration.

* Corresponding author. School of Pharmacy, University of Eastern Finland, P.O. Box 1627, 70211 Kuopio, Finland.
E-mail address: arto.urtti@uef.fi (A. Urtti).

http://dx.doi.org/10.1016/j.exer.2015.05.003

Intravitreal injection is an invasive procedure and, therefore, the dosing intervals should be long. The dosing intervals of intravitreal injections of antibodies, aptamers, soluble receptors and suspensions are often four to six weeks and sometimes even twelve weeks (Bashshur et al., 2008; Cheung and Eaton, 2013). This is based on the slow clearance, long half-life (about two to six days) and extremely high potency the macromolecules (anti-VEGF antibodies and soluble receptors) or slow dissolution and long residence time of suspension particles (corticosteroid suspensions). However, in the case of intravitreal solutions of small molecular drugs, the fast elimination rates (half-lives of 1–27 h) would lead to frequently repeated injections that are not possible in the clinical setting. Moreover, injections of the drug solutions intravitreally lead to high fluctuations in intravitreal drug concentrations. This is feasible only for the drugs with wide therapeutic index, otherwise the adverse effects would prohibit the clinical use. Controlled release formulations can maintain the intravitreal drug concentrations within the therapeutic index for prolonged periods, thereby allowing long dosing intervals of several months. Some controlled release implants are already in the clinical use for instance, fluocinolone acetonide intravitreal implant (Iluvien®) and dexamethasone intravitreal implant (Ozurdex®) (del Amo and Urtti, 2008; Sanford, 2013; Totan et al., 2015). Estimation of the time course of drug effects in the posterior eye segment is possible with pharmacokinetic modeling tools (Kontturi et al., 2014; Stewart and Rosenfeld, 2008).

After intravitreal administration, drugs distribute to the ocular tissues (lens, iris, ciliary body, retina). Distribution depends on the ability of drug to partition into the tissues and it is described as volume of drug distribution. Drug elimination may take place posteriorly through the blood-retina barrier (Duvvuri et al., 2003; Gupta et al., 2000; Maurice and Mishima, 1984; Shen et al., 2007) to the choroidal blood circulation that constitutes most of the ocular blood flow (del Amo et al., 2015; Roh et al., 2006). Intravitreal drug is eliminated also anteriorly via aqueous humor turnover and uveal blood flow. The importance of anterior and posterior routes depends on the drug properties (Maurice and Mishima, 1984): lipophilic drugs with high permeability in the blood-retina barrier are mostly eliminated posteriorly (e.g. fluconazole; vitreal clearance 0.753 ml/h (Gupta et al., 2000)), whereas elimination of large and hydrophilic compounds is restricted to the anterior route (e.g. bevacizumab; vitreal clearance 0.019 ml/h (Bakri et al., 2007; Christoforidis et al., 2011; del Amo et al., 2015)). These processes determine drug elimination in rabbit and human eyes and it is described as intravitreal clearance. Ocular pharmacokinetic parameters (i.e. volume of distribution and clearance) are the most informative, reliable and quantitative basis for the pharmacokinetic comparisons in terms of species, disease states, age, drug compounds and delivery systems.

Ocular pharmacokinetics has only rarely been studied in the human eye, because the invasive sampling from the human eye is ethically restricted and may influence pharmacokinetics. Therefore, ocular pharmacokinetics relies on animal models, mostly rabbits. Recently, the rabbit eye has been criticized for being a poor model of the human eye (Laude et al., 2010; Rowe-Rendleman et al., 2014). Therefore, we investigated all available intravitreal pharmacokinetic data in rabbits (del Amo et al., 2015) and humans (this review) and derived the pharmacokinetic parameters (clearance, volume of distribution) to compare systematically intravitreal pharmacokinetics in man and rabbit. We did not find any convincing evidence to justify the criticism of the rabbit model. Moreover, during the process of analyzing the intravitreal pharmacokinetic parameters in the rabbit eyes (del Amo et al., 2015), we noticed another remarkable problem: many published studies are based on suboptimal study designs, and actually 58% of the studies were discarded from the pharmacokinetic data analysis.

In this review, we summarize the current knowledge of intravitreal pharmacokinetics in rabbits and humans, and provide advice in intravitreal pharmacokinetic study design.

2. Intravitreal pharmacokinetics in rabbit eye

2.1. Introduction of concepts

The intravitreal pharmacokinetics is defined by the primary parameters: volume of distribution ($V_{ss,\ ivt}$) and clearance (CL_{ivt}) that describe drug distribution and elimination, respectively.

$V_{ss,\ ivt}$ can be compared to the anatomical volumes of the ocular tissues based on the principles from the drug distribution from plasma to the tissues (Jusko, 2006; Mager, 2006):

$$V_{ss,\ ivt} = V_{vitreous} + V_{lens} \times K_{p,\ lens} + V_{ciliary\ body} \times K_{p,\ ciliary\ body} + V_{retina} \times K_{p,\ retina} \cdots \quad (1)$$

where V values indicate the anatomical tissue volumes and K_p distribution coefficients of the drug between the tissue and vitreous. High K_p values indicate effective drug partitioning to the tissues, leading to $V_{ss,\ ivt}$ values bigger than the anatomical volumes.

Systemic volume of drug distribution at steady-state can be related to the anatomical volumes using Gillette equation (Gillette, 1971; Mager, 2006). In this case, the equation for the intravitreal drug delivery would be:

$$V_{ss,\ ivt} = V_{vitreous} + V_{lens} \times \frac{f_{u,\ vitreous}}{f_{u,\ lens}} + V_{ciliary\ body} \times \frac{f_{u,\ vitreous}}{f_{u,\ ciliary\ body}} + V_{retina} \times \frac{f_{u,\ vitreous}}{f_{u,\ retina}} \cdots \quad (2)$$

where V values indicate the anatomical tissue volumes and f_u terms indicate the fractions of unbound drug in the vitreous and surrounding tissues. Thus, in the context of intravitreal administration, $V_{ss,\ ivt}$ is related to the anatomical volumes ($V_{vitreous}$, $V_{tissues}$) and either 1) drug distribution between the tissues and vitreous humor (K_p) or 2) free fractions of the drug in the vitreous ($f_{u,\ vitreous}$) and tissues ($f_{u,\ tissue}$). Anyway, in both cases, high drug concentrations in the tissues increase the value of $V_{ss,\ ivt}$.

CL_{ivt} can be related to the ocular flows:

$$CL_{ivt} = Q_{ocular} \times E_{ocular} \quad (3)$$

where Q is the ocular flow and E is the extraction ratio in the tissue ($0 < E < 1$). Theoretical maximum for CL_{ivt} is equal to the ocular flows (aqueous humor and blood flows) representing completely flow-limited clearance without any membrane barrier limitations (e.g. blood-retinal barrier). On the contrary, at low values of E the clearance is limited by membrane permeation and defined as product of drug permeability in the membrane (P) and the membrane surface area (S):

$$CL_{ivt} = P_{ocular\ barriers} \times S_{ocular\ barriers} \quad (4)$$

After intravitreal injection, the drug is partitioning to some extent to the surrounding tissues and eliminated from the vitreous through aqueous humor turnover and blood-ocular barriers (Fig. 1). Membrane permeable drugs can cross the blood-ocular barriers, while poorly permeable drugs (e.g. macromolecules) will be cleared via aqueous humor turnover (Maurice and Mishima, 1984). All intravitreal drug will eventually end-up to the systemic

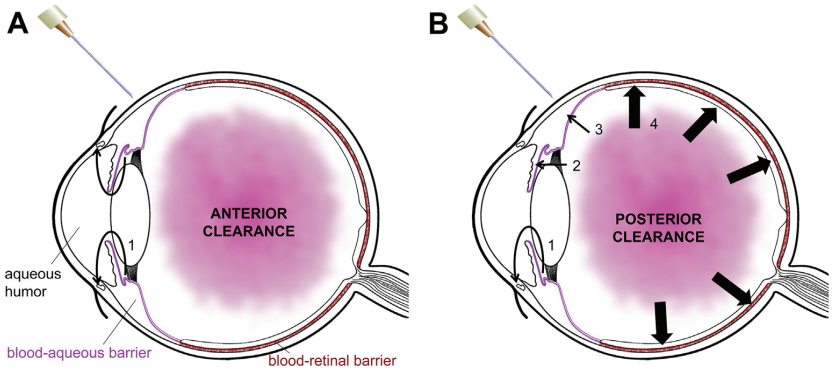

Fig. 1. Routes of drug elimination after intravitreal injection. (A) Anterior elimination of the drug in the aqueous humor flow (1). (B) Drug elimination through blood-ocular barriers. The drug permeates through the posterior iris epithelium into iris vein and is drained by vortex veins (2), through the non-pigmented ciliary epithelium to ciliary muscles and from the ciliary plexus to the episcleral veins (3), to the retinal capillaries and through the retinal pigment epithelium (RPE) into the choroid and systemic circulation (4) (del Amo et al., 2015).

circulation unless it is metabolized in the eye which is not habitual fate. However, the systemic circulation can be handled as a sink because the clearance in the human systemic circulation is much higher (10–100,000 ml/h) than the clearance in the eye (0.01–1.0 ml/h). Therefore, the concentrations in the systemic circulation are orders of magnitude lower than in the eye, and drug elimination from the eye is rate-limited by the ocular processes, and not affected by the drug concentrations in the blood circulation.

The primary pharmacokinetic parameters $V_{ss,\ ivt}$ and CL_{ivt} are useful in pharmacokinetic simulations and clinical translation. They allow estimation of average steady-state concentrations, concentration profiles, half-life ($t_{1/2,\ ivt}$) and amount of drug in the eye after administration of different doses or dosage forms (del Amo et al., 2015). $V_{ss,\ ivt}$ and CL_{ivt} can be linked to the fundamental factors, anatomy, physiology, and drug interactions with tissues, thereby providing understanding of ocular pharmacokinetics in the physiological context and generating tools for bottom-up simulation models (del Amo et al., 2015). Noteworthy, the most frequently used intravitreal pharmacokinetic parameter, $t_{1/2,\ ivt}$ depends on both drug distribution and elimination,

$$t_{1/2,\ ivt} = \frac{ln2 \times V_{ss,\ ivt}}{CL_{ivt}} \quad (5)$$

if the intravitreal concentration profile shows multi-exponential decline, the $t_{1/2,\ ivt}$ correspond to effective $t_{1/2,\ ivt}$. Even though $t_{1/2,\ ivt}$ is useful in defining the dosage intervals of the drug, it does not allow mechanistic analyses and simulations. Half-life cannot be linked to physiology and pathophysiological alterations in the eye.

2.2. Analysis of the literature

Recently, we developed a universal collection of $V_{ss,\ ivt}$, CL_{ivt} and $t_{1/2,\ ivt}$ values (del Amo et al., 2015). For that, we carried out a comprehensive literature search on intravitreal pharmacokinetic studies in healthy and normal rabbit eyes during 1947–2013. We set criteria for the data quality: at least four time-points, at least two replicates per point, and balanced sampling for at least a time-span of two $t_{1/2,\ ivt}$ of the drug (the derived parameters values are presented later in the Section 2.4). The criteria are needed for reliable determination of $V_{ss,\ ivt}$, CL_{ivt} and $t_{1/2,\ ivt}$ values. Surprisingly, only 42% of the literature reports fulfilled these quality criteria. The corresponding references and the data analysis are presented in our previous paper (del Amo et al., 2015). The remaining 58% (92 reports) had to be discarded due to inadequate data points or other problems (e.g. analytical issues, poor match between dose and initial concentration, solubility problems) that prevent reliable data analysis. Commonly, the problems were related to inadequate number of data points, poorly selected time spans and narrow concentration ranges. Table 1 illustrates some data quality problems that hamper the calculation of the pharmacokinetic parameters ($V_{ss,\ ivt}$, CL_{ivt} and $t_{1/2,\ ivt}$) or lead to unreliable estimates. For the analysis *Phoenix WinNonlin® software* (*version 6.3, Pharsight Inc., St. Louis, USA*) was used and accurate description of the workflow is described in Section 2.3.

Even though many intravitreal pharmacokinetic studies did not meet the normal quality standards, they give rough estimates of $t_{1/2,\ ivt}$ and range of drug concentrations after injection of a certain dose. Such information is valuable and important, but unfortunately not adequate for determination of pharmacokinetic parameters accurately.

2.3. Design of an intravitreal pharmacokinetic study

In a typical intravitreal pharmacokinetic study, drug is injected into the vitreal cavity in rabbits and, thereafter, drug concentrations are determined periodically. In most studies, the animals are sacrificed at different time intervals: the eyes are removed and the vitreous humor samples are assayed for drug concentrations. Continuous sampling with a microdialysis probe in the rabbit eyes has also been used (Atluri and Mitra, 2003). This approach reduces the number of animals, but reliable recovery estimates are needed in the determination of the drug yield (Duvvuri et al., 2003) and the duration of the experiments is often limited. In some cases, a radioactively labeled drug has been injected to the vitreous followed by imaging with positron emission tomography (Christoforidis et al., 2011, 2012). In all cases, the sampling times are crucial for obtaining reliable pharmacokinetic profiles and parameter values.

In rabbit studies, the number of test animals should be minimized based on 3R (Reduce, Refine, Replace) principles, but this should not lead to inadequate experimental design, unreliable pharmacokinetic profiles and parameters (Section 2.2.). Good practices of systemic pharmacokinetic data analyses should be applied with some modifications in ocular pharmacokinetics. The

Table 1
Typical examples of intravitreal data that cannot be used for reliable estimation of pharmacokinetic parameters are illustrated. These literature data were used for parameter estimation with Phoenix software following the advice from Section 2.3. The calculation of the estimated concentration at time 0 (C_0) is based on 1.15 ml rabbit vitreous volume (del Amo et al., 2015).

Missing initial data points	Missing intermediate data points	Missing data points in the terminal phase	Lack of adequate data points	Too short duration of the study
Candesartan (Lee et al. 2011) Dose = 1000 μg Estimated $C_0 \approx$ 870 μg/ml Albino rabbit	Moxifloxacin (Iyer et al. 2006) Dose = 200 μg Estimated $C_0 \approx$ 174 μg/ml Pigmented rabbit	Diclofenac (Durairaj et al. 2009) Equivalent dose = 279 μg Estimated $C_0 \approx$ 243 μg/ml Albino rabbit	Bevacizumab (Nomoto et al. 2009) Dose = 1250μg Estimated $C_0 \approx$ 1087 μg/ml Pigmented rabbit	Acyclovir (Hughes et al. 1996) Dose = 200 μg Estimated $C_0 \approx$ 174 μg/ml Pigmented rabbit
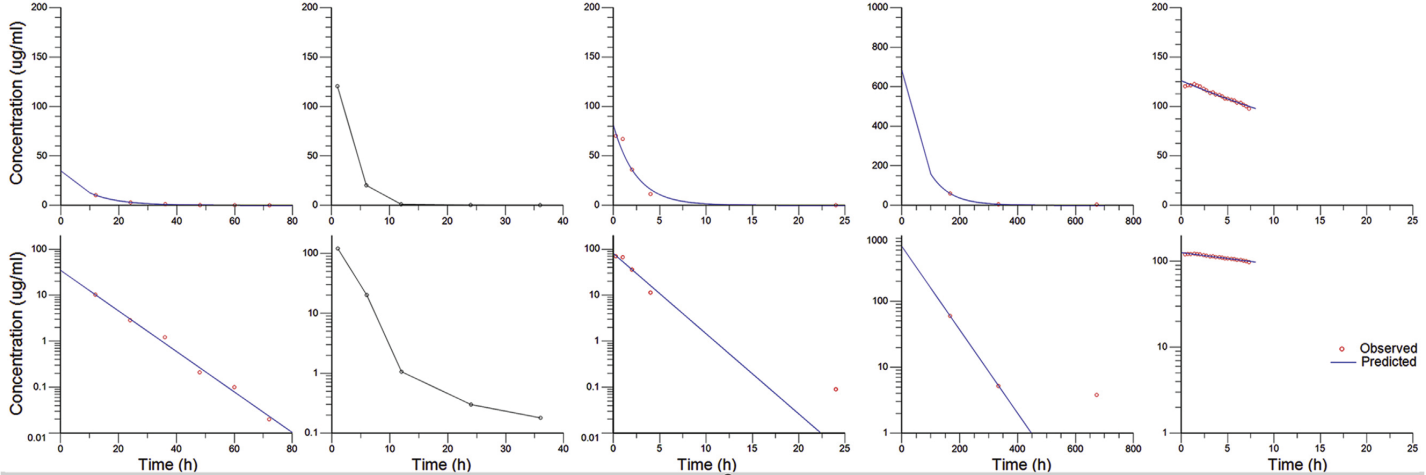				
Phoenix WinNonlin® data analysis				
One-compartment model with uniform weighting gave unrealistic parameter values: $V_{ss,ivt}$ = 28 ml, CL_{ivt} = 2.92 ml/h that were outside the range in the big data set [a] Correlation between parameters > 0.95 (unacceptable) The first sample is 1.2 % of the concentration at time zero. Most drug (98.8%) was eliminated before the first sample. Not enough initial data points for compartmental model fitting.	One- and two-compartmental analyses failed to fit the data. Not enough intermediate data points for compartmental model fitting.	One-compartment model with 1/Yhat weighting gave: $V_{ss,ivt}$ = 3.72 ml and CL_{ivt} = 1.494 ml/h (doubtful values comparing with the range[a]) It appears that the drug obeys two-compartmental kinetics, since the last data point is far above the fitted line. The single data point in the terminal elimination phase does not allow proper analysis with two-compartmental model. The last data point has too big role and this involves high risk of error. Not enough data points at the terminal phase for compartmental model fitting.	One-compartment model with uniform weighting. Correlation between parameters >0.95 (unacceptable); CV% > 30% (unacceptable); negative confidence intervals (unacceptable). Not enough data points for reliable compartment model fitting.	One-compartment model with uniform weighting gave: $V_{ss,ivt}$ = 1.59 ml and CL_{ivt} = 0.05 ml/h (unreliable value). The statistics were within the acceptable limits. However, the sampling time in this microdialysis study was too short and it did not allow reliable determination of the pharmacokinetic parameters. About 56% of the drug has not been eliminated at the time of the last sample. Not enough data points for reliable compartment model fitting.

a: The range values of $V_{ss,\ ivt}$ and CL_{ivt} in rabbit vitreous is 0.72–3.14 ml and 0.011–1.530 ml/h respectively (Fig. 2 and del Amo et al., 2015).

Table 2
Pharmacokinetic data analysis with curve fitting software.

Compartmental model
Select one- or two- compartmental model.
The experimental data are plotted in semi-logarithmic plot: logarithm of intravitreal concentration vs time.
Based on the shape of the plotted data one-compartmental (single slope) or two-compartmental (two distinct slopes) model may be feasible.
Weighting factor
Weighting is used to improve the curve fitting by giving more weight to the last data points with low concentrations.
The sum of squared residuals can be weighted by
• one (uniform weighting)
• $1/C_{obs}$ or $1/C_{calc}$ (1/Y or 1/Yhat respectively)
• $1/(C_{obs})^2$ or $1/(C_{calc})^2$ ($1/Y^2$ or $1/Yhat^2$ respectively)
The relative weight of small concentrations is increased with the use of the concentration or squared concentration in the denominator.
Y is the actual concentration and Yhat is the predicted concentration.
Goodness of fit
Goodness of fit describes how close the calculated curve is to the data points. The following criteria is used to evaluate the goodness of fit:
1) Calculated concentration curve should lie between the observed concentration points.
2) Signs of the residuals (i.e., $C_{obs} - C_{calc}$, shows either over-estimation or under-estimation) must change randomly. This indicates lack of systematic deviations.
3) Relative residuals (residual/C_{obs}) are not excessive at low concentrations.
4) Confidence intervals of the parameters are positive. This depends on the number of animals and data points, and the complexity of the pharmacokinetic model.
5) Coefficient of variation (CV%) should be less than 30%, preferably below 10%.
6) Correlation between various pharmacokinetic parameters should be < 0.95. This informs us that the parameters are independent from each other.
7) Sum of weighted squared residuals should be small enough.
8) Akaike's information criterion (AIC) is used to discriminate between models (for example, one- and two-compartment models) with the same weighting. The best model has the lowest AIC value.

pharmacokinetic parameters are determined using curve fitting software (e.g. *Kinetica®, Thermo Fisher Scientific Inc, Waltham, USA or Phoenix WinNonlin® software*) that are based on the method of least squares to fit the concentration curves. The objective is to minimize the difference between the observed and calculated concentrations (C_{obs} and C_{calc} respectively), *i.e.* sum of squared residuals $\Sigma(C_{obs} - C_{calc})^2$. These methods pool all the data from the experiment for maximal information gain. As illustrated in Table 1 inadequate data may not allow reliable estimation of pharmacokinetic parameters. Proper procedure in pharmacokinetic data analysis is presented in Table 2.

Usually, the kinetic analysis is done for each individual separately (e.g. plasma samples at different times), but this is not possible in intravitreal studies, because multiple sampling from the vitreous is not possible. All individual data points can be fitted simultaneously, and the fitted curve can be compared to the observed mean values or individual points. In any case, it is important to have adequate number of data points with proper time span and concentration range.

We propose that the following points should be taken into account in the design of intravitreal pharmacokinetic studies. Firstly, the drug dose should be soluble in the formulation and in the vitreous. This is not the case in many studies (some examples (Chin et al., 2005; Doft et al., 1985; Wingard et al., 1989)). Then, the resulting data does not allow reliable determination of CL_{ivt}, $V_{ss,\ ivt}$ and $t_{1/2,\ ivt}$ for the drug. Anyway, the obtained concentration profiles describe the properties of the formulation in drug delivery. Secondly, the dose should be reported, and if the drug is in salt form, the reporting should allow the estimation of dose as free acid or free base. Thirdly, at least six time points must be used at properly balanced intervals to describe drug distribution and elimination. The first data point should be shortly after injection and, thereafter, the data points should span at least three $t_{1/2,\ ivt}$ of the drug (*i.e.* at least 87% of the drug has been eliminated at that point). Fourthly, at least four to six replicate eyes should be used for each time point. Overall, this will results in 24–36 rabbit eyes (12–18 animals). Within the European Union the use of animals in scientific experiments should be rationally reduced (Directive 86/609/EEC). Properly conducted intravitreal pharmacokinetic study uses many rabbits, but it will yield reliable quantitation of pharmacokinetics (incl. $V_{ss,\ ivt}$, CL_{ivt}, $t_{1/2,\ ivt}$) that allows estimation of drug concentrations at different dosing regimens thereby reducing the need of animals in later experiments and in the long run.

2.4. Intravitreal pharmacokinetic parameters in rabbits

The universal collection of the intravitreal pharmacokinetic data in rabbits was followed by determination of the primary pharmacokinetic parameters (CL_{ivt} and $V_{ss,\ ivt}$). Only the studies that fulfilled the quality criteria were included in the analysis. The CL_{ivt} and $V_{ss,\ ivt}$ data are plotted against the molecular weight (MW) of the compounds in Fig. 2A–B.

The $V_{ss,\ ivt}$ values in rabbits are in the range 0.72–3.14 ml. Interestingly, there are no systematic differences in the $V_{ss,\ ivt}$ values of small molecules and macromolecules. Overall, the scope of $V_{ss,\ ivt}$ values is narrow (only 4-fold range) and in general the values are slightly greater than the anatomical volume of the vitreous humor (1.15 ml) (Fig. 2B). Volume of vitreous is bigger than the volumes of the surrounding tissues, such as iris, ciliary body, choroid, retina (0.050–0.059 ml) (Wiederholt et al., 1986; Wu et al., 1970) and lens (0.33–0.53 ml) (Zamudio and Candia, 2011). The small volumes of the tissues explain the narrow range of $V_{ss,\ ivt}$ values (see Eqs. (1) and (2)). The highest $V_{ss,\ ivt}$ value (3.14 ml) would be achieved with K_p (or $f_{u,\ vitreous}/f_{u,\ tissue}$) value of 2.8–4 if we use the average combined volume for the surrounding tissues (0.49–0.69 ml) in Eq. (1) or Eq. (2), proving that K_p values in the eye are moderate and do not have major impact on $V_{ss,\ ivt}$ values. It is therefore likely that the new drug candidates will have $V_{ss,\ ivt}$ in the range reported in Fig. 2B and del Amo et al. (2015). $V_{ss,\ ivt}$ values are similar or only moderately bigger than the anatomical volume of vitreal cavity and eye tissues, thereby ruling out the possibility that drug partitioning to the orbita would be significant. This is understandable, because the ocular blood flow removes drug effectively thereby minimizing its access to the orbita.

Drug elimination from the vitreous shows substantial differences among the compounds in the literature: CL_{ivt} values range from 0.011 to 1.530 ml/h (139-fold difference) and the values decrease clearly with increasing MW (Fig. 2A). Also, the $t_{1/2,\ ivt}$ values have a broad range (del Amo et al., 2015; Kidron et al., 2012), because the $t_{1/2,\ ivt}$ is dependent on CL_{ivt} and $V_{ss,\ ivt}$.

The CL_{ivt} of macromolecules are low (0.011–0.027 ml/h, Fig. 2A and D) because they are mainly eliminated via anterior route (Fig. 1A). Interestingly, CL_{ivt} of macromolecules are clearly less than

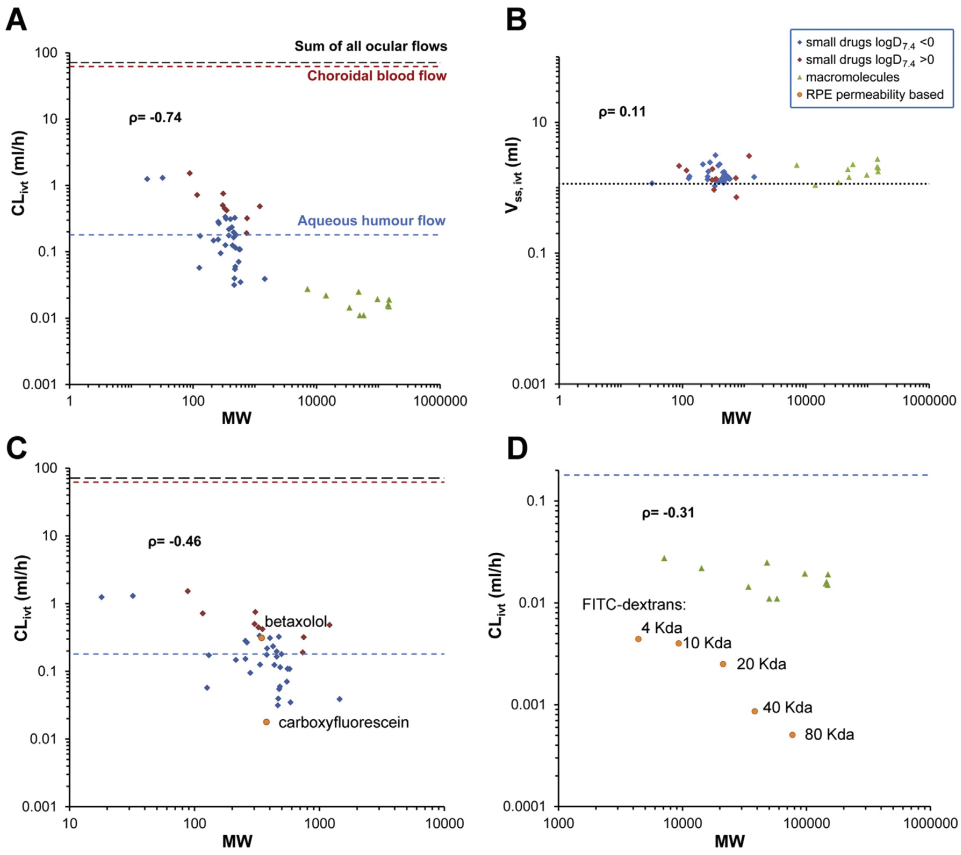

Fig. 2. The relationships between (A) MW and CL_{ivt} and (B) MW and $V_{ss,\ ivt}$ are presented for 40 small molecular compounds and 11 macromolecules after intravitreal injections in rabbits. The relationships between MW and CL_{ivt} of the small molecular compounds (C) and macromolecules (D) are presented. The diamonds represent the small MW compounds with Log $D_{7.4}$ below 0 (blue symbols) and Log $D_{7.4}$ above 0 (red symbols). The triangles represent the macromolecules. The circles represents intravitreal clearance via permeation across the RPE. These values were calculated based on permeability in bovine RPE-choroid membrane (Mannermaa et al., 2010; Pitkanen et al., 2005) and RPE surface area in rabbit (Reichenbach et al., 1994) using Eq. (4). In (A) the long dashed black line represents the sum of the ocular flow factors (choroidal, retinal, iridial and ciliary body blood flows, and aqueous humor flow), the short dashed lines correspond to the choroidal blood flow (red) and aqueous humor flow (blue). In (B) the dotted line represents the anatomical volume of the vitreous 1.15 ml. The ρ represent Spearman's rank correlation coefficient for small drugs and macromolecules. In the original publication (del Amo et al., 2015), the pharmacokinetic parameters of PF-04523655 were extracted from an abstract (Johnson, 2010). The original concentration curve became recently available and it was analyzed. However, the initial concentrations were too low for the administered dose. Therefore, the parameters of this drug were omitted from the figures.

the rate of aqueous humor turnover (0.18 ml/h) (Barany and Kinsey, 1949) suggesting that the access of drug from the vitreous to the anterior chamber is restricted. Presumably, CL_{ivt} of macromolecules via posterior route through blood-retina barrier is low, due to their low permeability in the RPE (Pitkanen et al., 2005). Intravitreal clearance across the RPE (CL_{RPE}) was calculated using the bovine RPE permeability for FITC-dextrans (Pitkanen et al., 2005) and surface area of the rabbit RPE (5.2 cm^2) (Reichenbach et al., 1994) according to Eq. (4) ($P \times S$). These CL_{RPE} values are 5–30 times lower than the CL_{ivt} values for the macromolecules in the same MW range (Fig. 2D). This suggests that only a small fraction (3–20%) of the macromolecule dose is eliminated through the RPE.

The wide range of CL_{ivt} of small drugs (0.031–1.530 ml/h) is probably determined by their ability to cross the blood-ocular barriers. High permeability across the barriers should lead to high CL_{ivt} values. Owing to the large surface area of the RPE and high blood flow in the choroid, it is probable that the compounds with high CL_{ivt} values are eliminated via posterior route (Fig. 1B). In our previous studies, the $t_{1/2,\ ivt}$ and CL_{ivt} of small drugs were determined by H-bond capacity and $LogD_{7.4}$ (del Amo et al., 2015; Kidron et al., 2012). These descriptors typically define membrane permeability, e.g. in the cornea (Kidron et al., 2010), intestinal wall (Linnankoski et al., 2006) and blood–brain barrier (Lanevskij et al., 2009; Liu et al., 2004). Accordingly, the calculated CL_{RPE} values for betaxolol and carboxyfluorescein, using permeability values of Pitkanen et al. (2005) and Mannermaa et al. (2010), are in the same range with CL_{ivt} values of lipophilic and hydrophilic small molecules, respectively, suggesting significant elimination through the RPE (Fig. 2C). Despite their ability to cross blood-retina barrier, the CL_{ivt} values of the small molecules are far below the value of choroidal blood flow showing that clearance is permeability-limited and not controlled by blood flow (Fig. 2A).

Some clinical biologics (e.g. ranibizumab, bevacizumab) are delivered intravitreally to the retinal and choroidal tissues. We should note that the effects of these drugs are dependent on their target concentrations and not on the quantity of drug that is eliminated through the blood-retina barrier. Therefore, therapeutic effects in the retina and/or choroid do not mean that the

posterior elimination pathway would be significant route for macromolecules. Therapeutic concentrations can be reached in the retina and/or choroid even though the posterior clearance would be an order of magnitude less than the anterior elimination.

3. Intravitreal pharmacokinetics in human eye

Intravitreal pharmacokinetic studies in humans are sparse, because the vitreous sampling is invasive and potentially risky procedure. There are, however, some studies that were carried out in patients who were selected for vitrectomy surgery or undergoing treatments for endophthalmitis, cytomegalovirus retinitis or choroidal neovascularization (Table 3). Typically, these studies reported only a few drug concentrations, usually from one individual and during the terminal elimination phase of the drug. For such data it is not possible to calculate the CL_{ivt} as it has been presented in Section 2.3. However, we did the following exercise to get rough estimates of CL_{ivt} (apparent CL_{ivt}), assuming one-compartment pharmacokinetics:

$$apparent\ CL_{ivt} = \frac{D_{ivt}}{AUC} \tag{6}$$

where D_{ivt} is the given intravitreal dose and AUC is area under the curve. The AUC values were calculated using equation (7):

$$AUC = \frac{C_0}{k_{elimination}} \tag{7}$$

where C_0 is the drug concentration in vitreous at time zero and $k_{elimination}$ is the first-order elimination rate constant. C_0 was calculated with equation (8):

$$C_0 = \frac{D_{ivt}}{V_{ss,\ ivt}} \tag{8}$$

where $V_{ss,\ ivt}$ was assumed to be equal to the human vitreous volume of 4 ml (Ruby et al., 2006). This is probably a reliable estimate, because the rabbit $V_{ss,\ ivt}$ values are limited in a narrow range (80% of the values in the dataset of 51 compounds were between 1.18 and 2.28 ml) (del Amo et al., 2015) and close to the anatomical volume of the vitreous. The $k_{elimination}$ was the slope of the curve defined by the calculated C_0 and the experimental concentration values. The apparent CL_{ivt} values are presented in Table 3. The same calculations for 2-fold higher $V_{ss,\ ivt}$ value (8 ml) were carried out and presented in Fig. A1 (versus rabbit CL_{ivt}) and A.2 (versus MW) in appendices. Estimation of CL_{ivt} and apparent CL_{ivt} values in human eyes enables universal rabbit-to-human comparison of intravitreal drug elimination (Fig. 3). Drug clearance in rabbit and human vitreous correlated well ($\rho = 0.91$; Rabbit $CL_{ivt} = 1.41 \times$ Human apparent $CL_{ivt} + 0.04$, units are ml/h; $R^2 = 0.82$) and absolute differences of the clearance values are in within 3-fold range (13/15

Table 3
Intravitreal drug concentrations in vitreous after intravitreal injection of drugs in humans. In the first panel, pharmacokinetic parameters are calculated by compartmental model (section 2.3, Doc. A) and in the second panel, the apparent CL_{ivt} is calculated according to the description given in section 3.

Drugs	Dose (μg)	Subjects	Time (h)	C (μg/ml)	$V_{ss,\ ivt}$ (ml)	CL_{ivt} (ml/h)	$t_{1/2,\ ivt}$ (h)	References
Bevacizumab	1250	Patients with choroidal neovascularization	24	92.70	3.17	0.025	160.8	(Zhu et al. 2008)
			48	165.00	9.39	0.042	154.4	Own calculations
			72	84.80				
			96	48.70				
			264	22.90				
			408	0.33				
			1032	1.39				
			1296	0.39				
			1776	0.022				
			2280	0.005				
			2424	0.003				

Drugs	Dose (μg)	Subjects	Time (h)	C (μg/ml)	Apparent CL_{ivt} (ml/h)	References
Bevacizumab	1250	Patients with choroidal neovascularization	48	166.0[a]	0.036	(Beer et al. 2006)
			696	0.5[b]		
Bevacizumab	1250	Patients with diabetic retinopathy	672	0.107	0.028	(Moisseiev et al. 2014)
			1344	0.019		
Cidofovir	20	AIDS patient with cytomegalovirus retinitis	24	0.673	0.336	(Taskintuna et al. 1998)
Dexamethasone phosphate	383[d]	Patients with postoperative endophthalmitis with and without core vitrectomy	66	0.023	0.472	(Gan et al. 2005)
			69	0.027		
			70	0.040		
			71	0.018		
			71	0.014		
			72	0.036		
Fomivirsen	165	Patients with cytomegalovirus retinitis	1	39.24[c]	0.068	(Bejanian et al. 1999)
			72	10.61		
			168	0.39		
			168	0.78		
			336	0.26		
Foscarnet	504[d]	AIDS patient with cytomegalovirus retinitis	23.25	51.53	0.152	(Diaz-Llopis et al. 1992)
Ganciclovir	200	AIDS patient with cytomegalovirus retinitis	51.4	1.17	0.292	(Henry et al. 1987)
Ganciclovir	2000	Patients with cytomegalovirus retinitis	24	212.0	0.172	(Morlet et al. 1996)
			24	165.4		
			24	138.2		
			24	102.2		
			24	152.8		

(continued on next page)

Table 3 (*continued*)

Drugs	Dose (μg)	Subjects	Time (h)	C (μg/ml)	Apparent CL_{ivt} (ml/h)	References
			24	92.2		
			72	59.8		
			72	10.0		
			72	20.8		
			72	19.4		
			72	6.8		
			72	23.4		
Gentamicin	50	Patients with postoperative endophthalmitis with and without core vitrectomy	63	0.90	0.092	(Gan et al. 2001)
			66	1.41		
			69	3.30		
			69	1.21		
			69	1.01		
			71	1.91		
			71	1.40		
			71	1.80		
			72	1.40		
			72	2.41		
			72	1.01		
			90	1.21		
			92	2.61		
Vancomycin	975[d]	Patients with postoperative endophthalmitis with core or entire vitrectomy	44	58.11	0.068	(Ferencz et al. 1999)
			48	137.85		
			72	182.36		
			72	25.05		
Vancomycin	200	Patients with postoperative endophthalmitis with and without core vitrectomy	63	2.59	0.084	(Gan et al. 2001)
			66	12.07		
			68	10.75		
			69	18.03		
			69	8.23		
			69	11.97		
			71	15.54		
			71	6.30		
			71	9.02		
			71	13.28		
			72	8.89		
			72	10.10		
			72	6.85		
			90	5.80		
			90	3.05		
			92	16.59		
			93	4.59		
Vancomycin	1000	Patients with postoperative endophthalmitis	48	125	0.100	(Haider et al. 2001)
			48	164		
			72	21		
			72	83		
Vancomycin	2000	Patients with postoperative endophthalmitis	48	161	0.100	(Haider et al. 2001)
			72	56		
			72	220		
			72	105		
			72	39		
Vancomycin	975[d]	Patients with exogenous endophthalmitis with core vitrectomy	24	133.7	0.132	(Raju et al. 2004)
			24	179.0		
			24	171.1		
			48	72.5		
			48	43.9		
Vancomycin	200	Patients with postoperative endophthalmitis with and without core vitrectomy	62	2.6	0.092	(Gan et al. 2005)
			66	12.0		
			68	10.8		
			69	12.0		
			69	8.2		
			71	15.5		
			71	9.0		
			71	8.9		
			71	6.3		
			71	16.6		
			72	6.8		
			93	4.6		

Footnote.

[a] The patient developed endophthalmitis 2 days after the drug injection, complete drug washout of previous treatment is assumed.

[b] The patient suffered retinal detachment 8 days before vitreous sampling.

[c] Average concentration of five patients. All other reported concentrations correspond to individual patient samples and only in Morlet's study (Morlet et al. 1996) two vitreous samples were taken from the same patient, for four patients.

[d] Equivalent dose.

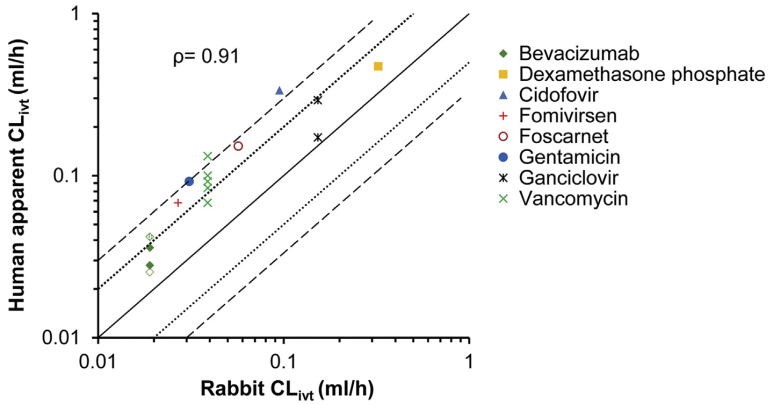

Fig. 3. Correlation between CL_{ivt} in rabbit versus human apparent CL_{ivt} (and CL_{ivt}). The dotted and dashed lines represent 2- and 3-fold deviation and the solid line represents the slope of 1.0. The open diamond correspond to bevacizumab CL_{ivt} calculated by Zhu et al. and the dotted one correspond to our calculations.

studies). The relationship of the apparent CL_{ivt} in human eye and MW was negative (Fig. B in appendices), like in rabbits (Fig. 2A). If higher value is used for human $V_{ss,\ ivt}$ (8 ml), the trends remain the same, and the CL_{ivt} difference is within 4-fold range (12/15 studies) (Fig. A1 and A2 in appendices). It is important to note that the individual values of apparent CL_{ivt} in human vitreous may not be accurate descriptors for the elimination of individual drugs. However, Fig. 3 shows good correlation and only moderate inter-species CL_{ivt} differences in the large pooled data from 15 studies. This supports the use of rabbit as a model in intravitreal pharmacokinetic studies. It is important to note that the human patients had different disease conditions (Table 3), but still no striking outliers were seen in the rabbit-to-man correlation in Fig. 3.

The experiment of Zhu et al. (2008) is the only human study that allows calculation of CL_{ivt} values with curve fitting (Table 3) though only one sample was available for each time point. It is important to note that bevacizumab has similar CL_{ivt} values (1.5- and 2.1-fold differences) in rabbit and humans (Fig. 3, Doc. A).

Intravitreal pharmacokinetics in human eyes is evaluated also by monitoring drug concentrations in the aqueous humor. Major concentration differences of bevacizumab in aqueous humor were seen after intravitreal injections in human (Krohne et al., 2008) and rabbit eyes (Nomoto et al., 2009). Based on this argument, the rabbit was considered not to be a good animal model for human eye (Rowe-Rendleman et al., 2014). However, that particular rabbit study (Nomoto et al., 2009) has some quality concerns: the first sample was taken only one week after the intravitreal injection and the assayed samples had exceptionally low concentrations. The authors compared their results with the rabbit study of Bakri et al. (Bakri et al., 2007) and justified the concentration differences based on the analytical method used. Nomoto et al. (2009) measured all variants of bevacizumab (free, in complex, fragments), but this kind of non-specific assay should lead to higher concentration values, not lower, than in Bakri's study. Then, it is interesting to plot together the existing rabbit and human data. The human bevacizumab data (Krohne et al., 2008; Meyer et al., 2011) is in line with Bakri's levels of bevacizumab in aqueous humor (Fig. 4). Similar conclusion is reached when AUC values of bevacizumab (normalized to 1 mg intravitreal dose) in aqueous humor are compared (Table 4): Nomoto's study (Nomoto et al., 2009) is clearly an outlier. Unfortunately, much criticism against rabbit model has been based on the comparisons of human data with Nomoto's rabbit data.

We carried out pharmacokinetic simulations of intravitreal bevacizumab using the measured pharmacokinetic parameters from the literature. We assumed that bevacizumab distributes in the vitreous as indicated by the $V_{ss,\ ivt}$ values (human 9.39 ml, rabbit 2.02 ml), its elimination takes place only via anterior route (CL_{ivt} = human 0.042 ml/h, rabbit 0.019 ml/h), and the elimination from the aqueous humor (volume 0.3 ml) takes place at the rate of aqueous humor outflow (human 0.14 ml/h, rabbit 0.18 ml/h) (Fig. 5, Table 5). Since blood-aqueous barrier does not allow permeation of proteins, the aqueous humor flow remains as the only route of bevacizumab elimination (Maurice and Mishima, 1984). The results

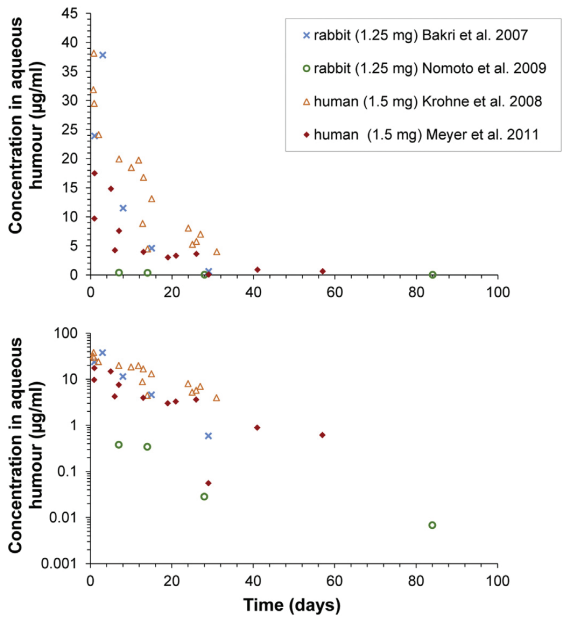

Fig. 4. Concentration of bevacizumab in aqueous humor versus time after intravitreal injection in rabbit (Bakri et al., 2007; Nomoto et al., 2009) and in human eyes (Krohne et al., 2008; Meyer et al., 2011) in arithmetic and semi-logarithmic scale.

Table 4
The AUC values (0 − infinity) of bevacizumab in aqueous humor after intravitreal injection in rabbit and human. The AUC values were dose normalized to 1 mg dose.

		AUC (μg*days)/ml	$AUC_{simulated}$ (μg*days)/ml
Rabbit	Bakri et al., 2007	234.6	231.5
	Nomoto et al., 2009	7.1	
Human	Krohne et al., 2008	325.2	297.3
	Meyer et al., 2011	131.8	

and structure of the simulation model are shown in Fig. 5. The simulated bevacizumab concentrations are in line with the real values, except the data of Nomoto et al. (Nomoto et al., 2009) that deviates substantially from the simulations (Figs. 4 and 5). The same conclusion is reached when AUC values of the simulations are compared to the experimental values (Table 4).

It is important to note that the drug concentrations in the aqueous humor are different from the concentrations in the vitreous. Moreover, the ratio of the concentrations (aqueous humor/vitreous) may not be constant for all compounds. Based on simulation, $AUC_{aqueous\ humor}/AUC_{vitreous}$ for small lipophilic compound (CL_{ivt} = 0.5 ml/h, $CL_{aqueous\ humor}$ = 1.2 ml/h (Schoenwald, 2003)) is 0.016. This means that the drug concentrations in the vitreous are approximately 50 times greater than in the aqueous humor. In the case of bevacizumab, the AUC-ratio is 0.095 meaning that approximately 10-fold higher concentrations are seen in the vitreous than in the aqueous humor.

4. Role of the vitreous in intravitreal pharmacokinetics

Many studies suggest that the vitreous plays a role in ocular pharmacokinetics, because the clearance of small MW drugs is faster in vitrectomized and lensectomized rabbit eyes than in either lensectomized or control rabbit eyes (Doft et al., 1985; Ficker et al., 1990; Jarus et al., 1985; Mandell et al., 1993; Pearson et al., 1993; Pflugfelder et al., 1987; Wingard et al., 1989). However, there are many changing variables in such studies (Doft et al., 1985; Ficker et al., 1990; Mandell et al., 1993; Wingard et al., 1989), and it is impossible to distinguish the specific effects of vitreous from the experiments with vitrectomized and lensectomized eyes (Jarus et al., 1985; Pearson et al., 1993; Pflugfelder et al., 1987). There are a few studies with vitrectomized rabbit eyes without lensectomy (Ahn et al., 2013, 2014; Christoforidis et al., 2013; Lee et al., 2010). In vitrectomized rabbit eyes, pharmacokinetics of bevacizumab and ranibizumab did not differ from the control rabbits (Ahn et al., 2013, 2014), while in another study small (1.8- and 1.3-fold) differences were seen for bevacizumab and ranibizumab, respectively (Christoforidis et al., 2013). Likewise, small increase in the elimination of FITC-dextrans was shown in the rabbit eyes after hyaluronidase treatment (Tan et al., 2011). We must be cautious in the interpretations because vitrectomy or enzyme treatment may endanger the integrity of the blood-ocular barriers (Knudsen et al., 2001; Mochizuki et al., 1992, 1993).

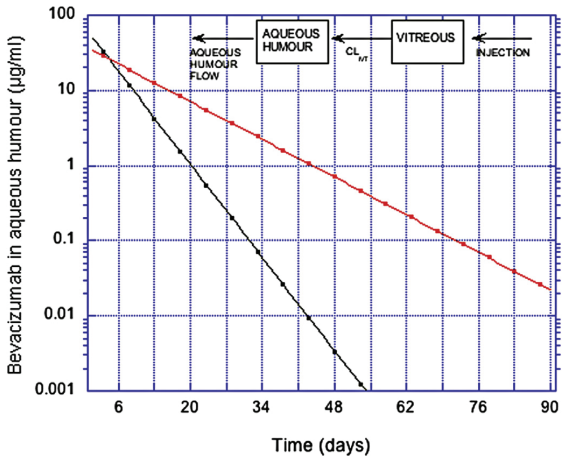

Fig. 5. The model structure and simulated bevacizumab concentrations in the human (in red) and rabbit (in black) aqueous humor are presented. The doses are as described in Fig. 3. (For interpretation of the references to color in this figure legend, the reader is referred to the web version of this article.)

Lee et al. (Lee et al., 2010) claimed a 10 times shorter $t_{1/2,\ ivt}$ for the vitrectomized rabbit as compared to the control rabbit. However, this study is misleading and data analysis is not reliable. In the operated eye, the half-life was calculated based on two experimental early data points, while additional later time point was included in the data analysis of the control eye. Moreover, the calculated $t_{1/2,\ ivt}$ in the control group was abnormally short considering that VEGF is a macromolecule. This problem has also been pointed out in other publications (Ahn et al., 2013, 2014). In conclusion, the study of Lee et al. (Lee et al., 2010) is an outlier among the studies on the vitreous effects on ocular pharmacokinetics. Most data does not support significant role of vitreous in drug elimination from the vitreous cavity.

Relatively minor effects of vitreous on ocular pharmacokinetics is understandable, because the vitreous is relatively loose structure that allows rapid diffusion of small molecular drugs and proteins (Gajraj, 2012; Maurice and Mishima, 1984; Pitkanen et al., 2003; Xu et al., 2000). Recently the mean pore size of the vitreous was analyzed to be 550 ± 50 nm, value that is two orders of magnitude greater than typical molecular diameter of a protein drug (Xu et al., 2013). Therefore, changes in the vitreous viscosity are not expected to have effects on drug diffusion and drug elimination from the eye. For example, diffusivity in the porcine and rabbit vitreous was similar (Gajraj, 2012) even though these species have difference in the viscosity of the vitreous. Furthermore, CL_{ivt} values show 139-fold range *in vivo* in rabbits (Fig. 2A). Compared to that range, the differences in the drug diffusion in the vitreous are negligible (Gajraj, 2012; Missel, 2012; Xu et al., 2000). Importantly, molecular permeability in the isolated RPE-choroid had 618-fold range of values depending on the lipophilicity and size of the compound (Pitkanen et al., 2005). Overall, permeability in the blood-retina barrier defines the range of CL_{ivt} values of drugs after intravitreal injections. In the case of small molecules, there is no correlation between MW and CL_{ivt} (Fig. 2C), but QSPR model with hydrogen bonding and $LogD_{7.4}$ describes the CL_{ivt} reliably (del Amo et al., 2015) showing clear dependence on blood-ocular barrier permeation.

For macromolecules the range of CL_{ivt} values is only about 3-fold, even though the MW range is 7122–149,000 (Fig. 2D). The CL_{RPE} values are much smaller than CL_{ivt} values indicating dominating role of the anterior elimination route, but yet CL_{ivt} values are clearly smaller than the rate of aqueous humor turnover (Fig. 2D). This is mainly due the restricted access of the drug from vitreous to the

Table 5
Comparison between the pharmacokinetically relevant anatomical and physiological parameters in the rabbit and human (or monkey) eye. The factors affecting the CL_{ivt} of macromolecules are marked by a dotted box. All parameters may affect the CL_{ivt} of small molecular drugs.

				Rabbit	*Human*	*References*
Physiological values affecting CL_{ivt}	Blood flow mediated CL_{ivt}	Barrier surface area	**Surface area of RPE**	520[a] mm^2	1204 ± 184[b] mm^2	(Reichenbach et al. 1994) (Panda-Jonas et al. 1994)
		Barrier permeability	**TEER of RPE layer**	179.2 ± 6 ohm.cm^2	79 ± 48 ohm.cm^2	(Koyano et al. 1993) (Quinn and Miller. 1992)
		Blood flows:	**Choroidal blood flow**	62 ml/h	43 ml/h	(Nilsson and Alm. 2012) (Sebag et al. 1994)
			Retinal blood flow	0.66 ml/h	0.26 ml/h	(Nilsson and Alm. 2012) (Feke et al. 1989)
			Ciliary body blood flow	4.91 ml/h	5.34[c] ml/h	(Nilsson and Alm. 2012) (Alm and Bill. 1973)
			Iridial blood flow	3.72 ml/h	1.02[c] ml/h	(Nilsson and Alm. 2012) (Alm and Bill. 1973)
	Aqueous humor flow mediated CL_{ivt}	Aqueous humor flow		0.18 ml/h	0.14 ml/h	(Barany and Kinsey. 1949) (Brubaker. 1982)
		Barrier between vitreous and anterior chamber		undefined	undefined	
Physiological values affecting $V_{ss,\ ivt}$ of all drugs		Ocular volumes:	**Vitreous volume**	1.15 ml	4 ml	(del Amo et al. 2015) (Ruby et al. 2006) (Zamudio and Candia. 2011)
			Lens weight	0.33 - 0.53 g	0.15 - 0.26 g	(Hemenger et al. 1995)
			Uveal tract & retina weight	0.16 g		(Wiederholt et al. 1986)
			Choroid weight	0.059 g		(Wu et al. 1970)
			Iris weight	0.057 g		(Wu et al. 1970)
			Ciliary body weight	0.050 g		(Wu et al. 1970)
		Tissue affinities:	$K_{p,\ ocular\ tissues}$	No data	No data	

Footnote: a: from adult rabbit; b: from humans between 2 and 90 year-old (50.7 ± 20.4 years); c: data from monkey, no human data available to our knowledge.

aqueous humor (i.e. bottleneck of the lens, ciliary body and lens) and partly due to the diffusion in the vitreous. Even though CL_{ivt} values of macromolecules may partly depend on their diffusivity in the vitreous, the values are spanning only a narrow range despite the large differences in the MWs. This is not surprising, because the pore size of non-liquefied vitreous (550 nm) is far greater than the size of protein drugs (about 5–10 nm) (Xu et al., 2013). Interestingly, CL_{ivt} values do not correlate with MW (Fig. 2D). This suggests that the role of vitreous may be related to the vitreous–proteins interactions, and not size related sieving effects.

Vitreous may have more significant effects on intravitreal pharmacokinetics in special cases. For example, highly cationic macromolecules, cationic nanoparticles and larger suspension particles show limited mobility and possible aggregation in the vitreous (Chin et al., 2005; Doft et al., 1985; Pitkanen et al., 2003; Wingard et al., 1989; Xu et al., 2013). These formulation aspects are, however, beyond the scope of this article.

5. Rabbit as an animal model in intravitreal pharmacokinetics

Successful translation of intravitreal pharmacokinetics from rabbit to man requires quantitative understanding of intravitreal pharmacokinetics in both. Unfortunately, there are only sparse data on human intravitreal pharmacokinetics. As presented in Sections 2 and 3, we have pooled all available data to calculate the primary pharmacokinetic parameters for the rabbit and human eye. The outcome does not support the criticism of rabbit as an animal model. Rather, it indicates that in general rabbit is a decent model in the vitreal pharmacokinetics.

$V_{ss,\ ivt}$ values depend on the anatomical volumes of the vitreous and surrounding tissues, and drug partitioning to the tissues (Section 2.1). Like in the rabbits, the human $V_{ss,\ ivt}$ values are expected to be close to human vitreous volume (4 ml), since the adjacent tissues are very small compared to the vitreous volume. Indeed, for bevacizumab (Zhu et al., 2008) the $V_{ss,\ ivt}$ in human was calculated as 3.2 ml and 9.4 ml (Table 3). These values were 1.6-fold and 4.5-fold higher than the $V_{ss,\ ivt}$ in rabbit (2.0 ml) (Bakri et al., 2007; Christoforidis et al., 2013; del Amo et al., 2015), while the difference in the vitreous volumes is between 2- and 3-fold (Table 5). Recently, Krohne et al. (2015) did not find significant impact of axial length and lens status on the pharmacokinetics of intravitreal ranibizumab and bevacizumab. This supports the notion that the $V_{ss,\ ivt}$ is relatively constant, mostly governed by the volume of the vitreous. On the contrary, systemic volumes of drug distribution span approximately 200,000-fold range (Obach et al., 2008). In conclusion, $V_{ss,\ ivt}$ in humans can be estimated with good accuracy based on the rabbit data and size difference of human and rabbit eye.

CL_{ivt} for small lipophilic molecules takes place mostly via RPE and choroid (Maurice and Mishima, 1984). The choroidal blood flow values in the rabbit and human are quite similar being about 85% of the total ocular blood flow (Table 5). It is known that both CL_{ivt} and RPE permeability are strongly affected by lipophilicity indicator ($LogD_{7.4}$) of the drug (del Amo et al., 2015; Pitkanen et al., 2005). Indeed, CL_{ivt} via RPE should be the product of drug permeability in the RPE and surface area of the RPE (Section 2.1, Eq. (4)). The RPE permeability in rabbit and human should be similar due to their similar trans-epithelial electrical resistance (TEER) values (Table 5), while the area of RPE is two to three times higher than in the rabbit. Therefore, CL_{ivt} of small lipophilic compounds is expected to be two or three times higher in man than in rabbit. This trend was

observed in Fig. 3. Apparent CL_{ivt} in humans was on average 1.4 times greater than the CL_{ivt} in rabbits. Anyway, the values are relatively similar and the correlation is good ($\rho = 0.91$, $R^2 = 0.82$).

One criticism has been based on the differences between the vasculature of the rabbit retina and the human retina. Nevertheless, in rabbit and human the retinal and choroidal blood flows are similar (Table 5) and the vascular walls as well (tight junctions in the retina; leaky vessels in the choroid). However, some issues of concern are related to the potential impact of the disease state on leakiness of the blood–ocular barriers, especially the RPE. Since CL_{ivt} is clearly permeability limited, changes in the rate–limiting membranes are expected to modify pharmacokinetics. This factor did not become evident in the data analysis based on the patients in Fig. 3, but we cannot exclude the possibility that some disease states might have significant impact on the intravitreal pharmacokinetics.

For macromolecules, anterior elimination via aqueous humor turnover is the main route of elimination. The rates of the aqueous humor turnover are similar in human and rabbit (Table 5), but these values are higher than the CL_{ivt} of macromolecules (Dejneka et al., 2008; del Amo et al., 2015; Eyetech Study Group, 2002; Leeds et al., 1997). Therefore, the access of the drug to the aqueous humor may limit its elimination in both rabbit and human eye. The CL_{ivt} values of bevacizumab in humans are 0.025 ml/h and 0.042 ml/h (Table 4), while in rabbit it is 0.019 ml/h (Bakri et al., 2007; Christoforidis et al., 2013; del Amo et al., 2015). The role of the barrier between vitreous and anterior chamber (lens, vitreous, zonules) remains unknown, but the data do not support major differences between man and rabbit.

In humans, the vitreous becomes more liquefied and less homogenous with the age, and this is associated with increased convective flow in the vitreal cavity (Maurice, 2001; Missel, 2012). Liquefaction and convection has been stated to be major pharmacokinetic differences between the rabbit and elderly patients (Laude et al., 2010). However, no significant difference in the intravitreal concentrations in patients with and without vitrectomy was observed in Gan's study (Gan et al., 2005) and the apparent CL_{ivt} value of vancomycin was not higher in vitrectomized patients (Ferencz et al., 1999) compared to non-vitrectomized patients (Haider et al., 2001) (Fig. 3, Table 2). Moreover, apparent CL_{ivt} values in elderly patients with and without vitrectomy were only moderately different from the CL_{ivt} values in healthy rabbits (Fig. 3, Table 2). Furthermore, Los (2008) showed that aging rabbit eye may be a good model for human vitreous liquefaction based on anatomical and histological analysis. Such a model may be a better approach than enzyme treatments to investigate the effect of the liquefying matrix or vitrectomy on vitreal drug elimination. Overall, even though vitreous humor may play a partial role in the elimination of macromolecules from the vitreal cavity, there is no evidence that the differences in the vitreal liquefaction or convection would cause significant changes in intravitreal pharmacokinetics (Fig. 3).

Drug metabolism in the liver is different in various species and, therefore, test methods based on human cells are being developed (Vellonen et al., 2014). The metabolic activity in the eye is relatively small if any. In general, intravitreal drugs are eliminated from the eye via elimination across the blood-ocular barriers and aqueous humor outflow, and not via metabolism (del Amo et al., 2015). Comparison between the rabbit and human data has not revealed metabolism derived species differences in vitreal drug elimination.

Even though the eye is partly immune protected site, there is a possibility that intravitreal injection of human protein or humanized antibody could cause immune response in the eye. Impact of immune response on intravitreal pharmacokinetics has not been demonstrated, even though Gaudreault et al. (2007) discussed this possibility. Formation of anti-drug antibodies can have substantial influence on systemic clearance of some protein-based drugs (Chen et al., 2013). The neutralizing antibodies are formed in a few weeks. Therefore, the immunological influence on intravitreal pharmacokinetics is expected to be minimal after a single injection, but may become evident during multiple dosing therapy.

Sometimes binding of drug to target proteins determines the drug clearance from the systemic circulation (Levy, 1994). For example, FcRN receptors mediate clearance of monoclonal antibodies from the systemic circulation so that the receptor turnover processes bring drug back to the blood circulation thereby prolonging the retention in the circulation (Ezan, 2013; Mager and Jusko, 2001). This leads sometimes also to receptor saturation and dose-dependent clearance, i.e. increasing clearance at higher doses. In principle, such mechanisms might operate within the eye, but so far they have not been shown to exist.

This review has concentrated on intravitreal pharmacokinetics of drugs in solution form. There is an increasing interest on ocular drug delivery systems for prolonged and controlled drug delivery to the posterior eye segment (del Amo and Urtti, 2008). The functionality of the dosage forms in the rabbit and human eye is beyond the scope of this review. Anyway, CL_{ivt} values are useful in the design of drug delivery systems, because the required release rate *in vivo* depends on the target concentration and CL_{ivt} (del Amo et al., 2015). Furthermore, the required drug payload in the dosage form is release rate multiplied by the dosing interval. As only small volumes can be injected intravitreally (maximum 100 μl), computational estimation of drug payload is very important aid in the design of prolonged action dosage forms for the retinal treatment. Overall, CL_{ivt} should be taken into account in the design of new intravitreal drug delivery systems.

6. Conclusions

In this review we have analyzed the data on intravitreal pharmacokinetics in rabbits and humans. Overall, based on the current data the rabbit is clinically predictable animal model for intravitreal pharmacokinetics, since both intravitreal volume of distribution and clearance values differ only moderately between rabbit and human. Intravitreal pharmacokinetic studies should be designed so that accurate values for clearance and volume of distribution are obtained. Further studies are needed in special cases, such as disease state effects, to complement the understanding of intravitreal pharmacokinetics.

Acknowledgments

This study was supported by the Finnish Cultural Foundation (E.d.A.) and Academy of Finland (A.U., project number 268868).

Appendix A. Supplementary data

Supplementary data related to this article can be found at http://dx.doi.org/10.1016/j.exer.2015.05.003.

References

Ahn, J., Kim, H., Woo, S.J., Park, J.H., Park, S., Hwang, D.J., Park, K.H., 2013. Pharmacokinetics of intravitreally injected bevacizumab in vitrectomized eyes. J. Ocul. Pharmacol. Ther. 29, 612–618.

Ahn, S.J., Ahn, J., Park, S., Kim, H., Hwang, D.J., Park, J.H., Park, J.Y., Chung, J.Y., Park, K.H., Woo, S.J., 2014. Intraocular pharmacokinetics of ranibizumab in vitrectomized versus nonvitrectomized eyes. Invest. Ophthalmol. Vis. Sci. 55, 567–573.

Alm, A., Bill, A., 1973. Ocular and optic nerve blood flow at normal and increased intraocular pressures in monkeys (Macaca irus): a study with radioactively labelled microspheres including flow determinations in brain and some other

tissues. Exp. Eye Res. 15, 15–29.
Atluri, H., Mitra, A.K., 2003. Disposition of short-chain aliphatic alcohols in rabbit vitreous by ocular microdialysis. Exp. Eye Res. 76, 315–320.
Bakri, S.J., Snyder, M.R., Reid, J.M., Pulido, J.S., Singh, R.J., 2007. Pharmacokinetics of intravitreal bevacizumab (Avastin). Ophthalmology 114, 855–859.
Barany, Y.E., Kinsey, V.E., 1949. The rate of flow of aqueous humor; the rate of disappearance of para-aminohippuric acid, radioactive rayopake, and radioactive diodrast from the aqueous humor of rabbits. Am. J. Ophthalmol 32, 177–188. Pt. 2.
Bashshur, Z.F., Haddad, Z.A., Schakal, A., Jaafar, R.F., Saab, M., Noureddin, B.N., 2008. Intravitreal bevacizumab for treatment of neovascular age-related macular degeneration: a one-year prospective study. Am. J. Ophthalmol. 145, 249–256 e2.
Beer, P.M., Wong, S.J., Hammad, A.M., Falk, N.S., O'Malley, M.R., Khan, S., 2006. Vitreous levels of unbound bevacizumab and unbound vascular endothelial growth factor in two patients. Retina 26, 871–876.
Bejanian, M., Lieberman, R.M., Goldstein, D.A., Engstrom, R.E., Boyer, D.S., Dunn, J.P., 1999. A pharmacokinetic study of intravitreal fomivirsen in patients with CMVR. Invest. Opthalmol. Vis. Sci. 40. S874–Abstract.
Brubaker, R.F., 1982. The flow of aqueous humor in the human eye. Trans. Am. Ophthalmol. Soc. 80, 391–474.
Cheung, L.K., Eaton, A., 2013. Age-related macular degeneration. Pharmacotherapy 33, 838–855.
Chen, X., Hickling, T., Kraynov, E., Kuang, B., Parng, C., Vicini, P., 2013. A mathematical model of the effect of immunogenicity on therapeutic protein pharmacokinetics. AAPS J. 15, 1141–1154.
Chin, H.S., Park, T.S., Moon, Y.S., Oh, J.H., 2005. Difference in clearance of intravitreal triamcinolone acetonide between vitrectomized and nonvitrectomized eyes. Retina 25, 556–560.
Christoforidis, J.B., Carlton, M.M., Knopp, M.V., Hinkle, G.H., 2011. PET/CT imaging of I-124-radiolabeled bevacizumab and ranibizumab after intravitreal injection in a rabbit model. Invest. Ophthalmol. Vis. Sci. 52, 5899–5903.
Christoforidis, J.B., Williams, M.M., Kothandaraman, S., Kumar, K., Epitropoulos, F.J., Knopp, M.V., 2012. Pharmacokinetic properties of intravitreal i-124-aflibercept in a rabbit model using PET/CT. Curr. Eye Res. 37, 1171–1174.
Christoforidis, J.B., Williams, M.M., Wang, J., Jiang, A., Pratt, C., Abdel-Rasoul, M., Hinkle, G.H., Knopp, M.V., 2013. Anatomic and pharmacokinetic properties of intravitreal bevacizumab and ranibizumab after vitrectomy and lensectomy. Retina 33, 946–952.
Dejneka, N.S., Wan, S., Bond, O.S., Kornbrust, D.J., Reich, S.J., 2008. Ocular biodistribution of bevasiranib following a single intravitreal injection to rabbit eyes. Mol. Vis. 14, 997–1005.
del Amo, E.M., Urtti, A., 2008. Current and future ophthalmic drug delivery systems. A shift to the posterior segment. Drug Discov. Today 13, 135–143.
del Amo, E.M., Vellonen, K., Kidron, H., Urtti, A., 2015. Intravitreal clearance and volume of distribution of compounds in rabbits: In silico prediction and pharmacokinetic simulations for drug development. Eur. J. Pharm. Biopharm. http://dx.doi.org/10.1016/j.ejpb.2015.01.003.
Diaz-Llopis, M., Chipont, E., Sanchez, S., Espana, E., Navea, A., Menezo, J.L., 1992. Intravitreal foscarnet for cytomegalovirus retinitis in a patient with acquired immunodeficiency syndrome. Am. J. Ophthalmol. 114, 742–747.
Doft, B.H., Weiskopf, J., Nilsson-Ehle, I., Wingard Jr., L.B., 1985. Amphotericin clearance in vitrectomized versus nonvitrectomized eyes. Ophthalmology 92, 1601–1605.
Durairaj, C., Kim, S.J., Edelhauser, H.F., Shah, J.C., Kompella, U.B., 2009. Influence of dosage form on the intravitreal pharmacokinetics of diclofenac. Invest. Ophthalmol. Vis. Sci. 50, 4887–4897.
Duvvuri, S., Gandhi, M.D., Mitra, A.K., 2003. Effect of P-glycoprotein on the ocular disposition of a model substrate, quinidine. Curr. Eye Res. 27, 345–353.
Eyetech Study Group, 2002. Preclinical and phase 1A clinical evaluation of an anti-VEGF pegylated aptamer (EYE001) for the treatment of exudative age-related macular degeneration. Retina 22, 143–152.
Ezan, E., 2013. Pharmacokinetic studies of protein drugs: past, present and future. Adv. Drug Deliv. Rev. 65, 1065–1073.
Feke, G.T., Tagawa, H., Deupree, D.M., Goger, D.G., Sebag, J., Weiter, J.J., 1989. Blood flow in the normal human retina. Invest. Ophthalmol. Vis. Sci. 30, 58–65.
Ferencz, J.R., Assia, E.I., Diamantstein, L., Rubinstein, E., 1999. Vancomycin concentration in the vitreous after intravenous and intravitreal administration for postoperative endophthalmitis. Arch. Ophthalmol. 117, 1023–1027.
Ficker, L., Meredith, T.A., Gardner, S., Wilson, L.A., 1990. Cefazolin levels after intravitreal injection. Effects of inflammation and surgery. Invest. Ophthalmol. Vis. Sci. 31, 502–505.
Gajraj, R.T.C., 2012. A Study of Drug Transport in the Vitreous Humor: Effect of Drug Size; Comparing Micro- and Macro-scale Diffusion; Assessing Vitreous Models; and Obtaining in Vivo Data. https://tspace.library.utoronto.ca/handle/1807/33202.
Gan, I.M., Ugahary, L.C., van Dissel, J.T., van Meurs, J.C., 2005. Effect of intravitreal dexamethasone on vitreous vancomycin concentrations in patients with suspected postoperative bacterial endophthalmitis. Graefes Arch. Clin. Exp. Ophthalmol. 243, 1186–1189.
Gan, I.M., van Dissel, J.T., Beekhuis, W.H., Swart, W., van Meurs, J.C., 2001. Intravitreal vancomycin and gentamicin concentrations in patients with postoperative endophthalmitis. Br. J. Ophthalmol. 85, 1289–1293.
Gaudreault, J., Fei, D., Beyer, J.C., Ryan, A., Rangell, L., Shiu, V., Damico, L.A., 2007. Pharmacokinetics and retinal distribution of ranibizumab, a humanized antibody fragment directed against VEGF-A, following intravitreal administration in rabbits. Retina 27, 1260–1266.
Gillette, J.R., 1971. Factors affecting drug metabolism. Ann. N. Y. Acad. Sci. 179, 43–66.
Gupta, S.K., Velpandian, T., Dhingra, N., Jaiswal, J., 2000. Intravitreal pharmacokinetics of plain and liposome-entrapped fluconazole in rabbit eyes. J. Ocul. Pharmacol. Ther. 16, 511–518.
Haider, S.A., Hassett, P., Bron, A.J., 2001. Intraocular vancomycin levels after intravitreal injection in post cataract extraction endophthalmitis. Retina 21, 210–213.
Hemenger, R.P., Garner, L.F., Ooi, C.S., 1995. Change with age of the refractive index gradient of the human ocular lens. Invest. Ophthalmol. Vis. Sci. 36, 703–707.
Henry, K., Cantrill, H., Fletcher, C., Chinnock, B.J., Balfour Jr., H.H., 1987. Use of intravitreal ganciclovir (dihydroxy propoxymethyl guanine) for cytomegalovirus retinitis in a patient with AIDS. Am. J. Ophthalmol. 103, 17–23.
Hughes, P.M., Krishnamoorthy, R., Mitra, A.K., 1996. Vitreous disposition of two acycloguanosine antivirals in the albino and pigmented rabbit models: a novel ocular microdialysis technique. J. Ocul. Pharmacol. Ther. 12, 209–224.
Iyer, M.N., He, F., Wensel, T.G., Mieler, W.F., Benz, M.S., Holz, E.R., 2006. Clearance of intravitreal moxifloxacin. Invest. Ophthalmol. Vis. Sci. 47, 317–319.
Jarus, G., Blumenkranz, M., Hernandez, E., Sossi, N., 1985. Clearance of intravitreal fluorouracil. Normal and aphakic vitrectomized eyes. Ophthalmology 92, 91–96.
Johnson, T.R., 2010. Pharmacokinetic and ocular distribution of PF-04523655 and RTP801-inhibiting siRNA, following intravitreal administration in rabbits. Invest. Ophthalmol. Vis. Sci. 51. E-Abstract 2442.
Jusko, W.J., 2006. Guidelines for collection and analysis for pharmacokinetic data. In: Burton, M.E. (Ed.), Applied Pharmacokinetics and Applied Therapeutics, fourth ed. Lippincott Williams & Wilkins, pp. 9–26.
Kidron, H., del Amo, E.M., Vellonen, K.S., Urtti, A., 2012. Prediction of the vitreal half-life of small molecular drug-like compounds. Pharm. Res. 29, 3302–3311.
Kidron, H., Vellonen, K.S., del Amo, E.M., Tissari, A., Urtti, A., 2010. Prediction of the corneal permeability of drug-like compounds. Pharm. Res. 27, 1398–1407.
Knudsen, L.L., Dissing, T., Hansen, M.N., Nielsen-Kudsk, F., 2001. Ocular fluorescein kinetics before and after vitrectomy on swine. Graefes Arch. Clin. Exp. Ophthalmol. 239, 832–839.
Kontturi, L.S., Collin, E.C., Murtomaki, L., Pandit, A.S., Yliperttula, M., Urtti, A., 2014. Encapsulated cells for long-term secretion of soluble VEGF receptor 1: material optimization and simulation of ocular drug response. Eur. J. Pharm. Biopharm. http://dx.doi.org/10.1016/j.ejpb.2014.10.005.
Koyano, S., Araie, M., Eguchi, S., 1993. Movement of fluorescein and its glucuronide across retinal pigment epithelium-choroid. Invest. Ophthalmol. Vis. Sci. 34, 531–538.
Krohne, T.U., Eter, N., Holz, F.G., Meyer, C.H., 2008. Intraocular pharmacokinetics of bevacizumab after a single intravitreal injection in humans. Am. J. Ophthalmol. 146, 508–512.
Krohne, T.U., Muether, P.S., Stratmann, N.K., Holz, F.G., Kirchhof, B., Meyer, C.H., Fauser, S., 2015. Influence of ocular volume and lens status on pharmacokinetics and duration of action of intravitreal vascular endothelial growth factor inhibitors. Retina 35, 69–74.
Lanevskij, K., Japertas, P., Didziapetris, R., Petrauskas, A., 2009. Ionization-specific prediction of blood-brain permeability. J. Pharm. Sci. 98, 122–134.
Laude, A., Tan, L.E., Wilson, C.G., Lascaratos, G., Elashry, M., Aslam, T., Patton, N., Dhillon, B., 2010. Intravitreal therapy for neovascular age-related macular degeneration and inter-individual variations in vitreous pharmacokinetics. Prog. Retin. Eye Res. 29, 466–475.
Lee, S.S., Ghosn, C., Yu, Z., Zacharias, L.C., Kao, H., Lanni, C., Abdelfattah, N., Kuppermann, B., Csaky, K.G., D'Argenio, D.Z., Burke, J.A., Hughes, P.M., Robinson, M.R., 2010. Vitreous VEGF clearance is increased after vitrectomy. Invest. Ophthalmol. Vis. Sci. 51, 2135–2138.
Leeds, J.M., Henry, S.P., Truong, L., Zutshi, A., Levin, A.A., Kornbrust, D., 1997. Pharmacokinetics of a potential human cytomegalovirus therapeutic, a phosphorothioate oligonucleotide, after intravitreal injection in the rabbit. Drug Metab. Dispos. 25, 921–926.
Levy, G., 1994. Pharmacologic target-mediated drug disposition. Clin. Pharmacol. Ther. 56, 248–252.
Linnankoski, J., Makela, J.M., Ranta, V.P., Urtti, A., Yliperttula, M., 2006. Computational prediction of oral drug absorption based on absorption rate constants in humans. J. Med. Chem. 49, 3674–3681.
Liu, X., Tu, M., Kelly, R.S., Chen, C., Smith, B.J., 2004. Development of a computational approach to predict blood-brain barrier permeability. Drug Metab. Dispos. 32, 132–139.
Los, L.I., 2008. The rabbit as an animal model for post-natal vitreous matrix differentiation and degeneration. Eye (Lond) 22, 1223–1232.
Mager, D.E., 2006. Quantitative structure-pharmacokinetic/pharmacodynamic relationships. Adv. Drug Deliv. Rev. 58, 1326–1356.
Mager, D.E., Jusko, W.J., 2001. General pharmacokinetic model for drugs exhibiting target-mediated drug disposition. J. Pharmacokinet. Pharmacodyn. 28, 507–532.
Mandell, B.A., Meredith, T.A., Aguilar, E., el-Massry, A., Sawant, A., Gardner, S., 1993. Effects of inflammation and surgery on amikacin levels in the vitreous cavity. Am. J. Ophthalmol. 115, 770–774.
Mannermaa, E., Reinisalo, M., Ranta, V.P., Vellonen, K.S., Kokki, H., Saarikko, A., Kaarniranta, K., Urtti, A., 2010. Filter-cultured ARPE-19 cells as outer blood-retinal barrier model. Eur. J. Pharm. Sci. 40, 289–296.

Maurice, D., 2001. Review: practical issues in intravitreal drug delivery. J. Ocul. Pharmacol. Ther. 17, 393–401.
Maurice, D.M., Mishima, S., 1984. Ocular pharmacokinetics. In: Anonymous Pharmacology of the Eye. Springer-Verlag.
Meyer, C.H., Krohne, T.U., Holz, F.G., 2011. Intraocular pharmacokinetics after a single intravitreal injection of 1.5 mg versus 3.0 mg of bevacizumab in humans. Retina 31, 1877–1884.
Missel, P.J., 2012. Computer modeling for drug delivery. In: Thassu, D., Chader, G.J. (Eds.), Ocular Drug Delivery Systems, first ed. CRC Press, Taylor & Francis group, pp. 59–94.
Mochizuki, K., Torisaki, M., Yamashita, Y., Komatsu, M., Tanahashi, T., 1993. Intravitreal flomoxef sodium in rabbits. Ophthalmic Res. 25, 128–136.
Mochizuki, K., Yamashita, Y., Torisaki, M., Komatsu, M., Tanahashi, T., Kawasaki, K., 1992. Intraocular kinetics of ceftazidime (Modacin). Ophthalmic Res. 24, 150–154.
Moisseiev, E., Waisbourd, M., Ben-Artsi, E., Levinger, E., Barak, A., Daniels, T., Csaky, K., Loewenstein, A., Barequet, I.S., 2014. Pharmacokinetics of bevacizumab after topical and intravitreal administration in human eyes. Graefes Arch. Clin. Exp. Ophthalmol. 252, 331–337.
Morlet, N., Young, S., Naidoo, D., Graham, G., Coroneo, M.T., 1996. High dose intravitreal ganciclovir injection provides a prolonged therapeutic intraocular concentration. Br. J. Ophthalmol. 80, 214–216.
Nilsson, S.F.E., Alm, A., 2012. Determination of ocular blood flows with the microsphere method.. In: Anonymous Ocular Blood Flow. Springer.
Nomoto, H., Shiraga, F., Kuno, N., Kimura, E., Fujii, S., Shinomiya, K., Nugent, A.K., Hirooka, K., Baba, T., 2009. Pharmacokinetics of bevacizumab after topical, subconjunctival, and intravitreal administration in rabbits. Invest. Ophthalmol. Vis. Sci. 50, 4807–4813.
Obach, R.S., Lombardo, F., Waters, N.J., 2008. Trend analysis of a database of intravenous pharmacokinetic parameters in humans for 670 drug compounds. Drug Metab. Dispos. 36, 1385–1405.
Panda-Jonas, S., Jonas, J.B., Jakobczyk, M., Schneider, U., 1994. Retinal photoreceptor count, retinal surface area, and optic disc size in normal human eyes. Ophthalmology 101, 519–523.
Pearson, P.A., Hainsworth, D.P., Ashton, P., 1993. Clearance and distribution of ciprofloxacin after intravitreal injection. Retina 13, 326–330.
Pflugfelder, S.C., Hernandez, E., Fliesler, S.J., Alvarez, J., Pflugfelder, M.E., Forster, R.K., 1987. Intravitreal vancomycin. Retinal toxicity, clearance, and interaction with gentamicin. Arch. Ophthalmol. 105, 831–837.
Pitkanen, L., Ranta, V.P., Moilanen, H., Urtti, A., 2005. Permeability of retinal pigment epithelium: effects of permeant molecular weight and lipophilicity. Invest. Ophthalmol. Vis. Sci. 46, 641–646.
Pitkanen, L., Ruponen, M., Nieminen, J., Urtti, A., 2003. Vitreous is a barrier in nonviral gene transfer by cationic lipids and polymers. Pharm. Res. 20, 576–583.
Quinn, R.H., Miller, S.S., 1992. Ion transport mechanisms in native human retinal pigment epithelium. Invest. Ophthalmol. Vis. Sci. 33, 3513–3527.
Raju, B., Thiagarajan, G., Das, T., Hyderabad Endophthalmitis Research Group, 2004. Modified high-performance liquid chromatography technique for detection of vancomycin in human vitreous. Ophthalmic Res. 36, 55–61.
Reichenbach, A., Ziegert, M., Schnitzer, J., Pritz-Hohmeier, S., Schaaf, P., Schober, W., Schneider, H., 1994. Development of the rabbit retina. V. The question of 'columnar units'. Brain Res. Dev. Brain Res. 79, 72–84.
Roh, S., Weiter, J.J., Duker, J.S., 2006. Ocular circulation. In: Anonymous Duane's Ophthalmology on CD-ROM, 2006 ed. Lippincott Williams & Wilkins. pp. (Chapter 5).
Rowe-Rendleman, C.L., Durazo, S.A., Kompella, U.B., Rittenhouse, K.D., Di Polo, A., Weiner, A.L., Grossniklaus, H.E., Naash, M.I., Lewin, A.S., Horsager, A., Edelhauser, H.F., 2014. Drug and gene delivery to the back of the eye: from bench to bedside. Invest. Ophthalmol. Vis. Sci. 55, 2714–2730.
Ruby, A.J., Williams, G.A., Blumenkranz, M.S., 2006. Vitreous humor. In: Anonymous. Lippincott Williams & Wilkins.
Sanford, M., 2013. Fluocinolone acetonide intravitreal implant (IluvienÂ®). Drugs 73, 187–193.
Schoenwald, R.D., 2003. Ocular pharmacokinetics and pharmacodynamics. In: Mitra, A.K. (Ed.), Ophthalmic Drug Delivery Systems, pp. 135–179.
Sebag, J., Tang, M., Brown, S., Sadun, A.A., Charles, M.A., 1994. Effects of pentoxifylline on choroidal blood flow in nonproliferative diabetic retinopathy. Angiology 45, 429–433.
Severn, P.S., Hamilton, R., 2015. The incidence of serious complications associated with intravitreal therapy in a quaternary ARMD service (2008-2014). Eye (Lond) 29, 150.
Shen, Y.C., Wang, M.Y., Wang, C.Y., Tsai, T.C., Tsai, H.Y., Lee, Y.F., Wei, L.C., 2007. Clearance of intravitreal voriconazole. Invest. Ophthalmol. Vis. Sci. 48, 2238–2241.
Stewart, M.W., Rosenfeld, P.J., 2008. Predicted biological activity of intravitreal VEGF Trap. Br. J. Ophthalmol. 92, 667–668.
Tan, L.E., Orilla, W., Hughes, P.M., Tsai, S., Burke, J.A., Wilson, C.G., 2011. Effects of vitreous liquefaction on the intravitreal distribution of sodium fluorescein, fluorescein dextran, and fluorescent microparticles. Invest. Ophthalmol. Vis. Sci. 52, 1111–1118.
Taskintuna, I., Rahhal, F.M., Capparelli, E.V., Cundy, K.C., Freeman, W.R., 1998. Intravitreal and plasma cidofovir concentrations after intravitreal and intravenous administration in AIDS patients with cytomegalovirus retinitis. J. Ocul. Pharmacol. Ther. 14, 147–151.
Totan, Y., Guler, E., Guragac, F.B., 2015. Dexamethasone intravitreal implant for chronic diabetic macular Edema resistant to intravitreal bevacizumab treatment. Curr. Eye Res. 1–7.
Urtti, A., 2006. Challenges and obstacles of ocular pharmacokinetics and drug delivery. Adv. Drug Deliv. Rev. 58, 1131–1135.
Vellonen, K.S., Malinen, M., Mannermaa, E., Subrizi, A., Toropainen, E., Lou, Y.R., Kidron, H., Yliperttula, M., Urtti, A., 2014. A critical assessment of in vitro tissue models for ADME and drug delivery. J. Control. Release 190, 94–114.
Wiederholt, M., Kossendrup, D., Schulz, W., Hoffmann, F., 1986. Pharmacokinetic of topical cyclosporin A in the rabbit eye. Invest. Ophthalmol. Vis. Sci. 27, 519–524.
Wingard Jr., L.B., Zuravleff, J.J., Doft, B.H., Berk, L., Rinkoff, J., 1989. Intraocular distribution of intravitreally administered amphotericin B in normal and vitrectomized eyes. Invest. Ophthalmol. Vis. Sci. 30, 2184–2189.
Wu, C.D., Müller, H.K., Hockwin, O., Noll, E., 1970. Determination of the wet and dry weight of Iris, ciliary body and choroid in man and in different animal species. Ophthalmic Res. 1, 124.
Xu, J., Heys, J.J., Barocas, V.H., Randolph, T.W., 2000. Permeability and diffusion in vitreous humor: implications for drug delivery. Pharm. Res. 17, 664–669.
Xu, Q., Boylan, N.J., Suk, J.S., Wang, Y., Nance, E.A., Yang, J., McDonnell, P.J., Cone, R.A., Duh, E.J., Hanes, J., 2013. Nanoparticle diffusion in, and microrheology of, the bovine vitreous ex vivo. J. Control. Release 167, 76–84.
Zamudio, A.C., Candia, O.A., 2011. Interaction between mechanical and osmotic forces in the isolated rabbit lens. Exp. Eye Res. 93, 798–803.
Zhang, K., Zhang, L., Weinreb, R.N., 2012. Ophthalmic drug discovery: novel targets and mechanisms for retinal diseases and glaucoma. Nat. Rev. Drug Discov. 11, 541–559.
Zhu, Q., Ziemssen, F., Henke-Fahle, S., Tatar, O., Szurman, P., Aisenbrey, S., Schneiderhan-Marra, N., Xu, X., Tubingen Bevacizumab Study Group, Grisanti, S., 2008. Vitreous levels of bevacizumab and vascular endothelial growth factor-A in patients with choroidal neovascularization. Ophthalmology 115, 1750–1755, 1755.e1.

9. Synopsis of the main results

The main results of the computational models and the comprehensive collation of the ocular data are summarized below:

1. Systemic pharmacokinetics

QSPR models for parallel prediction of systemic V_{ss} and f_u in humans were obtained based on a data set of 541 compounds (**I**):

$LogV_{ss}$= 0.2464 + 0.0909**LgS3** - 0.0269**LgS10** - 0.0099**LogS** + 0.3894**L3LgS** + 0.0465**$LogD_{10}$** + 0.0514**$LogD_{5.5}$** + 0.0010**%FU10** + 0.0004**MV** - 0.0005**W1** + 0.0023**D4** + 0.0174**HD**

f_u= 0.7052 + 0.0091**LgS3** - 0.0024**LgS10** + 0.0600**LogS** + 0.0277**L3LgS** - 0.0153 **$LogD_{10}$** - 0.0583**$LogD_{5.5}$** + 0.0009**%FU10** - 0.0007**MV** + 0.0001**W1** - 0.0025**D4** + 0.0026**HD**

where L3LgS is solubility profiling coefficient, LogS is the logarithm of solubility, LgS3 and LgS10 are the logarithms of solubility at pH 3 and pH 10, respectively, $LogD_{10}$ and $LogD_{5.5}$ are distribution coefficients at pH 10 and pH 5.5, respectively, %FU10 is % of fraction unionized at pH 10, MV is molar volume, W1 is hydrophilic volume, D4 is hydrophobic volume and HD is hydrogen bond donor. The cross-validation value of the model was Q^2 (leave-1/7-out) = 0.55. The model predicted the external test set: Q^2 = 0.50 for $LogV_{ss}$ and Q^2 = 0.54 for f_u. A foreign test set was also evaluated and the following predictions obtained: Q^2= 0.70 for $LogV_{ss}$ and Q^2 = 0.54 for f_u. In both cases, 101 drugs were used and the results were statistically significant in the Y-permutation test. The applicability domain of the model was successfully defined. Eleven descriptors were needed in the QSPR models for V_{ss} and f_u, these were related to lipophilicity, polarity and size of the molecule.

QSPR classification models were able to classify the drugs with high or low values of V_{ss} while classification of f_u was successful only for drugs with high V_{ss}. The predominant descriptors in the models were also related to molecular size, charge and lipophilicity.

2. Intravitreal pharmacokinetics

- Comprehensive collection of intravitreal values for $V_{ss,\ ivt}$, CL_{ivt} and $t_{1/2,\ ivt}$ in rabbit (40 small molecular weight compounds and 11 macromolecules) was generated (**III**). The CL_{ivt} and $t_{1/2,\ ivt}$ values showed wide ranges (0.011 – 1.530 ml/h for CL_{ivt} and 1.44 – 143.58 h for $t_{1/2,\ ivt}$). The range of $V_{ss,\ ivt}$ was narrow (0.72 – 3.14 ml). The wide range of CL_{ivt} values stemmed from the small molecular drug data (49-fold range). The CL_{ivt} range of macromolecules was narrow (2-fold).
- QSPR model for intravitreal half-life was constructed based on 40 intravitreal compounds (**II**):
  $Logt_{1/2}$= - 0.046 - 0.051**$LogD_{7.4}$** + 0.640**$LogH_{tot}$**

where $LogH_{tot}$ is the logarithm of the sum of hydrogen bond donors and acceptors. The Q^2 (leave-1/7-out) was 0.66. The model predicted the internal (Q^2= 0.76) and external (Q^2= 0.81) test sets and was statistically robust in the Y-permutation test. The applicability domain of the model was described by the value range of the molecular descriptors.

- Similarly, a QSPR model for intravitreal clearance of small molecular weight compounds was successfully built using 34 intravitreal drugs (**III**):

  $LogCL_{ivt}$ = -0.25269 - 0.53747**LogHD** + 0.05189$\mathbf{LogD_{7.4}}$

  where LogHD is the logarithm of the hydrogen bond donors. The Q^2 (leave-1/7-out) yielded 0.62. The model predicted internal (Q^2= 0.85) and external (Q^2= 0.92) test sets and was statistically robust in the Y-permutation test.

- Pharmacokinetic simulations of vitreal drug concentrations were carried out **(III)**. Intravitreal injections of drugs and drug delivery systems were simulated based on QSPR-derived CL_{ivt} values and typical $V_{ss, ivt}$ values. The simulations were used to estimate the relationships between drug dose, release rate, target concentration and duration of action.

- Most of the published pharmacokinetic studies involving intravitreal injection in the rabbits did not fulfill the quality criteria. Guidance was compiled on how to design an intravitreal pharmacokinetic study to be conducted in experimental animals (**IV**). A comprehensive rabbit-to-human comparison of intravitreal drug distribution and elimination revealed that intravitreal pharmacokinetics in rabbit and human eye were similar (**IV**). In the case of CL_{ivt} values, a good correlation was seen between rabbit and man. In both species, $V_{ss, ivt}$ values were in the range of the anatomical volume of vitreous humour.

- A comparison of CL_{ivt} with the calculated RPE mediated CL_{ivt} indicated that small molecules are mostly eliminated through the RPE, whereas macromolecules are primarily eliminated via the anterior route (**IV**). The data and analyses did not support the proposal that vitreous plays a significant role in drug elimination from the vitreal cavity.

10. General discussion and future prospects

In the present thesis, novel pharmacokinetic models have been investigated, developed and validated so that they can be exploited in the drug discovery and development process in the systemic and ocular routes of drug administration.

10.1. Systemic V_{ss} and f_u *in silico* prediction in humans

A QSPR was developed using linear PCA-PLS methods which allowed the parallel prediction of V_{ss} and f_u. Additionally, a non-linear Recursive Partitioning method was employed for classification models estimating either V_{ss} alone or V_{ss} together with f_u. Those molecular descriptors related to lipophilicity, charge and size were relevant in both QSPR approaches.

With the PCA-PLS method, a final equation for V_{ss} and f_u was obtained with Q^2Y (leave-1/7-out) of 0.55. The model predicted the external and foreign test sets reliably with Q^2 values ranging from 0.50 to 0.70 and both its statistical significance and applicability domains were defined. The QSPR model provided insights about which molecular determinants may govern systemic drug distribution. For example, the fraction of unionized drug at pH 10 (%FU10) and $LogD_{10}$ exhibited positive relationships with the values of V_{ss}. Higher values of %FU10 and $LogD_{10}$ were mostly found for basic drugs, and this is in line with the fact that the basic drugs have higher V_{ss} values than their acidic counterparts (Rodgers and Rowland, 2007). Charge was also relevant for the drug distribution as basic drugs bind to the acidic phospholipids present on the lipid membranes in the tissues (Rodgers and Rowland, 2007). Basic compounds may also be entrapped inside the acidic lysosomes within the cells (Ishizaki et al., 1998), whereas the lipophilic neutral forms tend to distribute into the adipose tissues.

On the other hand, the same descriptors exert an influence on f_u, but for most of them, the trend was opposite. The most influential descriptors on f_u were LogS (positive impact) and $LogD_{5.5}$ (negative impact). Highly soluble drugs tend to be free in plasma, whereas the lipophilic drugs prefer to bind to plasma proteins (Mayer and Van de Waterbeemd, 1985). Acidic drugs with high $LogD_{5.5}$ values bind to albumin which is the most abundant protein in human plasma (Kwon, 2001, Hall and Guyton, 2011) and this property leads to smaller f_u values.

Eleven *in silico* descriptors were necessary for the success of the model. This is a reflection of the complexity of systemic drug distribution, since there are a large number of different cellular and tissue binding sites as well as binding sites in plasma and factors that affect membrane permeation from plasma to the tissues (Rowland and Tozer, 2011, Toutain and Bousquet-Melou, 2004, Kwon, 2001, Pandit and Soltis, 2012). Overall, lipophilicity and solubility related descriptors were found to affect both V_{ss} and f_u, but in opposite directions.

The developed QSPR model that encompasses both V_{ss} and f_u is a useful tool for virtual screening of new compounds *in silico*. The model may help in the selection of drug

candidates and therefore it may well accelerate drug discovery. However, this is only one factor in the complicated world of drug discovery (van de Waterbeemd and Gifford, 2003). One must also note that in many cases the accuracy of predictions was only modest and a comparison with the PBPK models for V_{ss} (Poulin and Theil, 2002, Rodgers and Rowland, 2007) could prove to be illuminating. In the future, V_{ss} and f_u models may become integrated into pharmacokinetic and pharmacodynamic models (Xu and Mager, 2011, Theil et al., 2003). Nevertheless, there is still work to be done to improve the drug discovery and development process and to implement this kind of integrative approach (van de Waterbeemd and Gifford, 2003, Lombardo et al., 2003).

10.2. Intravitreal pharmacokinetics: assessment of the rabbit model

The rabbit is the most commonly used animal species in ocular pharmacokinetics (Maurice and Mishima, 1984, Prince, 1964). One goal of this thesis project was to evaluate the value of the rabbit when modelling intravitreal pharmacokinetics. This is an important topic since many ocular retinal diseases can be only treated and controlled by intravitreal injections. Only rarely have the intravitreal pharmacokinetics been investigated in humans due to the ethical constraints; animals have to used and the rabbit has been the most popular animal species in these kinds of studies (Maurice and Mishima, 1984). Nevertheless, the use of rabbits has been criticized, based on the anatomical and physiological differences between the rabbit and human eye (Bakri et al., 2007a, Bakri et al., 2007b, Vaishya et al., 2011, Rittenhouse and Pollack, 2000). Furthermore, although some investigators have claimed that there are pharmacokinetic differences between rabbit and man, often these discrepancies are attributable to inadequate sampling and assay problems (Nomoto et al., 2009, Lee et al., 2010). Nonetheless, based on these misleading studies, the rabbit model has even been criticized in a recent authoritative 'consensus' paper focusing on ocular drug delivery (Rowe-Rendleman et al., 2014).

The intravitreal pharmacokinetics in rabbits and humans were compared in a systematic manner. Apparent intravitreal clearance ($CL_{ivt,\ app}$) values of eight drugs were calculated based on the human patient studies. Interestingly, the apparent CL_{ivt} in humans correlated well with the values of rabbit CL_{ivt} displaying a Spearman's rank correlation coefficient of $\rho = 0.91$, (Rabbit $CL_{ivt} = 1.41 \times$ Human $CL_{ivt,\ app} + 0.04$, units are ml/h; $R^2 = 0.82$). The value of apparent CL_{ivt} in humans was, on average, 1.4 times greater than the corresponding CL_{ivt} value in rabbits. On the other hand, the intravitreal volume of distribution ($V_{ss,\ ivt}$) of bevacizumab in humans was larger than in rabbits (maximally 4.5-fold difference) (Zhu et al. 2008, Bakri et al. 2007, Christoforidis et al. 2013, III). These results demonstrated that the rabbit eye is a reasonable model for intravitreal pharmacokinetics: there is a good correlation in CL_{ivt} values and only modestly different absolute values. Therefore, translation from rabbit data to humans should be relatively easy and reliable. Pharmacokinetic similarity is based on the physiological and anatomical parameters: flows, blood-ocular barriers permeability and surface areas. These parameters are surprisingly similar in human and rabbit eye.

It has been claimed that there are differences in the viscosity of the vitreous between the healthy rabbit and elderly human patient eye and that this constitutes a major problem (Laude et al., 2010, Tan et al., 2011, Thakur et al., 2014). However, the data analyses did not provide support for this proposal. In fact, in the correlation conducted here between human $CL_{ivt, app}$ and rabbit CL_{ivt} values much of the human data included studies with elderly patients suffering from ocular diseases. Nevertheless, CL_{ivt} is clearly dependent on RPE permeability and diseases affecting the ocular epithelium may have an impact on the intravitreal pharmacokinetics. In this regard, further studies will be needed to dissect the role of retinal diseases in altering the intravitreal pharmacokinetics of small molecular weight drugs and macromolecules.

In conclusion, the rabbit is a useful animal model for the human eye and it can be used for preclinical studies of intravitreal pharmacokinetics.

10.3. Intravitreal clearance and half-life *in silico* predictions

In this work, a QSPR model for intravitreal half-life for small molecular drugs was built based on data of 47 compounds in experiments conducted in albino or pigmented rabbits. The pharmacokinetic studies selected were those in which the intravitreal concentrations had been measured during a time-span of not less than two half-lives. The final QSPR equation for $t_{1/2,\ ivt}$ (including albino and pigmented rabbits) was physiologically interpretable. The relevant descriptors were $LogD_{7.4}$ and the total hydrogen bonding capacity (the sum of donor and acceptor hydrogen bonds). $LogD_{7.4}$ showed a negative correlation with $t_{1/2,\ ivt}$, whereas hydrogen bonding showed a positive relationship with $t_{1/2,\ ivt}$. The ability of the QSPR model to predict $t_{1/2,\ ivt}$ was verified with an internal test set and a randomly chosen external test set. It is remarkable that $t_{1/2,\ ivt}$ can be reliably predicted with two descriptors that are known to affect membrane permeability (Kidron et al., 2010, Lanevskij et al., 2009, Linnankoski et al., 2006, Liu et al., 2004). Thus, this result supports the role of blood-ocular barriers in determining the vitreal elimination of small molecules. Moreover, these descriptors are related to the passive diffusion across barriers and thus it seems that active transport is not a major factor, at least for the 47 compounds used in the modelling because known substrates for these transporters (e.g. carbenicillin, quinidine) were not outliers in the model. From this data set, only 60% of the compounds could be included in the next study: QSPR models for intravitreal clearance and volume of distribution. The studies which had to be rejected had missing dose values or inadequate concentration profiles and these are values that are necessary for calculation of the primary pharmacokinetic parameters.

The quality of the published intravitreal pharmacokinetic data was unsatisfactory in many cases. The criteria applied for the inclusion in the CL_{ivt} and $V_{ss,\ ivt}$ analyses (at least four time-points and two replicates per point, balanced sampling during two $t_{1/2,\ ivt}$ or longer) were fulfilled in only 58% of the studies selected for inclusion in study III. Many reports displayed shortcomings such as inadequate data points, poor match between dose and initial concentration, solubility problems and thus it was not possible to make any reliable calculations of CL_{ivt} and $V_{ss,\ ivt}$. Indeed, sampling vitreous is not as simple task as obtaining

a blood specimen, it is an invasive technique and many rabbits are needed (12 - 18 animals) before one obtains sufficient data for the reliable estimation of the primary pharmacokinetic parameters. One aim of this thesis was to provide guidance about how best to design an intravitreal pharmacokinetic study in experimental animals.

It was possible to make reliable calculations of CL_{ivt} and $V_{ss,\ ivt}$ for the 42% of the cases and a final data set of 40 small molecules and 11 macromolecules was obtained. The chemical space of the intravitreal small molecules (molecular weight of 18 to1500 Da, LogP of -5 to 3, HD of 1 to 21, and hydrogen bond acceptor (HA) of 1 to 33) deviated from the "druggability" space of per oral administered drugs (i.e. molecular weight < 500, LogP < 5 and HD < 5, HA < 10) (Lipinski et al. 2001). This is not surprising because there are major differences in the physicochemical properties between oral drug administration and intravitreal injections. For example, hydrophilic and larger molecules can have a beneficially long residence time after injection into the vitreous, but these compounds may not have adequate per oral absorption or undergo good distribution to the tissues. Therefore, the "druggable" space for intravitreal compounds may differ from the rule-of-5 classification commonly used for orally administered drugs.

Prediction of the primary pharmacokinetic parameters ($CL_{ivt,}$ $V_{ss,\ ivt}$) is useful, because the resulting models can be integrated into pharmacokinetic simulation models to allow the prediction of drug concentrations in the vitreous after different dosing regimens. Furthermore, these parameters can be related to the anatomical volumes (for distribution), flow factors (blood flow, aqueous humour turnover) and blood-ocular barriers (for elimination) and they can help provide a mechanistic understanding of ocular pharmacokinetics.

Since the values of $V_{ss,\ ivt}$ of the compounds showed rather low variance (0.72–3.14 ml, 4-fold), it was not possible to build a QSPR model for $V_{ss,\ ivt}$. However, the narrow range of $V_{ss,\ ivt}$ represents new and useful information. These values are close to the typical anatomical volumes in the posterior segment of the rabbit eye, and therefore this indicates that the drug distribution to the surrounding tissues does not increase the $V_{ss,\ ivt}$ value significantly. Based on Eq. 3 and Eq. 8, one can conclude that $V_{ss,\ ivt}$ can be defined based on the anatomical volumes and $K_{p,\ T}$ or $f_u/f_{u,T}$ values in the posterior eye segment. There are two main reasons for the moderate $V_{ss,\ ivt}$ values: 1) the anatomical sizes of the surrounding ocular tissues are relatively small in comparison to the vitreous volume; 2) drug binding and partitioning to the ocular tissues is not extensive. The narrow range of $V_{ss,\ ivt}$ values is useful information, because without further experiments, one can assume with confidence that the $V_{ss,\ ivt}$ falls within a narrow range. Accordingly, values of 1.2 and 2.3 ml were used in the pharmacokinetic simulations, because 80% of the compounds have $V_{ss,\ ivt}$ values in this range.

Unlike the values of $V_{ss,\ ivt,}$ the values of CL_{ivt} displayed a broad, 49-fold, range allowing QSPR model building for the first time. The CL_{ivt} model for small molecules was able to predict the CL_{ivt} values of the internal and external test sets accurately (mean fold errors of 1.50 and 1.33, respectively) simply based on two descriptors: $LogD_{7.4}$ and hydrogen bond donor capacity. The model equations for CL_{ivt} and $t_{1/2,\ ivt}$ were based on similar descriptors (not identical). This indicates that the variance of $t_{1/2,\ ivt}$ values is attributable to the differences in the CL_{ivt} values. The values of $V_{ss,\ ivt}$ lie in such a narrow range that their

impact on the variance of $t_{1/2, ivt}$ is of low significance. The models were also physiologically interpretable as a higher $LogD_{7.4}$ value leads to a higher CL_{ivt} value (shorter $t_{1/2, ivt}$). This is likely due to the increased permeability in blood-ocular barriers, while increased hydrogen bonding results in a smaller CL_{ivt} value (longer $t_{1/2, ivt}$) as more polar compounds penetrate more slowly through the membranes. The only previous QSPR model which attempted to predict $t_{1/2, ivt}$ was done with a few descriptors and a miscellaneous compound set (macromolecules and small molecules) (Durairaj et al., 2009) and its performance was not properly validated (Durairaj et al., 2009).

The ocular pharmacokinetic data collection in this work is the most extensive conducted so far. It is anticipated that the data collection and the QSPR models for CL_{ivt} and $t_{1/2, ivt}$ will prove useful in ocular drug discovery and development, although one must be aware of the intravitreal chemical space of the QSPR models generated because some new drug candidates may fall outside of this chemical space (e.g. new analogs with LogP > 3).

Even though macromolecules could not be included in the QSPR model for CL_{ivt}, useful information was obtained. From 31 intravitreal pharmacokinetic studies with macromolecules, 13 studies met the selection criteria (11 compounds with molecular weights ranging from 7.1 kDa to 149 kDa). Both $V_{ss, ivt}$ and CL_{ivt} values showed a narrow distribution: 1.10 – 2.76 ml for $V_{ss, ivt}$ and 0.011 - 0.027 ml/h for CL_{ivt}, respectively. When compared to the small molecules, it seems that the macromolecules have similar $V_{ss, ivt}$ values but smaller CL_{ivt} values. When the CL_{ivt} of both sets, macromolecules and small molecular drugs, were plotted against molecular weight (18 Da - 149 kDa), a correlation was detected. Previously, Maurice and Mishima reported that the molecular weight exerts an influence on the vitreal elimination of those compounds that are eliminated anteriorly (Maurice, 1976, Maurice and Mishima, 1984). However, molecular weight does not affect the CL_{ivt} either of small compounds alone ($LogD_{7.4}$ and HD are the relevant descriptors) or macromolecules alone (no correlation between CL_{ivt} and molecular weight). Even though it was not feasible to create a QSPR model for CL_{ivt} of macromolecules (small set of drugs, only one descriptor available) physiochemical characterization of these macromolecules (e.g. charge, lipophilicity, molecular shape) could help clarifying the factors affecting their ocular clearance. Moreover, the comprehensive collection of intravitreal pharmacokinetic data compiled in this work could be useful in itself for the development of novel macromolecules for use in the treatment of ocular diseases.

Intravitreal drug clearance may occur via the anterior or posterior routes (Figure 7B) depending on the capability of the drug to cross the blood-ocular barriers, and in particular, the BRB (Maurice, 1976). Intravitreal clearance across RPE has been calculated for two small compounds (betaxolol and carboxyfluorescein) and for four FITC-dextrans based on their bovine RPE permeability values (Pitkanen et al., 2005). While the values for the small molecules were in the range of *in vivo* CL_{ivt} showing that significant elimination occurred through the RPE, the FITC-dextrans (4 – 80 KDa) were found to have values which were one order of magnitude lower than the *in vivo* CL_{ivt} of macromolecules. This finding supports the proposal that macromolecules are basically eliminated via the anterior route. This is the first attempt to quantify the RPE mediated CL_{ivt} and the result suggests that only about 3 - 20 % of the macromolecule drug may be eliminated via RPE. In the case of betaxolol, the role of RPE mediated CL_{ivt} was clearly more important.

10.4. Pharmacokinetic simulation of vitreal concentration of drugs

In the present thesis, the time-courses of drug concentrations in vitreous after intravitreal injection were simulated. In that part of the work, predicted values of CL_{ivt} and $V_{ss,\ ivt}$ were incorporated into the models. The value of CL_{ivt} was calculated based on the QSPR model using *in silico* values for $LogD_{7.4}$ and HD, while a typical range of $V_{ss,\ ivt}$ was employed. The simulated intravitreal pharmacokinetic profiles based on the predicted and real values matched well.

Moreover, the versatility of the simulation softwares made it possible to create different scenarios, e.g. drug release profiles from intravitreal drug delivery systems. A knowledge of the drug release rate from the delivery system, makes it possible to estimate the dose that is required to maintain the drug concentration within the therapeutic range for a certain time period. Such simulations can be undertaken based on the structure of the drug and the *in vitro* release rate from the delivery system. This can be advantageous in the evaluation of novel formulations and dosing regimens as well as in the design of pharmacokinetic studies conducted in experimental animals. The CL_{ivt}, potency and safety windows of the drug are relevant background information for this strategy. These simulations can be done early in the discovery phase (for the drug candidate) or later during drug development (for the drug in a novel delivery system). The same approach is applicable also for macromolecular drugs, even without a QSPR model, because the obtained values of $V_{ss,\ ivt}$ and CL_{ivt} fall within narrow ranges.

In conclusion, it is anticipated that the *in silico* tools developed in the present thesis will be of benefit in drug discovery and development in many ways, for example, by reducing and refining animal experiments, reducing the clinical attrition of investigational new drugs, and facilitating rational development of drug delivery systems. The results emerging from this thesis project should also make it possible to build relevant and reliable pharmacokinetic models for the human eye based on the translational information compiled here.

11. Summary and conclusions

The main outcomes of the thesis are summarized in the figure below.

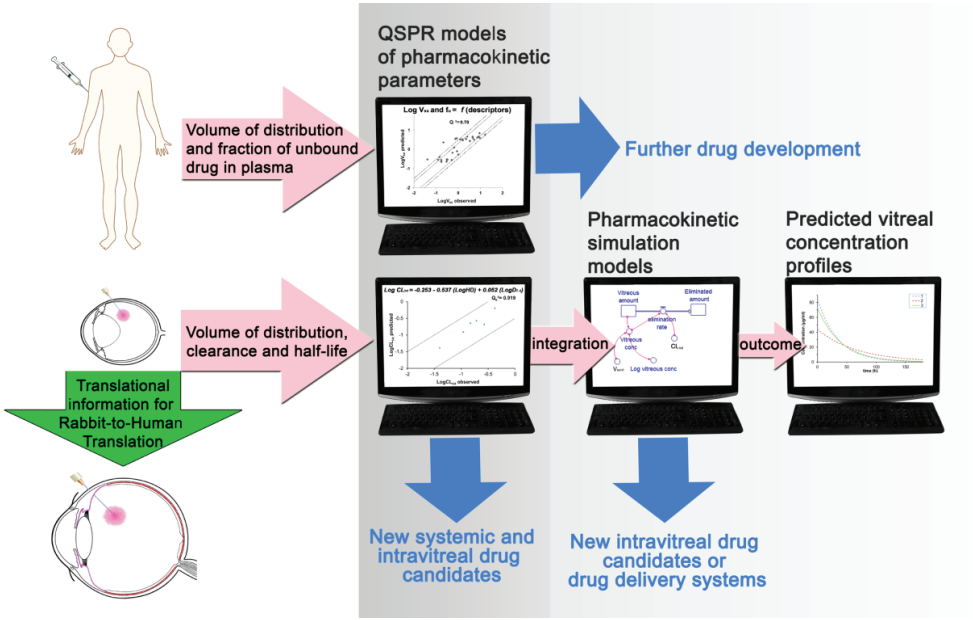

In this thesis project, new computational tools were built to permit pharmacokinetic predictions of drug candidates and drug delivery systems.

1. A QSPR model was built for the parallel prediction of volume of drug distribution and fraction of unbound drug in plasma in humans. Eleven descriptors were needed in the model. The model displayed adequate accuracy and predictability.

2. Comprehensive collections were obtained of data related to volume of distribution, clearance and half-life of intravitreally injected drugs in rabbits and humans. The volume of distribution had a narrow range of values, whereas clearance and half-life had broad variance.

3. Accurate QSPR models were built for intravitreal clearance and for prediction of the half-life of small compounds. $LogD_{7.4}$ and hydrogen bonding parameters adequately predicted the clearance and half-life.

4. Hybrid *in silico* tools integrating the CL_{ivt} QSPR model and $V_{ss,\ ivt}$ typical values in pharmacokinetic simulation models were built successfully. The concentration profiles of intravitreal compounds could be simulated reliably after administration of the drug either in solution or incorporated into delivery systems.

5. The translational value of the rabbit as an animal model for clinical intravitreal pharmacokinetics was assessed and demonstrated in a quantitative manner. No evidence was found to support crucial roles for vitreous viscosity or rabbit species differences in any of the critical parameters affecting ocular drug pharmacokinetics.

6. An improved framework was generated for connecting together the molecular structures, physiological factors and intravitreal pharmacokinetics.

References

Bakri, S.J., Snyder, M.R., Reid, J.M., Pulido, J.S., Singh, R.J., 2007a. Pharmacokinetics of intravitreal bevacizumab (Avastin). Ophthalmology 114, 855-859.

Bakri, S.J., Snyder, M.R., Reid, J.M., Pulido, J.S., Ezzat, M.K., Singh, R.J., 2007b. Pharmacokinetics of Intravitreal Ranibizumab (Lucentis). Ophthalmology 114, 2179-2182.

Balakin, K.V., Ivanenkov, Y.A., Savchuk, N.P., Ivashchenko, A.A., Ekins, S., 2005. Comprehensive computational assessment of ADME properties using mapping techniques. Curr. Drug Discov. Technol. 2, 99-113.

Bashshur, Z.F., Haddad, Z.A., Schakal, A., Jaafar, R.F., Saab, M., Noureddin, B.N., 2008. Intravitreal Bevacizumab for Treatment of Neovascular Age-related Macular Degeneration: A One-year Prospective Study. Am. J. Ophthalmol. 145, 249-256.

Berellini, G., Springer, C., Waters, N.J., Lombardo, F., 2009. In silico prediction of volume of distribution in human using linear and nonlinear models on a 669 compound data set. J. Med. Chem. 52, 4488-4495.

Bill, A., 1975. Blood circulation and fluid dynamics in the eye. Physiol. Rev. 55, 383-417.

Birkett, D.J., 2010. Pharmacokinetics made Easy, 2nd ed. McGraw-Hill.

Caldwell, G.W., Yan, Z., Tang, W., Dasgupta, M., Hasting, B., 2009. ADME optimization and toxicity assessment in early- and late-phase drug discovery. Curr. Top. Med. Chem. 9, 965-980.

Cheung, L.K., Eaton, A., 2013. Age-related macular degeneration. Pharmacotherapy 33, 838-855.

Cruciani, G., Crivori, P., Carrupt, P.-., Testa, B., 2000. Molecular fields in quantitative structure–permeation relationships: the VolSurf approach. Journal of Molecular Structure: THEOCHEM 503, 17-30.

Cunha-Vaz, J., 1979. The blood-ocular barriers. Surv. Ophthalmol. 23, 279-296.

Cunha-Vaz, J., Bernardes, R., Lobo, C., 2011. Blood-retinal barrier. Eur. J. Ophthalmol. 21 Suppl 6, S3-9.

DaCosta, J., Hamilton, R., Nago, J., Mapani, A., Kennedy, E., Luckett, T., Pavesio, C., Flanagan, D., 2014. Implementation of a nurse-delivered intravitreal injection service. Eye (Lond) 28, 734-740.

del Amo, E.M., Urtti, A., 2008. Current and future ophthalmic drug delivery systems. A shift to the posterior segment. Drug Discov. Today 13, 135-143.

Demir-Kavuk, O., Bentzien, J., Muegge, I., Knapp, E., 2011. DemQSAR: predicting human volume of distribution and clearance of drugs. J. Comput. Aided Mol. Des. 25, 1121-1133.

Dossarps, D., Bron, A.M., Koehrer, P., Aho-Glélé, L.S., Creuzot-Garcher, C., 2015. Endophthalmitis After Intravitreal Injections: Incidence, Presentation, Management, and Visual Outcome. Am. J. Ophthalmol. http://dx.doi.org/10.1016/j.ajo.2015.04.013.

Doweyko, A.M., 2008. QSAR: dead or alive? J. Comput. Aided Mol. Des. 22, 81-89.

Durairaj, C., Shah, J.C., Senapati, S., Kompella, U.B., 2009. Prediction of vitreal half-life based on drug physicochemical properties: quantitative structure-pharmacokinetic relationships (QSPKR). Pharm. Res. 26, 1236-1260.

Ekins, S., Mestres, J., Testa, B., 2007. In silico pharmacology for drug discovery: applications to targets and beyond RID B-3673-2009. Br. J. Pharmacol. 152, 21-37.

Eriksson, L., Johansson, E., Kettaneh-Wold, N., Trygg, J., Wikström, C., Wold, S., 2006a. Multi- and Megavariate Data Analysis, 2nd ed. Umetrics.

Eriksson, L., Andersson, P.L., Johansson, E., Tysklind, M., 2006b. Megavariate analysis of environmental QSAR data. Part I--a basic framework founded on principal component analysis (PCA), partial least squares (PLS), and statistical molecular design (SMD). Mol. Divers. 10, 169-186.

Eriksson, L., Jaworska, J., Worth, A., Cronin, M., McDowell, R., Gramatica, P., 2003. Methods for reliability and uncertainty assessment and for applicability evaluations of classification- and regression-based QSARs. Environ. Health Perspect. 111, 1361-1375.

Fagerholm, U., 2007. Prediction of human pharmacokinetics--evaluation of methods for prediction of volume of distribution. J. Pharm. Pharmacol. 59, 1181-1190.

Fan, J., de Lannoy, I.A.M., 2014. Pharmacokinetics. Biochem. Pharmacol. 87, 93-120.

Fatemi, M.H., Ghorbannezhad, Z., 2011. Estimation of the volume of distribution of some pharmacologically important compounds from their structural descriptors. Journal of the Serbian Chemical Society 76, 1003-1014.

Freddo, T.F., 2013. A contemporary concept of the blood-aqueous barrier. Prog. Retin. Eye Res. 32, 181-195.

Ghafourian, T., Barzegar-Jalali, M., Dastmalchi, S., Khavari-Khorasani, T., Hakimiha, N., Nokhodchi, A., 2006. QSPR models for the prediction of apparent volume of distribution. Int. J. Pharm. 319, 82-97.

Ghafourian, T., Barzegar-Jalali, M., Hakimiha, N., Cronin, M.T., 2004. Quantitative structure-pharmacokinetic relationship modelling: apparent volume of distribution. J. Pharm. Pharmacol. 56, 339-350.

Gleeson, M.P., 2007. Plasma protein binding affinity and its relationship to molecular structure: an in-silico analysis. J. Med. Chem. 50, 101-112.

Gleeson, M.P., Waters, N.J., Paine, S.W., Davis, A.M., 2006. In silico human and rat Vss quantitative structure-activity relationship models. J. Med. Chem. 49, 1953-1963.

Gombar, V.K., Hall, S.D., 2013. Quantitative Structure-Activity Relationship Models of Clinical Pharmacokinetics: Clearance and Volume of Distribution. J. Chem. Inf. Model. 53, 948-957.

Gupta, S.K., Velpandian, T., Dhingra, N., Jaiswal, J., 2000. Intravitreal pharmacokinetics of plain and liposome-entrapped fluconazole in rabbit eyes. J. Ocul. Pharmacol. Ther. 16, 511-518.

Hall, J.E., Guyton, A.C., 2011. Guyton and Hall Textbook of Medical Physiology, 12th ed. Saunders.

He, L., Jurs, P.C., 2005. Assessing the reliability of a QSAR model's predictions. Journal of Molecular Graphics and Modelling, 23, 503-523.

Hirono, S., Nakagome, I., Hirano, H., Yoshii, F., Moriguchi, I., 1994. Non-congeneric structure-pharmacokinetic property correlation studies using fuzzy adaptive least-squares: volume of distribution. Biol. Pharm. Bull. 17, 686-690.

International Transporter Consortium, Giacomini, K.M., Huang, S.M., Tweedie, D.J., Benet, L.Z., Brouwer, K.L., Chu, X., Dahlin, A., Evers, R., Fischer, V., Hillgren, K.M., Hoffmaster, K.A., Ishikawa, T., Keppler, D., Kim, R.B., Lee, C.A., Niemi, M., Polli, J.W., Sugiyama, Y., Swaan, P.W., Ware, J.A., Wright, S.H., Yee, S.W., Zamek-Gliszczynski, M.J., Zhang, L., 2010. Membrane transporters in drug development. Nat. Rev. Drug Discov. 9, 215-236.

Ishizaki, J., Yokogawa, K., Nakashima, E., Ohkuma, S., Ichimura, F., 1998. Uptake of basic drugs into rat lung granule fraction in vitro. Biol. Pharm. Bull. 21, 858-861.

Jones, H., Chen, Y., Gibson, C., Heimbach, T., Parrott, N., Peters, S., Snoeys, J., Upreti, V., Zheng, M., Hall, S., 2015. Physiologically based pharmacokinetic modelling in drug discovery and development: A pharmaceutical industry perspective. Clinical Pharmacology & Therapeutics 97, 247-262.

Karalis, V., Tsantili-Kakoulidou, A., Macheras, P., 2003. Quantitative structure-pharmacokinetic relationships for disposition parameters of cephalosporins. European Journal of Pharmaceutical Sciences 20, 115-123.

Karalis, V., Tsantili-Kakoulidou, A., Macheras, P., 2002. Multivariate statistics of disposition pharmacokinetic parameters for structurally unrelated drugs used in therapeutics. Pharm. Res. 19, 1827-1834.

Kidron, H., Vellonen, K.S., del Amo, E.M., Tissari, A., Urtti, A., 2010. Prediction of the corneal permeability of drug-like compounds. Pharm. Res. 27, 1398-1407.

Knibbe, C.A., Zuideveld, K.P., Aarts, L.P., Kuks, P.F., Danhof, M., 2005. Allometric relationships between the pharmacokinetics of propofol in rats, children and adults. Br. J. Clin. Pharmacol. 59, 705-711.

Kola, I., 2008. The state of innovation in drug development. Clin. Pharmacol. Ther. 83, 227-230.

Kola, I., Landis, J., 2004. Can the pharmaceutical industry reduce attrition rates? Nature Reviews Drug Discovery 3, 711-715.

Kotha, S., Murtomäki, L., 2014. Virtual pharmacokinetic model of human eye. Math. Biosci. 253, 11-18.

Kwon, Y., 2002. Handbook of Essential Pharmacokinetics, Pharmacodynamics and Drug Metabolism for Industrial Scientists, 1st ed. Kluwer Academic Publishers.

Lanevskij, K., Japertas, P., Didziapetris, R., Petrauskas, A., 2009. Ionization-specific prediction of blood-brain permeability. J. Pharm. Sci. 98, 122-134.

Laude, A., Tan, L.E., Wilson, C.G., Lascaratos, G., Elashry, M., Aslam, T., Patton, N., Dhillon, B., 2010. Intravitreal therapy for neovascular age-related macular degeneration and inter-individual variations in vitreous pharmacokinetics. Prog. Retin. Eye Res. 29, 466-475.

Leach, A.R., Gillet, V.J., 2007. An Introduction to Chemoinformatics, 2nd ed. Springer.

Lee, S.S., Ghosn, C., Yu, Z., Zacharias, L.C., Kao, H., Lanni, C., Abdelfattah, N., Kuppermann, B., Csaky, K.G., D'Argenio, D.Z., Burke, J.A., Hughes, P.M., Robinson, M.R., 2010. Vitreous VEGF clearance is increased after vitrectomy. Invest. Ophthalmol. Vis. Sci. 51, 2135-2138.

Li, H., Chen, Z., Xu, X., Sui, X., Guo, T., Liu, W., Zhang, J., 2011. Predicting human plasma protein binding of drugs using plasma protein interaction QSAR analysis (PPI-QSAR). Biopharm. Drug Dispos. 32, 333-342.

Lim, V.S., 1991. Recombinant human erythropoietin in predialysis patients. Am. J. Kidney Dis. 18, 34-37.

Linnankoski, J., Makela, J., Palmgren, J., Mauriala, T., Vedin, C., Ungell, A.L., Lazorova, L., Artursson, P., Urtti, A., Yliperttula, M., 2010. Paracellular porosity and pore size of the human intestinal epithelium in tissue and cell culture models. J. Pharm. Sci. 99, 2166-2175.

Linnankoski, J., Makela, J.M., Ranta, V.P., Urtti, A., Yliperttula, M., 2006. Computational prediction of oral drug absorption based on absorption rate constants in humans. J. Med. Chem. 49, 3674-3681.

Lipinski, C.A., 2000. Drug-like properties and the causes of poor solubility and poor permeability. J. Pharmacol. Toxicol. Methods 44, 235-249.

Lipinski, C.A., Lombardo, F., Dominy, B.W., Feeney, P.J., 2001. Experimental and computational approaches to estimate solubility and permeability in drug discovery and development settings1. Adv. Drug Deliv. Rev. 46, 3-26.

Liu, X., Tu, M., Kelly, R.S., Chen, C., Smith, B.J., 2004. Development of a computational approach to predict blood-brain barrier permeability. Drug Metab. Dispos. 32, 132-139.

Lombardo, F., Gifford, E., Shalaeva, M.Y., 2003. In silico ADME prediction: data, models, facts and myths. Mini Rev. Med. Chem. 3, 861-875.

Lombardo, F., Obach, R.S., Dicapua, F.M., Bakken, G.A., Lu, J., Potter, D.M., Gao, F., Miller, M.D., Zhang, Y., 2006. A hybrid mixture discriminant analysis-random forest computational model for the prediction of volume of distribution of drugs in human. J. Med. Chem. 49, 2262-2267.

Lüllmann, H., Mohr, K., Hein, L., 2011. Pocket Atlas of Pharmacology, 4th ed. Georg Thieme Verlag.

Mager, D.E., 2006. Quantitative structure-pharmacokinetic/pharmacodynamic relationships. Adv. Drug Deliv. Rev. 58, 1326-1356.

Mahmood, I., 2007. Application of allometric principles for the prediction of pharmacokinetics in human and veterinary drug development. Adv. Drug Deliv. Rev. 59, 1177-1192.

Maltarollo, V.G., Gertrudes, J.C., Oliveira, P.R., Honorio, K.M., 2015. Applying machine learning techniques for ADME-Tox prediction: a review. Expert Opin. Drug Metab. Toxicol. 11, 259-271.

Maurice, D.M., 1976. Injection of drugs into the vitreous body, in Leopold, I.H., Burns, R.P. (Eds.), Symposium on Ocular Therapy, 1st ed. John Wiley & Sons, pp. 59-72.

Maurice, D.M., Mishima, S., 1984. Ocular pharmacokinetics, in Sears, M.L. (Ed.), Pharmacology of the Eye, 1st ed. Springer-Verlag, pp. 19-116.

Mayer, J.M., Van de Waterbeemd, H., 1985. Development of quantitative structure-pharmacokinetic relationships. Environ. Health Perspect. 61, 295-306.

Meredith, T.A., 1993. Antimicrobial pharmacokinetics in endophthalmitis treatment: studies of ceftazidime. Trans. Am. Ophthalmol. Soc. 91, 653-699.

Moda, T.L., Montanari, C.A., Andricopulo, A.D., 2007. Hologram QSAR model for the prediction of human oral bioavailability. Bioorg. Med. Chem. 15, 7738-7745.

Ng, C., Xiao, Y., Putnam, W., Lum, B., Tropsha, A., 2004. Quantitative structure-pharmacokinetic parameters relationships (QSPKR) analysis of antimicrobial agents in humans using simulated annealing k-nearest-neighbor and partial least-square analysis methods. J. Pharm. Sci. 93, 2535-2544.

Nomoto, H., Shiraga, F., Kuno, N., Kimura, E., Fujii, S., Shinomiya, K., Nugent, A.K., Hirooka, K., Baba, T., 2009. Pharmacokinetics of bevacizumab after topical, subconjunctival, and intravitreal administration in rabbits. Invest. Ophthalmol. Visual Sci. 50, 4807-4813.

Obach, R.S., Lombardo, F., Waters, N.J., 2008. Trend Analysis of a Database of Intravenous Pharmacokinetic Parameters in Humans for 670 Drug Compounds. Drug Metab. Dispos. 36, 1385-1405.

Øie, S., Tozer, T.N., 1979. Effect of altered plasma protein binding on apparent volume of distribution. J. Pharm. Sci. 68, 1203-1205.

Pandit, N.K., Soltis, R.P., 2012. Introduction to the Pharmaceutical Sciences: An Integrated Approach, 2nd ed. Wolters Kluwer Lippincott Williams & Wilkins.

Paul, Y., Dhake, A.S., Parle, M., Singh, B., 2010. In Silico Quantitative Structure Pharmacokinetic Relationship Modelling for Quinolone Drugs: Biological Half-Life. Asian Journal of Chemistry 22, 4880-4890.

Peyman, G.A., Lad, E.M., Moshfeghi, D.M., 2009. Intravitreal injection of therapeutic agents. Retina 29, 875-912.

Pitkanen, L., Ranta, V.P., Moilanen, H., Urtti, A., 2005. Permeability of retinal pigment epithelium: effects of permeant molecular weight and lipophilicity. Invest. Ophthalmol. Vis. Sci. 46, 641-646.

Poulin, P., Theil, F.P., 2002. Prediction of pharmacokinetics prior to in vivo studies. 1. Mechanism-based prediction of volume of distribution. J. Pharm. Sci. 91, 129-156.

Prince, J.H., 1964. The Rabbit in Eye Research, 1st ed. Charles C. Thomas.

Ranta, V.P., Mannermaa, E., Lummepuro, K., Subrizi, A., Laukkanen, A., Antopolsky, M., Murtomaki, L., Hornof, M., Urtti, A., 2010. Barrier analysis of periocular drug delivery to the posterior segment. J. Control. Release 148, 42-48.

Ranta, V.P., Urtti, A., 2006. Transscleral drug delivery to the posterior eye: prospects of pharmacokinetic modelling. Adv. Drug Deliv. Rev. 58, 1164-1181.

Rittenhouse, K.D., Pollack, G.M., 2000. Microdialysis and drug delivery to the eye. Adv. Drug Deliv. Rev. 45, 229-241.

Rodgers, T., Rowland, M., 2007. Mechanistic approaches to volume of distribution predictions: understanding the processes. Pharm. Res. 24, 918-933.

Roh, S., Weiter, J.J., Duker, J.S., 2006. Ocular Circulation, in Tasman, W., Jaeger, E.A. (Eds.), Duane's Ophthalmology on CD-ROM, 2006 ed. Lippincott Williams & Wilkins. Chapter 5.

Rowe-Rendleman, C.L., Durazo, S.A., Kompella, U.B., Rittenhouse, K.D., Di Polo, A., Weiner, A.L., Grossniklaus, H.E., Naash, M.I., Lewin, A.S., Horsager, A., Edelhauser, H.F., 2014. Drug and gene delivery to the back of the eye: from bench to bedside. Invest. Ophthalmol. Vis. Sci. 55, 2714-2730.

Rowland, M., Tozer, T.N., 2011. Clinical Pharmacokinetics and Pharmacodynamics: Concepts and Applications, 4th ed. Lippincott Williams & Wilkins.

Saiakhov, R., Stefan, L., Klopman, G., 2000. Multiple computer-automated structure evaluation model of the plasma protein binding affinity of diverse drugs. Perspect. Drug Discov. Des. 19, 133-155.

Sanford, M., 2013. Fluocinolone Acetonide Intravitreal Implant (Iluvien®). Drugs 73, 187-193.

Sarao, V., Veritti, D., Boscia, F., Lanzetta, P., 2014. Intravitreal steroids for the treatment of retinal diseases. Scientific World Journal 2014, 989501.

Schmidt, S., Derendorf, H., 2014. Applied Pharmacometrics, 1st ed. Springer.

Severn, P.S., Hamilton, R., 2015. The incidence of serious complications associated with intravitreal therapy in a quaternary ARMD service (2008-2014). Eye (Lond) 29, 150.

Shardlow, C.E., Generaux, G.T., Patel, A.H., Tai, G., Tran, T., Bloomer, J.C., 2013. Impact of physiologically based pharmacokinetic modelling and simulation in drug development. Drug Metab. Dispos. 41, 1994-2003.

Shen, Y.C., Wang, M.Y., Wang, C.Y., Tsai, T.C., Tsai, H.Y., Lee, Y.F., Wei, L.C., 2007. Clearance of intravitreal voriconazole. Invest. Ophthalmol. Vis. Sci. 48, 2238-2241.

Sugano, K., Kansy, M., Artursson, P., Avdeef, A., Bendels, S., Di, L., Ecker, G.F., Faller, B., Fischer, H., Gerebtzoff, G., Lennernaes, H., Senner, F., 2010. Coexistence of passive and carrier-mediated processes in drug transport. Nat. Rev. Drug Discov. 9, 597-614.

Sui, X., Sun, J., Wu, X., Li, H., Liu, J., He, Z., 2008. Predicting the volume of distribution of drugs in humans. Curr. Drug Metab. 9, 574-580.

Sy, S.K.B., Wang, X., Derendorf, H., 2014. Introduction to Pharmacometrics and Quantitative Pharmacology with an Emphasis on Physiologically Based Pharmacokinetics, in Schmidt, S., Derendorf, H. (Eds.), Applied Pharmacometrics, 1st ed. Springer, pp. 1-64.

Tan, L.E., Orilla, W., Hughes, P.M., Tsai, S., Burke, J.A., Wilson, C.G., 2011. Effects of vitreous liquefaction on the intravitreal distribution of sodium fluorescein, fluorescein dextran, and fluorescent microparticles. Invest. Ophthalmol. Vis. Sci. 52, 1111-1118.

Teorell, T., 1937. Kinetics of distribution of substances administered to the body, I: the extravascular modes of administration. Arch. Int. Pharmacodyn. Ther. 57, 205-225.

Teorell, T., 1937. Kinetics of distribution of substances administered to the body, II: the extravascular modes of administration. Arch. Int. Pharmacodyn. Ther. 57, 226-240.

Tett, S.E., Cutler, D.J., Day, R.O., Brown, K.F., 1988. A dose-ranging study of the pharmacokinetics of hydroxy-chloroquine following intravenous administration to healthy volunteers. Br. J. Clin. Pharmacol. 26, 303-313.

Thakur, S.S., Barnett, N.L., Donaldson, M.J., Parekh, H.S., 2014. Intravitreal drug delivery in retinal disease: Are we out of our depth? Expert Opinion on Drug Delivery 11, 1575-1590.

Theil, F.P., Guentert, T.W., Haddad, S., Poulin, P., 2003. Utility of physiologically based pharmacokinetic models to drug development and rational drug discovery candidate selection. Toxicol. Lett. 138, 29-49.

Topliss, J.G., Edwards, R.P., 1979. Chance factors in studies of quantitative structure-activity relationships. J. Med. Chem. 22, 1238-1244.

Totan, Y., Guler, E., Guragac, F.B., 2015. Dexamethasone Intravitreal Implant for Chronic Diabetic Macular Edema Resistant to Intravitreal Bevacizumab Treatment. Curr. Eye Res. , 1-7.

Toutain, P.L., Bousquet-Melou, A., 2004. Volumes of distribution. J. Vet. Pharmacol. Ther. 27, 441-453.

Toutain, P.L., Bousquet-Mélou, A., 2004. Plasma terminal half-life. J. Vet. Pharmacol. Ther. 27, 427-439.

Tropsha, A., Gramatica, P., Gombar, V.K., 2003. The Importance of Being Earnest: Validation is the Absolute Essential for Successful Application and Interpretation of QSPR Models. QSAR & Combinatorial Science 22, 69-77.

Turner, J.V., Maddalena, D.J., Cutler, D.J., 2004. Pharmacokinetic parameter prediction from drug structure using artificial neural networks. Int. J. Pharm. 270, 209-219.

Urtti, A., 2006. Challenges and obstacles of ocular pharmacokinetics and drug delivery. Adv. Drug Deliv. Rev. 58, 1131-1135.

Vaishya, R.D., Ananthula, H.K., Mitra, A.K., 2011. Microdialysis for Vitreal Pharmacokinetics, in Kompella, U.B., Edelhauser, H.F. (Eds.), Drug Product Development for the Back of the Eye. Springer, pp. 21-45.

van de Waterbeemd, H., 2009. Improving compound quality through in vitro and in silico physicochemical profiling. Chem. Biodivers 6, 1760-1766.

van de Waterbeemd, H., Gifford, E., 2003. ADMET in silico modelling: towards prediction paradise? Nat. Rev. Drug Discov. 2, 192-204.

Vellonen, K.S., Malinen, M., Mannermaa, E., Subrizi, A., Toropainen, E., Lou, Y.R., Kidron, H., Yliperttula, M., Urtti, A., 2014. A critical assessment of in vitro tissue models for ADME and drug delivery. J. Control. Release 190, 94-114.

Votano, J.R., Parham, M., Hall, L.M., Hall, L.H., Kier, L.B., Oloff, S., Tropsha, A., 2006. QSAR modelling of human serum protein binding with several modelling techniques utilizing structure-information representation. J. Med. Chem. 49, 7169-7181.

Wang, H., Chhablani, J., Freeman, W.R., Beadle, J.R., Hostetler, K.Y., Hartmann, K., Conner, L., Aldern, K.A., Pearson, L., Cheng, L., 2011. Intraocular safety and pharmacokinetics of hexadecyloxypropyl-cidofovir (HDP-CDV) as a long-lasting intravitreal antiviral drug. Invest. Ophthalmol. Vis. Sci. 52, 9391-9396.

Wold, S., Sjöström, M., Eriksson, L., 2001a. PLS-regression: A basic tool of chemometrics. Chemometrics Intellig. Lab. Syst. 58, 109-130.

Wold, S., Trygg, J., Berglund, A., Antti, H., 2001b. Some recent developments in PLS modelling. Chemometrics Intellig. Lab. Syst. 58, 131-150.

Xu, C., Mager, D.E., 2011. Quantitative structure-pharmacokinetic relationships. Expert Opin. Drug Metab. Toxicol. 7, 63-77.

Xu, Q., Boylan, N.J., Suk, J.S., Wang, Y., Nance, E.A., Yang, J., McDonnell, P.J., Cone, R.A., Duh, E.J., Hanes, J., 2013. Nanoparticle diffusion in, and microrheology of, the bovine vitreous ex vivo. J. Controlled Release 167, 76-84.

Zhang, D., Luo, G., Ding, X., Lu, C., 2012a. Preclinical experimental models of drug metabolism and disposition in drug discovery and development. Acta Pharmaceutica Sinica B 2, 549-561.

Zhang, K., Zhang, L., Weinreb, R.N., 2012b. Ophthalmic drug discovery: novel targets and mechanisms for retinal diseases and glaucoma. Nat. Rev. Drug Discov. 11, 541-559.

Zhivkova, Z., Doytchinova, I., 2012. Prediction of steady-state volume of distribution of acidic drugs by quantitative structure-pharmacokinetics relationships. J. Pharm. Sci. 101, 1253-1266.

Zou, P., Yu, Y., Zheng, N., Yang, Y., Paholak, H.J., Yu, L.X., Sun, D., 2012. Applications of human pharmacokinetic prediction in first-in-human dose estimation. AAPS J. 14, 262-281.